THE ELECTRONIC SPECTRA OF SIMPLE MAIN GROUP INORGANIC AND ORGANOMETALLIC SYSTEMS

by

WILLIAM DUNCAN.

A Thesis presented for the Degree of Doctor of Philosophy.

UNIVERSITY OF EDINBURGH 1976.

DECLARATION.

The work included in this thesis is entirely my own work except where otherwise stated. Some of the results in Chapters 1, 2 and 3 have been published in collaboration with other members of this Department and reprints are to be found at the end of the thesis. They have not been submitted, in whole or in part, for any other Degree, at this or any other University.

DEDICATION.

To my Parents.

ACKNOWLEDGEMENTS.

I should like to thank my supervisors Dr. S. Cradock and Professor E.A.V. Ebsworth for their advice, encouragement and support. I am also deeply indebted to Drs. R.J. Donovan, H.M. Gillespie and S. Bell (University of Dundee) for assistance in obtaining (and interpreting) the vacuum ultra-violet spectra presented in Chapter 3.

I am most grateful to many others, but especially to Drs. R.A. Whiteford, K.M. McKay and W.J. Savage with whom I shared the laboratory facilities provided by the University of Edinburgh.

I would also wish to acknowledge my gratitude to the Science Research Council for the provision of a maintenance grant.

ABSTRACT.

The purpose underlying the researches described in this thesis is an attempt to understand the bonding and electronic structure of some simple inorganic and organometallic systems. The particular molecules chosen for study were the Selenium containing linear triatomic species OCSe, SCSe, CSe_2 and the main group metallocenes $M(C_5H_5)n$ n = 1, M = Tl & In ; n = 2, M = Pb, Sn & Hg.

In all cases the technique of ultraviolet photoelectron spectroscopy[1] was employed and the (vacuum) ultraviolet absorption spectra[2] of OCSe, SCSe & CSe_2 were also recorded. The major features of the photoelectron spectra were interpreted as arising from ionization from the filled valence levels obtained from simple schemes derived from Mulliken-Hund molecular orbital theory[3]. The absorption spectra were analysed in terms of transitions from these filled valence shell orbitals to the various empty valence and atomic like Rydberg[4] orbitals of the molecule. In addition, weaker features in the photoelectron spectra of CSe_2 and SCSe were attributed to formally forbidden one photon transitions involving simultaneous ionization and electronic excitation[5].

INDEX TO CONTENTS.

----------oOo----------

All references are to be found at the end of each chapter.

----------oOo----------

INDEX TO DIAGRAMS.

INDEX TO TABLES.

INTRODUCTION.

INTRODUCTION.

INTRODUCTION.

The results and their interpretation are presented in subsequent chapters. The purpose of this chapter is to provide an introduction to the theoretical and practical aspects of the spectroscopic techniques employed.

1. PHOTOELECTRON SPECTROSCOPY.

a) Introduction and theory.

When a molecule is irradiated by light of sufficiently short wavelength an electron may be ejected from one of the filled orbital levels. i.e.

$$\text{Molecule} + h\nu \longrightarrow (\text{Molecule})^{+} + \text{electron}$$

This process, called photoionization, forms the basis of photoelectron spectroscopy, which is concerned with the energy, intensity and distribution of these electrons.[6]

If the light source used is monochromatic, then a velocity analysis of the ejected electrons will, in simple systems, show a more or less discrete spectrum corresponding to the various states of the ion produced on photoionization. The spectrum thus obtained provides information on the relative order of the ionization potentials (IP's) of the various cationic states produced by ionization from successively higher binding energy orbitals.[7] In many cases, even for simple systems, there is no other way of obtaining such information and so the contribution made by photoelectron spectroscopy (p.e.s.) to our understanding of the ionic states of these molecules is considerable.[8] However, such information would be unlikely to arouse the intense interest of many chemists, who mainly deal with neutral or ground

state ionic species, were it not for the fact that according to Koopmans' Theorem[9], the ordering of the energy levels in the ionic state exactly parallels those of the neutral molecule and furthermore that the ionization potential of each particular orbital Ij, is equal in magnitude to its orbital energy ε_j; i.e. $I_j = -\varepsilon_j$. Thus by choosing to measure the ionic state energies, chemists have found an invaluable tool for probing the electronic structure of the neutral molecule with which they commonly deal.

In addition, the band structure observed in the photoelectron spectrum also reflect the changes in molecular geometry which take place on ionization. Such changes are closely related to the contribution which the particular orbital involved makes to the overall bonding of the molecule and so further comparison with the prediction of simple molecular orbital schemes may be made[10].

Since its discovery in the early 1960's,[11,12] the study of photoelectron spectroscopy has continued to develop at a rapid pace and is now a fully mature branch of spectroscopy. The availability of commercial spectrometers from Perkin Elmer[13] based on the original design of Turner has contributed much to this development. It has frequently been the subject of review articles[14,15,16,10,8] and several books[1,6,17] have also appeared - the one by Eland[6] being particularly good. The proceedings of several conferences[18,19,20] devoted to the subject have also been published and give some indication of the extent to which the subject has developed. Also of particular interest are the review chapters on photoelectron spectroscopy included in the Specialist Periodical Reports published by the Chemical Society[21].

In the experiments to be discussed in later chapters, the radiation used for photoionization is exclusively in the vacuum ultraviolet

region of the spectrum and generally will only ionize those electrons in molecular orbitals located in the valence shell. To probe deeper into the core region, Xray radiation is required[22]. Although basically similar in principle, as a result of the different instrumentation employed, the two branches of the subject XPS and UPS have developed separately and such division of the subject is likely to continue for some time yet. A major obstacle to their convergence is the poor resolution associated with the higher energy Xray sources,[23] and although recent attempts to bridge the gap between the two branches, including the use of intermediate energy sources[24] and the recording of valence level spectra with Xray sources[25] may help to emphasise the similarities, they also highlight the vastly superior resolution of UPS technique.

In recognition of the situation which exists at present, reference will only be made to XPS data, when it overlaps with or illuminates features observed in ultraviolet valence region spectra.

b) Instrumentation.

A diagramatic representation of a typical spectrometer is shown in Fig. I.[10] A detailed description of the actual spectrometer and the manner in which it was used to obtain the results to be presented, will be given in the Appendix on experimental methods. Here we will concentrate on the broader aspects of instrumentation and discuss the various essential component parts.

The most commonly used and useful ionization source is the He resonance line, He(I), with an energy of 21.22e.V. obtained by a high voltage, low current d.c. discharge in pure Helium. The output from such a system consists mainly of the He(I) line arising from the transition $He\ 1s^1 2p^1 \longrightarrow He\ 1s^2 (^1S)$. Higher members of the series arising from the $He 1s np (^1P) \rightarrow He\ 1s^2\ (^1S)$ transitions, usually denoted $He(I)_{\beta,\gamma,\delta}$ etc. usually occur to less than a few per cent and so the lamp output can be used directly without the need for a monochromator with its attendant loss in intensity.[26]

In addition, the use of the He(I) line is particularly helpful since the photoionization cross sections of most gases are near their maxima at this wavelength (584 nm).[27] Also, unlike the spectra obtained with the principal lines of the other inert gases e.g. Ne or Ar, there is less likelihood of autoionization effects causing anomalous intensity effects in the spectrum.[28]

Although most valence levels lie above 21 e.V. in energy, there are some levels mainly derived from atomic S orbitals, which occur in the range 21 to 40 e.V. and so are not accessible using He(I) radiation. However, by altering the conditions of the He discharge it is also possible to generate the He(II) line at 40.8 e.V.[29] and this will pro-:duce ionization from all valence levels except F 2s. This

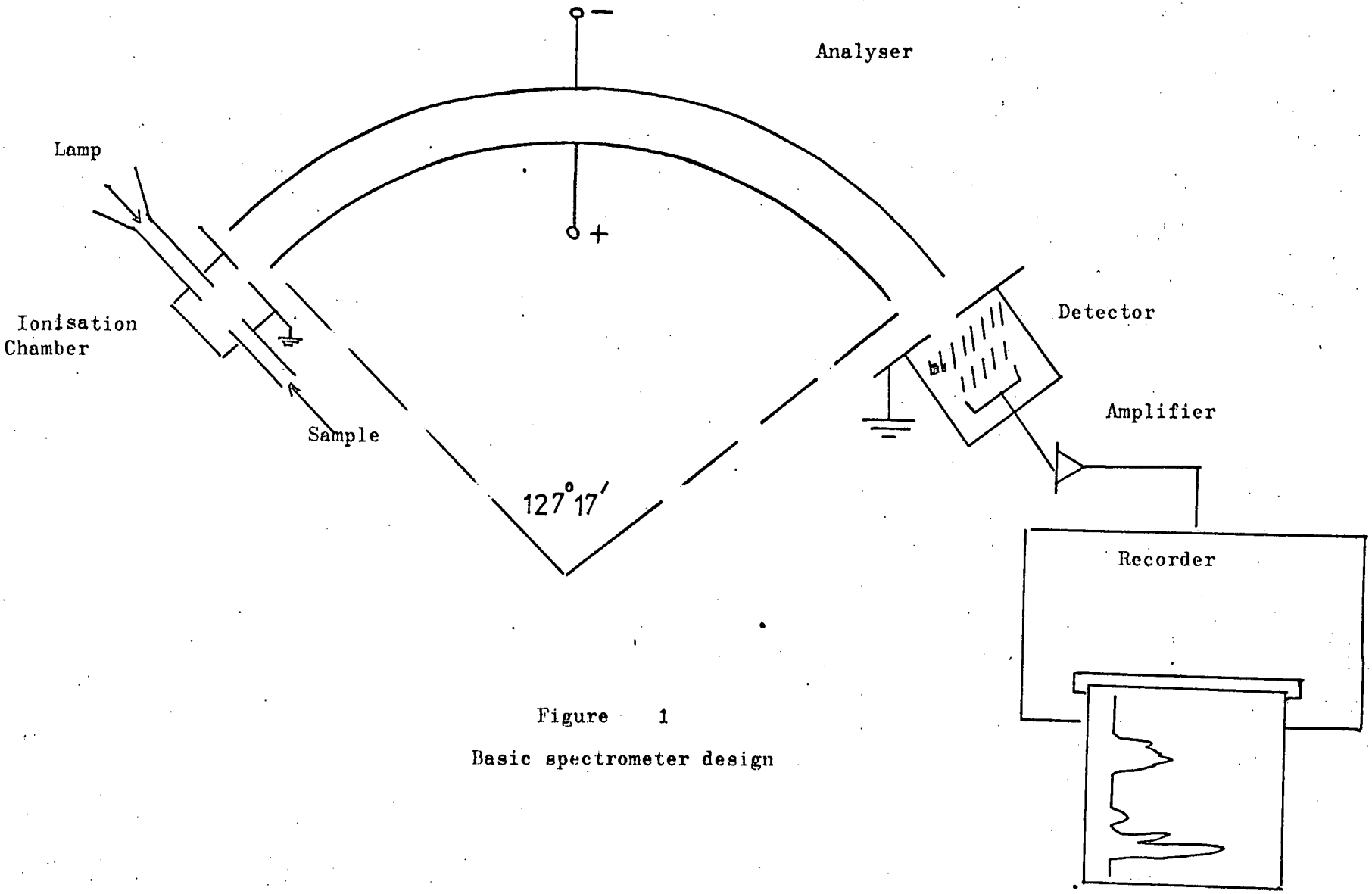

Figure 1

Basic spectrometer design

transition of $He^+(2p^1 \rightarrow 1s^1)$ occurs in discharges with a higher current density and lower Helium pressure than are required to produce He(I). However it is rarely possible to obtain a pure He(II) output without the use of filters[30] and particular care has to be exercised over the purity of the Helium used. He(II) photon fluxes of about 5% of the corresponding He(I) output are commonly used. However as a result of this, the useful range of He(II) ionization is restricted to below 28 e.V. since above this value He(I) ionization dominates the spectrum.

The reason for this is that the different photo-ejected electrons are analysed on the basis of their different kinetic energies Ej which are related to the ionization potential by the expression $Ej = h\nu - I.P.$ in the atomic case. In an He(I) source we know $h\nu$ is equal to 21.22 e.V. and so it is customary to record the IP's directly. However in the case of a mixed HeI/HeII output it is not possible to distinguish between an electron of the same kinetic energy arising from ionization by He(I) and He(II) photons even although they correspond to ionization from orbitals with very different binding energies.

Above an apparent IP of (40.8 - 21.2) = 19.6 e.V. the He(II) and He(I) spectra overlap. However as a result of the fact that most molecules have their first I.P's $\geq$ 8e.V. it is not until an apparent I.P. of about 28 e.V. that overlap resulting from the usually much higher intensity He(I) line, obscures the He(II) ionizations.

The earliest work[11,12] in photoelectron spectroscopy was performed using retarding field analysers[66] which gave an integral type spectrum. However the poorer resolution of cylindrical grid analysersquickly led to its replacement by the electrostatic 127° cylindrical analyser in which the voltage between two concentric plates

of $\frac{\pi}{\sqrt{2}}$ section, is continually varied to deflect electrons of different kinetic energies.[1] The several other types of analyser available and recent developments are described in detail in Refs.[1,6,21]

In the majority of photoelectron spectrometers the current produced by the different energy photoelectrons emerging from the deflection analyser is amplified using a 'cascade' type electron multiplier. After amplification by a factor of 10^9, the signal is taken to a pulse counter, which converts the pulses into an analogue voltage signal proportional to the number of pulses arriving per second. Counting rates between 1 and 10^5 electrons per second can conveniently be displayed on an X - Y plotter as a function of electron energy.

c) Theory of Ionization.

Before indicating the methods commonly employed in analysing the spectra thus obtained, it will be useful to discuss further the process of ionization.

The interaction between a molecule and a photon takes place via the electric dipole vector and this interaction is described according to the selection rules which detail the differences between the quantum numbers of the initial and final states for an allowed transition.[31]

For an atom or linear molecule, the change in angular momentum is

$$\Delta L = 0, \pm 1, \ldots\ldots \pm \ell$$

where ℓ = angular momentum of the ionized electron. In addition since only one electron of spin $\pm \frac{1}{2}$ is removed from the neutral system to form the ion, the change in multiplicity $(2S + 1)$ must be ± 1.[8]

In the application of these rules the initial state corresponds to the molecule plus incident photon and the final state to the ion plus free electron. However, these rules are much less restrictive for electronic excitation to the continuum than for transitions to bound states. This is a consequence of the fact that when the free electron leaves the molecule, it can do so with whatever angular momentum is required to satisfy the selection rules. Thus the outgoing electron can be regarded as an s,p,d or f wave carrying zero, one, two or three units of angular momenta or an appropriate mixture of these waves when two different angular momenta are possible under the selection rules.[32]

Photoionization usually corresponds to the removal of a single electron from the molecule without any change taking place in the

quantum numbers of the remaining electrons. The origin of this one electron transition selection rule is based on the fact that the initial and final states are described in terms of simple one electron orbital configurations. However this assumes that the electronic motions are wholly independent and when this is not strictly the case, then weak two electron transitions can occur with an intensity related to the degree of electron correlation.[33]

Koopmans' Theorem,[9] which strictly only applies to closed shell species, also relies on the validity of the one electron SCF orbital picture and is thus able to define the energy of a molecular orbital as the difference in energy between an electron at infinity from the molecular ion, and the same electron in the molecule. This energy also defines the ionization potential and so the simple relationship

$$I_j = -\varepsilon_j$$

quoted previously is obtained.

This is only valid when the interactions between the remaining electrons are unaffected by the removal of one of their numbers. The fact that this is usually true for most real systems stems from the fact that the main errors introduced in deriving Koopmans' Theorem are the neglect of correlation energy and reorganisation energy effects which although usually similar in magnitude, are of opposite sign.[34]

The application of Koopmans' Theorem has formed the basis of the analysis of most photoelectron spectra and provided the limitations and possible inaccuracies inherent in its application are borne in mind, it is a most useful and convenient assumption with which to begin any analysis.

It is usual to assume that discrepancies between calculated orbital energies and those derived using Koopmans' Theorem are a result of inaccuracies inherent in the calculation. However several examples are known where this is definitely not the case.

It is worth emphasising at this point that the molecular I.P's ob-:tained by photoelectron spectroscopy should only be properly compared with the orbital and eigenvalue solutions of an SCF Hamiltonian.

Although these delocalized molecular orbitals may be transformed by linear combinations into equivalent (hybrid) orbitals which are equally good solutions to the Schrodinger equations and suitable for describing properties of the molecular ground state, such as shape, the latter are not suitable for a discussion of the excited states. The correct set of wave functions are those which give the lowest energies under Koopmans' theorem and these correspond to the delocal-:ized orbitals, at least for the lowest ionic state of each symmetry.[36]

d) Interpretation of results.

Inspection of any molecular photoelectron spectrum indicates that the simple relationship

$$E = h\nu - I.P.$$

quoted earlier for the atomic case does not strictly apply to the molecular case. Instead of obtaining the single sharp line which the above equation would imply, we observe band envelopes with groups of closely spaced lines.

This is a consequence of the fact that ionization takes place from the molecular ground state to the various rotationally and vibrationally excited states of the ion as shown in Fig.2.

In this case the appropriate relationship defining the energy of the ejected photoelectron is

$$E = h\nu - I.P. - E_{vib,rot}$$

Except for the case of H_2[37] the changes in rotational energy have not been resolved although the most intense rotational transition corresponds to the $\Delta J = 0$ transition.

However the different vibrational levels can often be resolved and as transitions usually occur from the vibrational ground state of the molecule, the progression of peaks observed in the spectrum directly represents the various vibrational levels of the ion. The probability of a particular transition occurring between the ground state and a particular vibrational level in the ion is governed by the overlap of the vibrational wave functions of each state. This is given by the appropriate Franck-Condon factor for the transition and the relative intensity of each band is given by the square of this factor.[38] It should be emphasised, however, that the

Franck-Condon factors do not influence the total intensity, but only the relative importance of the various vibrational components.

The time scale on which ionization occurs is about 10^{-15}s. which is much faster than the time required for molecular vibration and in many cases, for molecular dissociation. As a result it is possible to denote the ionization process as vertical transitions between the potential energy surfaces, as shown in Fig. 2.

If the change in the potential energy surfaces occurring on ionization is small, then only those transitions in which the vibrational quantum numbers remain largely unchanged will be strong, since the vibrational wave functions for such levels are closely matched. In practice, this means that the adiabatic (0 - 0) transition is strongest, since the target molecules are usually in their vibrational ground states.

However, if there is a change in the position of the potential surface minimum (i.e. a different equilibrium internuclear distance) in the excited state, then the (0 - 0) transition will not be the strongest. The largest overlap (Franck-Condon factor) will then be for transitions between the molecular vibrational ground state and the higher vibrational quantum number levels of the ion in which the vibrational wave functions have large amplitudes at the molecular equilibrium internuclear distance. Thus vibrational modes which correspond most closely to the change in internuclear distances are most strongly excited and long vibrational progressions are observed. In this way, the shape of the band envelope directly reflects the changes which occur in the potential energy surfaces on ionization.

It is convenient to use these surfaces to define the different criteria for establishing the ionization potential energy of the

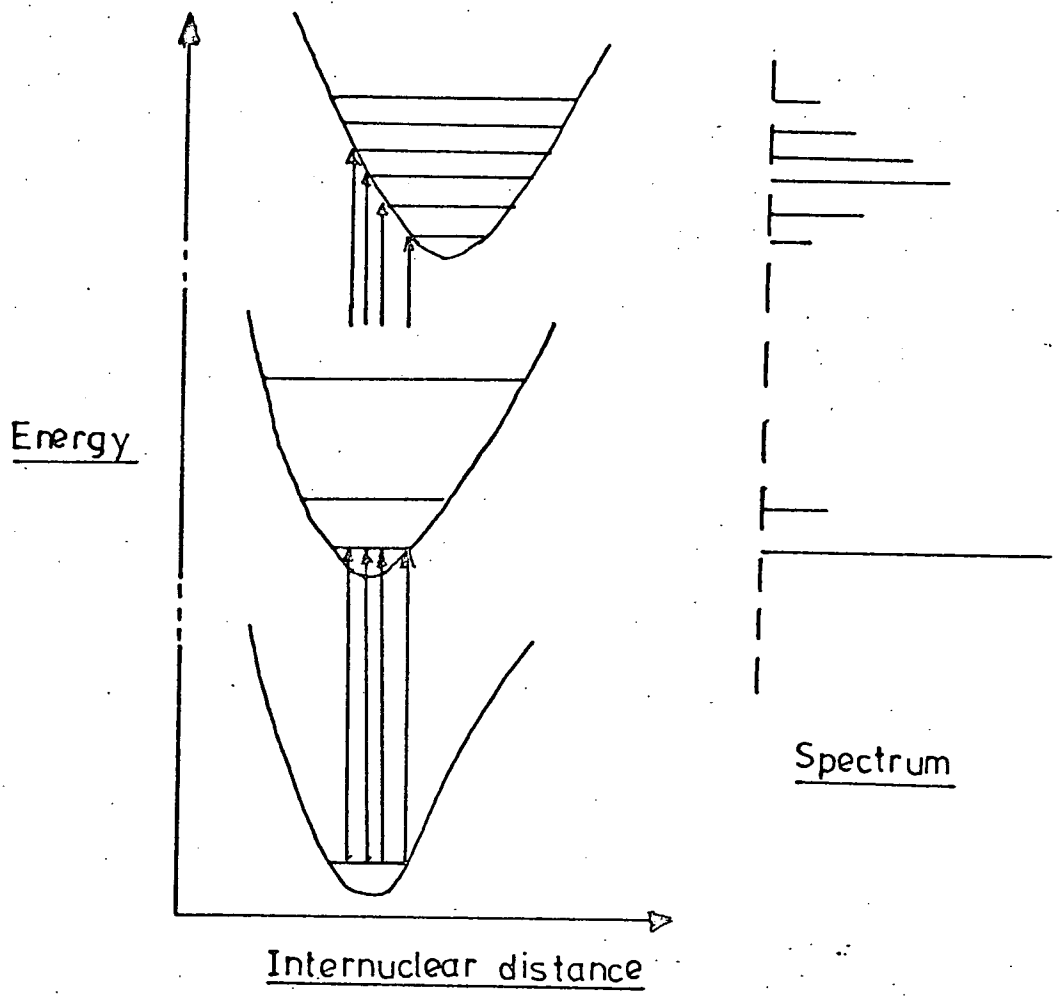

Figure 2.

Vibronic transitions.

band. The adiabatic ionization potential is the difference in energy between the vibrational (and rotational) ground states of the potential energy surfaces of the molecular and excited state species, i.e. the (0 - 0) band. In cases where this band is not clearly resolved, the ionization threshold is sometimes referred to as the adiabatic ionization potential.

The vertical ionization potential is given by the difference between the vibrational ground state of the molecule and that vibrational state of the ion obtained by a "vertical" transition at the molecular internuclear distance. Experimentally this usually corresponds to the point of maximum intensity in the photoelectron band.

The spacing of the lines in a band depends on the vibrational frequencies in the ion and the vibrational energies are given by the wellknown expression

$$E_{vib} = (v+\tfrac{1}{2})h\nu$$

v = vibrational quantum number.

and for an harmonic oscillator.

$$\nu = \frac{1}{2\pi}\sqrt{\frac{K}{\mu}}$$

K = force constant.

μ = reduced mass.

If the frequency in the ion is reduced in energy from its corresponding value in the ground state, this implies a reduction in the force constant. Now, although there is no rigorous relationship between K, (which defines the curvature at the base of the potential well), and bond strengths , a reduction in force constant is generally taken to imply a weaker bond. This weakening of the bond would suggest that an electron has been removed from a "bonding" level. Thus, a reduction in frequency between molecule and ion, is often taken as suggesting that ionization has occurred from a bonding orbital. Likewise if there is little change in frequency, this implies "non-bonding" character, and an increase in frequency usually taken to

indicate the "antibonding" character of the orbital from which ionization has taken place. In this way, a simple criterion, based on the change in vibrational frequency on ionization, can be used to establish the bonding characteristics of the various molecular orbitals.

Since this criterion is applied at equilibrium values near R_e, where the molecule and ion are stable and the SCF - MO approximation holds good, it is much more satisfactory than any thermochemical criterion based on the bond dissociation energy D. (i.e. the depth of the potential well). At the much larger internuclear distances near the dissociation limit, the SCF - MO's cease to be good approximations unless extensive configuration mixing is taken into account. In addition, as a consequence of the non crossing rule, the potential curve may short cut to another potential energy surface of the same symmetry but lower energy, and so play havoc with any thermochemical bonding criterion.[39]

Since, in principle, the valence shell orbitals can be delocalized over the entire molecule the interpretation of the p.e. spectrum obtained is not always a trivial matter. The problem has been likened to that in infra red spectroscopy where coupling of all the molecular normal modes may occur.[40] However the delocalization may be symmetry restricted and certain other types of orbital e.g. lone pairs, or aromatic Π levels, are usually easily recognised. Further aids to assignment include an examination of the fine structure of each band, its width and relative intensity. Comparison with the predictions of simple molecular orbital and symmetry considerations as well as recourse to calculations of varying degrees of sophistication are all frequently employed.[41]

In addition, comparison with the spectra of a related series of

molecules and "chemical intuition" can sometimes be the most effective way of analysing the spectra of the larger molecules.[42] By a combin-:ation of all these methods it has been possible to account for the major features in the spectra of most of the species studied to date.

e) Application and future activities.

An indication of the range of such studies and the problems investigated using p.e. spectroscopy may be obtained from a glance at the compilations of published spectra in refs. 10 and 21. From these it can be seen that the spectra of most stable volatile systems have now been recorded. The chemical applications of photo-electron spectroscopy have ranged from the contribution of d orbitals to the bonding in transition metal [43] and main group compounds, especially those of silicon and germanium,[44] to the substituent and steric effects in aromatic molecules.[45]

If as a result of the intense efforts of the last few years the subject has now reached maturity, it will perhaps not be too long before it enters a difficult period. The interest of many chemists, both organic and inorganic, is likely to diminish as the stock of readily accessible systems rapidly declines in number. Also, possible avenues of further research in areas such as the study of transient[46] or free radical species[47], angular distribution[48] or solid state studies[49] usually require substantial modification to the commercial spectrometers, the ready availability of which caused the subject to develop so quickly.

That there still remains a great deal of fascinating work to be done e.g. using high temperature molecular beam techniques[27,50], is not in doubt, but equally certain is the fact that the branching ratio of the subject between chemistry and physics is rapidly changing towards the advantage of the latter.[27]

OPTICAL SPECTROSCOPY.

a) Introduction.

Although the phenomena of photoionization has been known since at least the beginning of this century,[51] it was not until the fairly recent development of moderately high resolution electron energy analysers, that photo-electron spectroscopy became possible. On the other hand, the study of absorption of photons by atoms and molecules as a function of the photon energy, has continued to occupy the attention of spectroscopists since about the middle of last century. The contribution which these studies gave to the development of the atomic and quantum theories of matter would be difficult to underestimate.[52]

However, most of the work on the electronic spectra of atoms and simple systems (e.g. diatomics) had been performed by 1940, and as a result of the technical developments which took place during the second World War and immediately thereafter, the interest of many spectroscopists was directed to the lower energy regions of the electromagnetic spectrum e.g. the infra red, microwave and radio-frequency regions. Another major factor contributing to the comparative neglect of the electronic spectroscopy of molecules was that it had been found that the spectra of the larger molecules and indeed, some of the smaller ones e.g. methane, were mainly diffuse and therefore not readily amenable to analysis.[53]

Recently, however, with accurately determined ionization potentials for larger molecules readily obtainable from their photoelectron spectra, a renewed interest has been shown in the interpretation of their spectra in the vacuum ultra-violet.

As a result of this situation some of the best of the literature reviews[2,55,56,57,58] are none too recent, although the books by Robin[54] help to redress this situation. In addition, Samson has written an excellent recent account of the special instrumentation required in vacuum ultraviolet studies. The books by Herzberg[59,60] are classics and are essential reading for those seriously interested in the electronic structure of molecules.

b) Historical background.

The beginnings of optical spectroscopy were laid by Newton who observed that the spectrum produced by the passage of the sun's rays through a prism could be recombined into white light by another prism.[61] However, spectroscopy as we know it, did not begin until the early 19th century when Fraunhofer observed the dark lines in the sun's spectrum which bear his name.[62]

In about 1860 Bunsen and Kirchhoff were able to relate these lines to emission lines in light sources in the laboratory.[63] Not unnaturally, the visible region (7000 - 4000 Å) was the first to be investigated, but the development of photography enabled studies to be extended into the ultra violet which had been discovered earlier in the century by Ritter.[64]

However, the systematic study of the vacuum U.V. did not begin until about the 1890's, with the pioneering researches of Victor Schuman.[64a] It was he who first realised that in addition to removing the air, the oxygen content of which starts to absorb below 1900 Å, it was also necessary to replace the conventional quartz optics with natural fluorite, CaF_2, and to record the spectra using special largely gelatine free photographic emulsions.[64b] As a result of these modifications, he was able to reach wavelengths subsequently realised to be about 1250Å. The outstanding quality of the spectra recorded with such apparatus can be seen in the comparison of Schuman's spectrum of H_2, with that obtained using a modern 6m spectrometer, reproduced in an article by Tousey.[65] However it was Theodore Lyman[65a] who, by constructing a vacuum grating spectrograph according to the principle of Rowland[65b], was first able

to measure wavelengths and so place a wavelength scale on Schuman's spectra. Also, thanks to the absence of transmitting optics and using He sources, he was able to extend the limits of vacuum u.v. to approximately 500 $\mathring{A}$ and eventually succeeded in reaching 250 $\mathring{A}$. Since then the short wavelength limit has continued to be extended until it now overlaps with the soft Xray region at approximately 5$\mathring{A}$.

c) Techniques and instrumentation.

However, it would be completely wrong to suggest that most vacuum u.v. spectroscopists regularly pursue their studies up to anything near this limit. The reasons for this are to be found both in the instrumentation required to reach this limit and the fact that for most molecules, the spectra above the first ionization potential tend to be diffuse as a consequence of the autoionization or rapid dissoci-:ation of the superexcited states produced. In fact it is this pro-:blem, associated with all other resonance absorption techniques, which makes the estimation of the higher energy ionization potentials by photoelectron spectroscopy so valuable.

In addition the difference in spectroscopic techniques between 1800 and 2800 Å (say) is comparatively small since the changes in prisms, lenses, mirrors, windows and sources, although significant, do not necessitate fundamental changes in spectrometer optics. The only major difference is that below 2000 Å, oxygen must be removed from the light path. However the differences between 800 Å and 1800 Å are quite large, since there are no useful materials for prisms, lenses or windows and the reflectivity of mirrors is poor.[66] Below 500 Å, where He is no longer transparent, these difficulties become particularly acute and, once more, the instrumentation has to be modified substantially, mainly by the use of grazing incidence techniques.

For these reasons, although the entire region below 2000 Å is commonly called the "vacuum ultraviolet", it is convenient to sub-:divide this region into the various wavelength regions as shown below.[26]

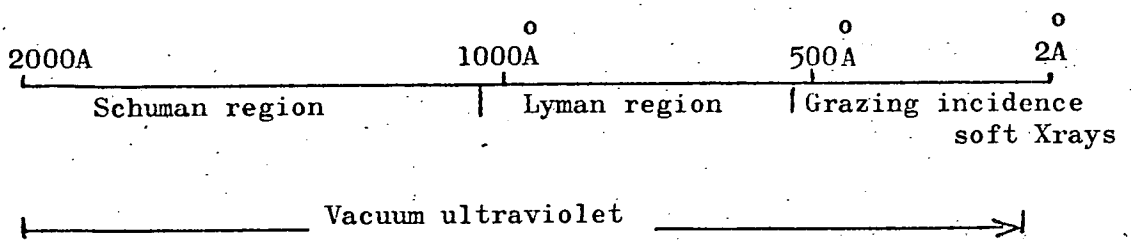

In the studies to be presented in Chapter 3 we will be concerned exclusively with spectra recorded in the Schuman region, the short wavelength cut off at 1050A, being the lower transmission limit of LiF.

An account of the spectrometers used in the present vacuum u.v. studies is given in the Appendix, but it will be useful at this stage to give a broad outline of the more important instrumental features, in this brief introduction to the subject.

The layout of a basic normal incidence spectrograph is shown in Fig. 3. At the heart of most spectrometers is the diffraction grating. This consists of a large number of parallel equidistant grooves ruled side by side on a suitable surface with a diamond point. The grating may be transparent (i.e. transmission grating) or more commonly, opaque to the incident radiation (i.e. a reflection grating). This latter type when ruled on a concave mirror eliminates the need for focussing and collimating lenses.[67]

The diffraction of such a grating is given by the expression

$$\pm n\lambda = \frac{A}{N}[\sin\alpha + \sin\beta]$$

where A = distance from first ruled line to last (often called linear aperture).

N = number of lines ruled on the grating.

n = order of spectrum i.e. 1,2,3 .....

α = angle of incident light of wavelength λ

β = angle of emergence of light.

both α and β are measured with respect to the normal.

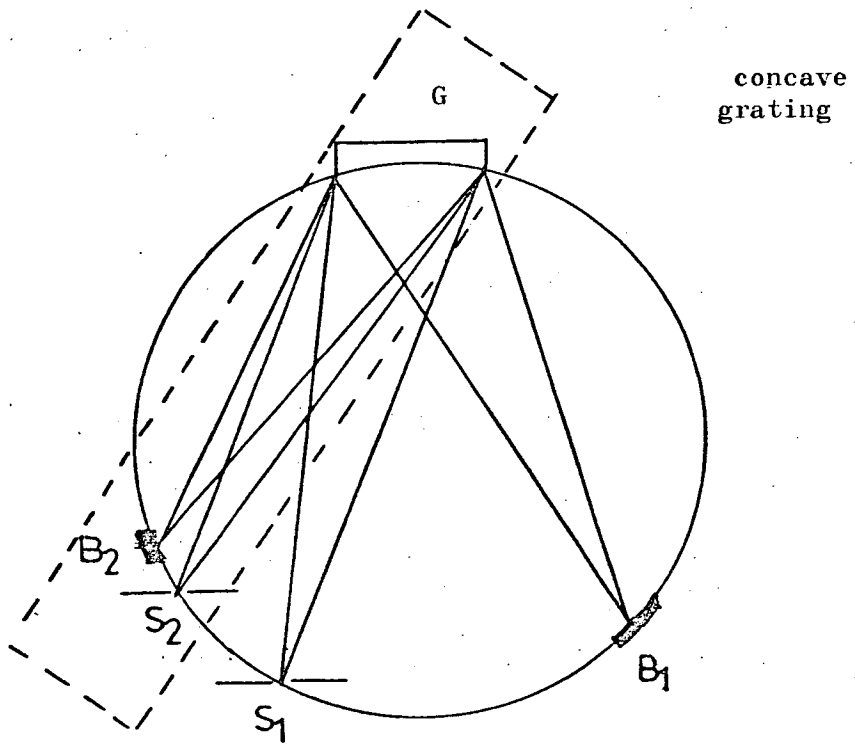

Figure 3.

Concave grating mounts. The slits S_1 and plate B_1 are in typical Paschen-Runge mount on the Rowland circle of the grating G. S_2 and B_2 are in Eagle mounting, which can be contained in an evacuted tube indicated by the dotted lines.

If the angle α is constant, then the angular dispersion of the incident radiation, is given by the expression:-

$$\frac{d\beta}{d\lambda} = \frac{n.N}{A\cos\beta}$$

Thus the dispersion varies directly with the order and number of lines per unit width. A more commonly used quantity is the linear dispersion (often called the plate factor) which is given by the expression

$$\frac{A\cos\beta}{n.r.N}$$

where r = radius of concave grating.

and is commonly expressed in $\mathring{A}$/mm.[26] The lower the plate factor, the better the resolution.

If the spectrum is recorded normal to the grating i.e. $\cos\beta = 1$ the wavelength is a linear function of the angle of emergence and the dispersion is constant. For practical reasons, it is usually necessary to record the spectrum slightly off normal incidence and as a result, the dispersion is not strictly linear and higher order correction terms are necessary to obtain accurate wavelength measurements.[26]

The resolving power of a plane grating, $R = \frac{\lambda}{d\lambda}$, and using the conventional Rayleigh criterion

$$\frac{\lambda}{d\lambda} = n.N$$

It is thus independent of the wavelength or spacing of the lines in the grating, but increases with increasing order number. Using a modified Rayleigh criterion it is also possible to use the same expression to describe the resolution of a concave grating provided the width W of the grating illuminated is less than (or equal to) $\frac{Wopt.}{1.18}$[68], where Wopt. is the optimum width of the grating and varies

with α and λ. Typical values for Wopt. are listed in the book by Samson.[26]

The fact that the incident radiation is diffracted into a variety of orders produces a substantial reduction in intensity in the particular order in which the spectrum is recorded. To overcome this, the grating is usually ruled so that the contours of the grooves concentrate the diffracted light into a definite direction. This technique is called "blazing," and the angle Θ which the groove makes with the vertical is known as the blaze angle as shown in the cross-section of a grating below.

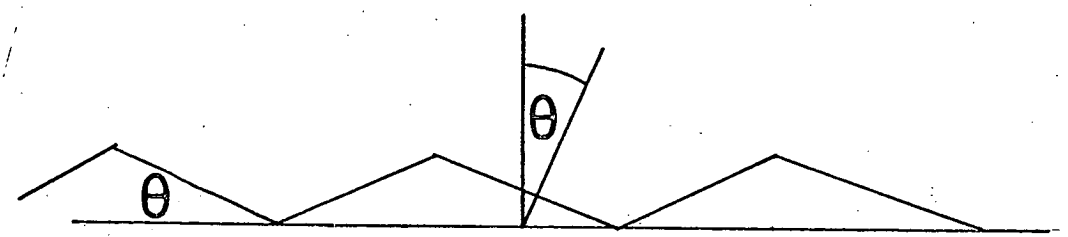

The grating may be mounted in a variety of ways. However Rowland showed that for a concave grating, the locus of the points at which the slit and its image in a horizontal plane are in focus, lie on a circle corresponding to the radius of the grating. This circle, called the Rowland circle, forms the basis of the Eagle and Paschen-Runge mounts as shown in Fig. 3. The details of these and other mountings, some of which are not based on the Rowland circle, are discussed fully in Chapter 3 of Samson's book.

The light sources used in vacuum U.V. studies can generally be divided into two types i.e.

a) Continuum sources, and

b) Line sources.

The continuum sources are used to provide information on the

absorption at all wavelengths but are usually not as intense as the line sources. The continua produced in high pressure discharges of H_2 and the inert gases are commonly used. These discharges can be sustained either by a condensed high voltage repetitive spark or by microwave excitation, although the intensity of the continua produced in the latter case is less intense.[69] However the ease of construction and long life time of the sources employed makes the electrode-less microwave technique particularly appealing and by employing longer exposure times, the reduced intensity factor is not prohibitive.

The useful ranges of the various continua are listed below:-

Gas	Useful range (Å)
H_2	1700 - 5000
Xe	1480 - 2000
Kr	1250 - 1800
Ar	1050 - 1550
Ne	740 - 1000
He	580 - 1100

and by using a suitable combination of lamps it is possible to cover the whole of the ultraviolet region up to 600 Å.

Another commonly employed source is obtained from the Lyman flash tube in which the energy of a capacitor bank of several μF is discharged at 15 - 25kV through a low pressure gas contained in a glass capillary tube.[70] Irrespective of the nature of the gas, the Lyman continuum extends from the visible to about 900 Å, the actual limit depending only on the capillary diameter and current densities used. The fact that such discharges are 'disruptive,' with the main discharge taking place in eroded wall material also leads to several problems, including a short useful lifetime and an

embarrassment of absorption lines. Despite this, these tubes still retain considerable appeal and the co-axial flash tube configuration is commonly employed in situations requiring high intensity sources over a relatively short period e.g. in flash photolysis experiments. Again more details are to be found in Samson's book.

The most popular method of recording vac.u.v. spectra is still the photographic plate. An alternative to the Schuman plate, with its almost gelatine free base, is to coat the emulsion with a fluorescent substance e.g. sodium salicylate, which converts the radiation to light of longer wavelength. In this way the extreme sensitivity of the Schuman plate to abrasion can be avoided although with a very slight loss in resolution.[71] For accurate measurement, glass plates are used in preference to cellulose strips. There have been many attempts to obtain spectra in a more direct fashion using techniques such as photoelectric emission, photionization of gases and solid state photodiodes.[26] For absolute intensity measurements such methods are essential.

d) Interpretation of results.

Having thus obtained and measured the spectrum, the next problem is the challenge of analysing the bands observed in terms of the electronic structure of the molecule. The details of how this has been performed for the CSe_2, OCSe and SCSe systems are given in Chapter 3. However it will be useful at this stage to set up the necessary framework, emphasising only the broader aspects of the interpretation of molecular electronic spectra.

In many cases, it has been possible to unravel the complexity of molecular electronic spectra by using concepts derived from atomic spectroscopy.[72] However in the molecular situation there exists the possibility of transitions which are without parallel in the atomic case. Thus it is convenient to classify the observed bands into two distinct classes.

i) intra valency transitions
and ii) extra valency transitions.

The difference between these is based on the assumption that the intra valency transitions take place within the nuclear framework, whereas the extra valency transitions take place between orbitals whose dimensions are so much greater than those of the nuclear framework that it may be approximated to a point. In this way we may expect to find strong parallels between the extra valency transitions and those observed in atomic spectra. The intra valency transitions on the other hand will follow a wholly different pattern and have no analogue in atomic spectra.

In some ways it is fortunate that the different types of transition are to be found in the different energy regions of the spectrum.

Thus it is common to find that the visible and near u.v. spectra (i.e. up to approximately 2000Å) consist mainly of intra valence transitions, whereas the vacuum (far) u.v. spectrum largely consists of extra valency transitions. Inevitably this "rule of thumb" does not hold for all systems and the distinction between these different class of transition is often, in itself, not particulary clear especially in the 45,000 - 60,000 cm^{-1} region.[54]

As the vac. u.v. spectra presented in Chapter 3 are dominated by the extra valency transitions it is appropriate to begin with them. A useful way of thinking about the states formed by such excitation is to consider them as a molecular ion, called the core, to which is added an electron, in one of the spacially large orbitals formed from those atomic orbitals of larger n, than were required to form the filled valence shell molecular orbitals.[66]

In this way the similarities between the results of vacuum u.v. and p.e. spectra are easily recognised. If the electron is sufficiently far away from the nucleus, the core will approximate to a unit positive change and so the energies of the various transitions should resemble those of atomic hydrogen, the frequencies ν of which, are given by the expression

$$h\nu = I - \frac{R}{n^2}$$

where I = series limit
R = Rydberg const. (109737 cm^{-1})
$n = 1, 2, 3 \ldots$

The earliest attempt to use such an equation to analyse multi-electron systems, was in the case of the alkali metal spectra.[73] Here it was expected that a similar system to hydrogen, with the optically excited electron in an orbit at a large distance from the

core, would exist. However, attempts to fit the wave numbers of the observed lines to the hydrogen atom formula were only successful when non integral values of n were used.

Thus the equation had to be modified to

$$h\nu = I - \frac{R}{n_e^2}$$

where the various symbols have their previous measuring and

$$n_e = (n - \delta).$$

n is again an integer and δ called the quantum defect, allows for the interaction of the Rydberg electron and the core. In this way it was possible to analyse the spectra into four series each characterised by a different value of δ depending on the angular momentum l of the electron and thus identified with transitions to the different s,p,d and f Rydberg series.

Comparison of the atomic electronic density $(4\pi r^2 \psi^2)$ for Na^+ and its 3s, 3p, 3d atomic orbitals shows that the extent of penetration into the core decreases in the order 3s, 3p, 3d, and this is exactly the same order as the decrease in quantum defect values. Thus the effect of penetration is to increase the term value from its corresponding value in the hydrogen atom system to produce positive values of δ. Thus in Na, the quantum defect associated with the highly penetrating ns orbitals, $\delta_{ns} = 1.4$; the less penetrating np orbitals have $\delta_{np} = 0.9$ and the almost non penetrating nd levels have $\delta_{nd} = 0$.

As n increases so the fractional part of the orbital involved in penetration will decrease and this is recognised in the Rydberg formula because as $n \longrightarrow \infty$ so $(n-\delta)^2 \longrightarrow n^2$.

In addition as it is the quantity $(n - \delta)$ and not n or δ

separately which is determined experimentally, the modified Rydberg equation gives a reasonable fit.

However, this does not complete the story of the quantum defect and we need to extend the theory to account for the fact that in Rb, for example, the 4d orbital has a value $\delta_{4d} = 1{\cdot}2$, whereas for Na, $\delta_{4d} = 0$.

An explanation for this has been given by Mulliken in his concept of "real precursors."[4] These correspond to occupied orbitals of the same symmetry but lower n value than the particular orbital under discussion and only those Rydberg orbitals without real precursors in the core have $\delta = 0$. Thus in Na, the 3d orbital has no real precursor, but acts as such for the 4d series in K, Rb, Cs, to make them more penetrating.

In this way the observed trends in δ may be explained. Rydberg orbitals can also have "virtual precursors" e.g. in the case of the 6s orbital of Na, the 1s and 2s are the real precursors and the 3s, 4s and 5s are the virtual precursors. In the 'Aufbau' of Rydberg orbitals each is built upon the framework of the preceding one and so the degree of penetration of the first member of the series will be reflected in all the higher energy Rydberg orbitals and so lead to $\delta > 0$. This "look alike" aspect of a Rydberg orbital and its nearest real (or virtual) precursor is called "recapitulation."

To varying degrees these concepts derived from atomic spectra will carry over into the interpretation of molecular spectra. However it is worth emphasising that we now have a useful criterion for establishing whether a particular molecular transition is of

Rydberg character or not. Thus Rydberg transitions are not only characterised by their absorption frequency ν, but also by their term value $T = I - h\nu = \frac{R}{(n - \delta)^2}$, so that increasing n by unity leads to the next member of the series. In the case of inter-valence shell transitions increasing n by one does not give the next level because such transitions do not occur in series.

In addition, it is usual to find that the Rydberg transitions in molecules resemble those of atoms in their sharpness. Inter-valence bands, on the other hand, are often broad, and when resolved, show extensive vibronic structure. This may be readily explained on the basis of the changes in potential surfaces on excitation used previously to account for the shapes of the band envelopes obtained in photoelectron spectra.[38] Thus as Rydberg orbitals are essentially non-bonding, transitions to them from bonding molecular orbitals are narrower than transitions to anti-bonding levels. The sharpest transitions of all will be from occupied non-bonding levels e.g. lone pair levels to the non-bonding Rydberg levels.

As the inter valence transitions mainly occur between bonding (or non-bonding) levels and unoccupied anti-bonding levels we would expect them to show considerable structure. However, the fact should be recognised that not all Rydberg transitions will be sharp and in cases where the uppermost occupied levels are strongly bond-:ing this is unlikely to be the case. The short lifetimes of the states produced on excitation from strongly bonding levels may also contribute to the diffuseness of the band shapes[76].

In a linear molecule the axial (rather than central) field of the core splits the terms of given n and l into $(l + 1)$ components,

according to the value of λ, which is the component of l along the molecular axis. Thus each of the Rydberg orbitals may be characterised by the quantum numbers (n, l, λ) and the modified many electron Rydberg equation, when applied to linear molecules should be written as[66]

$$T = IP - \frac{R}{n - \delta_{l\lambda}}$$

T = Term value.

The derivation of molecular Rydberg levels from their atomic counterparts is shown in Fig. 4, where it has been assumed that the spacing between the different λ components (core splitting) decreases with increasing n. Thus at high n values we are not able to distinguish between the p_σ and p_π levels and only one state called the 'p complex' is observed. A similar situation will apply to the d and f levels.

The spacing between the different n and l terms also decreases with increasing value of n and when the Δl splitting approaches that of Δn splitting, there is strong mixing of the different (n, l, λ) levels and n and l are no longer useful quantum numbers.

It is common to assume that $\delta_{l\lambda}$ remains constant, but in fact it changes slowly along the series. A more accurate expression is the Rydberg-Ritz formula in which

$$\delta_{l\lambda} = \alpha_{l\lambda} - \beta(n^*)^{-2}$$

n^* = effective principal quantum number

δ is plotted against $(n^*)^{-2}$ to determine α and β[77]

In most molecules, the ground state is usually closed shell and the Rydberg core open shell. Thus although penetration is still the prime cause of deviation from the hydrogenic term values and the values of δ ns, δ np, δ nd follow similar patterns as before, there is also the possibility that quantum mechanical exchange will

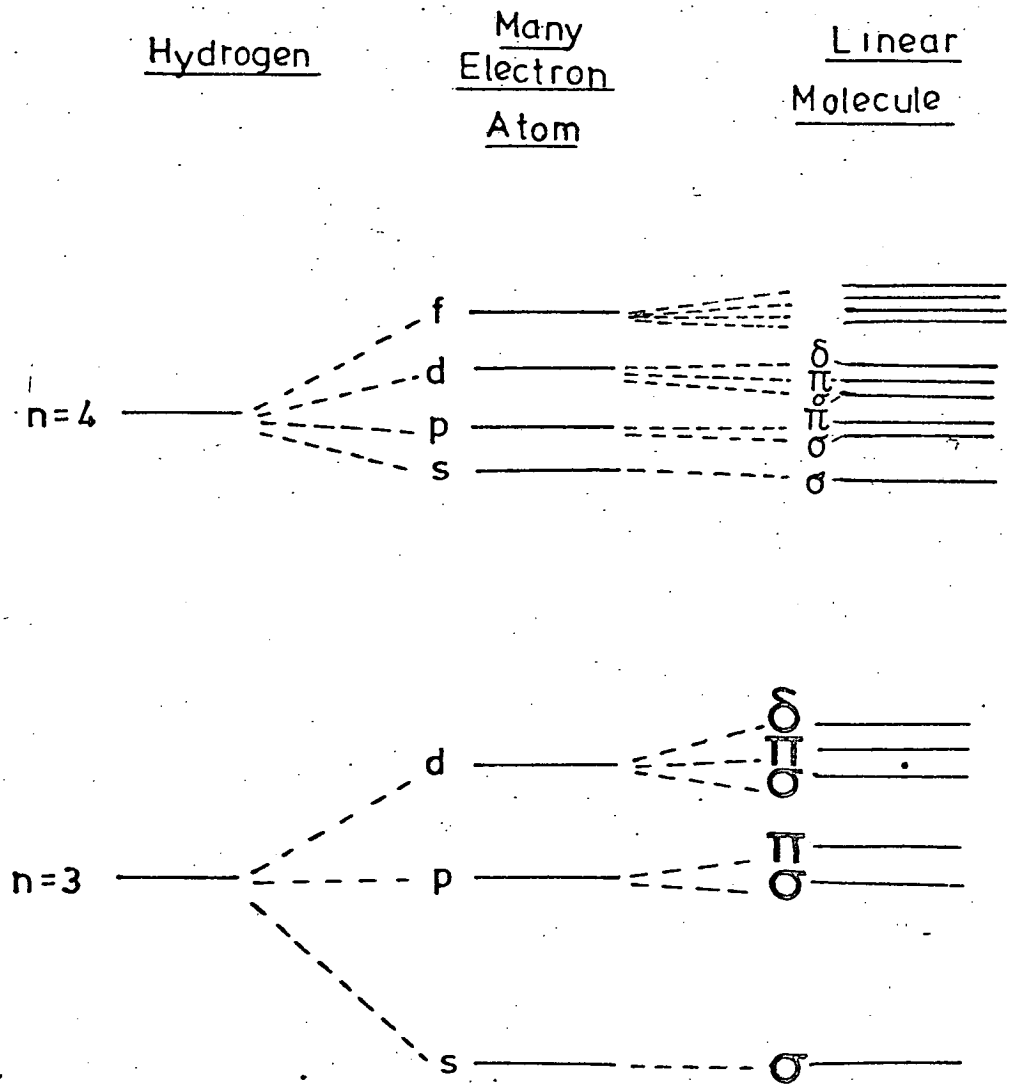

Figure 4.

Correlation between atomic and linear molecule Rydberg levels.

be involved. However, the exchange energy depends on the extent of the Rydberg to core overlap and so will be significant at low n and when there are no real precursors in the core.

The precursor concept is also of less use in the molecular case especially when the symmetry is low. As a result of there being many more Rydberg orbitals having the same symmetry as one of the core orbitals, a non-penetrating orbital on one centre may penetrate another, via two centre overlap, such that most Rydberg orbitals of low n have some penetration into the core. This will cause the lower members of the series to deviate from the term values predicted using the average quantum defect of the series.[54]

The requirement that the Rydberg orbitals are orthogonal to the core and to each other still remains valid in the molecular situation, and in fact can be responsible for spreading the Rydberg orbital to centres where the original core precursor has no density. In this way the recapitulation properties of the Rydberg wave function will be modified.

In the molecular case the choice of n is sometimes ambiguous. Some prefer to use the united atom states,[78] whereas others use the major atomic orbital component in a LCAO description at the internuclear distance.[79]

In the case of diatomics (and linear triatomics) it would appear that this latter classification is to be preferred.

An interesting feature associated with Rydberg transitions in a series of molecules containing elements from the same column in the periodic table e.g. the H_2X series where X = O, S, Se, Te, is that the term values remain fairly constant on going down the series.[80] In fact there is a slight drop. The term value is dependent on the expression $1/(n-\delta)^{-2}$ and as n increases by unity

at each step downwards but δ increases by almost the same amount, the quantity $(n - \delta)$ remains nearly constant.

This near constancy in term values can readily be appreciated from the fact that the corresponding orbitals in successive atoms are usually at least the same size and in many cases almost identi-:cal except for the innermost node. The close similarity of the S 3s and Se 4s orbitals shown in the paper by Adams[81] is a con-:vincing example of this effect.

Thus far we have presented a very encouraging picture of how the Rydberg states in molecules can readily be derived from their atomic counterparts and the spectra obtained so analysed. In reality, the situation inevitably tends to be much more complex and there are many reasons for the difficulties encountered in the analysis of molecular electronic spectra.

One of the most common is a result of the influence of inter-valence transitions which occur at similar energies to the Rydberg states and interact strongly with them e.g. NO. Furthermore a Rydberg orbital may possess a valence shell virtual orbital precur-:sor of the same symmetry and such pairs of orbitals are called "Rydberg - valence shell conjugates."

The distinction between such levels is frequently unclear and the Rydberg state may merge into the valence shell state at the higher frequency part of the band, close to the dissociation limit.[54] Such conjugate bands usually possess anomalously high intensities but usually only the lowest member of the Rydberg series will possess a conjugate valence shell partner.

As a result of this and other reasons, the first member of a

series may deviate significantly from the expected Rydberg formula position and the nature of the uppermost state is then in doubt.

In such cases the effect of the presence of a second "transparent" gas e.g. He at high pressure, on the vacuum u.v. spectrum of the species under investigation, can be most useful.[82] The Rydberg states, which involve the excitation of an electron into a large diameter orbit, are considerably more susceptible to perturbation by the high pressure gas than are the inter-valence excitations in which the transition is largely confined to the internuclear framework. Thus the Rydberg states often show assymetric pressure broadening as well as shifts to higher frequencies. The inter-valence transitions remain unaffected by pressures of perturber gases up to at least 150 atm.

The effect of recording vacuum u.v. spectra in condensed phases e.g. in matrices or in solution, is in many ways similar, but usually more extreme in its effect. Thus in organic glasses, the Rydberg transitions are usually "washed out" and the inter-valence bands shifted to lower frequencies.[83]

CORRELATION BETWEEN VACUUM ULTRAVIOLET SPECTRA AND PHOTO-ELECTRON SPECTRA.

Despite the quite distinct differences in techniques involved and the interpretation of the spectra so produced, there is really a very strong link between the results of photoelectron and vacuum ultraviolet spectroscopy. The information obtained using both can, in favourable cases, enable a very detailed picture of the various excited and ionic states of the system to be obtained. This in-:formation is largely complementary and where there is overlap, e.g. in the ionisation potentials obtained; the corroboration of the series limits estimated from the vacuum u.v. spectra by those obtained directly from p.e. spectra, is welcome proof of the essential correctness of the vacuum u.v. analyses.

In addition, knowledge of the first IP from p.e. data can be of particular value in the calculation of term values and hence the quantum defects, of the bands observed in the optical spectrum. The systematic nature of the series thus obtained can be used to produce tentative assignments and by the use of iterative procedures, successive refinements of the series and its limits can thus be ob-:tained. Even in those cases where extended Rydberg series are confidently assigned so that a value for the IP of considerably greater accuracy than is ever possible by p.e. spectroscopy, is ob-:tained; p.e. spectroscopy is still of great value in providing reliable values for the higher energy IPs.

Since all the members of a Rydberg series result from transi-:tions between one particular molecular orbital and successively high-:er energy orbitals approaching the IP, it is not only possible to use p.e. spectroscopy to examine the nature of the Rydberg core at

the series limit, but also, by assuming Koopmans' Theorem, to identify the originating molecular orbital.

This relationship between photoelectron spectroscopy and optical spectroscopy can also be inverted and it has been possible to deduce the ordering of the orbital levels in the photoelectron spectrum from the optical spectrum and a knowledge of the orbital symmetries as implied by the term values.[84]

As noted previously, high resolution photoelectron spectra can often reveal fine structure and in many cases the changes in geometry responsible for the vibronic pattern in the optical spectrum is closely matched by that observed in the photoelectron spectrum. Thus prior knowledge of the vibrational intervals and Franck Condon factors for the first band in the photoelectron spectrum can be invaluable in helping to identify the Rydberg origins in optical spectra showing extensive vibrational progressions. Likewise, it is also possible to use the much higher resolution of the electronic spectrum to help unravel the vibronic structure in a poorly resolved photoelectron band envelope.[85]

In addition to vibrational structure, the high resolution photoelectron spectrum can also give reliable estimates of the spin orbit splitting produced on ionisation from orbitally degenerate states. This is often similar enough in energy to that between corresponding Rydberg series to be of considerable assistance in the interpretation of the optical spectrum.

Thus in a system such as carbonyl selenide in which the bands of overlapping Rydberg series exhibit an extremely complex structure involving spin orbit splitting and progressions and sequences in both stretching modes, it would have been a considerably more

difficult task to assign the spectrum, had the photoelectron spectrum not been available.

It is the ready availability of such information as the photoelectron spectrum provides which will stimulate renewed interest in the high resolution spectra of complex molecules and contribute much to the expansion of this field in the near future.

REFERENCES.

1. D.W. Turner, A.D. Baker and C.R. Brundle; "Molecular Photoelectron Spectroscopy," Wiley Interscience, New York (1970).

2. P.G. Wilkinson; J. Molec. Spectros.; (1961), 6, 1.

3. R.S. Mulliken; J. Chem. Phys. (1935), 3, 720.

4. R.S. Mulliken; J. Amer. Soc. Chem. (1964), 86, 3183.

5. S. Cradock and W. Duncan; J. Chem. Soc. Faraday II, (1975), 71,1262.

6. J.H.D. Eland; "Photoelectron Spectroscopy", Butterworths (1974).

7. F.G. Herring; as reference 20, page 237.

8. W.C. Price; Adv. At. Mol. Phys. (1974), 10, 131.

9. T. Koopmanns; Physica, (1934), 1, 104.

10. R.L. DeKock and D.R. Lloyd; Adv. Inorg. Chem. Radiochem, (1974), 16, 68.

11. F.I. Vilesov, B.C. Kubator and A.N. Terenin; Dokl. Akad. Nauk S.S.S.R. (1961), 138, 1320.

12. D.W. Turner and M.I. Al-Joboury; J. Chem. Phys. (1962), 37, 3007.

13. Perkin-Elmer Ltd., Beaconsfield.

14. A.D. Baker; Accts. Chem. Res. (1970), 7, 549.

15. D.W. Turner; Chem. Brit. (1968), 4, 435.

16. S.D. Worley; Chem. Rev. (1971), 71, 195.

17. A.D. Baker and D. Betteridge; "Photoelectron Spectroscopy-Chemical and Analytical Aspects", Pergammon Press, Oxford (1971).

18. D.A. Shirley, (ed), "Electron Spectroscopy ". (Proceedings of the International Conference on Electron Spectroscopy held at Asilomar, Pacific Grove, California 1971), North Holland, Amsterdam (1972).

19. Faraday Discussions of the Chemical Society No. 54. "Discussion on the Photoelectron Spectra of molecules," Sussex 1972. Chemical Society Faraday Division.

20. C. Sandorfy, P.J. Ausloos, and M.B. Robin, eds. "Chemical Spectroscopy and Photochemistry in the Vacuum ultraviolet," D. Reidel Publishings Co., Holland 1974.

21. Electronic Structure and Magnetic Properties of Inorganic Compounds ed. P. Day. Volume I and Volume II A. Hamnett and A.F. Orchard, Volume III S. Evans and A.F. Orchard. Chemical Society.

22. K. Seighbahn, C. Nordling, G. Johansson, J. Hedman, K. Hamrin, U. Gelius, T. Bergmark, L.D. Werme, R. Manne and Y. Baer, P.F. Heden "E.S.C.A. applied to Free Molecules", North Holland, Publishers, Amersterdam, (1969).

23. U. Gelius and K. Seigbahn; in Reference 19, page 257.

24. M.O. Krause; Chem. Phys. Letts. (1971), 10, 65.

25. K. Seigbahn et. al.; J. Electron Spectros. (1972/73), 1, 131.

26. J.A.R. Samson, "Techniques of Vacuum ultraviolet Spectroscopy," Wiley, New York, 1967.

27. J. Berkowitz; in Reference 20, page 93.

28. P. Natalis, J. Delwiche and J.E. Collin; in reference 19, page 98.

29. A.W. Potts, H.J. Lempka, D.G. Streets and W.C. Price, Phil. Trans. Roy. Soc. London Ser. A. (1970), 268, 59.

30. A.W. Potts, T.A. Williams and W.C. Price; in Reference 19, page 104.

31. W.C. Price, in reference 8, page 157.

32. R.L. DeKock and D.R. Lloyd, in reference 10, page 70.

33. A.W. Potts and T.A. Williams, J. Electron Spectros.(1974), 3, 3.

34. W.G. Richards; Int. J. Mass Spectr. Ion Phys. (1969), 2, 419.

35. R.F. Fenske; Prog. Inorg. Chem. (1976), 21, 179.

36. C.C.J. Roothan; Rev. Mod. Phys. (1951), 23, 69.

37. L. Asbrink; Chem. Phys. Letts. (1970), 7, 549.

38. H.H. Jaffe and M. Orchin; "Theory and Applications of Ultra violet Spectroscopy." John Wiley and Sons, New York and London, (1962), page 134.

39. R.S. Mulliken in "Quantum Theory of Atoms, Molecules and the Solid State," ed. Lowdin, Academic Press, (1966), page 231.

40. R.L. DeKock and D.R. Lloyd; as reference 10, page 77.

41. G. Lauer, K.W. Schulte and A. Schweig; Chem. Phys. Letts. (1975), 32, 163.

42. S. Cradock and R.A. Whiteford; J. Chem. Soc. Faraday Trans.II, (1972), 68, 281.

43. S. Evans, A. Hamnett, A.F. Orchard and D.R. Lloyd; reference 19, page 227.

44. S. Cradock and E.A.V. Ebsworth; Chem. Comm. (1971), 57.

45. A.D. Baker, D.P. May and D.W. Turner; J. Chem. Soc., (1968), 22.

46. N. Jonathon, A. Morris, M.Okuda, K.J. Ross and D.J. Smith; in reference 19, page 48.

47. A.B. Cornford, D.C. Frost, F.G. Herring and C.A. McDowell, in reference 19, page 64.

48. J.A. Kinsinger and J.W. Taylor; Int. J. Mass Spectr. Ion Phys. (1972), 10, 445.

49. W.T. Bordass and J.W. Linnett, Nature (1967), 222.

50. J. Berkowitz; J. Chem. Phys., (1972), 56, 2766.

51. A. Einstein, Ann. Phys. (1905), 17, 132, ibid (1906), 20, 199.

52. C.A. Douglas-Clark; "The Fine Structure of Matter" Volume III, Chapman and Hall, London, (1938).

53. W.C. Price; in reference 20, page 1.

54. M.B. Robin; "Higher Excited States of Polyatomic Molecules", Volumes I and II, Academic Press, (1974/75).

55. W.C. Price; Adv. Spectros. (1959), 1,56.

56. J.C. Boyce; Rev. Mod. Phys. (1941), 13, 1.

57. A.D. Walsh; Chem. Soc. Revs. (1948), 2, 73.

58. W.R.S. Garton; Adv. At. Mol. Phys. (1966), 2, 93.

59. G. Herzberg; "The Electronic Spectra and Electronic Structure" of Polyatomic Molecules." Van Nostrand Reinhold, New York (1966).

60. G. Herzberg; "The Spectra and Structure of Free Radicals - An Introduction to Molecular Spectroscopy." Cornell University Press, Ithaca and London. (1971).

61. I. Newton; "Opticks" (London 1730), 4th Edition, Dover, New York 1952).

62. J. Fraunhofer; Gilberts Ann., (1817), 56, 264.

63. J. Bunsen and G. Kirchoff; Ab. handl. kgl. Akad. Wiss. Berlin (1861), page 63.

64. J.W. Ritter; Gilberts Ann. (1801), 7, 527, ibid., (1803), 12, 409.

64a. V. Schuman; Akad. Weiss. Wien. (1893), 102, 2A, 625.

64b. V. Schuman; Wien. Akad. Anzeiger (1892), 23, 230.

65. R. Tousey; Applied Optics, (1962), 6, 679.

65a. T.Lyman; Astrophys. J. (1906), 5, 349.

65b. H.A. Rowland; Phil. Mag. (1883), 16, 197.

66. A.E. Douglas in reference 20, page 113.

67. S. Walker and H. Straw; "Spectroscopy" Volume 2 Chapman Hall, London (1962), page 22.

68. T. Namioka; J. Opt. Soc. Amer. (1959), 49, 466.

69. R.E. Huffman, J.C. Larrabee and Y. Tanaka; Appl. Optics, (1965), 4, 1581.

70. W.R.S. Garton; J. Sci. Instr. (1953), 30, 119, ibid., (1959), 36, 11.

71. R. Allison and J. Burns; J. Opt. Soc. Amer. (1965), 55, 574.

72. H.G. Kuhn; "Atomic Spectra" Longmans, London, 1962.

73. J.R. Rydberg; Comptes Rendus .... (1890), 110, 394.

74. S. Walker and H. Straw; "Spectroscopy" Volume 1 Chapman Hall 1962.

75. J.C. Slater "Quantum Theory of Atomic Structure" Volume 1, McGraw Hill, New York (1960).

76. J.P. Byrne and I.G. Ross; Aust. J. Chem. (1971), 24, 1107.

77. R.B. Caton and A.E. Douglas; Can. J. Phys. (1970), 48, 432.

78. R.C. Nelson and W.J. Simpson; J. Chem. Phys. (1955), 23, 1146.

79. R.S. Mulliken; J. Amer. Chem. Soc. (1966), 88, 1849.

80. W.C. Price, J.P. Teegan and A.D. Walsh; Proc. Roy. Soc. London. Ser. A. (1950), 201, 600.

81. W.H. Adams; J. Amer. Chem. Soc. (1970), 92, 2198.

82. M.B. Robin and N.A. Kuebler; J. Molec. Spectros. (1970), 33, 247.

83. H.C. Longuet-Higgins and J.A. Pople; J. Chem. Phys. (1957), 27, 192.

84. P.J. Derrick, L. Asbrink, O. Edqvist, B.O. Jonsson and E. Lindholm; Int. J. Mass Spect. Ion Phys. (1971), 6, 203.

85. M.B. Robin as reference 54, Volume 1, page 74.

CHAPTER 1

THE PHOTOELECTRON SPECTRA OF CSe_2, SCSe and OCSe.

CHAPTER 1. Page No.

1. INTRODUCTION.

In this, and subsequent chapters we will examine the electronic structures of the triatomic molecules, CSe_2, SCSe, and OCSe,[1,2,3] as revealed by photoelectron and absorption spectroscopy in the vacuum ultra-violet.[4,5,6] Unlike the lighter members of the series to which they belong, i.e. CO_2, OCS and CS_2,[7] the extent of the spectroscopic information available for the Se containing species is extremely limited. The reasons for this are not too difficult to find. The compounds are not generally available commercially[8] and thus must be synthesised. This can only be achieved in disappointingly low yields and details of the synthetic routes employed are given in the Appendix. In common with most other volatile Se containing compounds, they possess extremely unpleasant smells even in low concentrations, - the stench of CSe_2 being particularly memorable! All the compounds are readily decomposed by heat and light; OCSe, the least stable, is also sensitive to water. All these factors, combined with the difficulty in obtaining pure samples, especially true in the case of CSe_2,[9] conspire to make these compounds unattractive to spectroscopists.

However, these debit factors must be weighed against several others. The trends observed in the spectra of the CO_2, COS, and CS_2 series can be much more clearly seen when the series is extended to include the Se containing analogues. In addition, the spectra contain several interesting features, largely connected with the presence of the Selenium. Also they are particularly suited for study in the vacuum ultra-violet because, unlike their oxygen and sulphur analogues, they all have I.P.s which lie below the LiF cutoff (110 n.m.), making it possible to observe the excited states of the molecule to the ionisation limit.

Thus, all the molecules in the CX_2, CXY (X,Y = O,S,Se) series

series are of considerable interest to spectroscopists. Much of this interest derives from the fact that the spectra of triatomic species provide a bridge between the spectra of atoms[10] (and diatomic species)[11] and those of more complex polyatomic molecules.[12] In addition, as the triatomic species to be discussed here are all linear both in their ground and many of their higher electronically excited and ionic states,[13] they may readily be compared with diatomic molecules, which are necessarily linear in all states.

2) RESULTS.

The He(I) photoelectron spectra of the molecules CSe_2, SCSe, and OCSe are shown in Figures 1, 2, and 3, with the results and assignments of the valence ionisation bands given in Table 1. A discussion of the weaker features observed in the spectra of these and other related molecules, will be deferred until the next chapter. Also included for the sake of completeness and to facilitate comparison, the spectra of CO_2, CS_2 and OCS adapted from Reference 7, are shown in Figure 4 and the results given in Table 2. All the spectra show four main bands in the region up to 21 e.V.

3) INTERPRETATION and DISCUSSION.

a) First band

The first band in both CSe_2 and SCSe consists of two intense well resolved (000) peaks. The splitting of the band is attributed to the fact that the orbitally degenerate states of linear ions, e.g. $^2\Pi$, $^2\Delta$, $^2\Phi$, divide into two components with different values of Ω, ($\Omega = \Lambda \pm S$). These components should be of equal intensity, with the component of higher Ω occurring at lower energy.[14] Thus, the first two peaks observed in the spectrum derive from the $X^2\Pi_{\frac{3}{2}g}$ and $X^2\Pi_{\frac{1}{2}g}$ states of the molecular ion. In CSe_2 like CS_2, the two peaks are of equal intensity, with no vibrationally excited states obvious, implying that the $1\pi_g$ level is essentially non-bonding. However, in SCSe the $X^2\Pi_{\frac{1}{2}}$ component appears to be slightly more intense than the $X^2\Pi_{\frac{3}{2}}$ component. The reason for this is that the (100) peak of the $X^2\Pi_{\frac{3}{2}}$ state underlies the (000) peak of the $X^2\Pi_{\frac{1}{2}}$ state, giving an enhanced overall intensity to the second band. The (100) peak of the $X^2\Pi_{\frac{1}{2}}$ state is clearly resolved and occurs at approximately

State of ion.	CSe_2	Electron Configuration.	Vibrational frequency. cm^{-1}
$X^2\prod g\frac{3}{2},\frac{1}{2}$	9·26 9·52	$2\sigma g^2\ 2\sigma u^2\ 1\pi u^4\ 1\pi g^3$	-
$A^2\prod u$	11·74	$2\sigma g^2\ 2\sigma u^2\ 1\pi u^3\ 1\pi g^4$	ν_1' 330
$B^2\Sigma^+ u$	13·61	$2\sigma g^2\ 2\sigma u^1\ 1\pi u^4\ 1\pi g^4$	ν_1' 300
$C^2\Sigma^+ g$	15·87	$2\sigma g^1\ 2\sigma u^2\ 1\pi u^4\ 1\pi g^4$	-

	OCSe	SCSe		OCSe	SCSe
				ν_1' ν_3'	ν_1' ν_3'
$X^2\prod\frac{3}{2},\frac{1}{2}$	10·37 10·57	9·58 9·76	$3\sigma^2\ 4\sigma^2\ 1\pi^4\ 2\pi^3$	2100 500	1280 -
$A^2\prod$	15·14	12·25	$3\sigma^2\ 4\sigma^2\ 1\pi^3\ 2\pi^4$	2000 600	- 425
$B^2\Sigma^+$	15·71	14·05	$3\sigma^2\ 4\sigma^1\ 1\pi^4\ 2\pi^4$	1850 -	- 480
$C^2\Sigma^+$	17·92	16·02	$3\sigma^1\ 4\sigma^2\ 1\pi^4\ 2\pi^4$	2080 640	- 480

TABLE 1.

	CS_2	CO_2		CS_2	CO_2
				ν_1' ν_3'	ν_1' ν_3'
$X^2\prod g\frac{3}{2},\frac{1}{2}$	10·06 10·12	13·87	$2\sigma g^2 2\sigma u^2 1\pi u^4 1\pi g^3$	- 1170	1220 1420
$A^2\prod u$	12·83	17·60	$2\sigma g^2 2\sigma u^2 1\pi u^3 1\pi g^4$	560 -	1110 -
$B^2\Sigma^+ u$	14.47	18·80	$2\sigma g^2 2\sigma u^1 1\pi u^4 1\pi g^4$	600 -	1270 1400
$C^2\Sigma^+ g$	16·19	19·40	$2\sigma g^1 2\sigma u^2 1\pi u^4 1\pi g^4$	600 800	1390 1470

	OCS		OCS	
			ν_1'	ν_3'
$X^2\prod\frac{3}{2},\frac{1}{2}$	11·19	$3\sigma^2 4\sigma^2 1\pi^4 2\pi^3$	650	2000
$A^2\prod$	15·52	$3\sigma^2 4\sigma^2 1\pi^3 2\pi^4$	790	2050
$B^2\Sigma^+$	16·04	$3\sigma^2 4\sigma^1 1\pi^4 2\pi^4$	-	
$C^2\Sigma^+$	17·96	$3\sigma^1 4\sigma^2 1\pi^4 2\pi^4$	970	2170

TABLE 2.

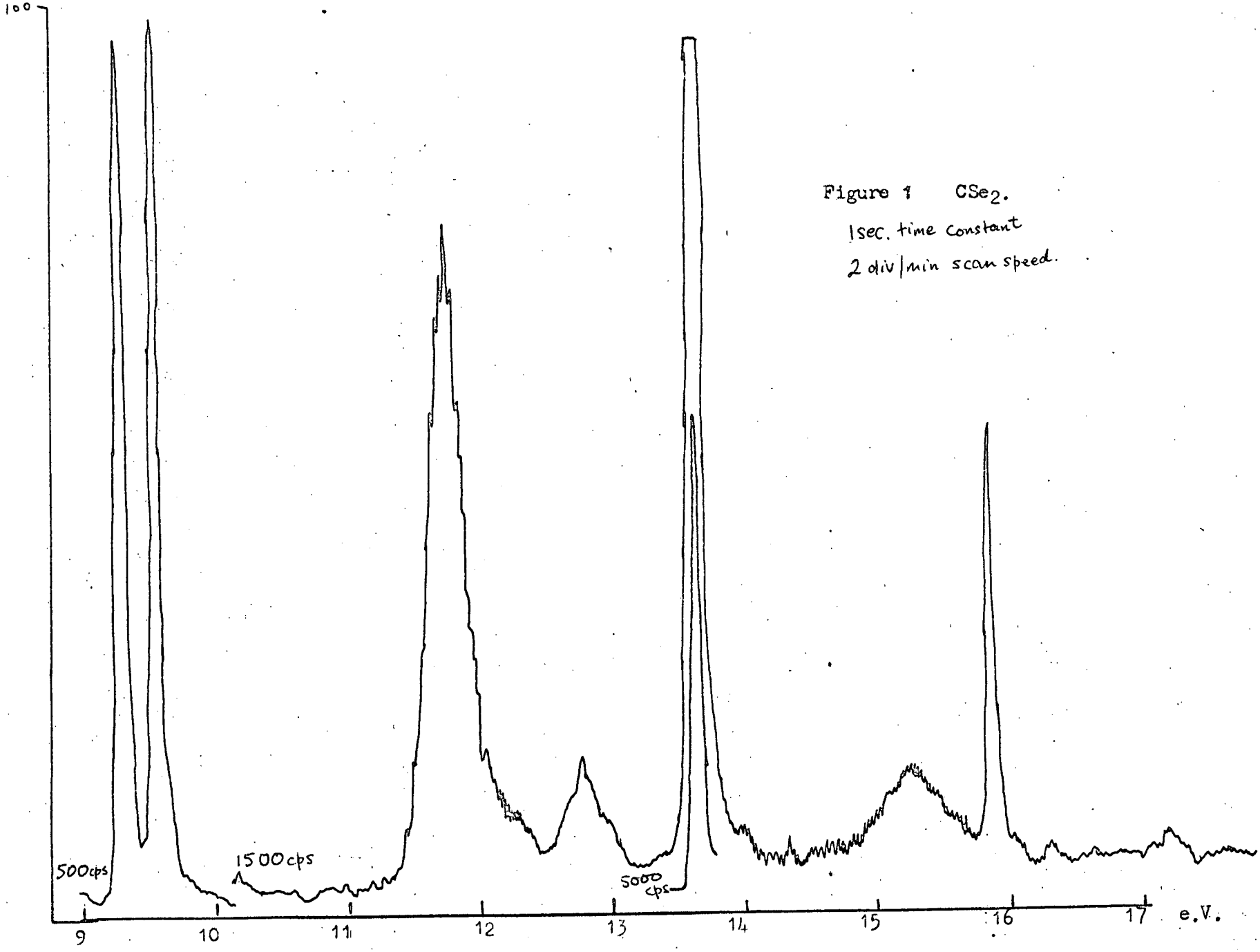

Figure 1 CSe_2.
1sec. time constant
2 div/min scan speed.

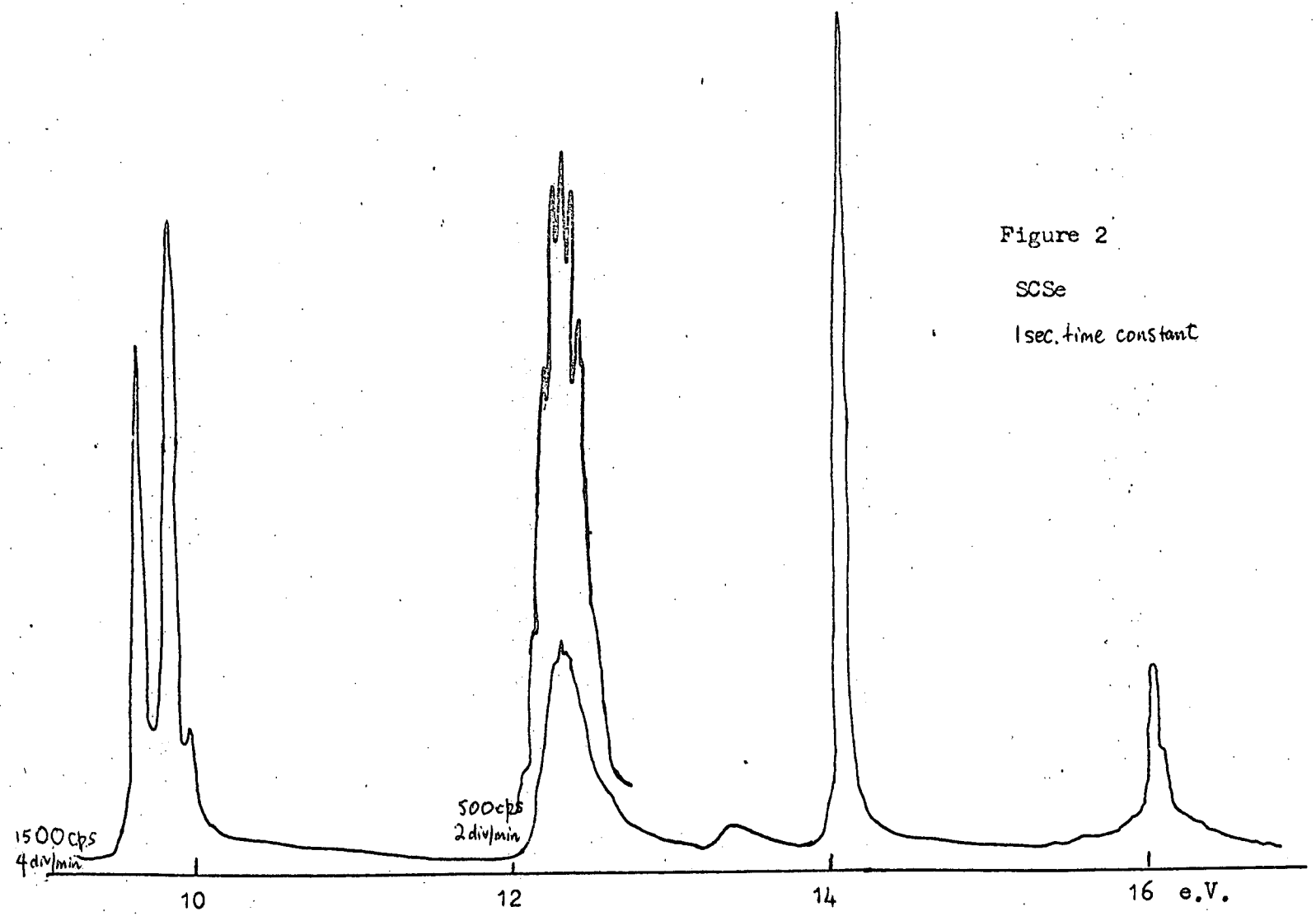

Figure 2

SCSe

1 sec. time constant

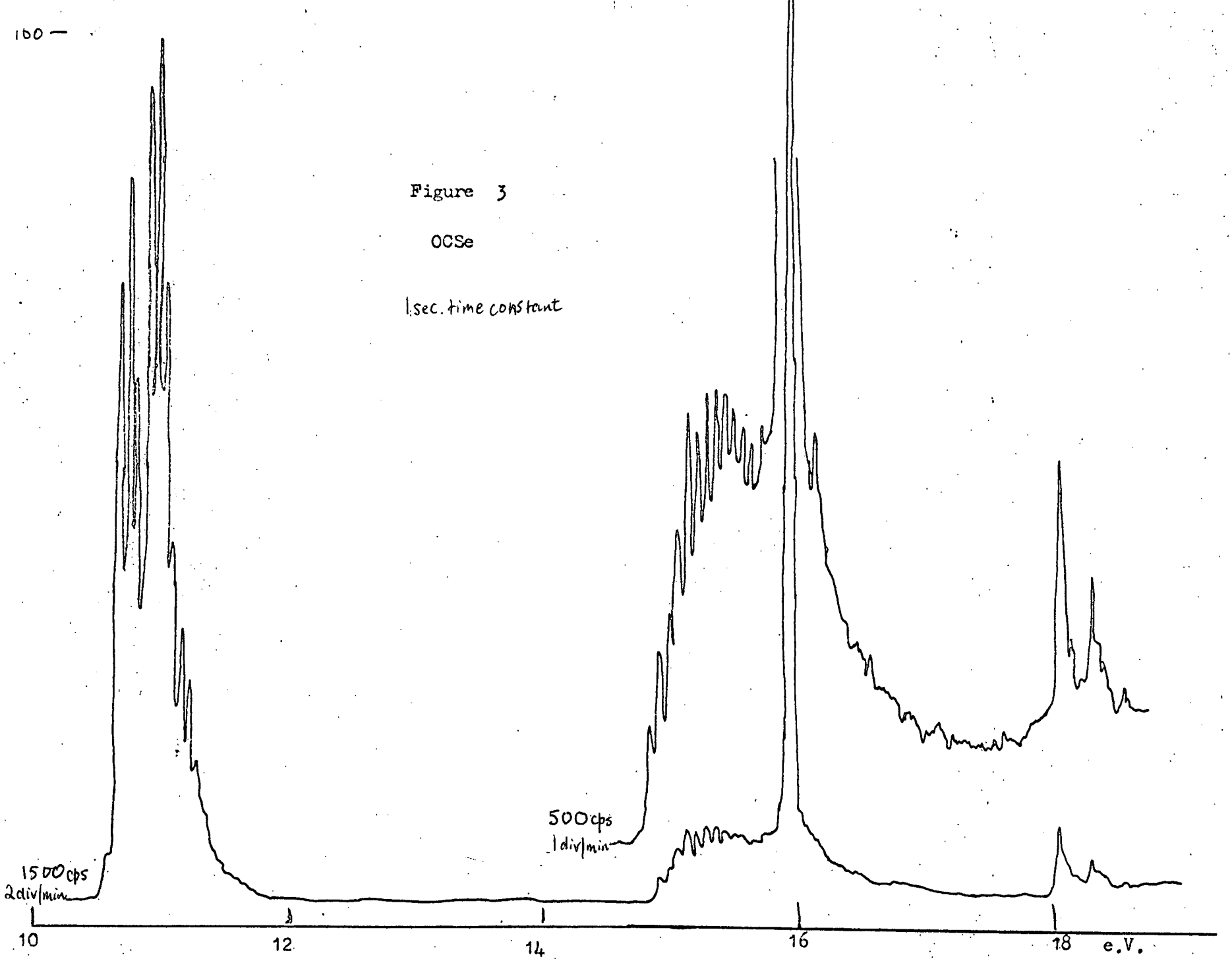

Figure 3

OCSe

1 sec. time constant

Figure 4.

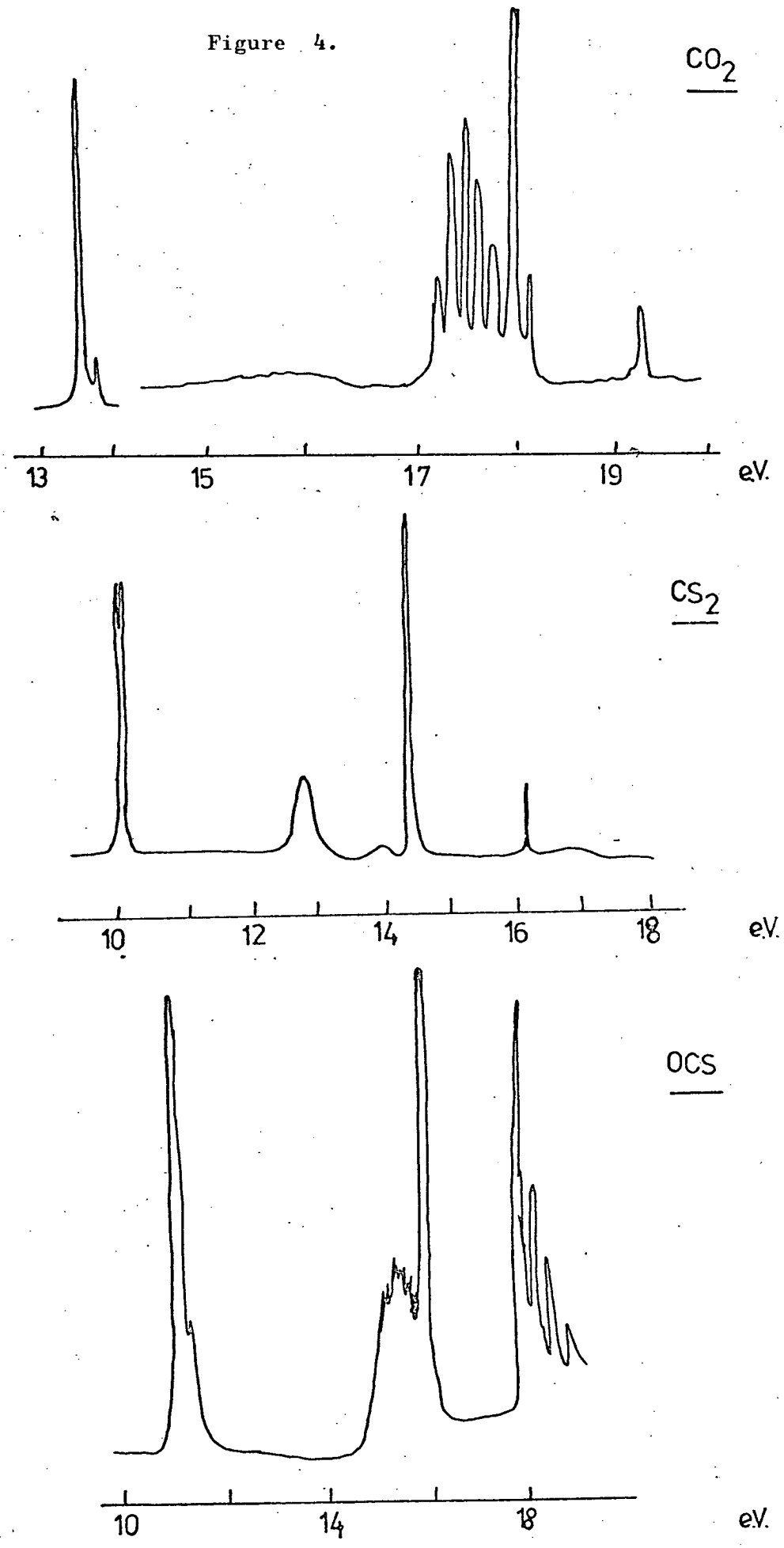

1280 cm^{-1} above the (000) band. The corresponding frequency in SCSe is 1435 $cm.^{-1}$ [9] and the small reduction in frequency and low intensity (low Franck-Condon factors) of the vibrational peaks, implies that the uppermost level in SCSe, 2π has only a slightly bonding character [15] and, as expected, closely resembles the uppermost level in CS_2 and CSe_2.

In analysing the vibrational progressions observed in photoelectron spectra, a useful aid to assignment are the vibrational selection rules for all electronic transitions including ionisation. These are based on the Born-Oppenheimer approximation and the application of the Franck Condon principle which assumes that the probability of a particular vibrational transition is given by the factor $|\langle X_{v'} | X_{v''} \rangle|^2$ where $X_{v'}$ and $X_{v''}$ are the vibrational wavefunctions in the upper and lower states between which the transition takes place.

In addition, the direct product of the representations to which $X_{v'}$ & $X_{v''}$ belong, must be (or contain) the totally symmetric representation of the point group of the molecule and the ion.[14] Thus the selection rules may be expressed as[16]

i) any number of quanta of a vibrational mode symmetric to a symmetry species is allowed, and

ii) only zero or an even number of quanta of a vibrational mode antisymmetric to a symmetry species is allowed.

Applying these rules to the systems under discussion we find that for CX_2 species only ν_1 is allowed in single quanta, with ν_2 and ν_3 appearing in double quanta. However for CXY species both ν_1 and ν_3 can appear in single quanta, with ν_2 still appearing in double quanta. In addition, these double quantal excitations are expected to be very weak.

Even for triatomic systems (which possess only three fundamental vibrational modes) it is often not sufficient to compare the vibra-:tional frequencies between the ion and molecule to make the appropriate

assignment. For example in CSe_2 with values of ν_1'' and ν_2'' of 368 and 308 cm^{-1} it would have been impossible to assign the observed ionic frequency of 330 cm^{-1} (seen in the next band) to ν_1' were it not for the fact that we know from the vibrational selection rules above that ν_2' cannot appear in single quanta.

The first band in the OCSe, Figures 3 and 5, is different from the corresponding band in CS_2 and CSe_2 as it clearly involves many vibrationally excited states of the ion. In part, the apparent complexity of the band derives from overlap of the vibrational components of the $X^2\Pi_{\frac{3}{2}}$ state with those of the $X^2\Pi_{\frac{1}{2}}$ state. This again is reflected in the apparently enhanced intensity of the $X^2\Pi_{\frac{1}{2}}$ component. However the pattern of vibrationally excited states of the $X^2\Pi_{\frac{1}{2}}$ state can readily be analysed in terms of progressions involving both ν_1 and ν_3. The ν_3 vibration is reduced from 642 cm^{-1} [9a] in the neutral molecule to approximately 500 cm^{-1} in the ion; ν_1 increases in value from 2020 cm^{-1} in the molecule to 2100 cm^{-1} in the ion.

Thus we have a situation in which one frequency goes up and the other goes down in energy. This apparent contradiction of the simple rules about bonding and antibonding character as deduced from the change in vibrational frequencies should be seen for the over-simplification which it represents in polyatomic species. In the present example, the frequencies ω_1, and ω_3 possess the same symmetry Σ^+ and so may interact. The extent of this coupling will determine the final values of ν_1 and ν_3 observed in both the molecule and the ion. Thus it would appear that the coupling in the ion is even greater than in the neutral molecule and so the ν_1' and ν_3' are pushed even further apart. The net result is that one frequency goes up,

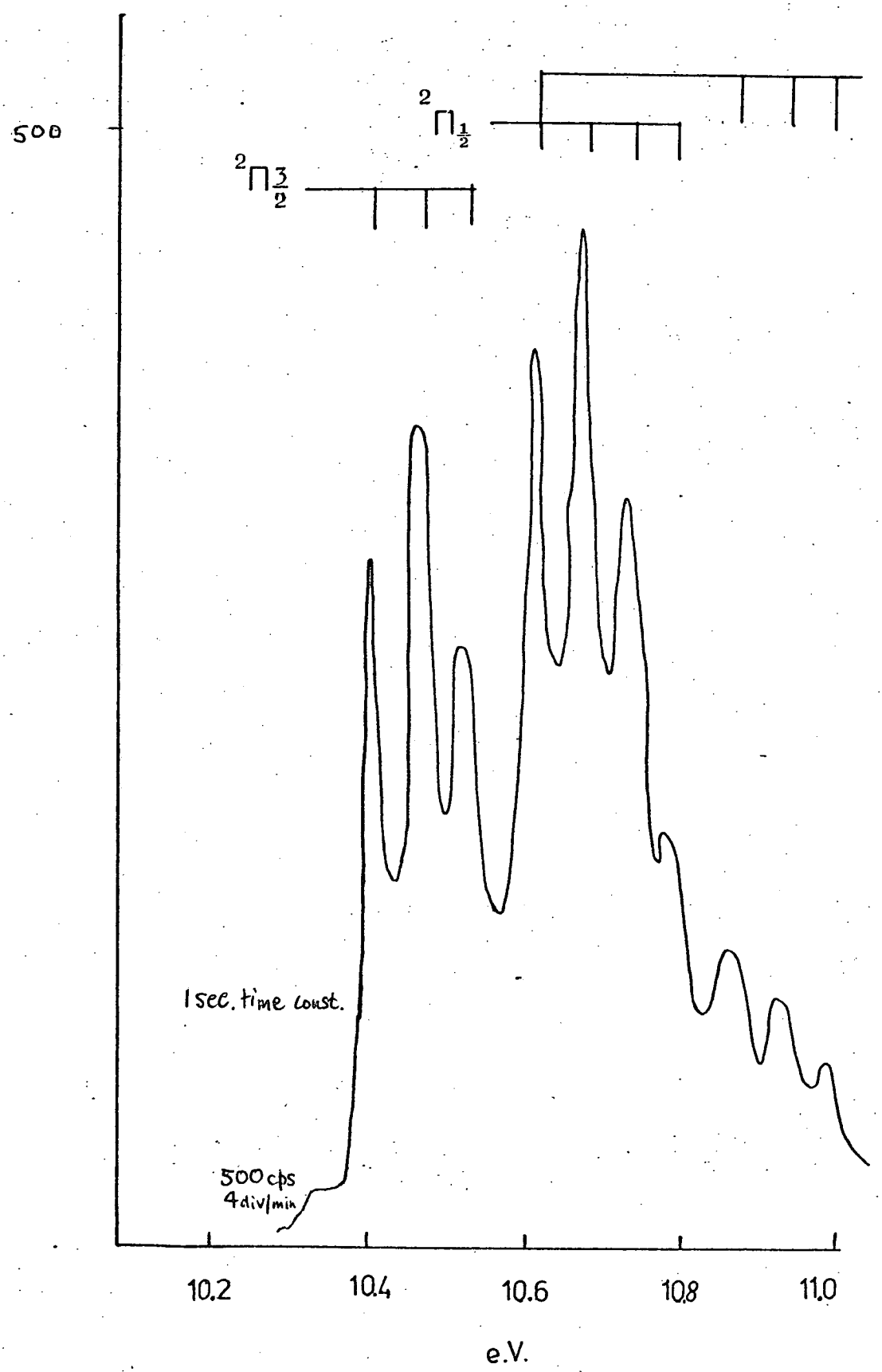

Figure 5

Detail of the first band of OCSe.

the other down, when compared with neutral molecule values.

An identical set of vibrational progressions in ν_1 and ν_3 exists for the $X^2\Pi_{\frac{3}{2}}$ state, but except for the first three members of the (00n) series, these overlap with and are not resolved from the $X^2\Pi_{\frac{1}{2}}$ state vibrational progressions.

i) Spin orbit coupling in the first band.

Analysed in this way the energy between the $X^2\Pi_{\frac{3}{2}}$ and $X^2\Pi_{\frac{1}{2}}$ components, (the spin orbit coupling), is 10.57 - 10.37 = 0.20 e.V. (1610 $cm.^{-1}$) The corresponding values for CSe_2 and CSSe are 0.26 e.V and 0.18 e.V. respectively. At first sight, it may appear strange that the spin orbit splitting in OCSe is larger than that in SCSe. However, it is obvious, both on comparing the energy and spin orbit splitting of these bands with those of the corresponding bands in the sulphur and oxygen analogues, that the highest occupied level in the Selenium containing species, $1\pi g$ (or 2π), is largely derived from Se $4p_\pi$ orbitals. Thus from qualitative energy and size considera-:tions, the possible contribution from $O2p_\pi$ to this level in OCSe would be expected to be less than that of S $3p_\pi$ in SCSe. As a result we observe that the spin orbit coupling in $OCSe^+$ is greater than in $SCSe^+$, i.e. it is nearer to the value of CSe_2^+.

It is possible, and also instructive, to discuss this not only in a qualitative manner, but also in a quantitive fashion.[17] It is known that the energies of the spin orbit components are given by the expression:-

$$E = E_o + \varsigma\Lambda\Sigma \qquad \text{——— (1)}$$

and for a Π state ($\Lambda = 1$), the spacing of the components is equal to ς. In the $^2\Pi$ and $^2\Phi$ states of a linear ion the magnitude of the splitting depends on the proportions of the different orbitals

making up the molecular orbital, ($\psi = \sum_{\mu} c_{\mu} \cdot \varphi_{\mu}$)

i.e. $$\zeta = \sum_{\mu} c_{\mu}^2 \cdot \zeta_{\mu} \qquad \text{——————(2)}$$

For the systems under discussion, the electrons of the 2π orbital are largely located on the outer atoms and so the spin orbit splitting of the $^2\Pi$ states should be approximately equal to the atomic splitting parameter for the outer atoms, ζ_x. Thus taking the observed spin orbit splitting values in CO_2, CS_2 and CSe_2, gives $\zeta_{CO_2} = \cdot 020$ e.V., $\zeta_{CS_2} = 0.054$ e.V. and $\zeta_{CSe_2} = 0.26$ e.V., which compare favourably with the values obtained from atomic spectra.[18] However there is a small difference, e.g. the atomic spin orbit splitting in S, $3s^2 3p^4\ (^3P)$ is 382 cm^{-1}, which is slightly smaller than the value of 436 cm^{-1} derived from the CS_2^+ spectrum. This discrepancy may be accounted for by the modification of the π g orbitals which occurs on ionisation. Thus we should really compare the spin orbit value obtained from CS_2^+ with that of S^+, which has been estimated to be 452 cm^{-1},[19] and in which case the correlation is much better. A similar, but larger difference in ζ values between Se and CSe_2 exists (·21 e.V. and · 26 e.V. respectively) for the same reasons.

However using the ζ values derived above and the observed spin orbit splitting in OCSe and SCSe we may write, using equation (2).

$$\zeta_{OCSe} = c_O^2 \zeta_O + c_{Se}^2 \zeta_{Se} = \cdot 02\, c_O^2 + .26 c_{Se}^2 = .20$$
$$\zeta_{SCSe} = c_S^2 \zeta_S + c_{Se}^{\prime 2} \zeta_{Se} = \cdot 054 c_S + .26 c_{Se}^{\prime 2} = .18$$

and solving these equations for Co^2, Cs^2, Cse^2 and Cse^2 using the normalisation equation $Cx^2 + Cy^2 = 1$ (X, y = O,S,Se) to produce a pair of simultaneous equations in each case, we obtain the results

$$\zeta_{OCSe} = .24 \zeta_{O2p_\pi} + .76 \zeta_{Se\,4p_\pi}$$
$$\zeta_{SCSe} = .38 \zeta_{S3p_\pi} \; .62 \zeta_{Se\,4p_\pi} .$$

Thus it is the substantially higher contribution of $S3p_\pi$ (with its

fairly small ϱ value) to the 2Π level in SCSe compared with the correspondingly lower contribution of $O2_{p\pi}$ to the 2Π level in OCSe, which results in the larger spin orbit splitting observed in the latter.

It is also instructive to perform an identical analysis on the spin orbit splitting in OCS^+ in which case we find

$$\varrho_{OCS} = 0.26\varrho_{O2p\pi} + 0.74\varrho_{S3p\pi}$$

The Cx^2 and Cy^2 values are very close to those found for OCSe and reflect the fact that the differences between $S3_{p\pi}$ and $Se\ 4_{p\pi}$ are much smaller than the corresponding differences between $O2_{p\pi}$ and $S3_{p\pi}$.

It is the information which the p.e. spectra of CSe_2 and OCSe give about the I.P.s, vibrational structure and spin orbit coupling of this uppermost $^2\Pi$ state which are invaluable in the assignment of the vacuum ultra-violet spectra of these molecules. We shall return to this in Chapter 3, where we shall see in detail how the overall band contour of the $^2\Pi$ state is reflected time after time in the successive Rydberg states leading to the $X^2\Pi$ ionisation limit.

b) Second band.

The second band in both CSe_2 and SCSe is comparatively broad with an overall width of approximately 0.6 e.V. and consists of a regular resolvable vibrational progression extending up to $\upsilon = 8$ or 9. In CSe_2^+ the observed frequency is 330 cm^{-1} and as discussed previously may be assigned to ν_1' and should be compared with ν_1'' in CSe_2 of 368 cm^{-1}. Likewise in $SCSe^+$, the observed frequency ν_3, is reduced from a ground state value of 506 cm^{-1} to 425 cm^{-1} in the ion. The extent of the band envelope, and the reduction in frequency occurring in the ion, both indicate that there is a substantial bonding character to this level.

The second band in OCSe is again clearly different both in energy and band contour from the corresponding bands in CS_2 and CSe_2.

There are (at least) 14 resolvable peaks extending from an adiabatic I.P. of 14.62 e.V. for about 1 e.V., before breaking off into the third band, Figure 6. The spacing of the progressions, (approximately 0.075 e.V.) is not strictly regular, and by analogy to the analysis of a similar band in OCS,[7] may be interpreted as involving both ν_3' and ν_1' modes in progressions of the type (n00), n01), (n02).

There can be little doubt that the second band in CSe_2 and SCSe correlates with the second band observed in the spectrum of CS_2. Largely on the basis of the fact that the $^2\Sigma_u^+ \longrightarrow X^2\Pi_{g(i)}$ transition for CS_2^+ [19] is identical in energy to the difference between the first and third I.P.s of CS_2, the second band of CS_2 has been assigned to ionisation from the $^2\Pi u$ state. Also, emission studies of the $A^2\Pi_u \longrightarrow X^2\Pi_g$ transition of CO_2 [20] and the $^2\Pi \longrightarrow X^2\Pi_{(i)}$ transition COS[21] confirm that the second band in the spectrum of these molecules arises from ionisation of the second π level. Thus, there would appear to be no good reason to doubt that the second band in the spectra of CSe_2, SCSe and OCSe also arises from ionisation of the $1\pi_u$ (or 1π) level.

In contrast to the previous $\pi_{(g)}$ level, this orbital is delocalised over the whole molecule, with greatest density at the central carbon atom. Thus, we would expect the spin orbit splitting of the peaks to be small and to be comparable to that of atomic carbon. In CO_2^+ ($A^2\Pi_u$) [14] the splitting has been observed to be 0.0118 e.V. and although it may be expected to increase on going down the series, because of the small contributions from the terminal atoms it remains too small to be seen under the normal conditions of resolution in photoelectron spectroscopy.

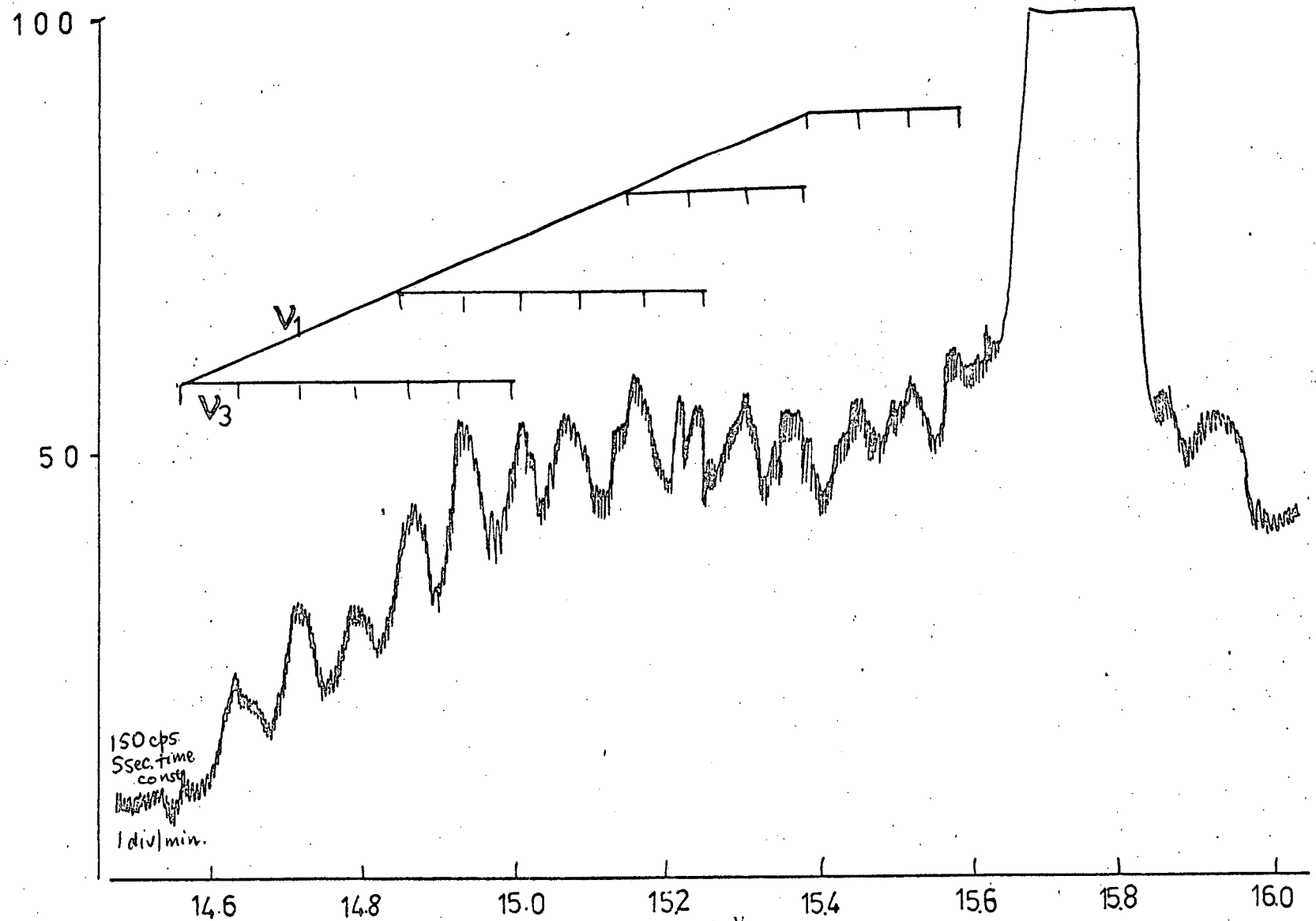
100
50
ν_1
ν_3
150 cps
5sec. time
const.
1 div/min.
14.6
14.8
15.0
15.2
15.4
15.6
15.8
16.0
e.V.

Figure 6

c) Third and fourth valence bands.

The third valence ionisation band, the strongest in all the spectra, can be clearly seen to consist of an intense (000) peak in all cases. The associated vibrational structure is weak. In CSe_2 the (100) band is at approximately 300 cm^{-1} higher energy, (compare $\nu_1''(X\,^1\Sigma_g^+)$ = 368cm^{-1} and $\nu_1'A^2\Pi_u$ = 330cm^{-1}) and in SCSe the (001) band is at approximately 480 cm^{-1} above (000), (compare $\nu_3''(X^1\Sigma^+)$= 506cm^{-1} ; $\nu_3'(A^2\Pi)$ = 425cm^{-1}). The identification of the vibrational features of this band in OCSe is more problematical as a consequence of the overlap with the previous band, but a weak feature at approximately 1850 cm^{-1} higher energy may be assigned to the (100) band.

The fourth valence ionisation appears much less intense and the possible causes of this are discussed later. In CSe_2 the band consists entirely of a sharp (000) component with no vibrational features apparent. In SCSe a weak (001) band is observed at approximately 480 cm^{-1} to higher energy than the (000) peak. Again the corresponding band in OCSe is different, clearly showing resolved vibrational progressions in ν_1 and ν_3 with frequencies of 2080 and 640 cm^{-1} respectively which are very close to their electronic ground state values.

In all the molecules under discussion, the third and fourth bands may be attributed to ionisation from the valence levels σu and σg derived from atomic p_σ and S levels. Despite their sharpness and general lack of extensive vibrational features, their contribution to the bonding (especially the σu level) may be greater than the simple application of these criteria usually imply. This may be explained as a result of the shortening of the bond lengths caused by the higher energy π bonds, leading to an effective cancellation of the +ve and

-ve overlap. This makes the orbital appear "non-bonding" at the internuclear distance, when the criteria used to establish this, are the change in bond length and curvature of the base of the potential energy curve. However, if the contribution to the bond dissociation energy i.e. the depth of the potential well, is considered instead, then as the bond length increases, as on dissociation, the effective cancellation of +ve and -ve overlap no longer applies, and so the orbital will show considerable bonding power.[14] However an alternative explanation of this phenomenon is that it occurs as a result of mixing of these σ levels with higher binding energy σ levels. These have been observed in the Xray photoelectron spectrum and are of the appropriate symmetry to mix with the σ levels under discussion. If strong mixing occurs then the extent of bonding (and anti-bonding) character which these levels would exhibit would be reduced and could give the appear-:ance of non-bonding character.

d) Correlation of electronic energy levels in linear triatomic systems.

Thus we have seen how the four bands in each of the spectra may be explained as due to ionisation from the uppermost valence levels, which in order of increasing I.P. are $2\pi, 1\pi, 4\sigma, 3\sigma$.
To emphasise the trends in orbital character and the trends in their energies, a correlation diagram of the observed ionic states of CO_2 through to CSe_2, is presented in Figure 7. The information which it contains is largely self-explanatory, with the effect of substitution of S by Se, having much less effect than that of O by S, clearly apparent. Also included, for comparison, are the known ionic state energies of other linear triatomic molecules containing 16 valence level electrons.[7,22,23] Several features are worthy of comment.

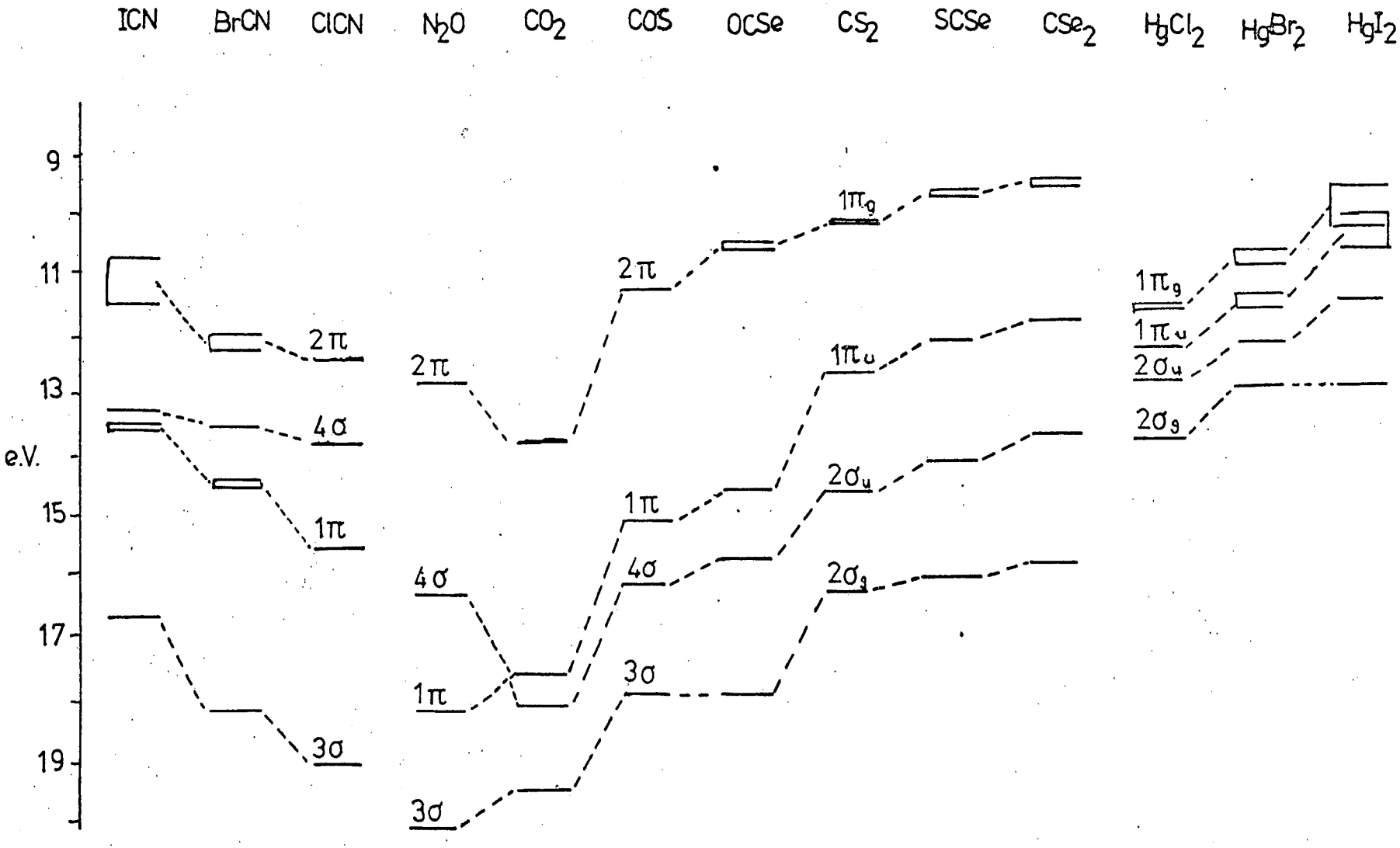
ICN
BrCN
ClCN
N_2O
CO_2
COS
OCSe
CS_2
SCSe
CSe_2
$HgCl_2$
$HgBr_2$
HgI_2
9
11
13
15
17
19
e.V.
2π
4σ
1π
3σ
2π
4σ
1π
3σ
2π
1π
4σ
3σ
1πg
1πu
2σu
2σg
1πg
1πu
2σu
2σg

Figure 7

Only in the mercuric halides is the ordering of the orbital energies the same as in the CX_2, CXY (X,Y = O,S,Se) systems. In the XCN (X = O, Br, I) and N_2O molecules, the 4σ level is higher than the 1π level. This change is illustrated in the molecular orbital energy diagrams shown in Figure 8. These diagrams have been constructed from the known orbital energies of CO, CS and N_2 as determined by p.e. spectroscopy[7,24] and the atomic energy levels of O,N,Se, determined from optical spectra.[18] In them we can see the composition of the triatomic molecular orbitals in terms of the corresponding orbital energies of their atomic and diatomic components. In particular, we can see that the $\sigma(u)$ level in the ABC systems is formed interaction of the $\sigma(g)$ level in AB with the p_σ levels of C. In CO_2 and CS_2, these levels are sufficiently similar in energy to interact strongly enough to push the $\sigma(u)$ level below the $\pi(u)$ level. However in N_2O the larger difference between the σg level of N_2 and the O_{2p_σ} level reduces the extent of the interaction between them and so the 4σ level remains above the 1π level. However, in the OCS and OCSe systems where there is a fairly large energy difference between the CO 2σ level and the uppermost $p\sigma$ level of S or Se, the molecular 4σ level formed from them is only just pushed below the 1π level and in fact overlaps with its higher vibrational levels.

The trends observed in the spin orbit splittings of the $^2\Pi$ states are also worthy of comment. Thus in the HgX_2 and XCN (X = Cl, Br, I), the spin orbit splitting on the first band is largely derived from the halogen p_π levels and we see a marked increase in the splitting on going down the series. This effect also occurs for similar reasons in the first band of the CX_2, CXY (X,Y = O,S,Se) systems. However for the Hg X_2 and CX_2, CXY molecules, the $1\pi u$

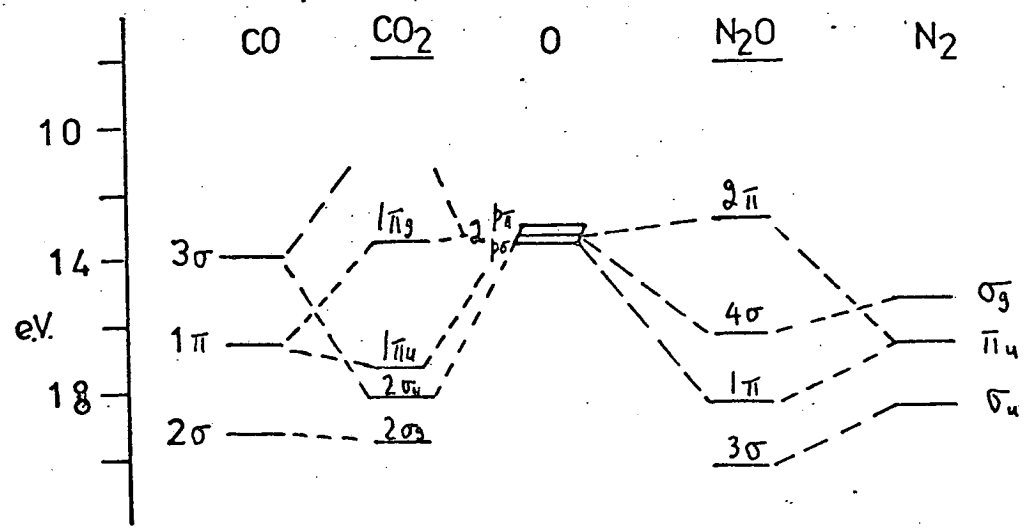
CO
CO2
O
N2O
N2
10
14
18
eV.
3σ
1π
2σ
1πg
1πu
2σu
2σg
2p π
2p σ
2π
4σ
1π
3σ
σg
πu
σu

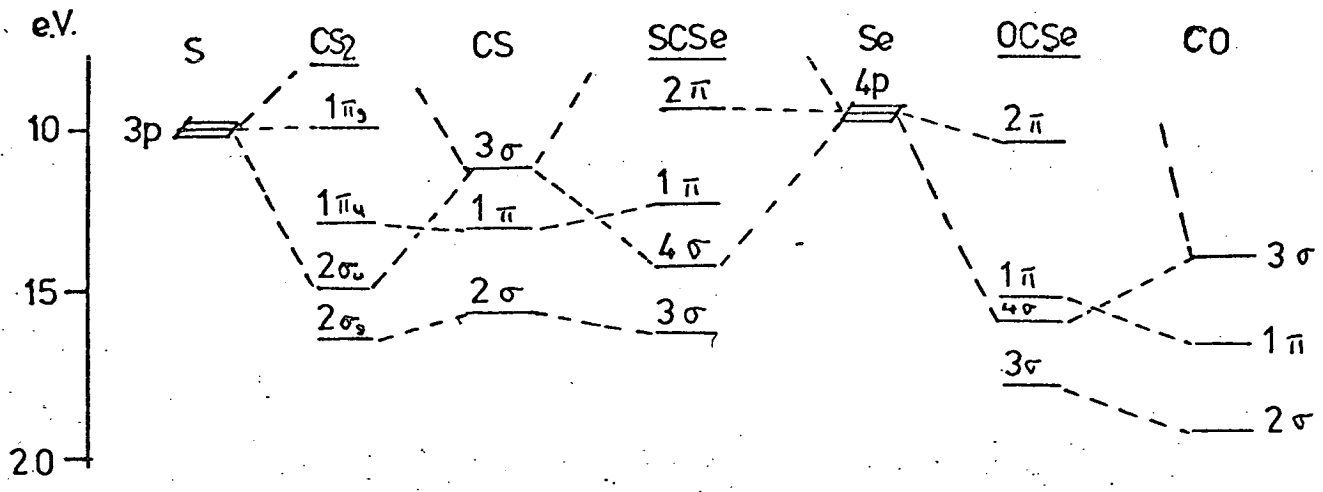
eV.
10
15
20
S
CS2
CS
SCSe
Se
OCSe
CO
3p
1πg
1πu
2σu
2σg
3σ
1π
2σ
2π
1π
4σ
3σ
4p
2π
1π
4σ
3σ
3σ
1π
2σ

Figure 8

level is spread over the molecule with high density at the central atom. In the HgX_2 spectra, this results in a considerable spin orbit splitting of the $^2\Pi u$ levels, associated with the large atomic splitting value of mercury, ζHg. By contrast, the ζ value of Carbon, being very much smaller, no splitting is observed in the p.e.s of the $A^2\Pi u$ states of the CX_2 systems. However in XCN molecules the $B^2\Pi\frac{1}{2},\frac{3}{2}$ level contains some halogen p_π character and so the splitting of the different Ω levels increases on going down the series.

e) Relative band intensities between He(I) and He(II) spectra.

In connection with studies of the weak bands to be discussed in the next chapter, the spectra of all the CX_2, CXY molecules were recorded using He(II) radiation, and the spectra are shown in Figures 5 to 10 of that chapter. It is interesting to compare the trends observed in the relative peak intensities for the different bands in the spectra obtained with He(I) radiation with those obtained using He(II) radiation.

Taking the intensity of the $4\sigma(u)$ band as unity, the corresponding relative intensities are given in Table 3. The intensities are summed over all the vibrational components, this being especially important for the 1π level.

The most striking feature is the marked increase in intensity of the 1π and 3σ bands in all spectra, relative to the 4σ bands, on going from He(I) to He(II). In CS_2, CSSe and CSe_2 systems the 1π band dominates the He(II) spectrum. Comparison with the relative intensities shown in the valence region Xray p.e. spectra (ESCA), would be useful and although the spectra have been obtained for CO_2, COS and CS_2, except in the case of CS_2, the 1π and 4π levels are not resolved and so their relative intensities unobtainable.[25]

	He (I)			He(II)		
Molecule	$1\pi u$	$4\sigma(2\sigma u)$	$3\sigma(2\sigma g)$	$1\pi(u)$	$4\sigma(2\sigma u)$	$3\sigma(2\sigma g)$
CO_2	1.2	1	0.1	1.24	1	0.45
OCS	0.75	1	0.13	2.5	1	1.0
OCSe	0.4	1	0.14	1.7	1	0.9
CS_2	1.4	1	0.3	4.5	1	0.75
SCSe	1.1	1	0.25	3.0	1	0.55
CSe_2	1.3	1	0.2	2.25	1	0.25

TABLE 3.

Relative photoionisation cross-sections in He(I) and He(II) spectra of linear triatomic species.

It should be noted however that the 3σ level is of considerable intensity in the ESCA spectra.

The causes of these changes observed on varying the ionising source from He(I) to He(II) and eventually to Mg K_α are complex.[26] Apart from the instrumental factors associated with the decreased sensitivity of electrostatic analysers to lower energy electrons, which is particularly important in the case of He(I) spectra, several other factors have been identified for closed shell species.[27]

For orbitals composed from the same set of atomic orbitals, the relative cross-section for ionisation is proportional to the number of equivalent electrons available to be ionised. Thus ionisations from fully occupied π levels should be twice as intense as those from σ levels, and in addition the intensity of the various σ levels should be equal. However the relative intensities also depend on the atomic orbitals from which the m.o's are derived and factors such as their size, number of nodes and localisation can be of considerable importance. Although no hard and fast rules exist, some helpful generalisations have been made.[28] Thus in He(I) spectra the cross-section for ionisation increases on going down a group, with a large increase between the first and second rows (e.g. O to S). This trend is partially reversed on going to He(II). In addition, the cross-sections for ionisation of "s" type orbitals decreases relative to those of "p" type as the periodic table is crossed from left to right. Thus the ESCA results on CO_2, OCS and CS_2[25] indicate that "2s" character is seen roughly ten times stronger than "2p" but "3s" and "3p" have roughly the same intensity. Therefore the relative contribution of the different atomic orbitals will contribute significantly to the observed intensity patterns and the

changes in intensity between He(I) and He(II) spectra.

Ab initio calculations of the relative atomic populations of the various molecular orbitals in CO_2, CS_2 and COS have been published [25] and using these it is possible to deduce the major atomic contributions to the corresponding molecular orbitals in CSe_2, OCSe and SCSe as shown in Table 4. It is instructive to use these results to examine the pattern of corresponding relative intensities in the light of the trends in photoionisation cross-sections quoted previously.

On a purely statistical basis, it might be expected that the $2\sigma u$ and $2\sigma g$ levels in CO_2, CS_2 and CSe_2 would show roughly the same relative intensity. However, although both levels contain about the same relative proportion of terminal atom p_σ and s character, they contain markedly different contributions from C_{2p} and C_{2s} atomic orbitals. Thus in the He(I) spectrum, we would expect the $2\sigma u$ level to be the more intense, but in the He(II) spectrum, the $2\sigma g$ level, with its C_{2s} contribution, should increase in relative intensity, as observed. In OCS, OCSe and SCSe the 4σ and 3σ levels contain completely different a.o's, largely derived from the terminal atoms. The relative intensity pattern in the He(I) spectrum conforms to the rule that cross-sections for ionisation increase on going down a group, so that in OCSe the intensity of the 4σ level (largely derived from Se 4p /4s a.o's) is considerably greater than that of the 3σ level which is mainly composed of O 2s/2p a.o's. Likewise this effect is predicted to be less marked in the He(II) spectrum, as observed.

The intensity of the 4σ level in the He(I) spectra of OCSe and OCS is, relative to that of the 1π level, exceptionally high, but this again may be explained in terms of the different a.o. contribu-:tions to these levels. The 1π level is composed mainly of O_{2p_π} a.o.s whereas the 4σ level is derived from Se $4p_\sigma$ (in OCSe), and

Valence Level.	CSe_2
$1\pi g$	$Se4p_{\bar{\pi}}$
$1\pi u$	$Se4p_{\pi}$ + $C2p_{\bar{\pi}}$
$2\sigma u$	$Se4p_{\sigma}$ + Se4s + $C2p_{\sigma}$
$2\sigma g$	$Se4p_{\sigma}$ + Se4s + C2s
$1\sigma u$	Se4s + $C2p_{\sigma}$
$1\sigma g$	Se4s + C2s

OCSe	Valence Level.	SCSe
$Se4p_{\bar{\pi}}$	2π	$Se4p_{\bar{\pi}}$
$O2p_{\bar{\pi}}$ + $C2p_{\pi}$	1π	$S3p_{\bar{\pi}}$ + $C2p_{\pi}$
$Se4p_{\sigma}$ + Se4s + $C2p_{\sigma}$	4σ	$Se4p_{\sigma}$ + Se4s + $C2p_{\sigma}$
$O2p_{\sigma}$ + O2s + C2s	3σ	$S3p_{\sigma}$ + S3s + C2s
Se3s + $C2p_{\sigma}$ + C2s	2σ	Se4s + $C2p_{\sigma}$ + C2s
O2s + C2s	1σ	S3s + C2s

TABLE 4.

Predicted major atomic orbital character of the upper valence levels in CSe_2, SCSe and OCSe.

so would be predicted to be much more intense in the He(I) spectrum. Again, as predicted, this effect is reversed in the He(II) spectrum and in this case the double degeneracy of the 1π level results in its considerable intensity.

Thus on the basis of the relative a.o. contributions to each of the m.o's it is possible to account qualitively for the grosser features of the relative intensity patterns and their behaviour on changing to a higher energy ionising source.

REFERENCES.

1. S. Cradock and W. Duncan: Molecular Physics (1974), 27, 837.

2. S. Cradock and W. Duncan: J.C.S. Faraday Trans. II (1975), 71,1262.

3. D.C. Frost, S.T. Lee, and C.A. McDowell: J. Chem. Phys.(1973), 59, 5484.

4. S. Cradock, R.J. Donovan, W. Duncan, H.M. Gillespie: J.C.S. Faraday Trans. II, (1975), 71, 156.

5. S. Cradock, R.J. Donovan, W. Duncan, H.M. Gillespie: Chem. Phys. Letts. (1975), 31, 344.

6. E.J. Finn and G.W. King: J. Molec. Spectros. (1975), 56, 39.

7. D.W. Turner et.al.: Molecular Photoelectron Spectroscopy, (Wiley), 1970.

8. Strem Chemicals Ltd.

9. T. Wentink, J. Chem. Phys. (1958), 29, 188.

9a. M. Bavia, G.D. Lonardo, C. Galloni and A. Trombetti, J.C.S. Faraday II, (1972), 68, 615

10. H.G. Kuhn; Atomic Spectra (2nd Edition) 1969, Longmans, London.

11. G. Herzberg: Spectra of Diatomic Molecules (2nd Edition), 1950. Van Nostrand Reinhold, New York.

12. G. Herzberg; Electronic Spectra and Electronic Structure of Polyatomic Molecules, 1966. Van Nostrand Reinhold, New York.

13. R.S. Mulliken, Rev. Mod. Phys. (1942), 14, 204.
A.D. Walsh, J. Chem. Soc. (1953), 2260, and following articles.

14. J.H.D. Eland: Photoelectron Spectroscopy, 1974, page 128. Butterworths, London.

15. A.D. Baker, Accs. of Chem. Res. (1970), 3, 17.

16. C.R. Brundle, and D.W. Turner; Intern. J. Mass Spectr. Ion Phys. (1969), 2, 195.

17. As reference 14, page 132.

18. C.E. Moore; Atomic Energy Levels. Vols. I, II, III: National Bureau of Standards, Washington D.C.

19. J.H. Callomon, Proc. Roy. Soc. (London), Ser. A. (1958), 244,220.

20. S. Mrozowski; Phys. Rev. (1947), 72, 691; as reference 7, page68.

21. S. Leach, J. Chim. Phys. (1964), 61, 1493.

22. J.H.D.Eland; Intern. J. Mass Spectr. Ion Phys. (1970), 4, 37.

23. E. Heilbronner, V. Hornung, K.A. Muzkat; Helv. Chimica Acta. (1970), 53, 347.

24. N. Jonathon, A. Morris, M. Okuda, K.J. Ross, and D.J. Smith: Chem. Phys. Letts. (1972), 13, 334.

25. C.J. Allan, U. Gelius, D.A. Allison, G. Johansson, H. Seigbahn, K. Seigbahn, J. Electron Spectros. and Related Phenomena,(1972/73), 1, 131.

26. A. Hamnett and A.F. Orchard: Electronic Structure and Magnetism of Inorganic Compounds. Volume 3, Chapter 4, Chemical Society 1974.

27. J.H.D. Eland. as reference 14, page 13.

28. W.C. Price, A.E. Potts, D.G. Streets in Electron Spectroscopy ed. D.A. Shirley, page 187, 1972. North Holland, Amsterdam.

CHAPTER 2.

FORBIDDEN TRANSITIONS IN THE He(I) and He(II) SPECTRA OF LINEAR TRIATOMIC MOLECULES.

CHAPTER 2.

1. INTRODUCTION.

In the preceding chapter we have seen how the major features of the photoelectron spectra of the CY_2, CXY(X,Y = O,S,Se) series can be accounted for on the basis of ionisation from each of the four upper-most valence shell levels. However in the spectra of these (and other related molecules) weaker features are observed which cannot be accounted for on this basis and it is the purpose of this chapter to explain how they may arise.

In trying to interpret their occurrence, we will obtain a deeper insight into the process of photoionisation and of the excited ionic states in which these molecules can exist.

2. BACKGROUND.

Factors which may produce weak features in the p.e. spectrum may be classified as being due to:-

a) trace impurities in and/or decomposition of the original sample.

b) ionisation from minority emission lines due to impurities in the lamp.[1]

c) forbidden transitions.

Only when the possibility of factors (a) and (b) has been ruled out can the possibility of forbidden transitions be considered. Although some wrong assignments have appeared in the literature,[2] it is usually not too difficult to ascertain when factors (a) or (b) apply, since there is usually a change in relative peak areas between that of the impurity features and those of the pure compound on varying the experimental conditions. In addition the purity of a sample may be checked by several methods, e.g. infra-red or mass spectroscopy[3] and the predicted positions of bands arising from likely lamp impurity emission lines may be readily calculated and compared with the features

observed.

An example of bands arising from such minority emission lines is shown in Figure 1. It is mainly in the high I.P. (i.e. low electron kinetic energy) region of the He(I) spectrum that these minority emission lines can prove troublesome. However in this case, they are readily recognised from the sharp line character and separation as being identical in origin to the first band in the spectrum, arising from ionisation of the 2Π level of SCSe by O(I), H(I) and N(I) lines

The first example of these forbidden transitions was observed in the spectrum of carbon disulphide,[8] the so called 'fifth band', although it was not immediately recognised as such. It was originally thought to be due to ionisation from the largely S_{3s} based level corresponding to the $D^2\Sigma u^+$ state. However an ab initio calculation on CS_2 places this level at 27.8 e.V. A broad band in the Xray p.e. spectrum at approximately 26.5 e.V has been attributed to this level and the more tightly bound $1\sigma g$ level.[9]

Another interesting feature of this weak band is the fact that in contrast to all other bands in the spectra of linear triatomics, this particular band is continuous in nature and shows no resolvable features. This had been attributed to a short lifetime, as a result of rapid dissociation, of the state of CS_2^+ formed. If this were the case then dissociation should lead directly to a single set of products with most of the available energy being converted into translational energy of the fragments.

However this system has been studied using photoelectron - photoion coincidence techniques[10] and the results are opposite to those expected for a rapid fragmentation process. In fact, the observation of S_2^+ ions indicates that the dissociation process is slow and that a short lifetime cannot be responsible for its continuous

Figure 1

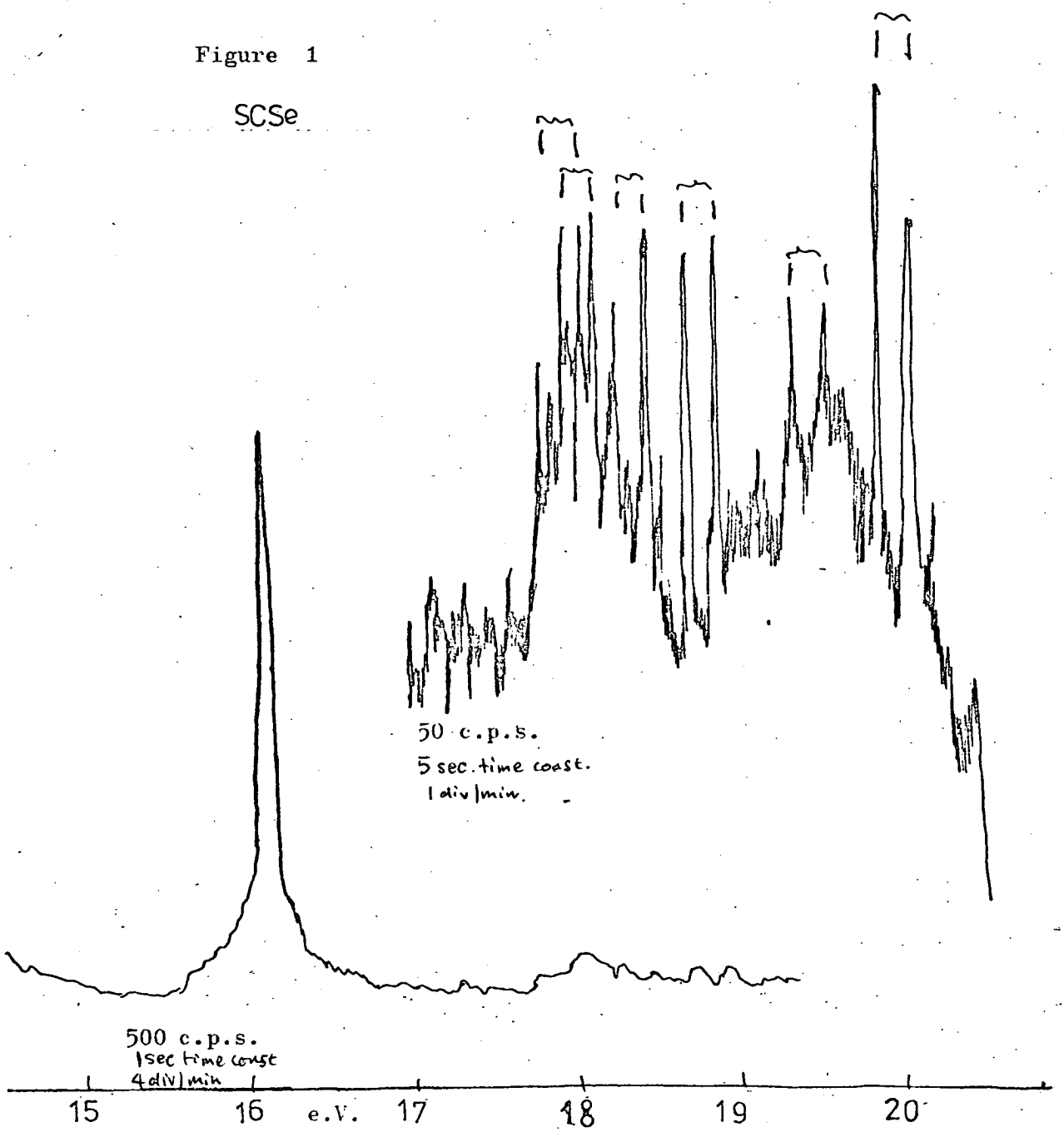
SCSe
50 c.p.s.
5 sec. time coast.
1 div/min.
500 c.p.s.
1 sec time const
4 div/min
15
16
e.V.
17
18
19
20

appearance.

Thus it would appear that an anomalous band which does not correspond to simple ionisation from any of the valence levels, exists in the spectrum of CS_2. In addition, the genuineness of this band is not in doubt, having been observed using spectroscopically pure samples of CS_2 and under a variety of experimental conditions. All this would point to the existence of this band being due to a forbidden process.

3. RESULTS.

It was therefore of interest to see whether the same process would also permit the observation of similar bands in other CY_2, CXY (X,Y = O,S,Se) species.

Close inspection of the photoelectron spectra presented in the previous chapter reveals such bands only in the He(I) spectra of CSe_2 and SCSe, as shown in Figures 2 and 3 of this chapter.

4. DISCUSSION.

Two related questions immediately arise:-

i) How do the forbidden bands become weakly allowed in these systems?

ii) Why do only some of the spectra in such a closely related series show these bands, while others do not?

a) Selection rules for ionisation.

In order to understand the existence of such forbidden bands it is necessary to reconsider the expression:-

$$I \propto |\langle \Psi_i | M | \Psi_f \rangle|^2$$

where I = intensity, Ψ = total electronic wavefunction of initial state (i) and final state (f), M = dipole moment vector.

Normally it is possible to interpret the p.e. spectra of closed

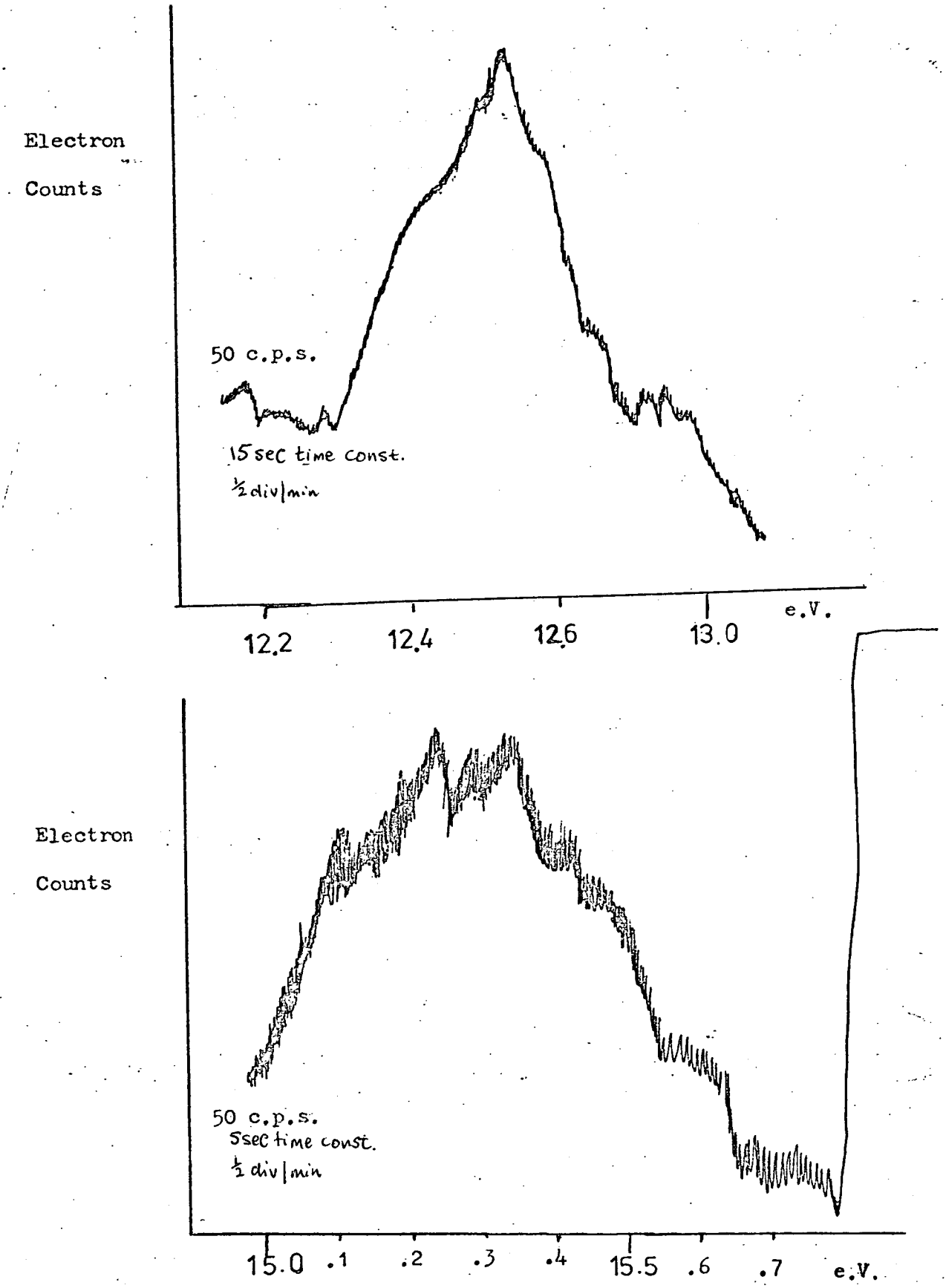

Forbidden bands in CSe_2.

Figure 2 .

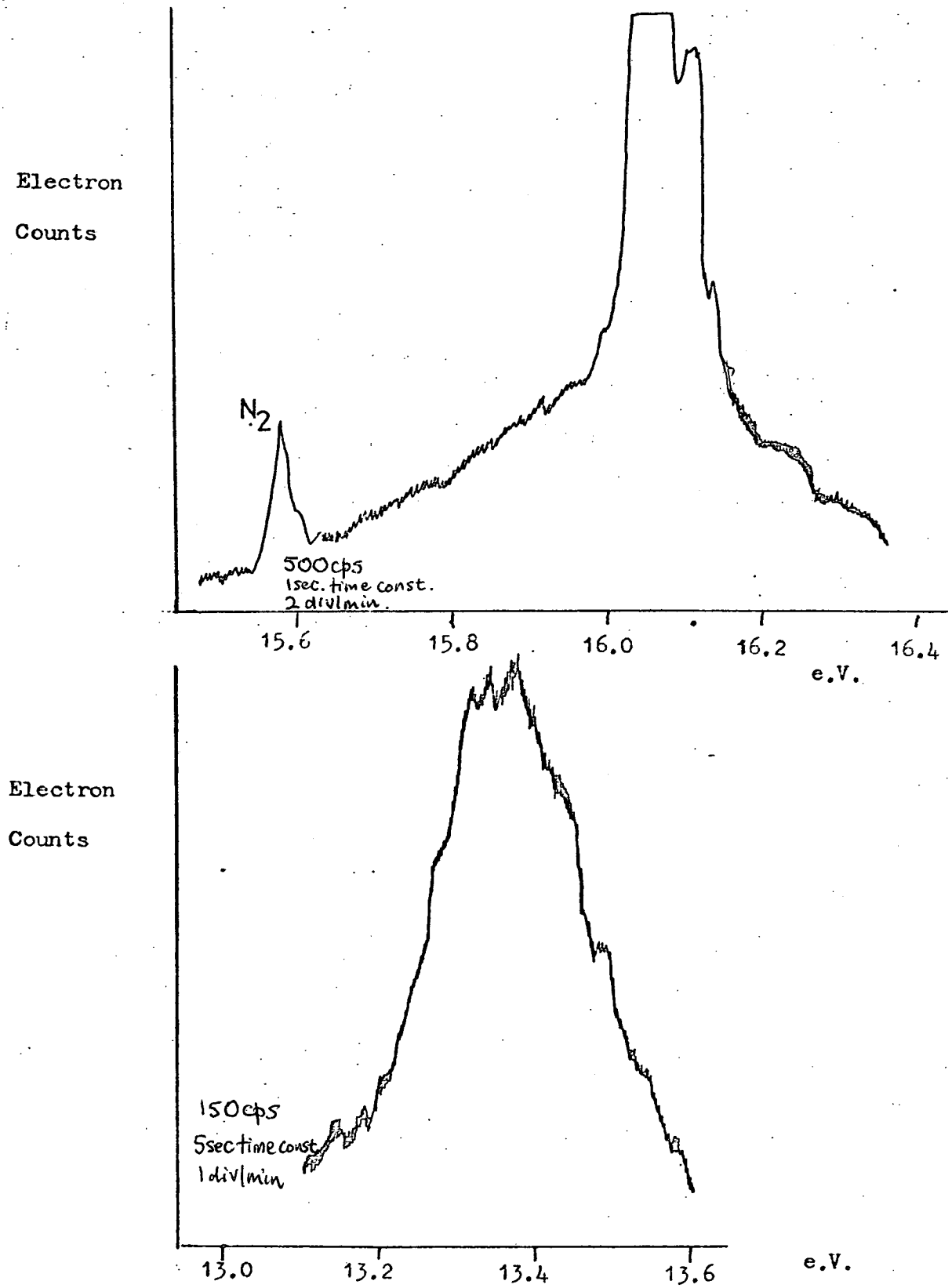

Figure 3. Forbidden bands in SCSe.

shell molecules on the basis of one band to each valence level as there are no orbitals from which ionisation is symmetry forbidden.[4] That the transition should involve removal of only one electron to the continuum, leaving all others unaffected, is a consequence of the fact that the ground and excited state wave functions are usually well described in terms of antisymmetrised single-electron configurations i.e. Slater type determinants. It is thus assumed that both the ground and excited states share a common core of (N-1) electrons, the orbitals of which are orthogonal to the orbital in the ground state containing the electron to be ionised.[5] Thus there is only one electronic state produced on ionisation from each molecular level of a closed shell species, and so only one band produced in the spectrum, corresponding to ionisation from that level. A proof that two electron excitations are formally forbidden for orbitals of the type discussed above, is given in reference 7.

b) Configuration mixing effects.

However it is known that such an analysis ignores effects such as electron correlation. As a result, the best wave function for a particular state is not necessarily that corresponding to the simple central field approximation[6] description of that state. An improved wave function may be obtained by taking appropriate linear combinations of all those wavefunctions derived from states of identical symmetry[11]

i.e. $$\Psi_j = a_j\varphi_1 + b_j\varphi_2 + c_j\varphi_3 + \ldots\ldots m_j\varphi_n$$

Thus any excited ionised state will nominally consist in part of an electron configuration of the same symmetry, directly accessible to photoionisation by removal of one electron. The intensity of the transition to such an excited ionised state will be governed by the square of the appropriate configuration mixing co-efficient m_j.

Such a situation has been described as "intensity borrowing by configuration mixing,"[12] as the intensity of the formally allowed band (corresponding to the one electron transition) is reduced; the sum of the squares of the configuration mixing co-efficients being equal to unity. In this way, the weaker bands are regarded as having borrowed intensity from the allowed transition(s).

However only those ideal configurations of identical spin, parity ($\sum 1$) and J value may mix with the predominant configuration to produce the new wave function and so result in new bands. Thus we need only consider excited states of the same term manifold as those ionic states produced on direct ionisation.

In the CY_2 species under discussion we must consider alternative $^2\Pi g$, $^2\Pi u$, $^2\Sigma u^+$, $^2\Sigma g^+$ states.

c) Energy cycles for ionisation and excitation.

The energy of these electronically excited ionic states may conveniently be analysed in terms of the cycle shown in Figure 4.[13] This involves alternative ionisation and excitation paths. From the p.e. spectrum[14] we can obtain reliable values for I1, and from the optical spectrum[15] we may obtain values for the various E2 transitions. However we cannot obtain experimentally determined values for either I2 or E1, but as a first approximation may assume, I1 = I2. This would seem reasonable, as it is the same electron which is ionised from the same orbital in each case.

Thus we may use the right hand path of Figure 4 to estimate the energy of the excited ion.

It should be noted that although the left hand path may also be used, it is much less reliable to assume E2 = E1, as the former involves $a, b^4 c^0 \longrightarrow b^3 c^1$ excitation, but the latter $a, b^3 c^0 \longrightarrow b^2 c^1$

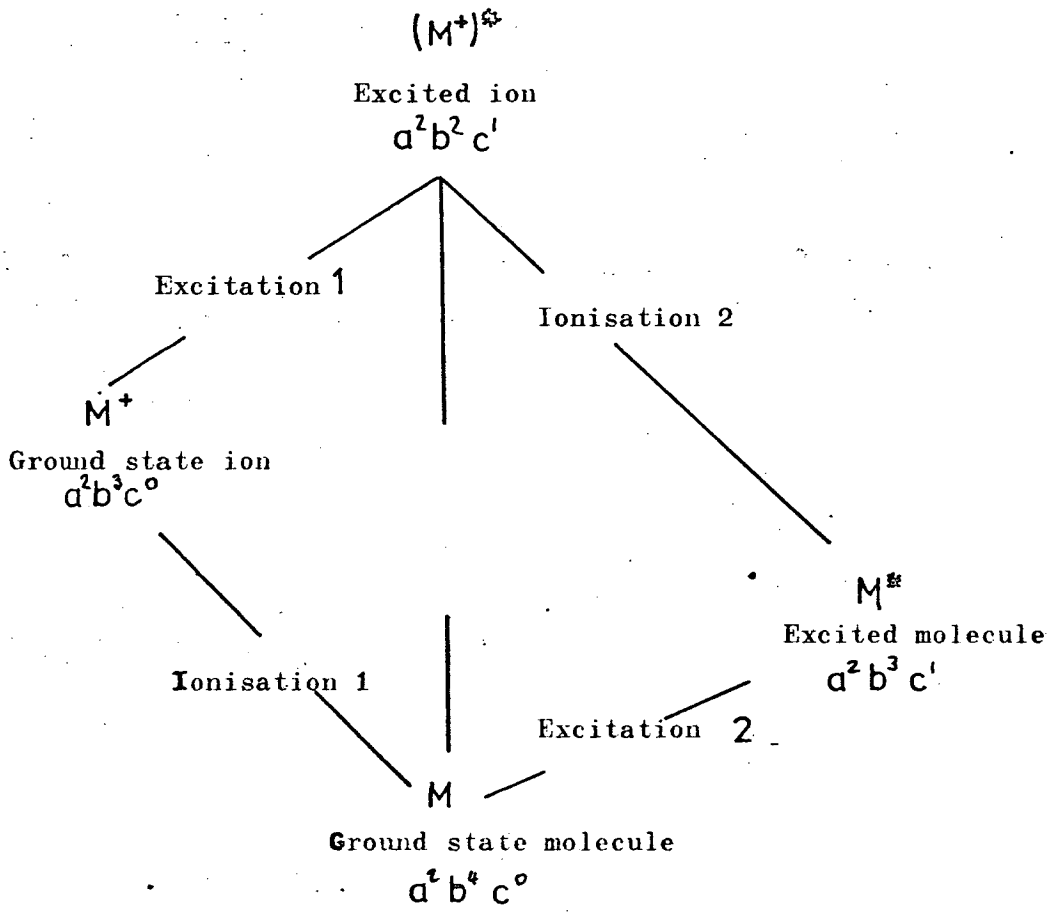
$(M^+)^*$
Excited ion
$a^2b^2c^1$
Excitation 1
Ionisation 2
M^+
Ground state ion
$a^2b^3c^0$
M^*
Excited molecule
$a^2b^3c^1$
Ionisation 1
Excitation 2
M
Ground state molecule
$a^2b^4c^0$

Figure 4.

transition. Such are the magnitudes of the configuration splittings observed in the electronic spectra of these molecules that it would be misleading to regard both E1 and E2 as purely $c^0 \longrightarrow c^1$ transitions.

The first excited state in these molecules, corresponding to the configuration $(....1\pi_u^4 \; 1\pi_g^3 \; 2\pi_u^1)$ can give rise to 6 states for a linear molecule [16]

i.e. $^1\Sigma_u^+$, $^1\Delta_u$, $^1\Sigma_u^-$, $^3\Sigma_u^+$, $^3\Delta$, $^3\Sigma_u^-$.

According to the selection rules which are discussed fully in the next chapter, only the transition $^1\Sigma_g^+ \longrightarrow {}^1\Sigma_u^+$, will be fully allowed. However states of the configuration $(..1\pi_g^3 \; 2\pi_u^1)$ are almost certainly non-linear and so the $^1\Sigma_g^+ \longrightarrow {}^1\Delta_u$ transition is allowed by a vibronic interaction mechanism involving bending. Thus the energies of the first two strong band systems observed in the visible/ultraviolet spectrum of these molecules correspond to the transitions to the $^1\Delta_u$ and $^1\Sigma_u^+$ states respectively and their energies are listed in Table 1.

The corresponding excitation in the $^2\Pi_g$ state leads to the configuration $(....1\pi_g^2 \; 2\pi_u^1)$ and this gives rise to five states. These may be derived as follows: the $1\pi_g^2$ part of the configuration generates $^1\Delta_g$, $^1\Sigma_g$ and $^3\Sigma_g$ states, each of which combines with the remaining $2\pi_u$ electron as follows:-

$$\begin{array}{lcll} \underline{(\pi_g)^2} & & \underline{(\pi_u)^1} & \underline{\pi_g^2\pi_u^1} \\ {}^1\Delta_g & \times & {}^2\Pi_u & \rightleftharpoons \; {}^2\Phi_u \; + \; {}^2\Pi_u \\ {}^1\Sigma_g & \times & {}^2\Pi_u & \longrightarrow \; {}^2\Pi_u \\ {}^3\Sigma_g & \times & {}^2\Pi_u & \rightleftharpoons \; {}^2\Pi_u \; + \; {}^4\Pi_u \end{array}$$

i.e. the excited ion configuration $(...1\pi_g^2 \; 2\pi_u^1)$ gives rise to a $^2\Phi_u$, $^4\Pi_u$ and <u>three</u> $^2\Pi_u$ states. [17]

Of these the $^2\Pi_u$ states are of the same symmetry as the states produced on ionisation of the $1\pi_u$ valence levels.

Optical Transition Energies (e.V.) from $^1\Sigma_g^+$ state.

Molecule	$^1\Sigma g^+ \rightarrow (..1\pi g^3 2\pi u^1)$		$^1\Sigma g^+ \rightarrow (.1\pi g^3\ 3\sigma g^1)$	$^1\Sigma g^+ \rightarrow (..1\pi g^3 3\sigma u^1)$
	$^1\Delta u$	$^1\Sigma u^+$	$^1\Pi g$	$^1\Pi u$
CO_2	8.4	11.1	10.6	~ 12
OCS	5.2	8,1	~ 8.0	~ 9.2
CS_2	3.9	6,3	6.8	~ 8
SCSe	3.5	5.7	~ 6.4	~ 7.6
OCSe	4.9	5.8	7.2	8.4
CSe_2	3.3	5.4	6.1	7.3

TABLE 1.

Molecule	$^1\Sigma g^+ \rightarrow {}^2\Pi g$	$^1\Sigma g^+ \rightarrow {}^2\Pi u$		$^1\Sigma g^+ \rightarrow {}^2\Pi u$	
		calculated	observed	calculated	observed.
CO_2	13.8	22.2	22.6	24.9	27.2
OCS	11.2	16.4	-	19.3	20.1
CS_2	10.1	14.0	14.1	16.4	17.1
SCSe	9.6	13.1	13.3	15.3	16.0
OCSe	10.4	15.3	-	16.2	-
CSe_2	9.3	12.6	12.7	14.7	15.3

TABLE 2.

Comparison of observed and calculated energies of excited $^2\Pi$ states.

In order to calculate the energy of these $^2\Pi u$ states let us return to the cycle in Figure 4. As an example, we shall use the CSe_2 system.

First of all we should note that ionisation of a $1\pi g$ electron from the $^1\Delta u$ ($\ldots 1\pi g^3\ 2\pi u^1$) configuration leads to $^2\Pi u$ and $^2\Phi u$ states and a similar ionisation from the corresponding $^1\Sigma u^{\pm}$ states leads to the remaining two $^2\Pi u$ states. Thus it is valid to use the excitation energies corresponding to these $^1\Delta u$ and $^1\Sigma u^{\pm}$ states followed by ionisation from the $1\pi g$ level to generate the excited $^2\Pi u$ states. However as the $^1\Sigma g^+ \rightarrow {}^1\Sigma u^-$ transition is strongly forbidden it is not possible to estimate the energy of the $^2\Pi u$ state derived from it.

Using the known excitation energies to the $^1\Delta u$ and $^1\Sigma u^+$ states in CSe_2 and the first I.P., we estimate that the other $^2\Pi u$ states will occur at apparent I.P's of 9.3 + 3.3 = 12.6 e.V and 9.3 + 5.4 = 14.7e.V respectively. These predictions may be favourably compared with the weak bands observed at 12.7 e.V and 15.3 e.V.

d) Comparison of observed and predicted results.

The results, along with those for other molecules in the series are presented in Table 2. The correlation is quite reasonable when due allowance is made for the gross simplifications assumed in deriving the predicted values. The principal value of the predictions is that they give a good idea of where to expect these features, which being very weak can easily be missed. From the results in Table 2 we can see that we would not expect to see these forbidden bands in the He(I) spectrum of CO_2 but that they should occur in the He(II) spectrum, i.e. Figure 5(b). Also the fact that they are not observed in the He(I) spectra of OCS and OCSe is due to the fact that they

occur in regions of the spectrum so dominated by the intense valence transitions that they are obscured by them.

It is perhaps worth stressing at this point that although we have discussed these features in terms of ionisation and excitation sequences, and have used an energy cycle based on such schemes to estimate their energies, there can be no question that they arise by other than one photon processes. Since the He(I) resonance line does not produce a continuum in the ultra-violet, it is not possible for such bands to arise from stepwise ionisation and excitation processes. The mechanism for their formation is an allowed simultaneous two electron transition induced by one photon as a result of configuration mixing with a fully allowed ionic state of the same symmetry.

e) Vibrational structure in forbidden bands.

Another feature of all these bands worthy of comment is their continuous nature. It was shown in the case of CS_2^+, that this was not due to lifetime broadening.[10] However the explanation of the origin of these bands in terms of transitions to electronically excited states of the ion with the configuration $(\ldots 1\pi u^4\ 1\pi g^2\ 2\pi u^1)$ readily provides an explanation for this diffuseness. It is well known from the electronic spectra of the neutral molecules, that on populating the $2\pi u$ level, the nuclear skeleton ceases to be linear.[18] This is responsible for the highly complex pattern of vibronic structure associated with the $^1\Delta u$ and $^1\Sigma u^+$ transitions. Likewise, the equilibrium position in these excited $^2\Pi u$ states of the ion will also be non-linear, for the $2\pi u$ level is again populated. As a result of the partial relaxation of the selection rules occurring in a linear $\rightarrow$ non linear transition, excitation of the low frequency bending mode as well as Renner Teller complications could lead to a highly

structured band, which under the resolution of the spectrometer would appear diffuse.

5. FORBIDDEN BANDS IN He(II) SPECTRA.

As there is little confusion between these "weak" features and the main valence bands, an understanding of these bands is not really essential to the interpretation of the major features of the He(I) spectra. Nevertheless, it is pleasing to be able to account for all the bands observed.

a) Reasons for the proliferation of forbidden bands in He(II) spectra.

However in the interpretation of the He(II) spectra of these molecules it is essential to consider the possibility of these "forbidden" bands. In fact in the region above 20 e.V. they dominate the He(II) spectra as shown in Figures 5 to 10.

As a consequence of the strong He(I) output still present in the discharge, the He(II) line only allows ionisations up to about 25 e.V. to be distinguished from that due to He(I). Nevertheless in the region up to 25 e.V. many new weak features are observed in all the spectra.

The reasons why the He(II) spectra, compared with the He(I) spectra, are so dominated by these weak configuration mixing features may be explained as follows:-

i) The absence of any valence level ionisations in the region 20 - 25 e.V. means that these weak formally forbidden bands are not obscured by the much more intense valence bands. In fact this may be the reason why so few configuration mixing bands are observed in He(I) spectra.

ii) The forbidden bands generally appear much stronger in the He(II) spectra than in the He(I) spectra. This effect is most noticeable in the He(II) spectrum of

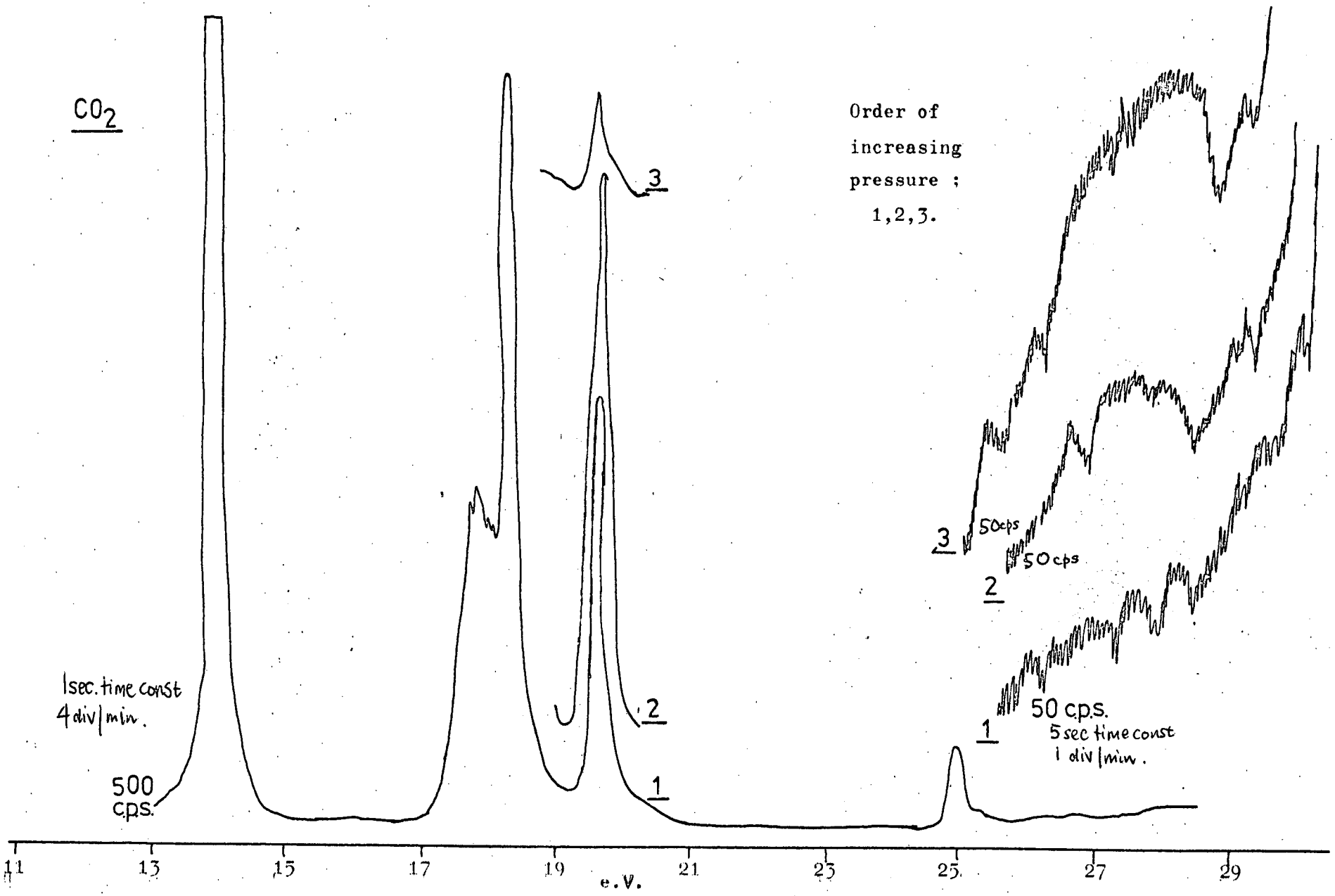
CO_2
Order of increasing pressure ; 1,2,3.
3
2
1
1sec. time const
4 div/min.
500 cps.
50cps
50cps
50 c.p.s.
5 sec time const
1 div/min.
11
13
15
17
19
21
23
25
27
29
e.V.

Figure 5.

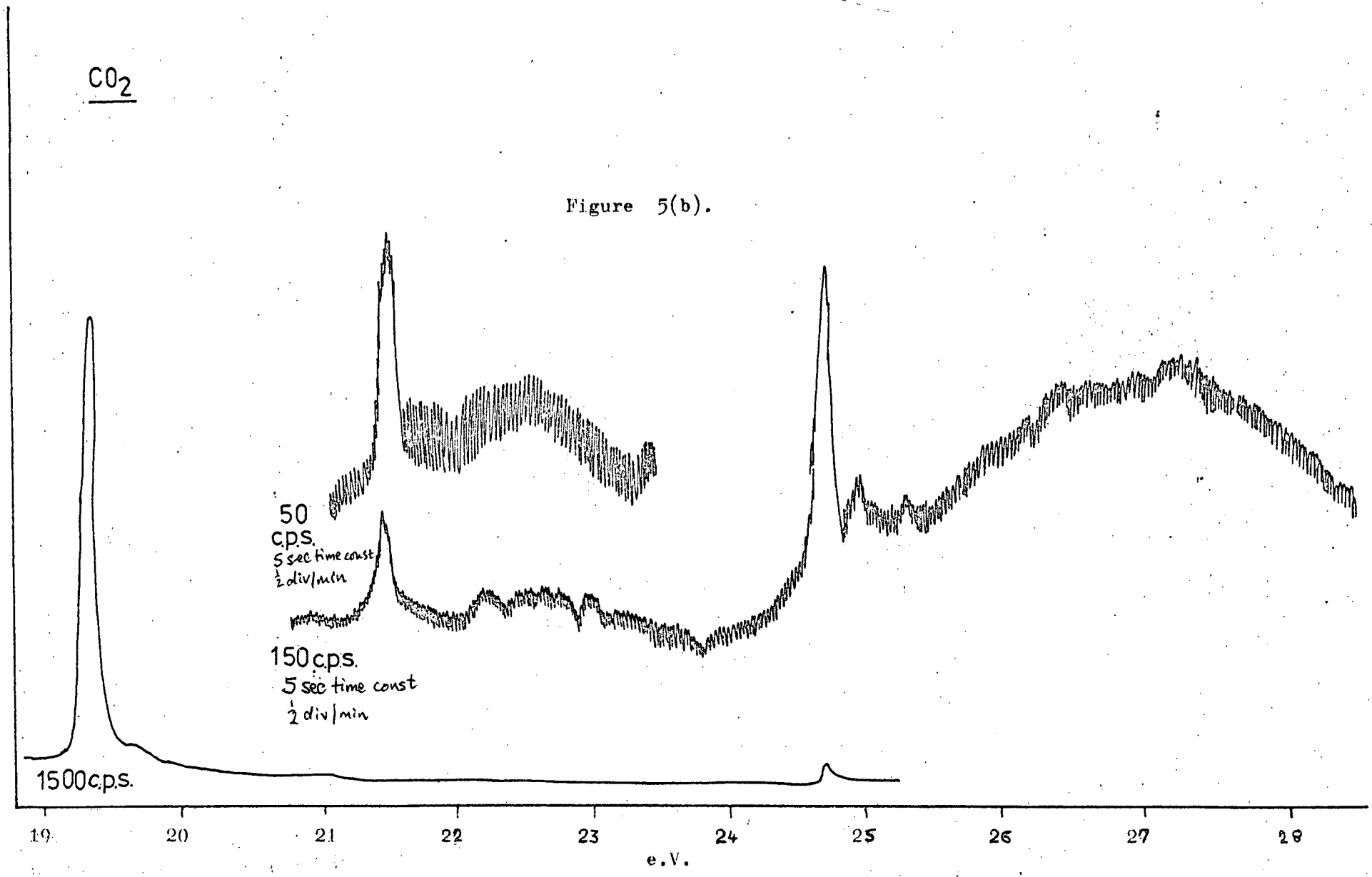
CO_2
50
c.p.s.
5 sec time const
½ div/min
150 c.p.s.
5 sec time const
½ div/min
1500 c.p.s.
19
20
21
22
23
24
25
26
27
28
e.V.

Figure 5(b).

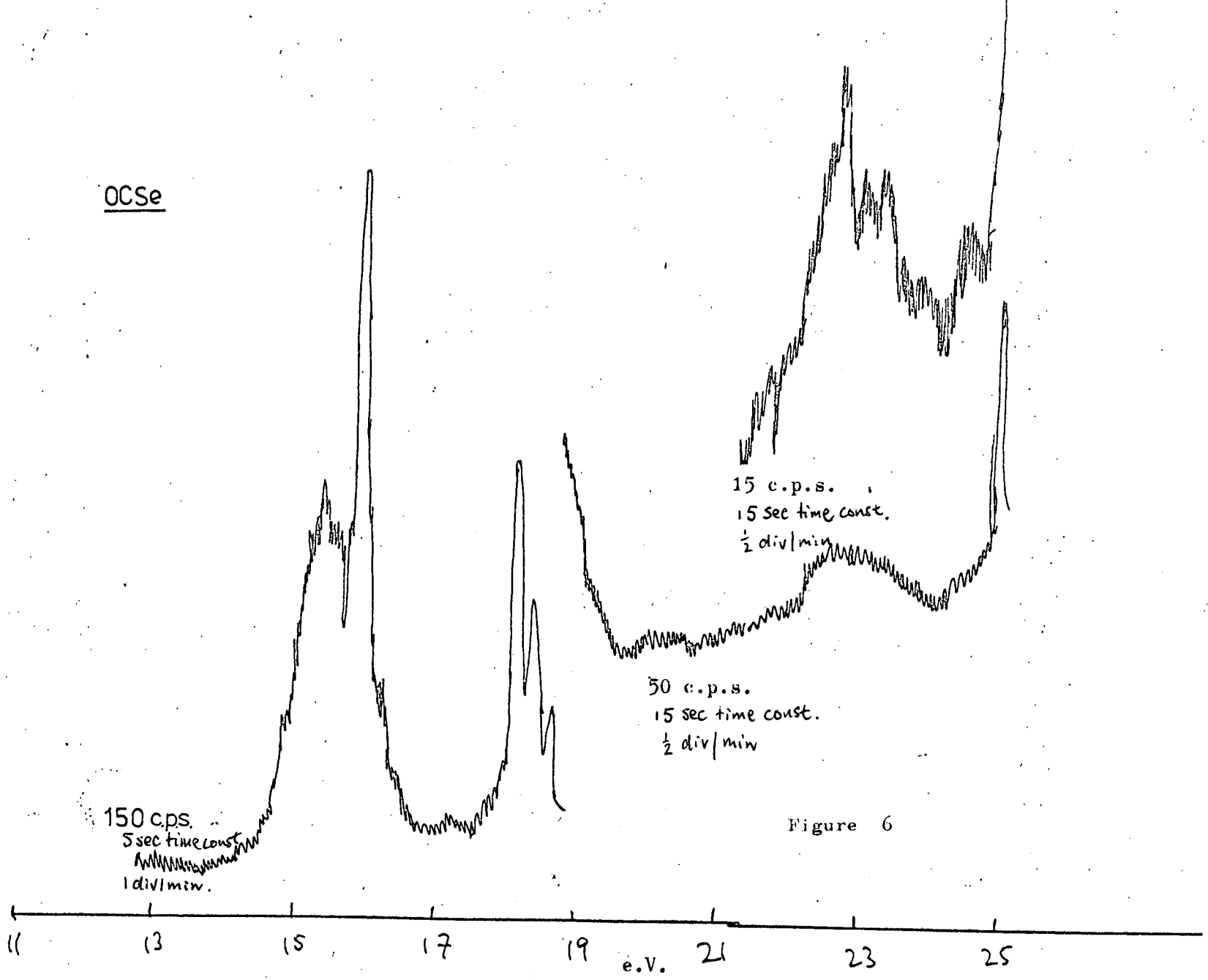
OCSe
150 c.p.s.
5 sec time const.
1 div/min.
50 c.p.s.
15 sec time const.
½ div/min
15 c.p.s.
15 sec time const.
½ div/min
11
13
15
17
19
e.V.
21
23
25

Figure 6

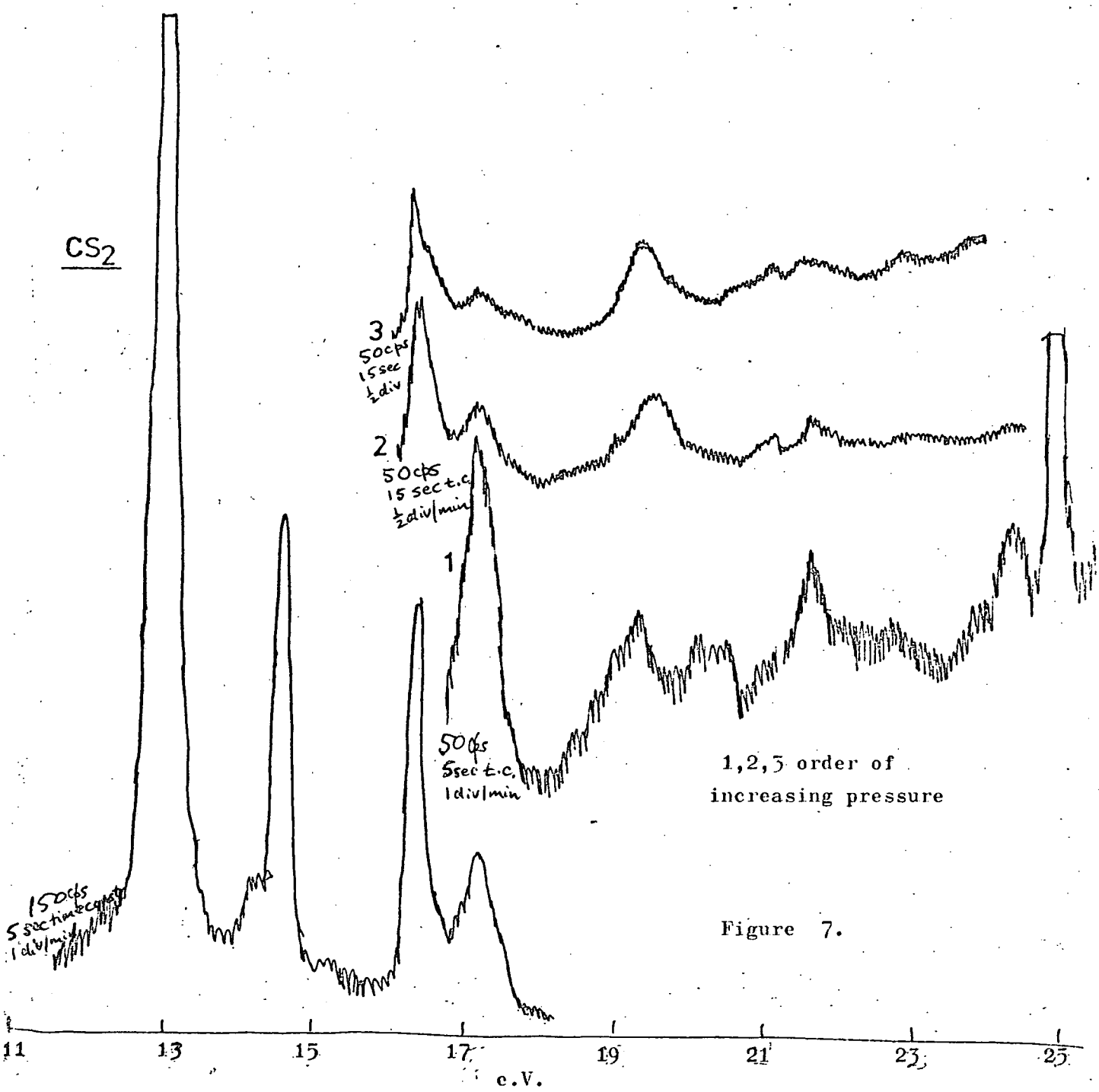
CS2
3
50cps
15sec
½div
2
50cps
15 sec t.c
½div/min
1
50cps
5sec t.c.
1div/min
1,2,3 order of
increasing pressure
11
13
15
17
19
21
23
25
e.V.

Figure 7.

SCSe

Figure 8

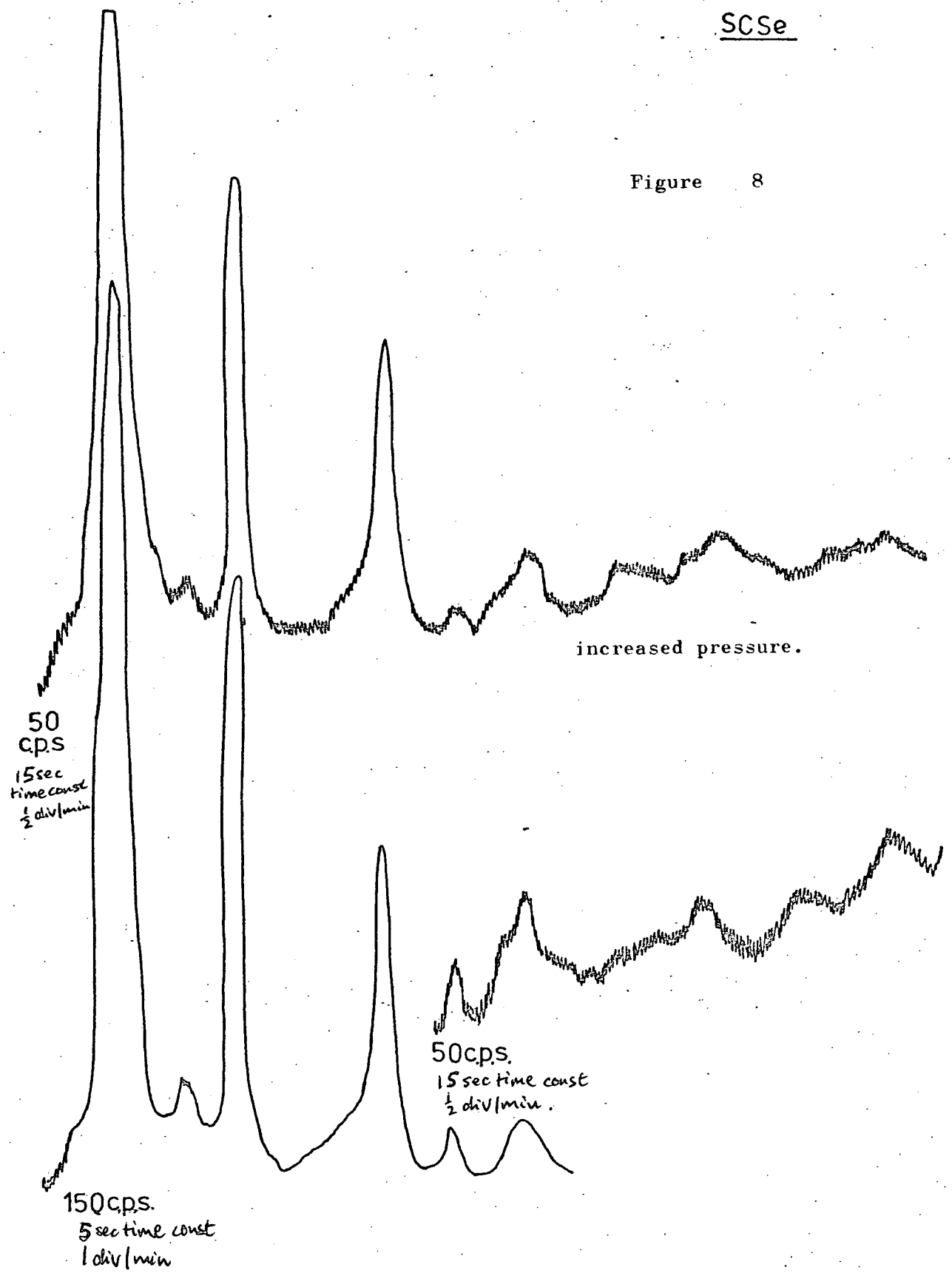

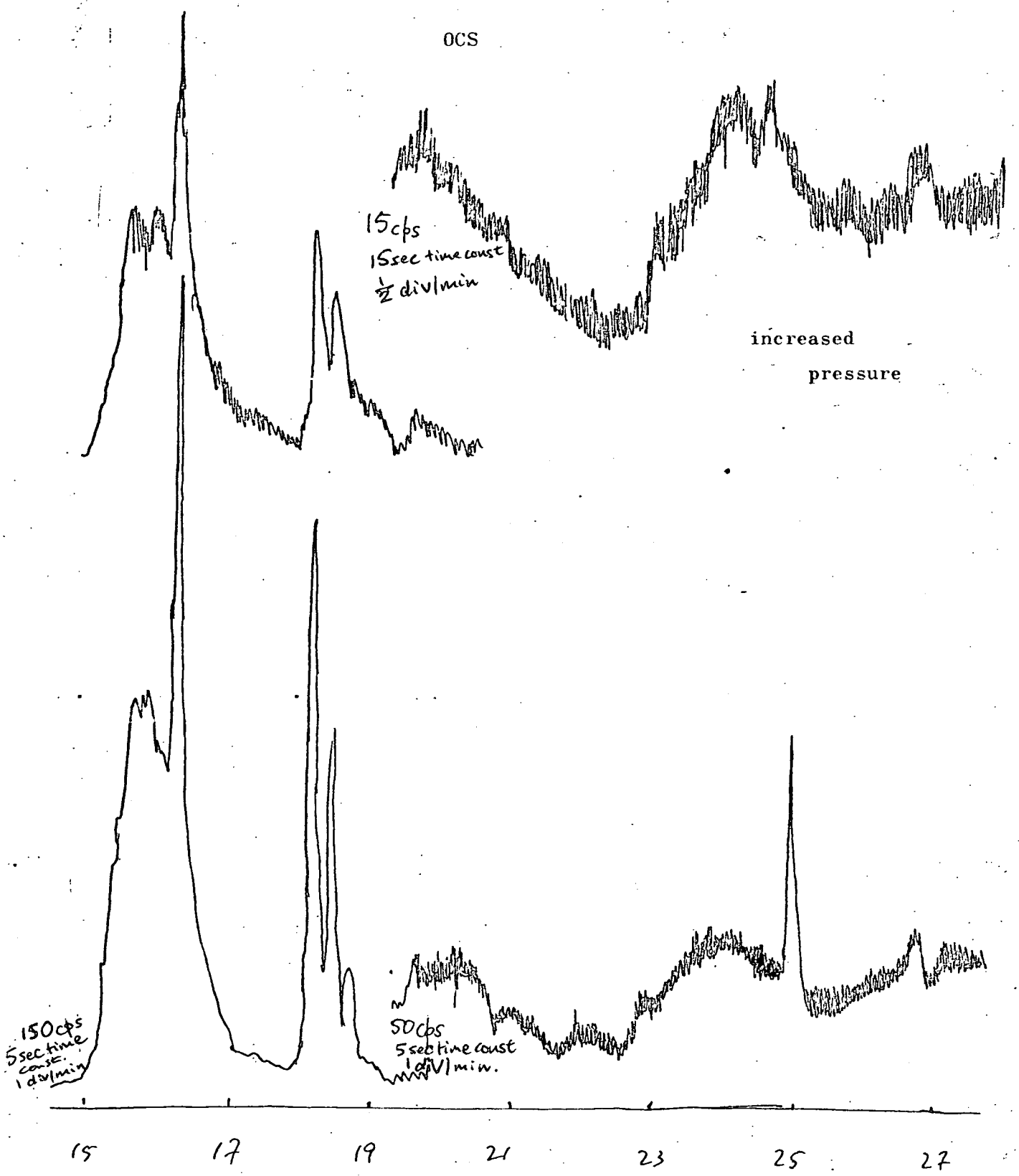
OCS
15cps
15sec time const
½ div/min
increased
pressure
150cps
5sec time
const.
1 div/min
50cps
5sec time const
1 div/min.
15
17
19
21
23
25
27

Figure 9.

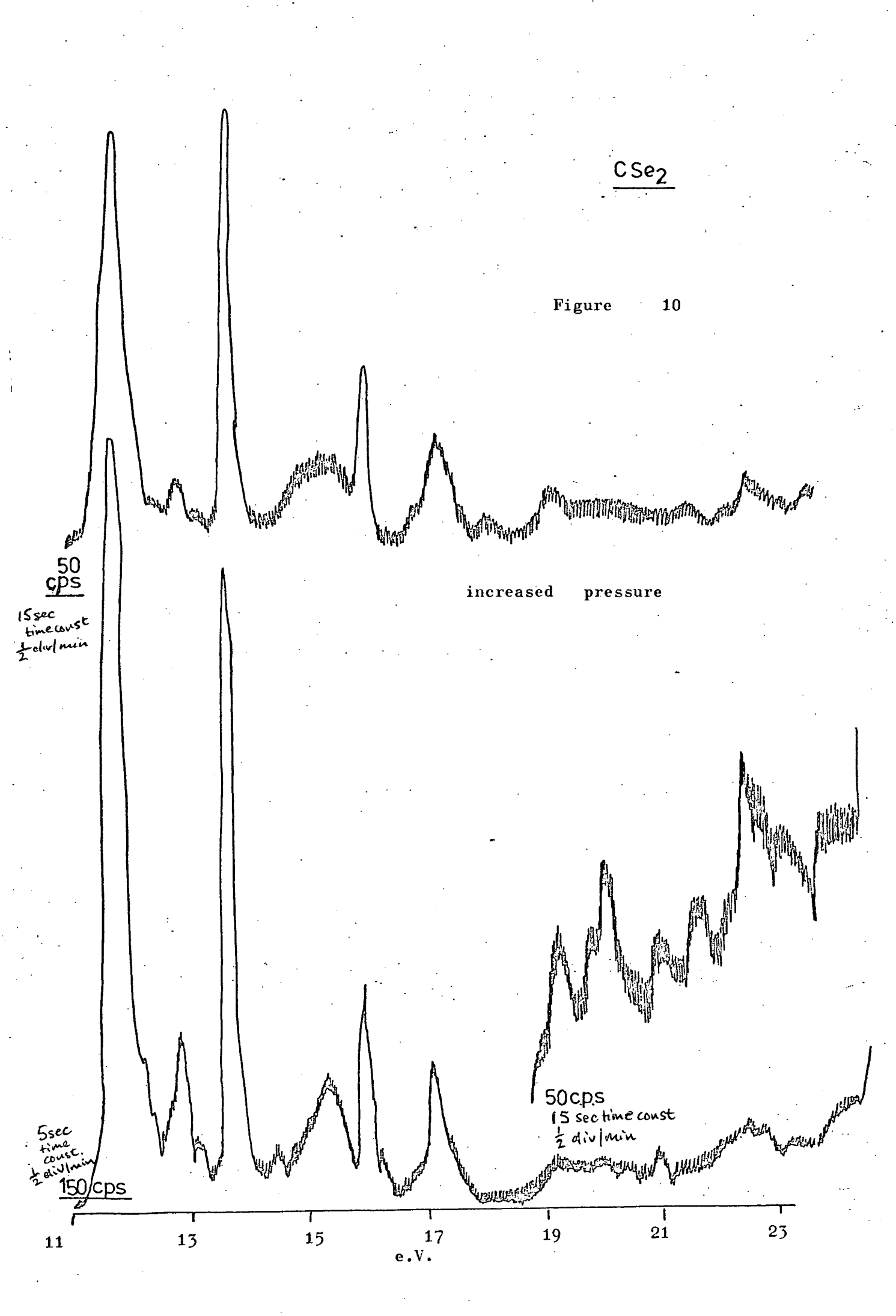
CSe_2
50 cps
15 sec time const
½ div/min
increased pressure
50 c.p.s
15 sec time const
½ div/min
5 sec time const.
½ div/min
150 cps
11
13
15
17
19
21
23
e.V.

Figure 10

CSe_2 Fig.10 where the configuration mixing bands at 15.3 and 17.1 e.V. are of comparable intensity to the $(2\sigma g)^{-1}$ band at 16.2 e.V. It is also worth noting that relative to the fully allowed valence level ionisation bands, the intensity of these forbidden bands increases on going down the series CO_2 to CSe_2. This implies that in the lighter molecules, the configuration mixing coefficients for the higher energy excited ionic states (mj) are much smaller, with the one electron description of the wavefunctions more reliable, than is the case in the heavier analogues, where configuration mixing is an important factor.

iii) There are many excited ionised states of the correct symmetry to mix with and borrow intensity from the allowed $^2\Sigma_g^+$, $^2\Sigma_u^+$, $^2\Pi_u$ states.[6] While it was only necessary to consider two of these excited states to account for the weak features in the He(I) spectrum, many of the others lie in the higher energy region of the spectrum and are only accessible using He(II) radiation.

(b) Discussion and assignments.

Although all the He(II) spectra reveal many of these forbidden bands there are not enough of them for all the possible configuration mixing states to be populated. There are 34 possible excited ionised states derived from atomic p orbitals alone, which can mix with and borrow intensity from the fully allowed states. The major problem associated with assigning these observed features to the most likely excited ionic states, is that there are several near coincidences in

the energies predicted from ionisation and excitation cycles, and the band envelopes are often sufficiently broad to encompass several possible predictions. As a result our analysis does not allow us to formulate the selection rules which must apply to these bands - that approximate selection rules must exist cannot be in doubt, otherwise we would observe many more bands.

The excited ionic states derived by ionisation from all upper valence levels of the various known excited states of these molecules are given in Table 3. From it we observe that only in the case of ionisation from the σ levels of the $^1\Delta$ state do we generate ionic states of different symmetry to the fully allowed ionic states. In Table 4 the calculations of the excited ionic states produced using the ionisation + excitation schemes detailed in Figure 3 are presented. These may be compared with the forbidden features observed in the He(I) and He(II) spectra.

It should be noted that several alternative assignments exist. For example, it is possible that the bands listed in Table 2 and which were assigned to the second, higher energy, $^2\Pi u$ state, could also be assigned to the $^2\Pi g$ state (.... $1\pi u^3\ 1\pi g^3\ 2\pi u^1$) derived from the $^1\Sigma g \longrightarrow {}^1\Delta u$ excitation followed by ionisation from the πu level.

Nevertheless, the bands observed may be accounted for on the basis of transitions to excited ionic states deriving intensity from configuration mixing intensity borrowing.

(c) Pressure effects in He(I) and He(II) spectra.

In coming to this conclusion it was necessary to verify that none of the bands was "pressure dependent," as this would imply a multi-step process leading to its formation. The He(II) spectra of these molecules recorded at higher pressures of the sample in the

Excited neutral state.	Ionisation from	Final excited ionic states.	Electron configuration.
$^1\Delta_u$	$1\pi g$	$^2\Pi u + {}^2\Phi g$	$(..\ 1\pi_u^4 . 1\pi g^2 . 2\pi u^1)$
	$1\pi u$	$^2\Pi g + {}^2\Phi g$	$(..\ 1\pi u^3 . 1\pi g^3 . 2\pi u^1)$
	$2\sigma u$	$^2\Delta g$	$(2\sigma g^2 . 2\sigma_u^1 . 1\pi u^4 . 1\pi g^3 . 2\pi u^1)$
	$2\sigma g$	$^2\Delta u$	$(2\sigma g^1 . 2\sigma_u^2 . 1\pi u^4 . 1\pi g^3 . 2\pi u^1)$
$^1\Sigma_u^{\pm}$	$1\pi g$	$^2\Pi u + {}^2\Pi u$	$(..\ 1\pi u^4 . 1\pi g^2 . 2\pi u^1)$
	$1\pi u$	$^2\Pi g + {}^2\Pi g$	$(..\ 1\pi u^3 . 1\pi g^3 . 2\pi u^1)$
	$2\sigma u$	$^2\Sigma g$	$(2\sigma g^2 . 2\sigma u^1 . 1\pi u^4 . 1\pi g^3 . 2\pi u^1)$
	$2\sigma u$	$^2\Sigma u$	$(2\sigma g^1 . 2\sigma u^2 . 1\pi u^4 . 1\pi g^3 . 2\pi u^1)$
$^1\Pi g$	$1\pi g$	$^2\Sigma g + {}^2\Delta g$	$(..\ 1\pi u^4 . 1\pi g^2 . 3\sigma g^1)$
	$1\pi u$	$^2\Sigma u + {}^2\Delta u$	$(..\ 1\pi u^3 . 1\pi g^3 . 3\sigma g^1)$
	$2\sigma u$	$^2\Pi u$	$(2\sigma g^2 . 2\sigma u^1 . 1\pi u^4 . 1\pi g^3 . 3\sigma g^1)$
	$2\sigma g$	$^2\Pi g$	$(2\sigma g^1 . 2\sigma u^2 . 1\pi u^4 . 1\pi g^3 . 3\sigma g^1)$
$^1\Pi u$	$1\pi g$	$^2\Sigma u + {}^2\Delta u$	$(..\ 1\pi u^4 . 1\pi g^2 . 3\sigma u^1)$
	$1\pi u$	$^2\Sigma g + {}^2\Delta u$	$(..\ 1\pi u^3 . 1\pi g^3 . 3\sigma u^1)$
	$2\sigma u$	$^2\Pi g$	$(2\sigma g^2 . 2\sigma u^1 . 1\pi u^4 . 1\pi g^3 . 3\sigma u^1)$
	$2\sigma g$	$^2\Pi u$	$(2\sigma g^1 . 2\sigma u^2 . 1\pi u^4 . 1\pi u^3 . 3\sigma u^1)$

TABLE 3.

$^1\Delta(u)$	CO_2		CS_2		CSe_2		OCS		OCSe		SCSe	
	calc	obs	calc	obs	calc	obs	calc	obs	calc	obs	calc	obs
$1\pi g$	22·2	22·6	14·0	14·1	12·6	12·7	16·4	–	15·3	–	13·1	13·3
$1\pi u$	26·0	27·2	16.75	17·1	15·05	15·3	20·7	20·1	20·1	20	15·55	15·7
$^1\Sigma(u)^+$												
$1\pi g$	24·9	27·2	16.4	17·1	14·9	15·3	19·3	20·1	16·2	–	15·3	15·7
$1\pi u$	28·7	27·2	19.15	19·0	17·15	17·1	23·6	23·5	20·9	–	17·95	18·1
$2\sigma u$	29·2	29·5	21.05	21·35	19·0	19·4	24·1	23·5	21·5	–	19·75	–
$2\sigma g$	30·5	29·5	22.5	22·3	21·3	21·2	26·1	26·4	23·7	23·0	21·7	22·0
$^1\Pi(g)$												
$1\pi g$	24·4	–	17·3	17·1	15·4	15·3	19·2	–	17·6	–	16·0	15·7
$1\pi u$	28·2	27·2	20·05	20·2	17·84	–	23·5	23·6	22·3	22·4	18·65	18·11
$2\sigma u$	29·4	29·5	21·95	21·56	19·7	19·4	24·0	23·5	22·9	22·4	20·45	20·6
$2\sigma g$	30·0	29·5	23·4	23·9	22·0	21·7	26·0	26·4	25·9	–	22·4	22·0
$^1\Pi u$												
$1\pi g$	25·8	27·2	18·3	18·9	16·7	17·1	20·4	20·14	18·8	–	17·2	17·2
$1\pi u$	28·6	29·5	21·08	21·35	19·14	19·4	24·7	–	23·5	23·6	19·85	–
$2\sigma u$	30·8	–	22·95	–	21·0	21·2	25·2	–	24·1	24·1	21·65	–
$2\sigma g$	31·4	–			23·3	23·6	27·2	–	26·3	23·6	23·1	–

TABLE 4.

Comparison of predicted and observed energies of excited ionic states of $^2\Pi u$, $^2\Pi g$, $^2\Sigma u^+$, $^2\Sigma g^+$, symmetry.

target region are shown in Figures 5 to 10. Only in the case of CO_2, Figure 5, did any of the weak features increase in intensity with increased pressure and only then with a small shift in position.

The effect of increased pressure of sample is shown in Figure 11 where the number of electron counts (per second) is plotted against the number of turns of the inlet needle valve for the observed bands of CO_2. In using the number of turns of the inlet needle valve as a co-ordinate axis we are assuming that the sample pressure in the target region increases with the number of turns. Unfortunately it was not possible to measure the pressure directly in the target region of the spectrometer with sufficient accuracy to determine whether or not the pressure increased linearly with the number of turns although, such a condition is not essential to our argument.

The overall shape of the curves produced by the valence bands shows that the number of counts increases rapidly with pressure until it reaches a plateau between 4 and 7 turns, but instead of continuing to rise it then slowly falls, eventually to zero, with ever increasing pressure. This indicates that at higher sample pressures, the photo-ejected electrons interact with the parent molecule instead of reaching the analyser. The electrons may be scattered as a result of this interaction, but since the detection system is only designed to accept those electrons emitted perpendicular to the photon beam, this will not only result in a considerable reduction in intensity, but is also likely to produce a diffuse background to the band. However for certain electrons with particular energies it is possible for the interaction to result in electron impact type phenomena[20] and this should give rise to new fairly well defined bands.

Thus the pressure dependence of the band in CO_2 at 27 e.V. Figure 5 is in marked contrast to that exhibited by the valence

Figure 11

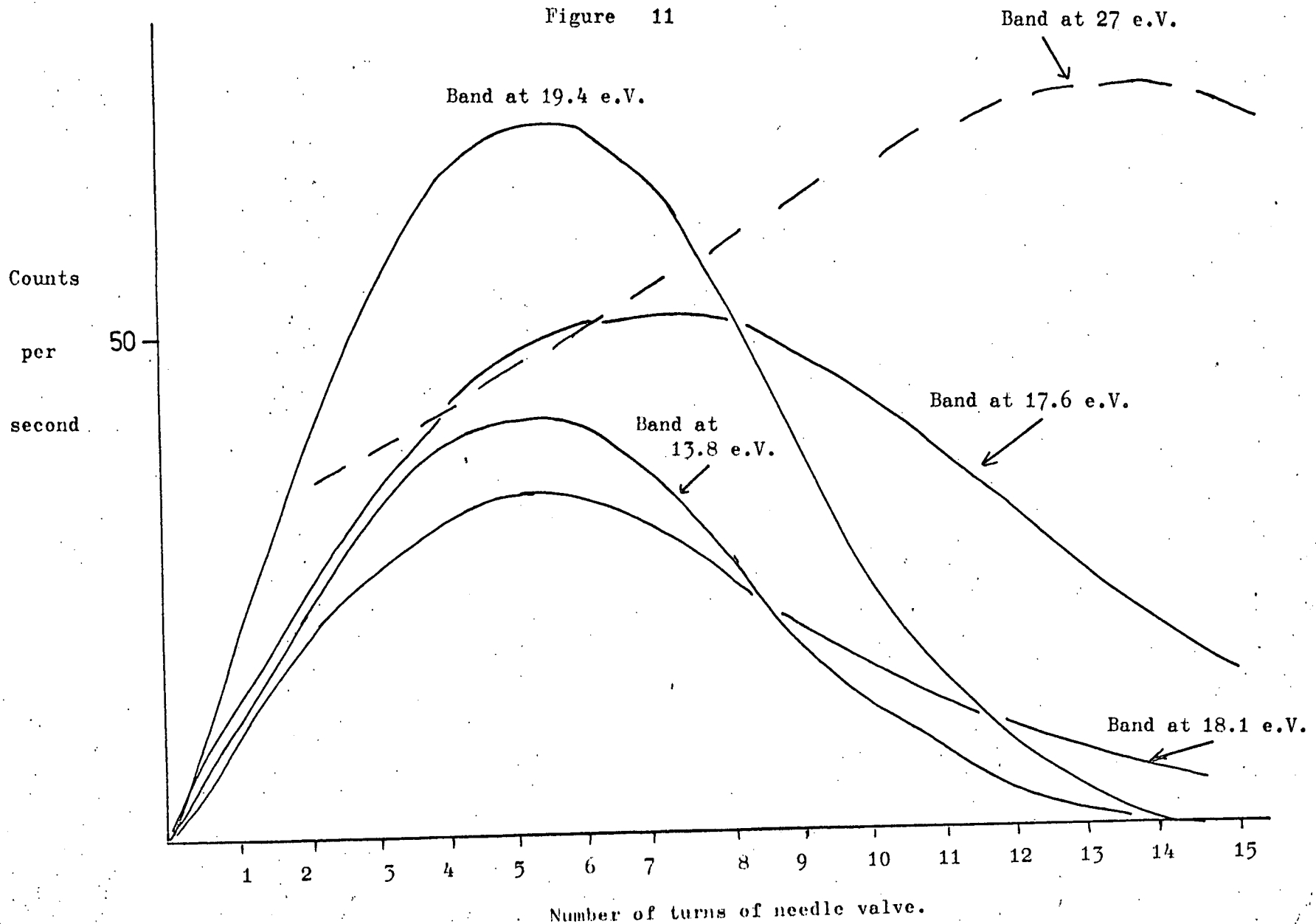
Band at 27 e.V.
Band at 19.4 e.V.
Counts
per
second
50
Band at 17.6 e.V.
Band at
13.8 e.V.
Band at 18.1 e.V.
1
2
3
4
5
6
7
8
9
10
11
12
13
14
15
Number of turns of needle valve.

bands. In this case, the number of counts continues to rise, reaching a high plateau, at pressures when the valence bands have all but disappeared. It is therefore likely that the band observed in 27 e.V. is an example of such an electron impact interaction and may be tentatively assigned to a process such as,

$$CO_2 + h\nu_{40.8\ e.V.} \longrightarrow CO_2^{+}\ (X^2\Pi g) + e^{-}(27\ e.V.)$$

$$e^{-}(27\ e.V.) + CO_2 \rightarrow e^{-} + [CO_2]^{*} \longrightarrow CO_2^{+}(X^2\Pi g) + e^{-}(27 - I)\ e.V.$$

$$I = 13.8\ e.V.$$

Thus as a result of impact by the 27 e.V. electron, another electron with a Kinetic Energy of 13.2 is ejected. This would appear at an apparent I.P. of (40.8 - 13.2) = 27.6 e.V. Furthermore we would expect the appearance of such a band to depend on the pressure of CO_2 since the probability of electron capture increases with increasing pressure.

Other examples of electron molecule interactions have been noted in the He(I) spectrum of CO_2 when recorded with high sample pressures and the lack of observed structure in the bands attributed to the instability of the compound negative ions.[21] The effect of increasing the sample pressure on the He(I) spectrum of OCS is shown in Figure 12. Here it is observed that the $A^2\Pi$ band almost disappears under the $B^2\Sigma$ band which now shows considerably enhanced vibrational structure when compared with the lower pressure spectrum. In addition the higher I.P. $C^2\Sigma$ band is almost buried under the high background of randomly scattered electrons.

However, no pressure effects, analogous to those of CO_2 , were observed in the He(II) spectra of the other molecules in this series and so we may confidently assign all the weak bands observed in their spectra as arising from configuration mixing of states of the same term manifold as the allowed simple one electron ionisation states.

Figure 12

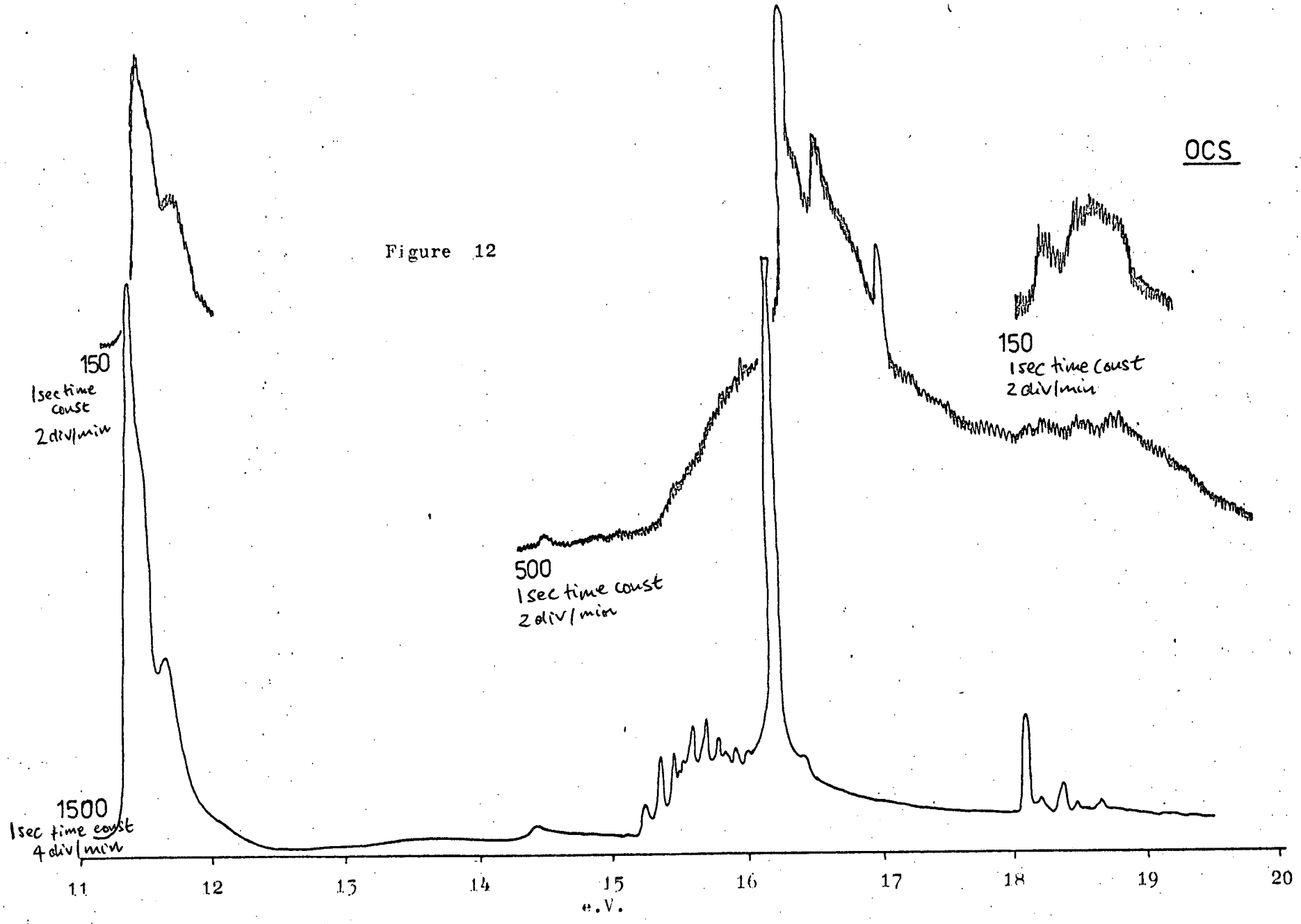
OCS
150
1sec time coust
2div/min
500
1sec time coust
2div/min
150
1sec time coust
2div/min
1500
1sec time coust
4div/min
11
12
13
14
15
16
17
18
19
20
e.V.

REFERENCES.

1. A.D. Baker and D. Betteridge; Photoelectron Spectroscopy; Pergamon Press, 1972.

2. D.C. Frost, C.A. McDowell and D.A. Vroom; Chem. Phys. Letts. (1967), 1, 93.

3a. K. Nakamoto; Infra-red Spectra of Inorganic and Co-ordination Compounds; Wiley Interscience 2nd Edition (1970).

b. R.S. Draco; Physical Methods in Inorganic Chemistry; Reinhold Publishing Corporation, London. (1965).

4. R.L. DeKock, D.R. Lloyd; Adv. Inorg. Chem. and Radiochem. (1974), 16, 65.

5. A.L. Stewart; Adv. At. Mol. Phys. (1967), 3, 1.

6. A.W. Potts, and T.A. Williams; J. Elect. Spectros. (1974), 3, 3.

7. H.H. Jaffe and M. Orchin; Theory and Application of Ultra-violet Spectroscopy; Wiley and Sons, New York and London. (1962), 123.

8. D.W. Turner, C. Baker, A.D. Baker, C.R. Bundle; Molecular Photoelectron Spectroscopy; Wiley Interscience (1970).

9. C.J. Allan, U. Gelius, O.A. Allison, G. Johansson, H. Seigbahn and K. Seigbahn; J. Electron Spectros. (1972/73), 1, 131.

10. B. Brehm, J.H.D. Eland, R. Frey and A. Kustler; Int. J. Mass. Spect. Ion Phys. (1973), 12, 213.

11. W.G. Richards and J.A. Horsley; Ab initio mo. calculations for Chemists, O.U.P. (1970), 37.

12. J.C. Lorquet and C. Cadet; Int. J. Mass Spectr. Ion Phys. (1971), 463.

13. S. Cradock and W. Duncan; Journal of the Chem. Soc. Faraday Trans. II. (1975), 71, 1262.

14. D.C. Frost, S.T. Lee and C.A. McDowell; J. Chem. Phys. (1973), 59, 5484.

15. A.B. Callear and W.J.R. Tyerman; Trans. Farad. Soc. (1965). 61, 2395.

16. J.W. Rabalais, J.M. McDonald, V. Scherr and S.P. McGlynn; Chem. Rev. (1971), 71, 73.

17. G. Hezberg; "Electronic Spectra and Electronic Structure of Polyatomic Molecules" Van Nostrand (1966).

18. A.D. Walsh; J. Chem. Soc. (1953), 2266.

19. G. Duxbury; to be published, (personal communication).

20. I.C. Walker; Annual Reports; (1974), 71, 49.

21. D.G. Streets, A.W. Potts and W.C. Price; Int. J. Mass Spectr. Ion Phys. (1972/73), 10, 123.

CHAPTER 3

THE ELECTRONIC SPECTRA OF CSe_2, SCSe and OCSe.

CHAPTER 3. Page No.

1) INTRODUCTION.

a) Selection Rules.

In the previous chapters we have examined in detail the various ionic states of CSe_2 , SCSe, OCSe produced by electronic transitions from the filled valence shell levels into the continuum.

In this chapter we will again be concerned with electronic transitions produced by vac. u.v. radiation, from the filled valence shell levels, but this time into successively higher energy bound states of the neutral molecule.

As observed in the Introduction, such excitations may be classified into -

(a) intervalence transitions

(b) extravalence (Rydberg) transitions.

on the basis of their successive term values.[1]

However, the intensity of both is again governed by an expression of the type

$$D = \left| \langle \Xi_i | M | \Xi_f \rangle \right|^2$$

D = dipole strength , M = dipole moment vector

Ξ_i = overall wave function for state i

Ξ_f = overall wave function for state f.

similar to that encountered previously in the explanation of photoelectron band intensities.[2] The conditions under which such expressions vanish identically (i.e. equal zero) again yield the selection rules. In the case of an electronic transition to a bound state, the selection rules are of much more assistance in choosing between possible assignments, than is usually the case in photoelectron spectra. This is a consequence of the fact that whereas the photo ejected electron can assume whatever angular

momentum is required to satisfy the selection rules without affecting the energy of the transition,[3] in the case of an electron in a bound orbit, these different values of ℓ correspond to transitions to different states.

The selection rules for electronic transitions in linear molecules are similar to those of diatomic molecules except that due allowance has to be made for the influence of the larger number of vibrational modes.[4]

It is often possible to use the symmetry properties of the wave functions to predict whether or not the integral will vanish. These symmetry based selection rules stem from the fact that the product $\Psi_i \times \Psi_f$ must transform as (belong to) the same symmetry species as at least one of the components of M. However, as the three components of M can <u>at most</u> belong to only three different symmetry species, and in molecules of high symmetry e.g. $C_{\infty v}$, $D_{\infty h}$ may only belong to two, $\Psi_i \times \Psi_f$ may belong to a symmetry species to which M does not belong.

This would correspond to a forbidden transition. It is also the case that when an integrand is an odd function of the integration co-ordinates, the integrand will vanish.[2]

We should also distinguish clearly between rigorous electric dipole selection rules and approximate selection rules which depend on the extent to which assumptions, such as the Born-Oppenheimer approximation[5] or the coupling conditions,[6] are valid.

The rigorous selection rules[7] for an electric dipole transition in a linear molecule are

$$\Delta J = 0, \pm 1 \quad ; \quad J = 0 \not\leftrightarrow J = 0.$$

J = total angular momentum.

which is identical to the atomic case, assuming zero nuclear spin.

As the symmetry properties of the molecular wave functions do not depend on the coupling conditions, transitions between rotational levels governed by -

$$+ \leftrightarrow - , \qquad + \not\leftrightarrow + , \; - \not\leftrightarrow -$$

and when applicable -

$$s \leftrightarrow a , \qquad a \not\leftrightarrow a , \; s \not\leftrightarrow s$$

also applies.

For linear molecules -

$$g \leftrightarrow u , \qquad g \not\leftrightarrow g , \; u \not\leftrightarrow u$$

The additional selection rules depend on the coupling conditions. Thus in situations where the electronic states may be identified according to the value of Λ as $\Sigma, \Pi, \Delta, \Theta$ then only transitions between states such that

$$\Delta \Lambda = 0, \pm 1 \quad \text{are allowed.}$$

This permits $\Sigma \leftrightarrow \Sigma$, $\Sigma \leftrightarrow \Pi$ but not $\Sigma \leftrightarrow \Delta$ transitions. In addition when both initial and final states have $\Lambda = 0$, it can be shown that

$$\Sigma^{+} \leftrightarrow \Sigma^{+} \qquad \Sigma^{-} \leftrightarrow \Sigma^{-} \quad \text{but} \quad \Sigma^{+} \not\leftrightarrow \Sigma^{-}$$

Provided spin orbit coupling is not too large, the total spin angular momentum remains unchanged in a transition i.e. $\Delta S = 0$, and prevents transitions between states of different multiplicity. Furthermore when $\mathcal{\Sigma}$ is a good quantum number (i.e. Hunds case (a))

$$\Delta \mathcal{\Sigma} = 0$$

(n.b. do not confuse $\mathcal{\Sigma}$ with Σ which is a state with $\Lambda = 0$.)

When Ω the axial component of J, is also conserved i.e. Hund's cases (a) and (e),[5] then

$$\Delta \Omega = 0, \pm 1 \; ; \quad \text{except for } J = 0 \text{ when } \Omega : 0 \not\leftrightarrow \Omega = 0$$

For singlet to singlet transitions this is equivalent to the $\Delta \Lambda = 0, \pm 1$ rule and prevents the appearance of Q branches in $^1\Sigma \longleftrightarrow {}^1\Sigma$ transitions.

In other cases where Ω and Λ are not defined, then similar selection rules hold for the quantum numbers defining the angular momentum.

Detailed proofs of these selection rules are given in Reference 8, but it will be instructive to consider in a far less rigorous fashion the g $\longleftrightarrow$ u and spin multiplicity rules, as examples of how such rules may be derived.[2]

Thus for molecules with a centre of symmetry the transition moment will be zero unless the overall function is gerade (g). Now all components of M are necessarily ungerade (u) and so the product $\Psi_i \times \Psi_f$ must also be (u) for the total integral to be (g). This can only happen if Ψ_i is (g), and Ψ_f is (u), or vice versa, but not if both Ψ_i or Ψ_f are either u or g. In this way only g$\leftrightarrow$ u is allowed.

In transitions which involve a change of spin e.g. singlet to triplet, the transition moment may be written as equal to -

$$\int \Psi_i \alpha M \Psi_f \beta \, d\tau \, d\sigma$$

where α and β are spin wave functions of opposite sign.

This may be arranged to give

$$\int \Psi_i M \Psi_f \int \alpha \beta \, d\sigma$$

$d\sigma$ = volume element of spin co-ordinates

However, the integrand $\alpha \beta$ is an odd function and so the total integral vanishes. Thus singlet to triplet transitions are forbidden.

As a consequence of these rules only a few of the large number of transitions which otherwise would be possible are seen to occur.

Furthermore proposed assignments should correspond to transitions which obey these rules.

However in practice the situation tends to be less well defined and "forbidden transitions" may be observed as a result of interaction with the magnetic dipole or electric quadrupole vector of the radiation. These interactions each possess distinct selection rules and a transition forbidden by the electric dipole selection rules may be allowed under these new selection rules.[4]

However, such interactions tend to be very much weaker than the electric dipole transitions and rarely contribute to the major spectral features.

A more common cause of forbidden transitions occurring with reasonable intensity is due to violations of the approximate selection rules when the quantum numbers involved are no longer wholly valid. Thus although we have shown that singlet to triplet transitions are formally forbidden, they may occur as a result of spin orbit coupling effects. Thus although it is useful to distinguish between states on the basis of their multiplicity, by assuming that the orbital and spin angular momenta are independent, such an assumption is not always wholly valid. As a result of the small interaction which exists between states of identical total angular momentum, the spin orbit integrals of the form :-

$$\int {}^{1}\underline{\Psi}_{i} \, . \, M \, . \, {}^{3}\underline{\Psi}_{f}$$

do not vanish identically, and their use in the appropriate secular leads to two final wave functions of the form:

$$\underline{\Psi} = \alpha \, {}^{1}\underline{\Psi} + \beta \, {}^{3}\underline{\Psi}$$

of which one possesses largely singlet and the other mainly triplet character.

Thus the admixture of small amount of singlet character into what would have been an otherwise wholly triplet function , results in transitions to this state with intensities proportional to the mixing co-efficient α^2 .

Coupling Schemes.

In the higher quantum levels of the lighter elements and in most of the Rydberg states of the heavier elements, the spin momenta of the Rydberg and core electrons are sufficiently reduced for (L,S) coupling schemes to be no longer valid.[4]

Instead we must employ (J,j) coulpling which allows for the interaction of the core electron spin with its own angular momentum. In this scheme the spin and orbital angular momentum of each electron is coupled to form a resultant angular momentum with quantum number j_i, i.e.

$$L_i + S_i = J_i$$

and the electrostatic interactions cause these individual J_i values to couple and form a resultant J.

$$\text{i.e.} \quad J = \Sigma J_i : J_i = \Sigma j_i , \Sigma j_{i-1}$$

Thus we have a situation in which there is strong interaction between states of similar J value and not too surprisingly, we find the $\Delta S = 0$ and ΔL selection rules do not apply as S and L are no longer good quantum numbers. Instead the selection rules are -

$$\Delta J = 0, \pm 1 \text{ and } \Delta j = 0, \pm 1.$$

Unfortunately, at high quantum number levels other perturba-:tions may occur but a clear example of this change in coupling schemes is to be found in PII. As can be seen in Figure 1, at low n, the $^1P_1$ and $^3P_{0,1,2}$ states corresponding to the configuration

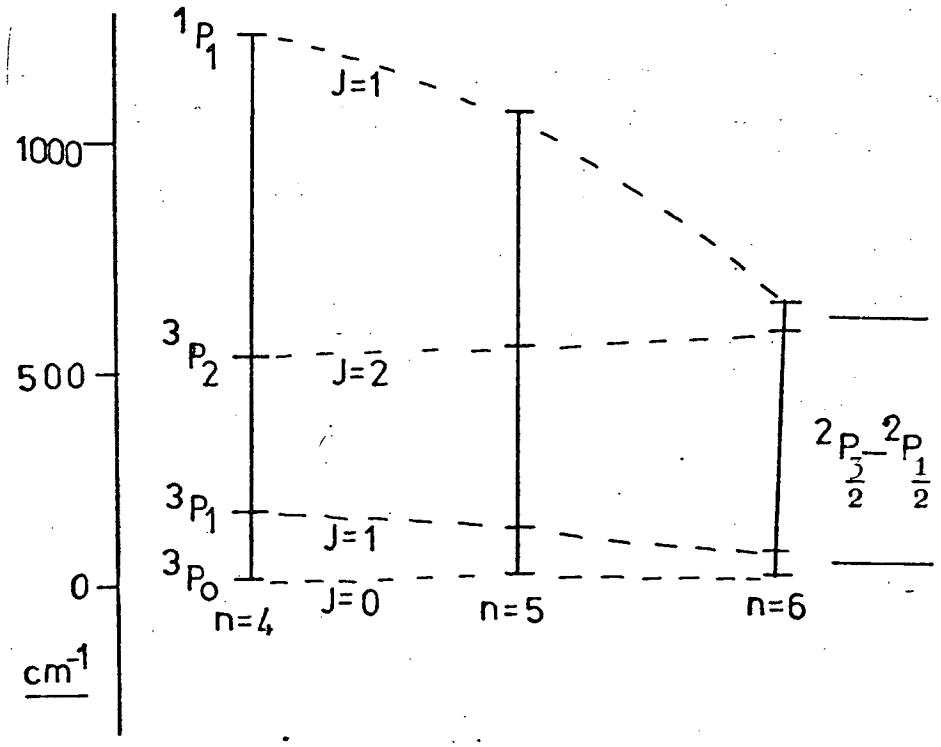

Figure 1

Coupling schemes in P(II).

ns n′p, (n + 1) n′p. etc. are clearly distinguished on the basis of multiplicity, however as n increases, the energy of $^1P_1$ and $^3P_2$ states approach each other, as do the energies of the $^3Po,_1$ levels.

In the limit the separation between $^1P_1$ / $^3P_2$ level and the $^3P_o/^3P_1$ levels approaches that of the $^2P_{\frac{3}{2}} - {}^2P_{\frac{1}{2}}$ separation in PIII.

Thus if there is a change in coupling scheme on going to higher quantum levels, then there should be a corresponding change in the observed splittings between different multiplet components of the series. Furthermore if no change in multiplet splitting is observed with increasing n, and the splitting is close to the spin orbit coupling of the ion, then the coupling may be assumed to be (J,j) throughout. The molecular analogue of (J,j) coupling is (Ω_c, ω) coupling. In this Ω_c is the total angular momentum of the core and ω that of the Rydberg electron. It should be emphasised , however, that both (Λ,S) and (Ω_c,ω) coupling schemes lead to exactly the same number of multiplet states and the same values of J. Only their energy separation is different.

Selection Rules for Triatomic Species.

Whereas the breaches of the selection rules discussed thus far apply equally well to diatomics and other linear molecules, there are two other causes of breakdown of the selection rules which do not apply in the diatomic case. Thus, if on excitation, the nuclear geometry does not remain linear, but bends in the excited state so formed, certain quantum numbers or symmetries are no longer defined and so some of the selection rules do not apply. Also, if strong vibronic interactions exist in one of the states involved in a transition forbidden by electric dipole selection rules, then this interaction may cause certain vibronic transitions (but not the 0-0 band) to become allowed. Thus although a $^1\Sigma_g^+ \longleftrightarrow {}^1\Sigma_g^+$ transition is forbidden, if a σ_u^+ vibration is singly excited, the resulting vibronic transition would be $^1\Sigma_u^+ \longleftrightarrow {}^1\Sigma_g^+$ and thus allowed.[4]

Furthermore, it should be recognised that unlike the situation for diatomics where there are no selection rules for the vibronic transitions, this is not the case for all linear molecules. Thus although the relative intensity in both systems are given by the Franck Condon factors

i.e. $\left| \int \chi_{v'} \chi_v \, d\tau_v \right|^2$

these must be totally symmetric for the particular vibrational transition to be allowed. Only if there are no symmetry operations to which the integrand is antisymmetric will the integral be non-vanishing.

In the case when there are two (or more) totally symmetric vibrations then we obtain not only progressions in each of the vibrations, but also in combinations of them. This can result in a

considerably more complex vibrational pattern for a linear triatomic than for a diatomic, as shown in Figure 2.

The degenerate bending mode in linear molecules $\Pi(u)$ is non totally symmetric and only transitions in even values of Δv_k can occur. Such vibrations are also characterised by the quantum number l_k for which the selection rule $\Delta l_k = 0$ applies. In addition the intensity of successive transitions in non-totally symmetric vibrations always declines rapidly, whereas in totally symmetric vibrations the relative intensity pattern can often reach its maximum only at high v_k. The reason for this, based on the differences in potential surfaces between ground and excited states, has been discussed previously in relation to photoelectron spectra band envelopes.

As in diatomics, we can also find sequence structure on the low energy side of the vibrational progressions. As shown in Figure 3 these sequences correspond to groups of band with the same Δv_k but as $v' < v''$ so the (0-0), (1-1), (2-2) transitions occur at successively lower energies. However, unlike diatomics, it is now possible to have sequences in single quanta of all totally symmetric modes and in double quanta of non totally symmetric modes. Both types of sequences exhibit similar relative intensity patterns and in the case of the excitation of the bending mode frequency, the higher statistical weight can lead to moderate intensity.

Further complications can arise from transitions to or from orbitally degenerate states e.g. $^1\Pi$ or $^1\Delta$. As a result of vibronic interaction, a splitting occurs in the vibrational levels of the degenerate state in which one or more quanta of the degenerate bending vibrations is excited. These splittings, call Renner-Teller

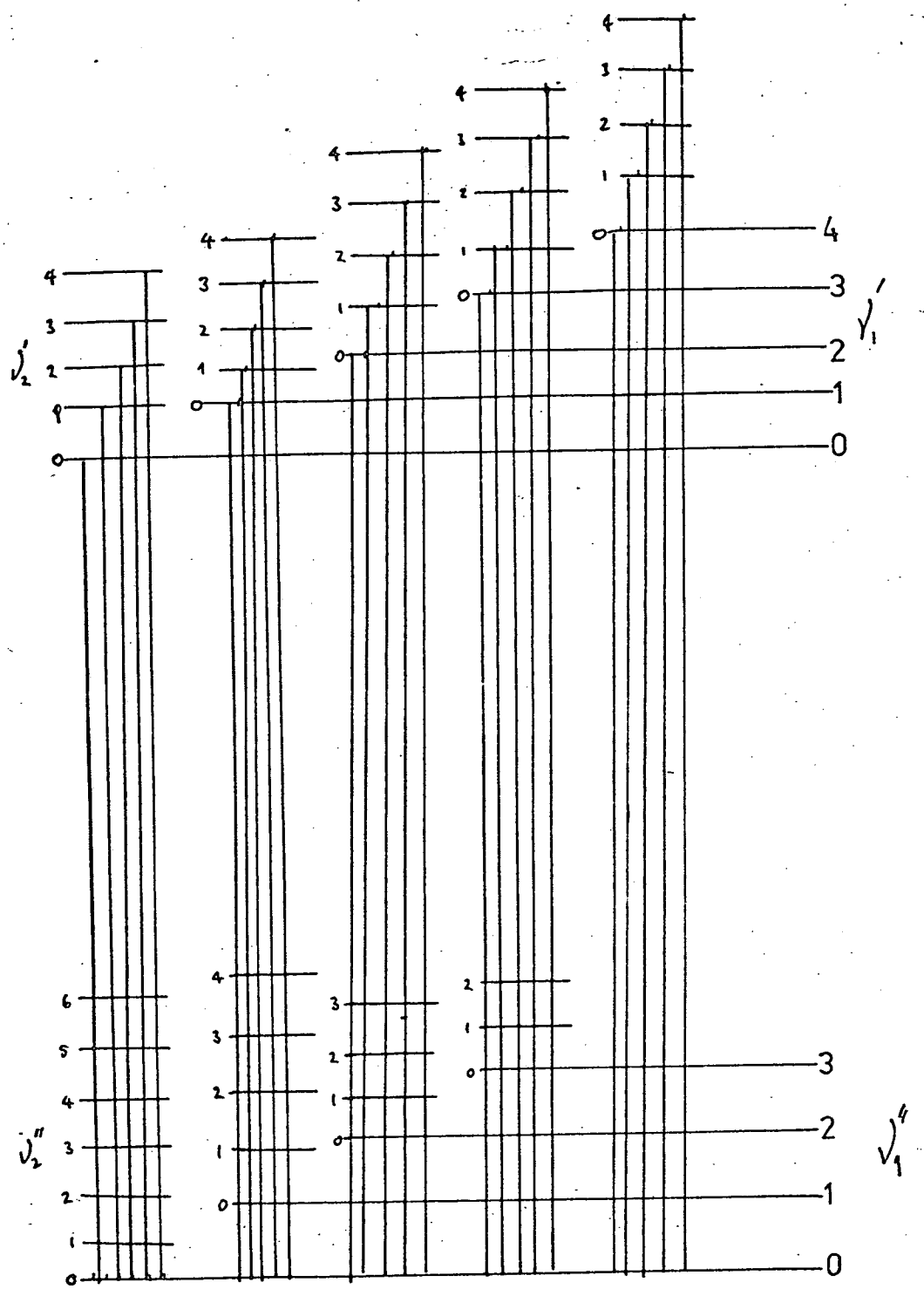

Figure 2

Progressions in two totally symmetric vibrations ν_1 and ν_2.

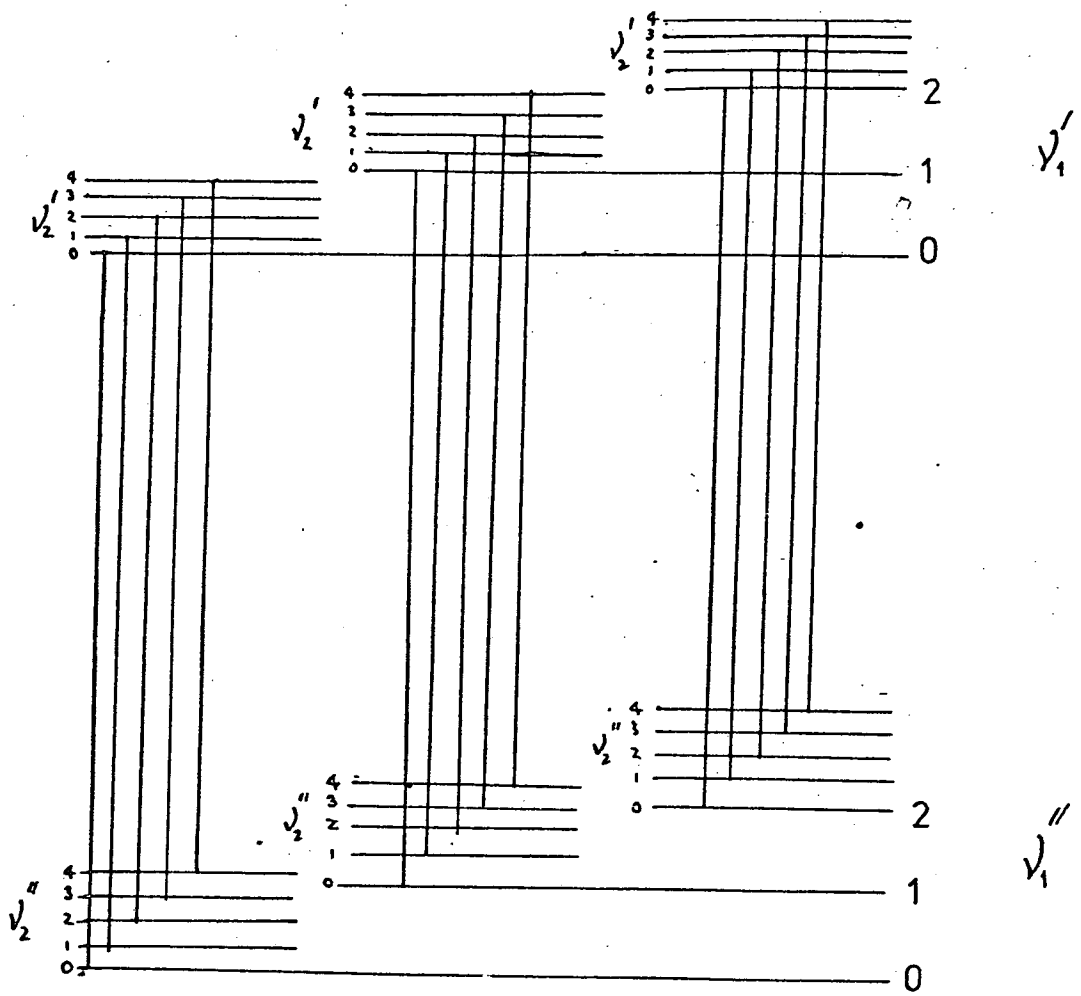

Figure 3

Sequence structure.

splittings,[4] can result in several more transitions being observed as shown in Figure 4. When the separation of the Renner-Teller components is large, analysis of the resultant spectrum can be difficult. A detailed account of this phenomena and its effect on the electronic spectra of triatomic molecules has appeared recently.[10]

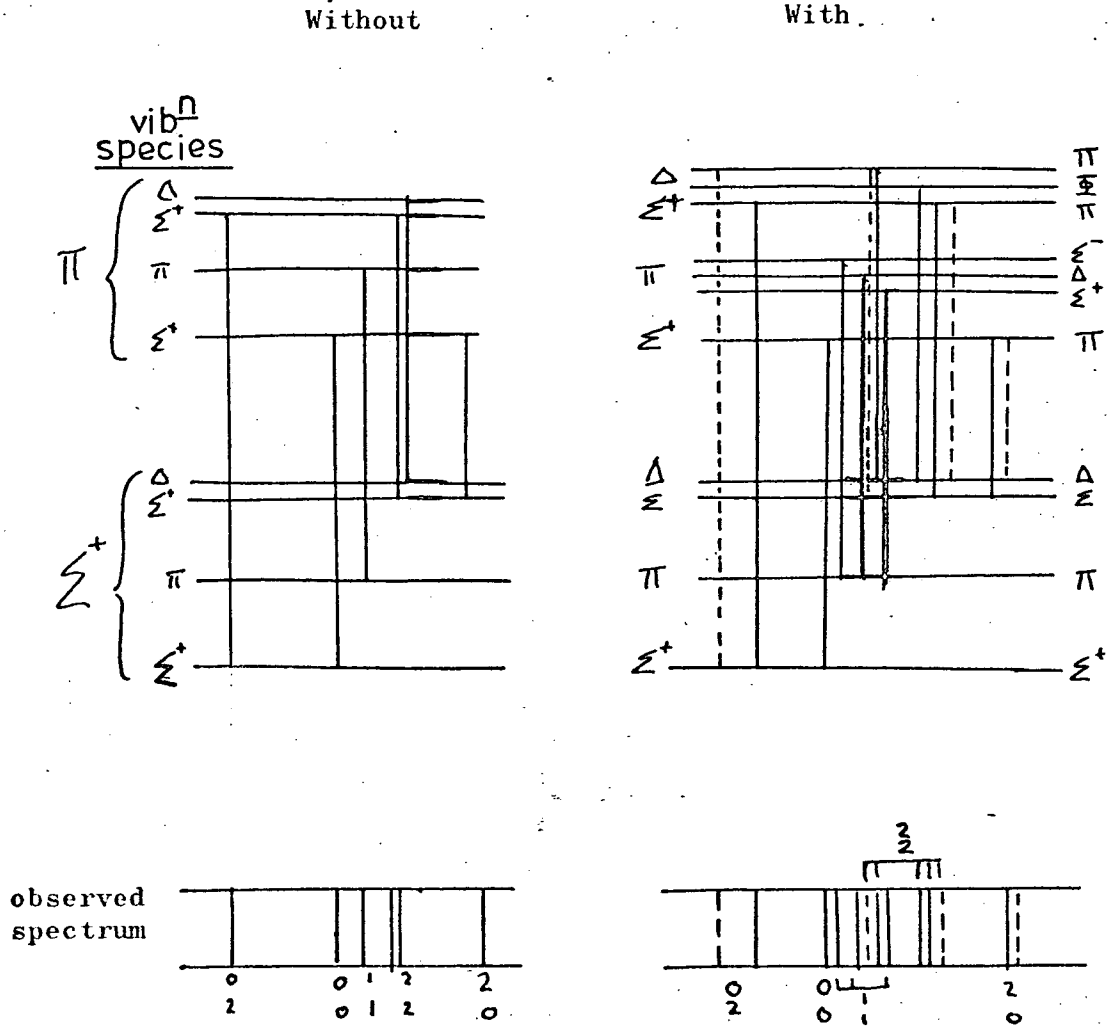

Figure 4

Renner Teller Effect.

2. THE VISIBLE/u.v. SPECTRUM of CSe_2, SCSe and OCSe.

a) Selection rules.

We are now able to use the selection rules given above to identify the allowed transitions in CSe_2. The selection rules for the other Se containing triatomics SCSe and OCSe will be basically similar, although the g and u restrictions do not apply.

From the analysis of the photoelectron studies, we have established that the electronic ground state of CSe_2 may be written

$$(\ldots 2\sigma_g^2\ 2\sigma_u^2\ \ 1\pi_u^4\ \ 1\pi_g^4)\ {}^1\Sigma_g^+$$

As the lowest energy empty valence shell orbitals are the $2\pi_u$ and $3\sigma_g$ levels, we expect the low energy electronic spectrum to arise from the following transitions:-

$$(\cdots\cdots 1\pi_g^4) \longrightarrow (\ldots 1\pi_g^3\ 2\pi_u^1) : {}^1\Sigma_g^+ \rightarrow {}^1\Sigma_u^+, {}^1\Delta_u, {}^1\Sigma_u^-, {}^3\Sigma_u^+, {}^3\Delta_u, {}^3\Sigma_u^-.$$

$$(\cdots\cdots 1\pi_g^4) \longrightarrow (\cdots 1\pi_g^3\ 3\sigma_g^1) : {}^1\Sigma_g^+ \rightarrow {}^1\Pi_g, {}^3\Pi_g.$$

$$(\ldots 1\pi_u^4\ 1\pi_g^4) \longrightarrow (1\pi_u^3 1\pi_g^4\ 2\pi_u^1) : {}^1\Sigma_g^+ \rightarrow {}^1\Sigma_g^+, {}^1\Delta_g, {}^1\Sigma_g^-, {}^3\Sigma_g^+, {}^3\Delta_g, {}^3\Sigma_g^-.$$

According to the selection rules, only the ${}^1\Sigma_g^+ \rightarrow {}^1\Sigma_u^+$ transition will be allowed, all the others being forbidden either by parity, multiplicity or $\Delta\Lambda$ selection rules.

b) Use of Walsh diagrams

However we know from the Walsh diagram for CO_2 [11], reproduced in Figure 5, that when the $2\pi_u$ level is occupied, the nuclear geometry no longer remains linear, but will bend. As a result, we must consider the correlation between linear and bent states shown below:-

Bent state.	Polarisation	Linear state.
${}^1A_1$	$\perp$	${}^1\Sigma_g^+$ ${}^1\Pi_u$ ${}^1\Delta_g$
${}^1A_2$	forbidden	${}^1\Sigma_u^-$ ${}^1\Pi_g$ ${}^1\Delta_u$
${}^1B_1$	$\perp$	${}^1\Sigma_g^-$ ${}^1\Pi_u$ ${}^1\Delta_g$
${}^1B_2$	$\parallel$	${}^1\Sigma_u^+$ ${}^1\Pi_g$ ${}^1\Delta_u$

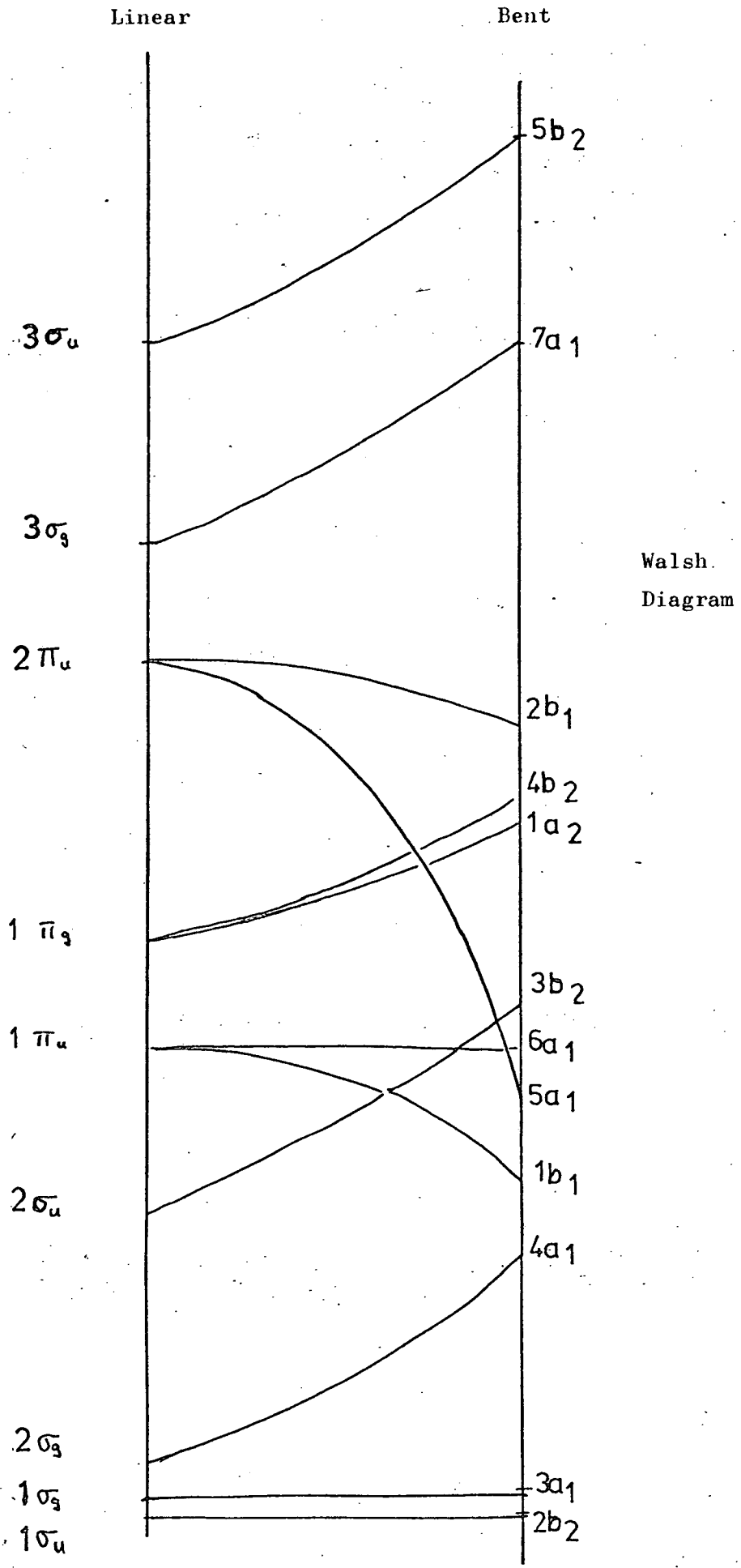
Linear
Bent
$3\sigma_u$
$3\sigma_g$
$2\pi_u$
$1\pi_g$
$1\pi_u$
$2\sigma_u$
$2\sigma_g$
$1\sigma_g$
$1\sigma_u$
$5b_2$
$7a_1$
$2b_1$
$4b_2$
$1a_2$
$3b_2$
$6a_1$
$5a_1$
$1b_1$
$4a_1$
$3a_1$
$2b_2$
Walsh
Diagram

Figure 5

Thus when a vibronic interaction involving a bent state is taken into account, it is possible for the transition $^1\Sigma_g^+ \longrightarrow {}^1\Delta_u$ to become allowed.

Again using the Walsh diagram we can see that when the $3\sigma g$ level is occupied, the nuclear framework is again likely to be linear. Although parity forbidden, the $^1\Sigma_g^+ \longrightarrow {}^1\Pi_g$ transition may become allowed by vibronic coupling of the σ u vibrational mode. However, if allowed, the $^1\Sigma_g^+ \rightarrow {}^1\Pi_g$ transition would be expected to show Renner-Teller effects.

Thus of the 14 possible transitions only 3 are likely to be observed. In order of increasing energy these will be:-

$$^1\Sigma_g^+ \longrightarrow {}^1\Delta_u \quad (\ldots 1\pi_g^3\, 2\pi_u^1)$$
$$^1\Sigma_g^+ \longrightarrow {}^1\Sigma_u^+ \quad (\ldots 1\pi_g^3\, 2\pi_u^1)$$
$$^1\Sigma_g^+ \longrightarrow {}^1\Pi_g \quad (\ldots 1\pi_g^3\, 3\sigma_g^1)$$

However the fact that the appearance of the first and last of these is due to a partial breakdown of the selection rules should be reflected in decreased intensity of the bands corresponding to these transitions, compared with that of the fully allowed $^1\Sigma_g^+ \longrightarrow {}^1\Sigma_u^+$ transition.

c) Results and discussion

The visible/near ultraviolet spectra of CSe_2, SCSe and OCSe are presented in Figures 6, 7, 8, and the assignments given in Table 1. As expected there are strong similarities between the spectra[14] although there are regular shifts in the relative energy of the same transition occurring in the different molecules. Generally the transition energies in OCSe are the highest and those in CSe_2 the lowest. Thus both CSe_2 and SCSe are coloured yellow as a result of absorption in the visible from the $^1\Sigma_{(g)}^+ \longrightarrow {}^1\Delta_{(u)}$

POSTGRADUATE LECTURE COURSES.

TITLE OF LECTURE.	LECTURER(S)	NO. OF LECTURES	COMMENT.
^{13}C n.m.r. and Fourier Transform n.m.r.	Dr. Shaw (Varian Associates)	5	Postgraduate Lectures.
Xray and u.v. photoelectron spectroscopy.	Dr. Whan Dr. Cradock	5	Postgraduate Lectures.
Molecular Spectroscopy	Dr. Rae (Dept. of Physics) Dr. Donovan	5	Postgraduate Chemical Physics Lectures.
Vibrational Spectroscopy	Dr. Cradock	5	Postgraduate Lectures.
High Speed Liquid Chromatography	Prof. Knox Dr. Done	5	Postgraduate Lectures.
Theoretical Chemistry	Dr. Palmer	5	Honours class Optional Course
Aspects of Fluorine Chemistry	Dr. Rankin	5	Honours class Optional Course.
Fortran Computing Course	E.R.C.C. (Alison House)	1 week	

Also attendance at Departmental (Wednesday morning) and Inorganic group evening seminars.

TABLE 1.

Near u.v. and visible spectra.

Molecule	(cm^{-1}) band max.	Assignment.	Comment.
CSe_2 (See Fig. 6)	~ 26,500	$X\,^1\Sigma_g^+ \rightarrow\, ^1\Delta_u$	Weak. diffuse v.complex vibrational structure.
	~ 44,000	$X\,^1\Sigma_g^+ \rightarrow\, ^1\Sigma_u^+$	V.strong diffuse.
	~ 49,000	$X\,^1\Sigma_g^+ \rightarrow\, ^1\Pi_g$	W. diffuse.
SCSe (See Fig. 7)	~ 28,500	$X\,^1\Sigma^+ \rightarrow\, ^1\Delta$	Weak. Sharp. V. complex vibrational structure.
	~ 45,600	$X\,^1\Sigma^+ \rightarrow\, ^1\Sigma^+$	V. Strong, diffuse vibrational structure.
OCSe (See Fig. 8)	~ 40,500	$X\,^1\Sigma^+ \rightarrow\, ^1\Delta$	W. diffuse vibrational structure.
	> 50,000	$X\,^1\Sigma^+ \rightarrow\, ^1\Sigma^+$	V. strong, diffuse vibrational structure.

Figure 6. CSe_2.

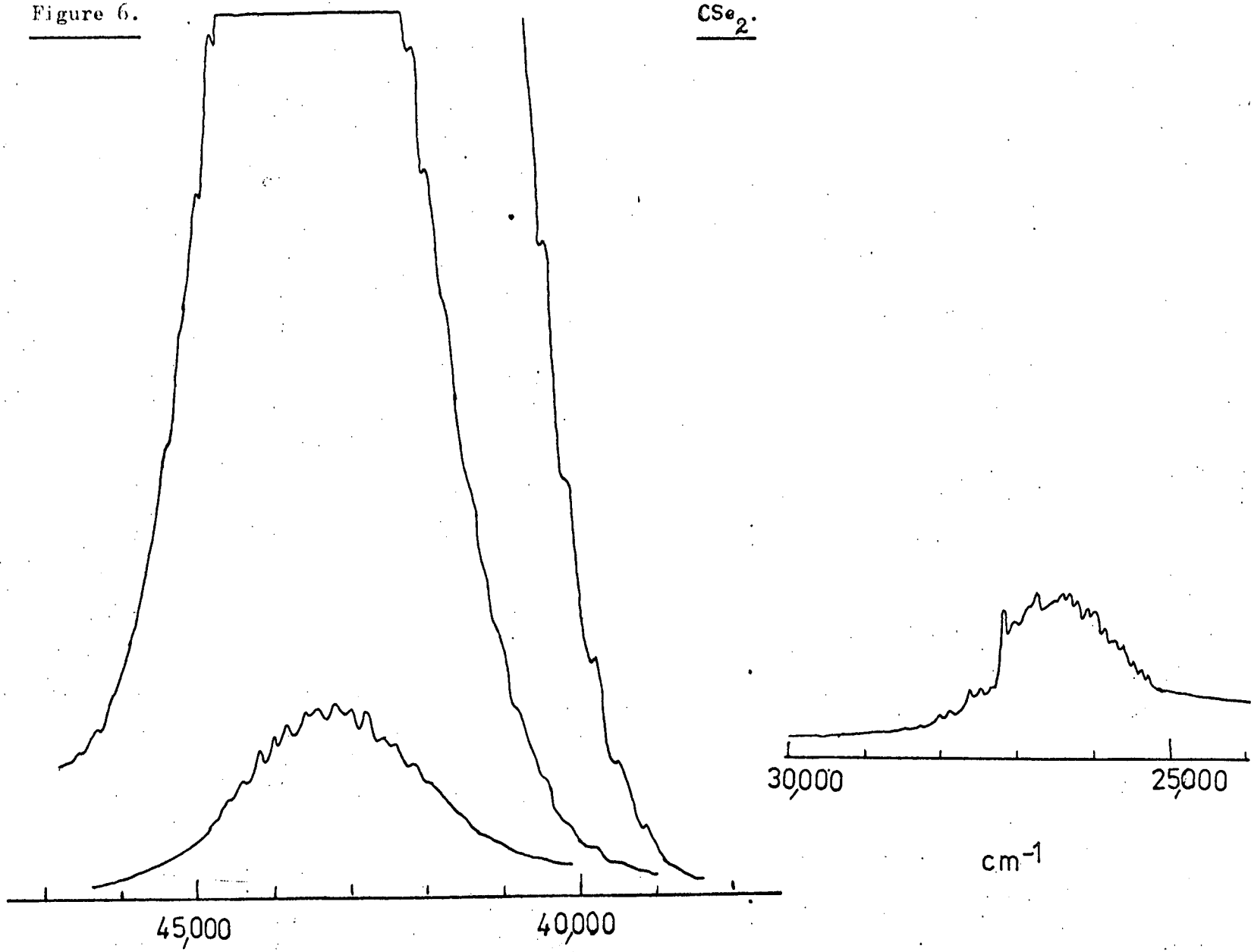

Figure 7. SCSe.

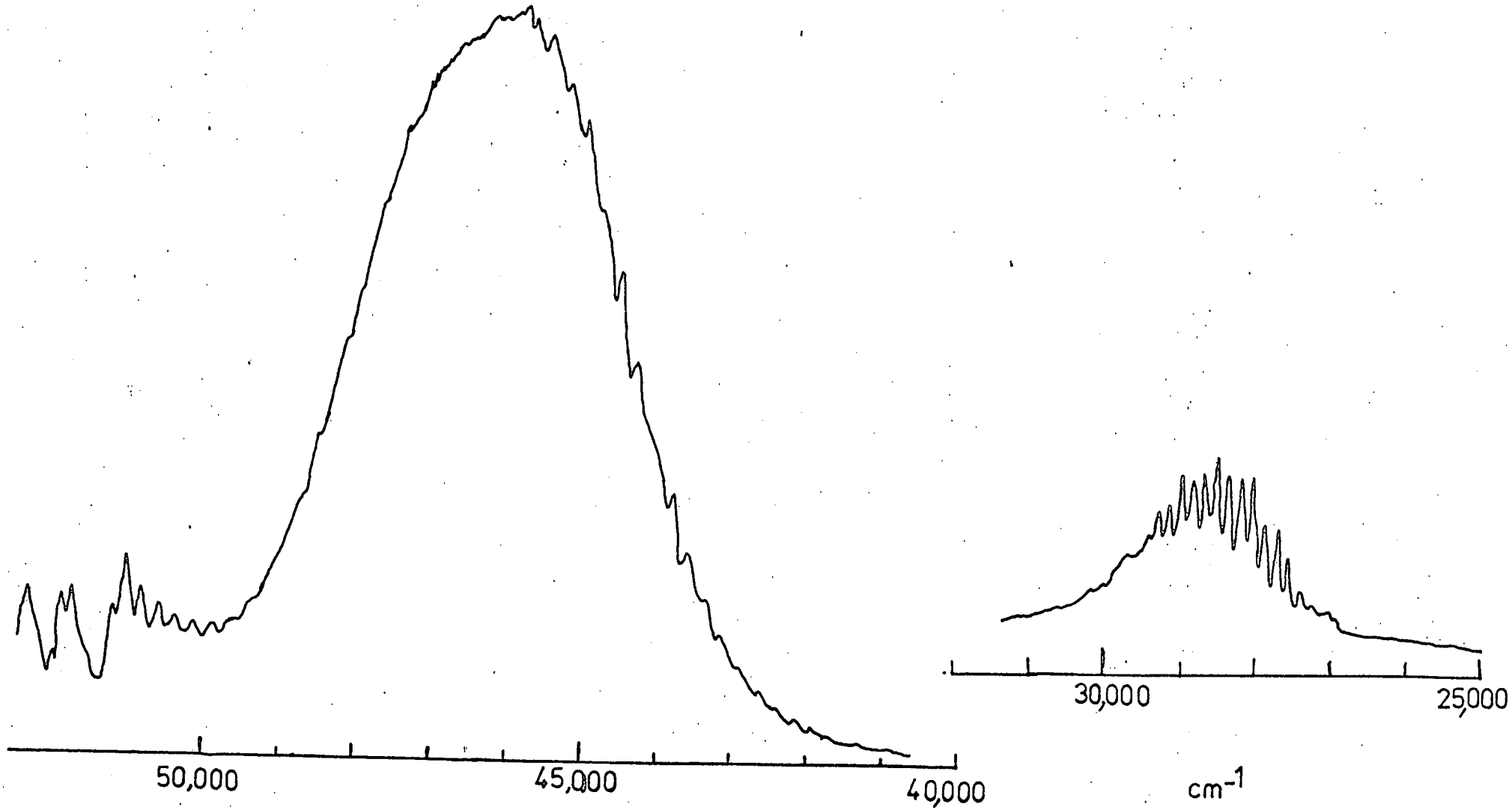

Figure 8.

OCSe.

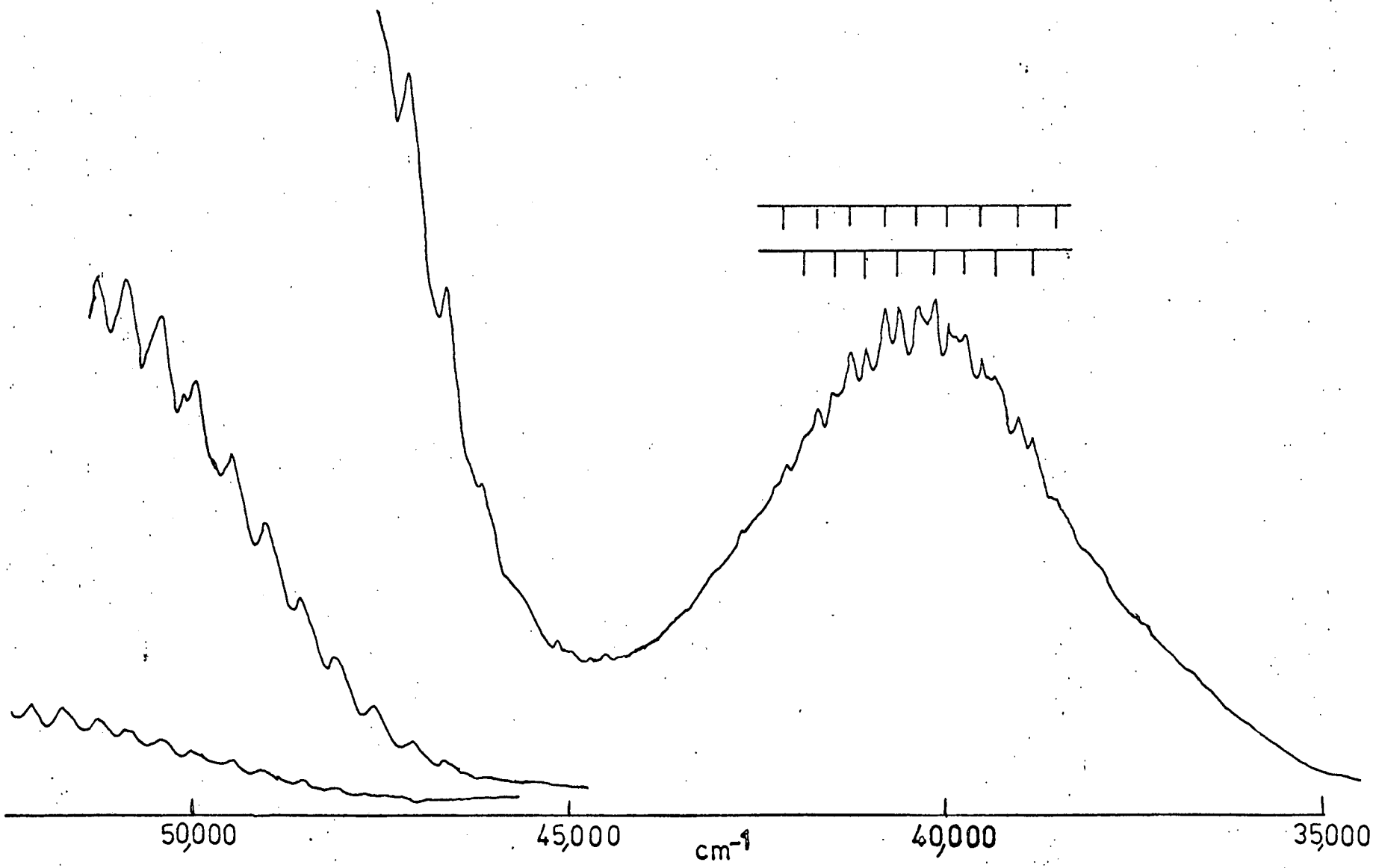

transition. The corresponding transition in OCSe occurs in the near u.v. and so OCSe is colourless. As a consequence of the non-linear geometry arising from occupation of the $2\pi_u$ level and the Renner-Teller effects associated with transitions to orbitally degenerate states, the vibrational structure of the $^1\Sigma_g^+ \longrightarrow {}^1\Delta_u$ is particularly complex and has, in the case of CSe_2 and OCSe been studied by King and his co-workers using isotopically pure selenium compounds.[12,13] The vibrational structure of the $^1\Sigma_g^+ \longrightarrow {}^1\Sigma_u^+$ transition is diffuse, even under high resolution, although an analysis has been proposed for OCSe.[13,13a]

3. THE VACUUM ULTRAVIOLET SPECTRA of CSe_2, SCSe and OCSe.

a) Selection rules

We may again use the selection rules to help decide which Rydberg transitions will be allowed.

From the p.e. results we know that the only complete Rydberg series we can expect to observe are those converging to the $^2\pi g$ limit ($\ldots 1\pi g^3$). Thus it is appropriate to characterise the Rydberg state as being formed from a $^2\Pi g$ ionic core with the Rydberg electron in an orbit with $l = 0, 1, 2$.

This will result in the following states:-

Core.	×	Rydberg electron.	=	Total Rydberg State.
πg	×	σu	=	Π_u
πg	×	πu	=	$\Sigma_u^+ \; \Sigma_u^- \; \Delta_u$
πg	×	δu	=	$\Pi_u \; \Phi_u$

Assuming (Λ, S) coupling to apply, each of these states may exist in singlet or triplet forms but by the spin multiplicity selection rule, only those transitions to the singlet component will be allowed. Also, according to the other selection rules, we would predict only the $^1\Sigma_g^+ \longrightarrow {}^1\Pi_u$ and $^1\Sigma_g^+ \longrightarrow {}^1\Sigma_u^+$ transitions to be fully allowed. Thus only those transitions involving electronic excitation from the $1\pi g$ level to the σu, πu and δu Rydberg levels will be observed.

The symmetry of the various Carbon and Selenium Rydberg levels is given in Table 2, where it can be seen that transitions to all Se ns, np and nd Rydberg levels will be allowed whereas only transitions to C np Rydberg series would be possible. As Rydberg transitions are essentially "atomic" they tend to follow the atomic $\Delta l = \pm 1$ selection rule[9] so that the transitions to the np_σ level are expected to be much

C	ns	σg
	np	$\sigma u + \pi u$
	nd	$\sigma g + \pi g + \delta g$
Se	ns	$\sigma g + \sigma u$
	np	$\sigma g + \sigma u$
	np	$\pi g + \pi u$
	nd	$\sigma g + \sigma u$
	nd	$\pi g + \pi u$
	nd	$\delta g + \delta u$

TABLE 2.

stronger than those to the np_π level, for which $\Delta l = 0$. In the case of the nd levels the selection rules allow transitions to both the $nd\sigma$ and nd_δ components.

b) Results.

The vacuum ultraviolet spectra of CSe_2, SCSe and OCSe are presented in Figures 9, 10,11. Although undoubtedly very complex, the almost complete absence of diffuse structureless bands has made it possible to carry out a detailed analysis of all the spectra and the results are given in Tables 3,4,5. Again there are stronger similarities between the spectra of SCSe and CSe_2, than between those of OCSe and CSe_2.

This was also noted previously in the comparison between the first band in the p.e. spectrum of each compound. Thus whereas the $X^2\Pi g\,\frac{1}{2}, \frac{3}{2}$ states of CSe_2 showed no vibrational structure, the corresponding $X^2\Pi\,\frac{1}{2},\frac{3}{2}$ band of OCSe clearly showed progressions in ν_1 and ν_3, and this difference is also apparent in the Rydberg series.

c) Identification of Rydberg series in molecules.

The assignments of the Rydberg series are carried out using a set of Rydberg term tables. In these, the different term values for quantum defects from 1.00 to 0.01, in steps of 0.01, are listed for increasing n. A copy of such a set of term tables is included in an appendix to this chapter. Knowing the I.P. from the p.e. spectrum it is possible to calculate the term value of each band directly and using the Rydberg term tables we obtain the associated values of the quantum defect δ and N. Now if a band belongs to a Rydberg series, then for a particular value of δ, increasing N by unity should lead to the term value of the next member.

Figure 9. The Absorption Spectrum of CSe_2 between 150 and 130 n.m.

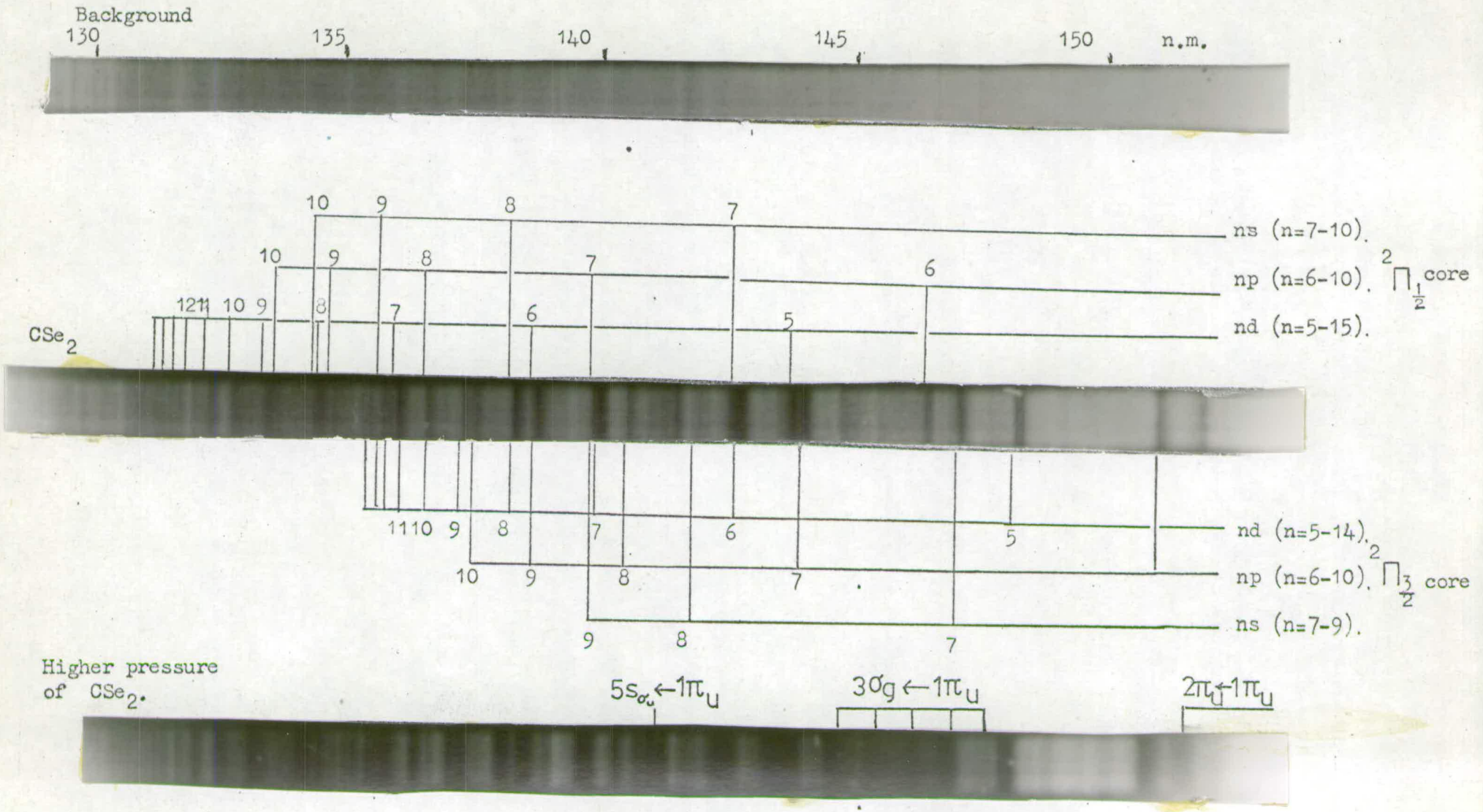

TABLE 3. RYDBERG SERIES FOR CSe_2. BAND ORIGINS (To) cm^{-1}

nd Series.

n	$^2\Pi_{\frac{1}{2}}$ core ν	δ	Comment	n	$^2\Pi_{\frac{3}{2}}$ core ν	δ	Comment	Spin orbit coupling.
4	64270	1.04	w	4	61960	1.06	w	2300
5	69531	1.12	s.	5	67390	1.12	s	2141
6	72082	1.19	s	6	70004	1.16	s	2078
7	73562	1.19	s	7	71429	1.19	s	2133
8	74444	1.20	s	8	72312	1.19	s	2132
9	75013	1.19	s	9	72876	1.19	m	2137
10	75403	1.19	s	10	73260	1.21	s	2148
11	75667	1.19	s	11	73540	1.19	m	2137
12	76878	1.20	m	12	73741	1.18	m	2137
13	75990		m	13	73900		w	2090
14	76150		w	14	74020		v.w	2130
15	76250		v.w	15	74070		v.w	2220
16	76320		v.w	16	74110		v.w.	2210
17	76380		v.w					
	Series limit 76813				Series limit			

TABLE 3 (Contd.)

RYDBERG SERIES FOR CSe_2.

BAND ORIGINS (To) cm^{-1}

nd Series.	$^2\Pi_{\frac{1}{2}}$ core			$^2\Pi_{\frac{3}{2}}$ core				
n	ν	δ	Comment.	n	ν	δ	Comment	Spin orbit coupling.
5	57610	2 61	v.s	5	55497	2 61	v.s	2113
6	68269	2 42	s	6	66225	2 40	s	2044
7	71444	2 48	v.s	7	69440	2 42	v.s	2004
8	73239	2 46	s	8	71124	2 44	s	2115
9	74267	2 44	m	9	72134	2 43	s	2133
10	74859	2 40	m	10	72780	2 45	m	2115
11	75313	2 46	m	11	73169	2 48	w	2144
ns Series								
5	52312	2 89	m	5	50000	2 89	s	2312
6	64583	3 01	m	6	62150	3 04	w	2433
7	70053	2 97	s	7	67944	2 96	s	2109
8	-	-	-	8	-	-	-	-
9	73714	3 03	m	9	71505	3 12	m	2236
10	74516	3 10	m	10	72280	3 24	w	2236
11	75041	3 14	m	11	72865	3 22	w	2176

The Absorption spectrum of CSe_2 between 170 and 185 n.m.

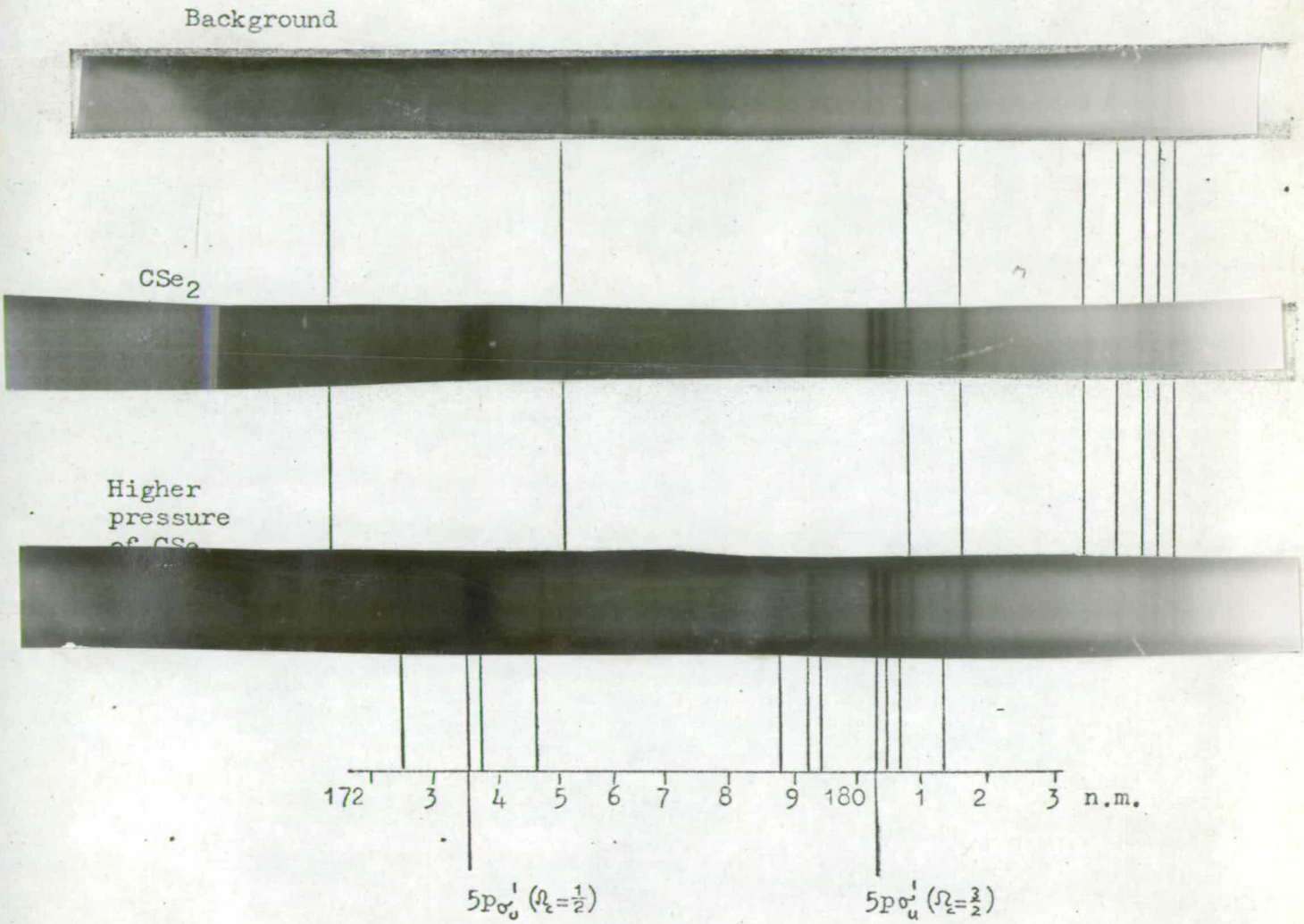

Figure 9 (See Table 3).

Table 3

Absorption Spectrum of CSe_2 between 210 nm and 170 nm

λ(vacuum)/*nm	Intensity	ν/cm^{-1}	Description	Assignment vibration	Assignment electronic (upper state)
~205		~48,780	continuum		$^1\Pi_g(\ldots 1\pi_g^3 3\sigma_g^1)$
203.0 min	m	49,260	resonance		$^3\Pi_{u,o}(\ldots 1\pi_g^3(\Omega_c=\frac{1}{2})5s\sigma_u^1)$ see text
201.9_8 max		49,510			
200.0_0	m	50,000	broad, diffuse**	(0,0)	$^1\Pi_{u,1}(\ldots 1\pi_g^3(\Omega_c=3/2)5s\sigma_u^1)$
198.2_0	w	50,454	" " **	ν_2?	
197.4_4	w	50,648	diffuse**	$2\nu_1$?	
196.4_8	w	50,896	broad, diffuse**	$2\nu_2$?	
196.0_3	w	51,013	diffuse	$3\nu_1$?	
195.4_3	vw	51,169		$\nu_1+\nu_3-\nu_1$	
195.3_0	w	51,203		ν_3	
193.9_9	vw	51,549	diffuse	$2\nu_1+\nu_3-\nu_1$	
193.8_6	m	51,584	"	$\nu_1+\nu_3$	
191.3_4	vw	52,263	sharp	$\nu_1(1,1)$	$^1\Pi_{u,1}(\ldots 1\pi_g^3(\Omega_c=\frac{1}{2})5s\sigma_u^1)$
191.1_6	m	52,312	"	(0,0)	

Table 3

λ(vacuum)/*nm	Intensity	ν/cm^{-1}	Description	Assignment vibration	Assignment electronic (upper state)
181.6_0	vw	55,066		$\nu_1(1,2)$	
181.4_3	w	55,118	sharp	(0,1)	
181.1_1	vw	55,215		?	
180.5_8	m	55,377	sharp	$(2,2)^+$	
180.3_8	s	55,438	"	(1,1)	
180.1_9	vs	55,497	"	(0,0)	$^1\Pi_u(\ldots 1\pi_g^3(\Omega_c=3/2)5p\sigma_u^1)$
179.3_6	vw	55,754	diffuse	(2,1)	
179.1_6	m	55,816	"	(1,0)	
178.6_9	vw	55,963		?	
178.6_0	vw	55,991		?	

Table 3

λ(vacuum)/*nm	Intensity	ν/cm^{-1}	Description	Assignment vibration	Assignment electronic (upper state)
174.7_3	w	57,231		$\nu_1(0,1)$	$^1\Pi_u(\ldots 1\pi_g^3(\Omega_c=\frac{1}{2})5p\sigma_u^1)$
173.7_5	s	57,554	diffuse	(1,1)	
173.5_8	vs	57,610	"	(0,0)	
172.6_3†	vw	57,927	"	(1,0)	

* wavelengths accurate to ±0.05 nm.

** other weaker diffuse bands in this region.

\+ Si emission line at 180.8 nm may obscure the (3,3) band.

† other very weak bands in the region 173.6-172.6 nm.

The Absorption Spectrum of SCSe between 120 and 180 n.m.

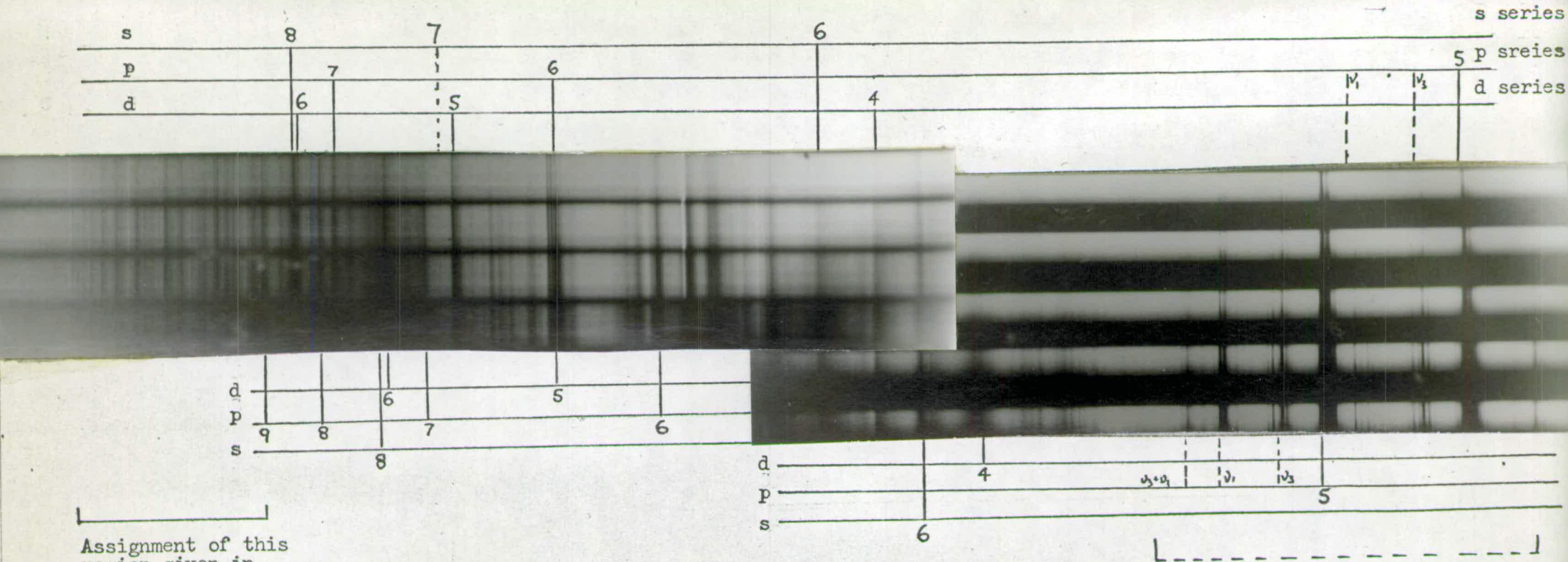

Assignment of this region given in Figs. 10a &10b.

See Table 4d for assignment of weaker features in this region.

75 74 73 72 71 70

$X10^3$ c.m.$^{-1}$.

Figure 10.

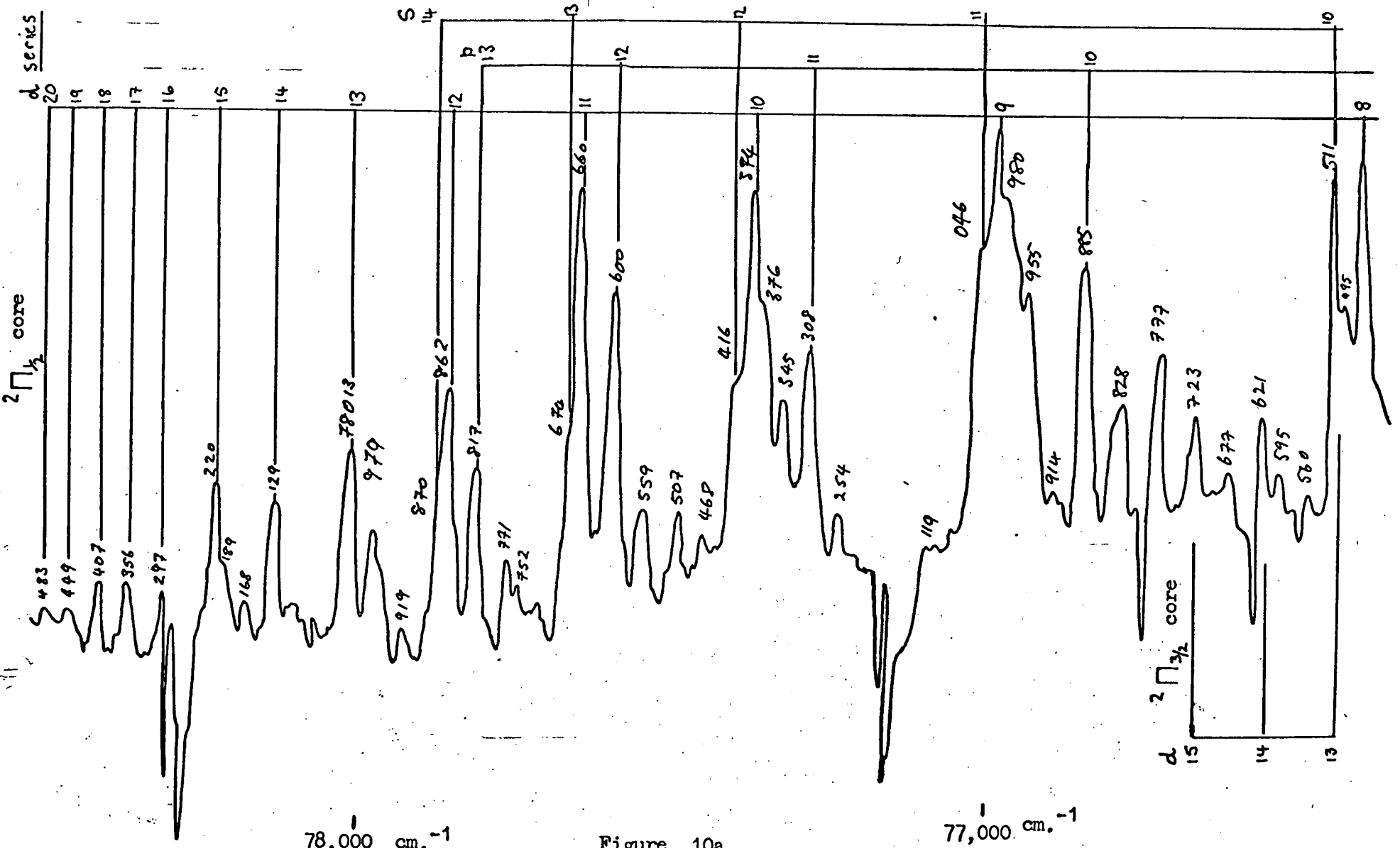

78,000 cm.$^{-1}$ 77,000 cm.$^{-1}$

Figure 10a.

Figure 10b.

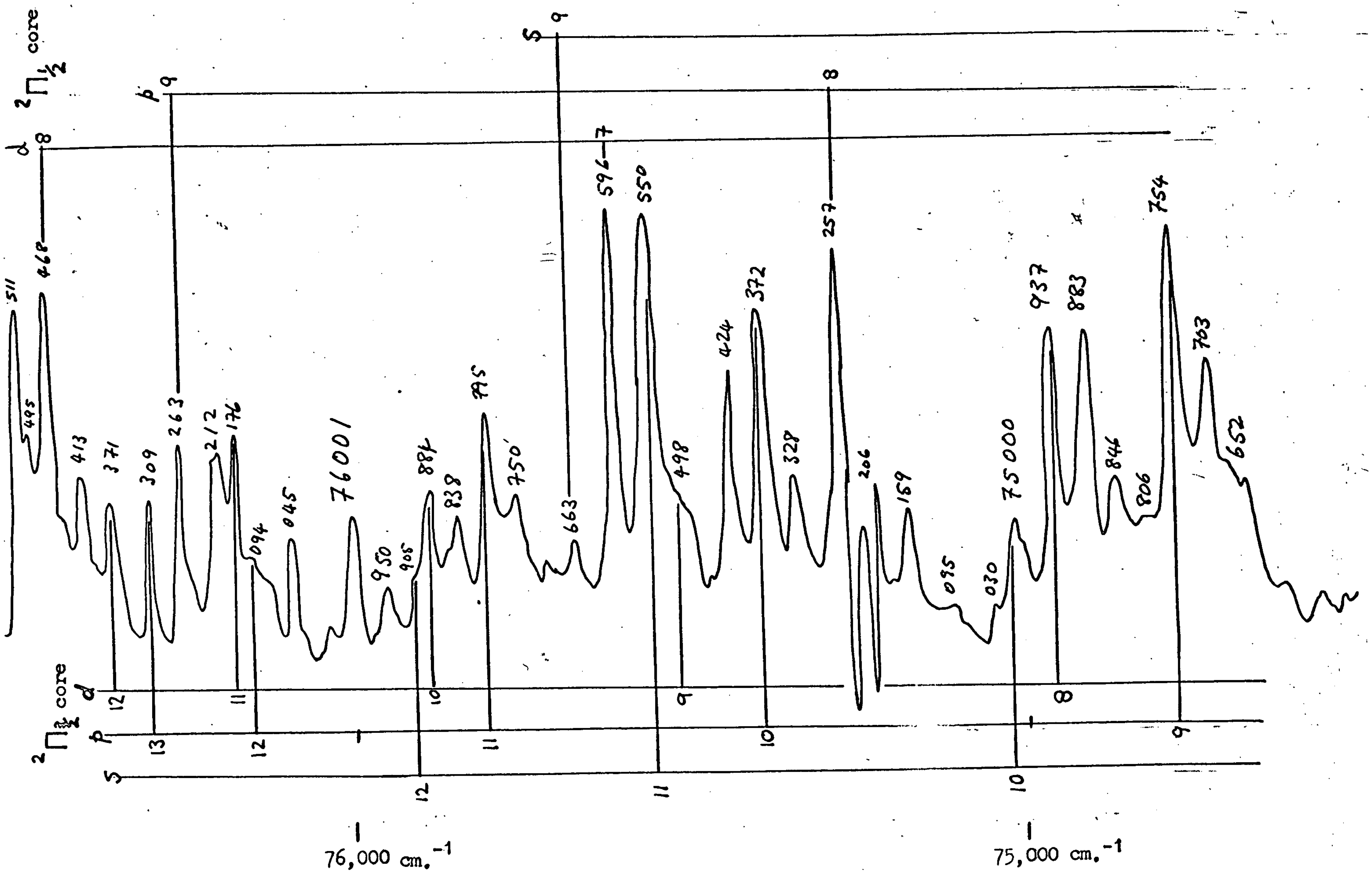

TABLE 4. RYDBERG SERIES FOR SCSe. BAND ORIGINS (To) cm^{-1}

nd Series.

$^2\Pi_{\frac{1}{2}}$ core				$^2\Pi_{\frac{3}{2}}$ core				
n	ν	δ	Comment	n	ν	δ	Comment	Spin orbit coupling.
4	65399	1·14	w. diffuse	4	64000†	1.12	w. diffuse	1399
5	71536	1·14	s.	5	69999	1.12	s. overlapped	1537
6	74189	1·12	m. overlapped	6	72665	1.13	m.	1524
7	75596	1·14	m. sharp	7	74067	1.17	m. overlapped	1529
8	76468	1·13	m. sharp	8	74936	1.17	m. sharp	1532
9	77018	1·14	m. sharp	9	75498	1.18	w. diffuse	1520
10	77394	1·14	m. sharp	10	75884	1.18	w. sharp	1510
11	77660	1·15	m. sharp	11	76176	1.10	w. sharp	1485
12	77863	1·14	w. sharp	12	76368	1.11	w. sharp	1495
13	78013	1·14	w. sharp	13	76511	1.16	m. sharp overlapped	1502
14	78130	1·13	w. sharp	14	76621	1.23	w. overlapped	1509
15	78223	1·12	w. sharp	15	76723	1.14	w.	1500
16	78297	1·12	v.w					
17	78356	1·13	v.w					
18	78407	1·12	v.w					
19	78449	1·12	v.w					
20	78483	1·15	v.w					

†band partially obscured by emission lines.

TABLE 4 Contd. RYDBERG SERIES FOR SCSe. BAND ORIGINS (To) cm^{-1}

np Series.

	$^2\Pi_{\frac{1}{2}}$ core			$^2\Pi_{\frac{3}{2}}$ core			
n	ν	δ	Comment	n	ν	δ	Comment	Spin orbit coupling.
5	59885	2 59	v.s ‡	5	58336	2 59	v.s ‡	1545
6	70043	2 46	s. overlapped	6	68432	2 48	m. diffuse	1611
7	73503	2 44	m. diffuse	7	71998	2 45	m.	1505
8	75257	2 43	m. sharp	8	73751	2 44	s.	1506
9	76263	2 41	m. sharp	9	74754	2 43	m.	1509
10	76887	2 41	w. sharp	10	75372	2 44	m.	1515
11	77308	2 40	w. sharp	11	75795	2 44	w.	1513
12	77602	2 40	w. sharp	12	76094	2 44	w. diffuse	1508
13	77818	2 39	w. sharp	13	76309	2 44	w. sharp	1509

‡ (000-000) band. Details and assignment of other bands in this region given in Table 4(d).

TABLE 4 Contd. RYDBERG SERIES FOR SCSe. BAND ORIGINS (To) cm^{-1}

ns Series.

n	$^2\Pi_{\frac{1}{2}}$ core ν	δ	Comment	n	$^2\Pi_{\frac{3}{2}}$ core ν	δ	Comment	Spin orbit coupling.
5	53253	2·93	m. sharp	5	51734	2·93	w. diffuse	1519
6	66175	3·05	w. diffuse	6	64800	3·03	w. diffuse	1375
7	(71638)		*	7	70126		*	
8	74207	3·11	m. overlapped	8	72738	3·04	w. (?)	1469
9	75665	3·08	w. broad	9	74164	3·08	w. overlapped	1501
10	76511	3·06	m. sharp	10	75005	3·08	w.	1506
11	77044	3·08	w. (shoulder)	11	75548	3·07	m. sharp	1496
12	77416	3·07	w. (shoulder)	12	75904	3·11	w. overlapped	1512
13	77674	3·09	w. (shoulder)					
14	77870	3·09	w. (shoulder)					

* calculated value, weak very complex absorption in this region due to intervalence bands.

$^2\Pi_{\frac{1}{2}}$ core series limit : 78792 cm^{-1}

$^2\Pi_{\frac{3}{2}}$ core series limit: 77294 cm^{-1}

Table 4 Absorption Spectrum of SCSe between 210n.m. and 170 n.m.

	Frequency ($cm.^{-1}$)	Comment	Assignment
a.	49660	w.broad	
	49901	w.broad	
	50134	w.broad	
	50382	w.broad	
	50829	m.broad	
	51207	m.broad	
b.	51034	m.broad	$4\sigma^2\ 2\pi^3\ (\Omega=\frac{3}{2})\ 5\sigma^1$
	51734/878	s.broad	$4\sigma^2\ 2\pi^3\ (\Omega=\frac{3}{2})\ 5s_\sigma^1$
	52305/396	s.overlapped	$4\sigma^2\ 2\pi^3\ (\Omega=\frac{1}{2})\ 5\sigma^1$
	53254	s.sharp	000-000 $4\sigma^2\ 2\pi^3\ (\Omega=\frac{1}{2})\ 5s_\sigma^1$
	52750	w.	000-001 "
	52907	w.	000-010 "
	53920	w.	001-000(?) "
c.	51584		
	52586		
	52845		
	53520		
	54205		
	54847		
	55548		

Table 4 (Contd.) Absorption Spectrum of SCSe between 210 and 170 n.m.

d. Assignment (Electronic)	Wavelength. cm^{-1}	Assignment (Vibrational)	Wavelength. cm^{-1}	Assignment (Electronic).
$^2\Pi_{\frac{3}{2}}$				$^2\Pi_{\frac{1}{2}}$
	57788	001-002		
	57837	000-001	59387	
	58151	004-004		
	58190	003-003	59747	
	58223	002-002	59767	
	58280	001-001	59831	
(...5p)	58336	000-000	59885	(...5p)
	58426	?	-	
	58659	?	-	
	58730	002-001	60301	
	58787	001-000	60351	
	59460	200-100	61015	
	59530	100-000	61077	
	-	202-101	61404	
	-	101-000	61451	

Figure 11 : The Absorption Spectrum of OCSe between 145 and 115 n.m.

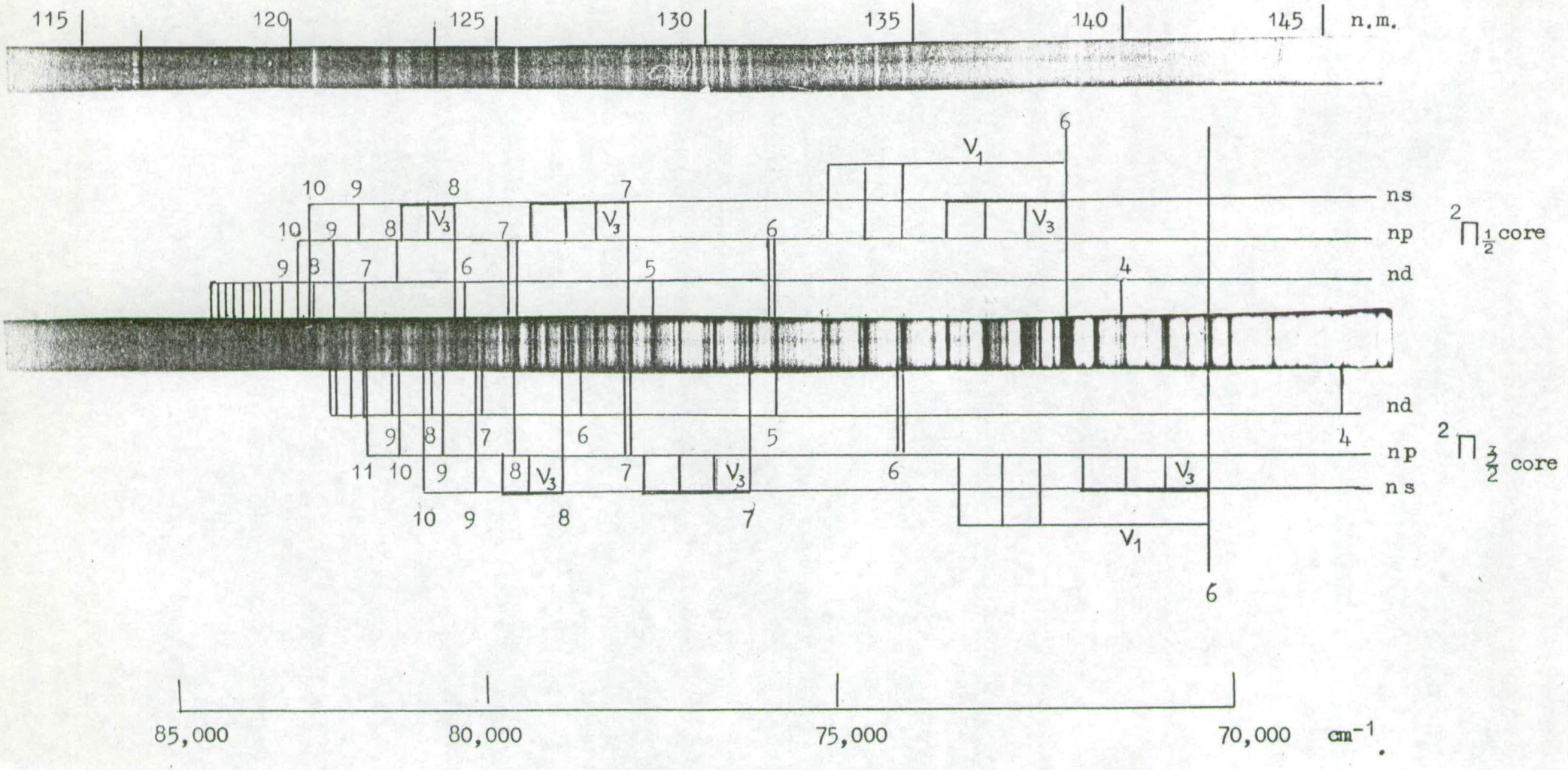

TABLE 5. RYDBERG SERIES FOR OCSe. BAND ORIGINS (To) cm^{-1}

nd Series. $^2\Pi_{\frac{1}{2}}$ core

n	ν	δ	Comment.
4	71336	1 20	
5	77664	1 22	
6	80556	1 21	
7	82094	1 17	
8	82976	1 17	
9	83521	1 27	
10	83870	1 31	
11	84225	1 02	
12	84381	1 20	
13	84540	1 18	
14	84651	1 24	
15	84756	1 12	

Series Limit 85531 cm^{-1}.

$^2\Pi_{\frac{3}{2}}$ core

n	ν	δ	Comment	Spin orbit coupling.
4	69493	1 20		1843
5	75887	1 21		1777
6	78714	1 23		1842
7	80233	1 23		1861
8	81091	1 28		1875
9	81687	1 27		1834
10	82094	1 24		1776
11	-	-	-	-
12	82574	1 25		1807

Series Limit 83524 cm^{-1}.

TABLE 5 (Contd.) RYDBERG SERIES FOR OCSe. BAND ORIGINS (To) cm^{-1}

np Series.

	$^2\Pi_{\frac{1}{2}}$ core			$^2\Pi_{\frac{3}{2}}$ core			
n	ν	δ	Comment.	n	ν	δ	Comment.	Spin orbit coupling.
5	66210	2.61		5	64388	2.60		1882
	66292	2.60			64534	2.59		1758
6	75887	2.59		6	74146	2.58		1741
	75957	2.58			74230	2.56		1727
7	79721	2.58		7	78005	2.54		1716
	79834	2.53			78100	2.51		1734
8	81568	2.61		8	79796	2.58		1722
9	82684	2.56		9	80872	2.57		1812
10	-	-		10	81568	2.51		-
11	83788	2.56						
12	84089	2.58						
13	84329	2.52						
14	84490	2.54						

TABLE 5 (Contd.) RYDBERG SERIES FOR OCSe. BAND ORIGINS (To) cm^{-1}

ns Series.

	$^2\Pi_{\frac{1}{2}}$ core			$^2\Pi_{\frac{3}{2}}$ core			
n	ν	δ	Comment.	n	ν	δ	Comment.	Spin orbit coupling.
6	72038	3.13		6	70247	3.12		1781
7	7°004	3.13		7	76267	3.11		1777
8	80673	3.14		8	78929	3.11		1744
9	82094	3.17		9	80354	3.12		1740
10	82976	3.16		10	81198	3.14		1778

Thus, in principle, all that is necessary, is to tabulate the absorption frequency, ν; calculate the term value; $(I - \nu)$; and note the corresponding value of δ and N for each band in the spectrum. From such a tabulation the various series characterised by the same value of δ and sequential N can then be identified.

However, even in the atomic case such an ideal situation is unlikely to occur. In the molecular case the possibilities for perturbation from the expected Rydberg term values is considerably greater and it is the extent of such deviations which can make the interpretation of molecular Rydberg spectra a challenge.[15]

Thus, there is inevitably a considerable degree of "trial and error" in trying to fit the observed bands into Rydberg series and the ambiguities which arise are often best resolved by cross-correlation of related spectra.

It is usually appropriate to treat the results using standard "best fit" techniques.[16] However one of the major difficulties in the initial stages of the analysis arises from the fact that although the absorption frequencies may be accurate to $\pm$ 1cm^{-1} (or better), the term values calculated using I.P.s determined from p.e. spectra are often only accurate to $\pm$ 100 cm^{-1}! Especially at the higher n values, where the bands tend to be quite closely spaced, this level of inaccuracy is sufficiently large to make assignment of successive members virtually impossible. Thus we may have to rely on experience, or trends in other features, such as band shape and intensity to estimate the series. Thus we normally expect the intensity of successive members of a series to decrease regularly and rapidly with increasing n. This is a consequence of the fact that the oscillator strength of a Rydberg transition is governed by an expression of the form

$\langle \phi c/M/\phi_R \rangle$ and as n increases, the overlap between the core wave function ϕc and that of the Rydberg electron ϕ_R decreases. In the case of an unperturbed atomic series the oscillator strength is expected to decrease as n^{-3}.[17]

Thus by inspection it may be possible to identify members of the series to nearer the limit than would have been possible on the basis of poorly estimated term values. Provided we have correctly chosen the members of the series we can now extrapolate the series to its limit and obtain a more accurate value for the I.P. This process can then be repeated several times and at each stage a more accurate value for the I.P. and hence the term values is obtained. When a sufficiently accurate value for the I.P. is obtained it is possible to reverse the process and use the I.P. to calculate the term values for a given value of δ. These may then be compared with experimental values and any obvious discrepancies noted. In such a procedure the choice of a suitable value of δ is usually that of the terminal members, rather than the initial members of the series, as these usually lie considerably off the positions predicted using average δ values. It is also this often quite large change in δ between the early members which makes series identification particularly difficult in the preliminary stages.

The reasons for such deviations, as well as the methods by which it may be possible to check whether or not a band actually belongs to the Rydberg series, were discussed in the Introduction.

d) Analysis of Rydberg series in CSe_2, SCSe and OCSe.

There are three other factors which make preliminary identification of the Rydberg series more difficult in the particular

molecules under discussion. The first of these is the fact that, as we have seen previously in the p.e. spectrum, the $X^2\Pi(g)$ state to which the ns, np and nd series converge, is split by spin orbit coupling. Thus it is necessary to characterise the observed Rydberg series according to the Ω value of the core, with the $\Omega = \frac{3}{2}$ core series lying to lower energy than the series with $\Omega = \frac{1}{2}$ core. Thus instead of there being only three Rydberg series to identify, there are now six. Furthermore, there is not only considerable overlap but there are also several coincidences between the two series and were it not for the fact that the splitting between the different core series so closely resembles that of the ion, then identification of the different Ω components would have been considerably more difficult.

The presence of these two closely lying limits means that in the initial stages of the analysis it is necessary to evaluate term values for every transition to <u>both</u> series limits. However only one of these will properly predict the next series member and so it is usually possible to identify the particular core to which it belongs. Unfortunately the several cases of coincidence between the different core series can produce considerable ambiguity in the early stages of analysis.

When the members of a particular series have been identified, it is useful to examine the spectrum, and by inspection to identify the corresponding members of the same n and δ , but with different core state, Ω . This is possible because of the strong resemblance in band shape and relative intensity between the different core series.

In the p.e. spectra, the $^2\Pi_{\frac{3}{2}}$, $_{\frac{1}{2}}$ states were observed to be equally intense. However in the optical spectrum the $(\Omega = \frac{1}{2})$ core series is generally more intense than the $(\Omega = \frac{3}{2})$ core series.

An explanation for this is that we have assumed (Ω_c, ω) coupling to exist in all the Rydberg states. Certainly this would appear reasonable, as there is no major change in the value of the splittings observed between the different components on going down the series from high to low n. This would suggest that there has been little change from (Ω_c, ω) coupling. However it is still likely that there is some (Λ, S) coupling character present, especially in the lower n series members and to that extent we may alternatively label the different components as $^1\Pi$ and $^3\Pi$. By the spin multiplicity selection rules we would expect the transitions to the $^3\Pi$ components to be forbidden and that to the $^1\Pi$ component fully allowed. It is this residual "forbiddeness" which may account for the slightly decreased intensity of the $\Omega = \frac{3}{2}$ core component.

In addition the difference in intensity between the corresponding members of a series with different core Ω value decreases with increasing n, as (Ω_c, ω) coupling becomes even more valid with higher n.

Another feature causing some problems in series identification is the fact that there is a near integral difference between the quantum defects of the ns and nd series. Now the observed term value is related to the value of $(n - \delta)^2$ and so the ns and nd series tend to merge together. This is especially true near the series limit where only the d series are clearly observed. In fact in the CSe_2 and SCSe spectra the ns series members are really rather poorly defined. In OCSe, on the other hand, although there is still a tendency for the s and d series to merge together, the ns series is particularly strong and well defined.

The third difficulty was only really acute in the case of OCSe. The problem arises from the fact that only the term values of the

(000) band will correctly predict the next (000) members of the series. Thus the complete tabulation of all the bands, term values and associated quantum defects contains much redundant and indeed misleading information as a result of including vibrationally excited states. Largely by inspection and trial and error it is possible to identify which are the electronic origins and which are the vibrationally excited states. In OCSe where the overall band envelopes consist of two overlapping bands, corresponding to the different core states, each of which exhibits long progressions in ν_1 and ν_3, it is doubtful whether a satisfactory analysis could have been started without the aid of the information available from the photoelectron studies.

e) Discussion of results.

Despite these several complications it has proved possible to analyse the spectra in considerable detail [18, 19,20] and the results given in Tables 3, 4, 5 are largely self-explanatory. However there still remain a few features which it is difficult to account for in a wholly satisfactory manner.

For instance in CSe_2 the $1\pi g \longrightarrow Se5p$ ($\Omega = \frac{3}{2}$) core transition is sharp whereas the corresponding transition to the higher energy ($\Omega = \frac{1}{2}$) core is diffuse. An analogous but even more complex situation exists in CS_2 where the much smaller energy difference between the different core states leads to considerable overlap of the upper vibrational members of the lower core state, and the diffuse envelope of the upper core state. By contrast in SCSe, see table 4, the vibrational members of both core states are clearly resolved, with no apparent diffuseness present. A possible reason for the diffuse-:ness in CS_2 and CSe_2 is that the potential energy surfaces may lie

so that the vibrational members of the upper state are predissociated by curve crossing to that of the lower state.[4]

i.e.

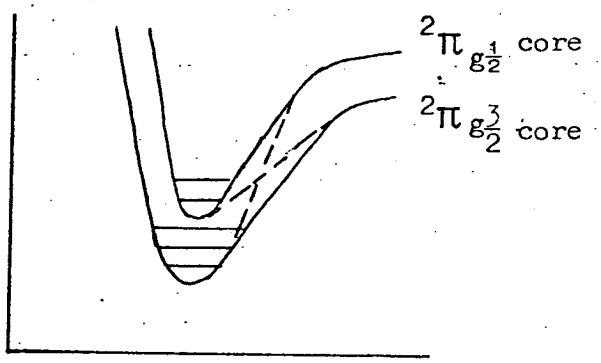

However the reason why such a situation does not apply in SCSe (or OCSe) is not at all obvious, although it may be connected with the absence of g and u symmetry in these latter molecules. However, had such an effect leading to diffuseness of the vibrational members of the ($\Omega = \frac{1}{2}$) core existed in OCSe, it is doubtful whether it would have been possible to analyse the spectrum. In CSe_2 and SCSe the other Rydberg series members only exhibit weak vibrational structure, if any, implying that the potential curves for these states lie almost directly above the potential curves for the ground state. This emphasises the essentially 'non-bonding' nature of the Rydberg orbitals.

Another puzzling feature, which occurs only in OCSe, is an apparent splitting of the initial members of the $2\pi \longrightarrow np$ series. Again, there is no wholly satisfactory explanation, but as it is confined to the early members of the series it might indicate that it arises from transitions to the $p\pi$ and $p\sigma$ levels of the 'p complex'[15] but that in the higher n values the splitting is too small to be observed.

f) Higher energy intervalence transitions.

When all the Rydberg series have been identified the remaining bands are either the higher energy valence level transitions or else the early members of other Rydberg series converging to the next I.P. Both types of band tend to be fairly weak and diffuse as a result of rapid dissociation or autoionisation effects. However it is often possible to distinguish between these two types of band using information obtained from the photoelectron spectrum and the results are presented in Table 6.

g) Configuration mixing effects.

One other particularly interesting feature observed in the spectra of CSe_2 and OCSe are apparent emissions such as shown in Figures 12, 13. Such 'window' effects have been noted previously in a few other molecules e.g.naphthalene[21] and have been the subject of a theoretical analysis.

The theory[22, 23] as originally developed was concerned with the autoionisation windows observed in the spectra of heavy atoms[24] and although such windows have also been observed in a few molecules e.g. SF_6,[25] the theory has mainly been employed to explain effects such as those reported here.

These arise as a result of configuration mixing between a discrete Rydberg state and a dissociation continuum of the same symmetry and energy leading to interference effects between the levels.[26] Depending on the magnitude and sign of certain parameters, especially the line profile index q, a variety of line shapes, ranging from totally destructive interference on one side and constructive on the other, may result,[27] as shown in Figure 14.

Table 6.

Higher Energy Intervalence Transitions.

CSe_2

Transition.	(cm^{-1})	Comment.
$3\sigma_u \leftarrow 1\pi_g$	~ 58,000	w. diffuse.
$2\pi_u \leftarrow 1\pi_u$	~ 65,000	m. diffuse.
$3\sigma_g \leftarrow 1\pi_u$	~68,500	w. diffuse.

SCSe

$6\sigma \leftarrow 2\pi$	~ 64,000	v. broad diffuse.
$3\pi \leftarrow 1\pi$	66,800 67,600 68,000 68,400	broad diffuse.
	~ 71,000	v.w. complex vibrational structure.
	~ 72,800	

OCSe

$5\sigma \leftarrow 2\pi$	~ 58,300	strongly mixed with Rydberg levels.
$6\sigma \leftarrow 2\pi$	67,500	

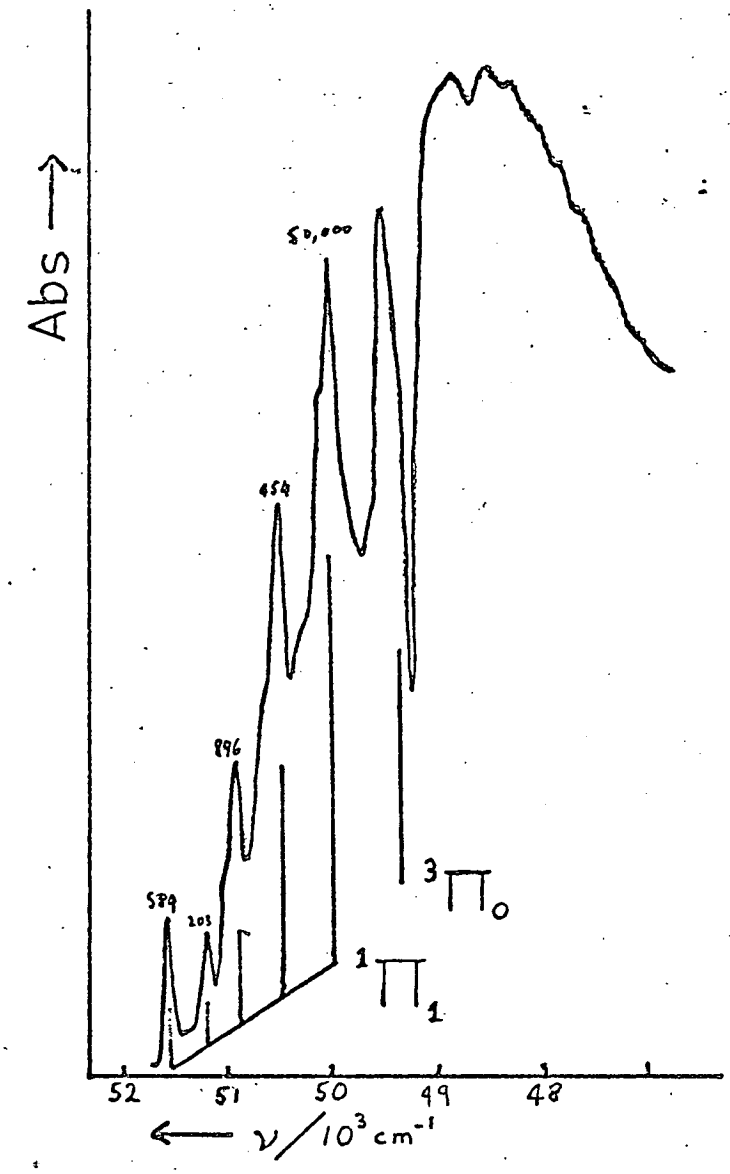

Figure 12

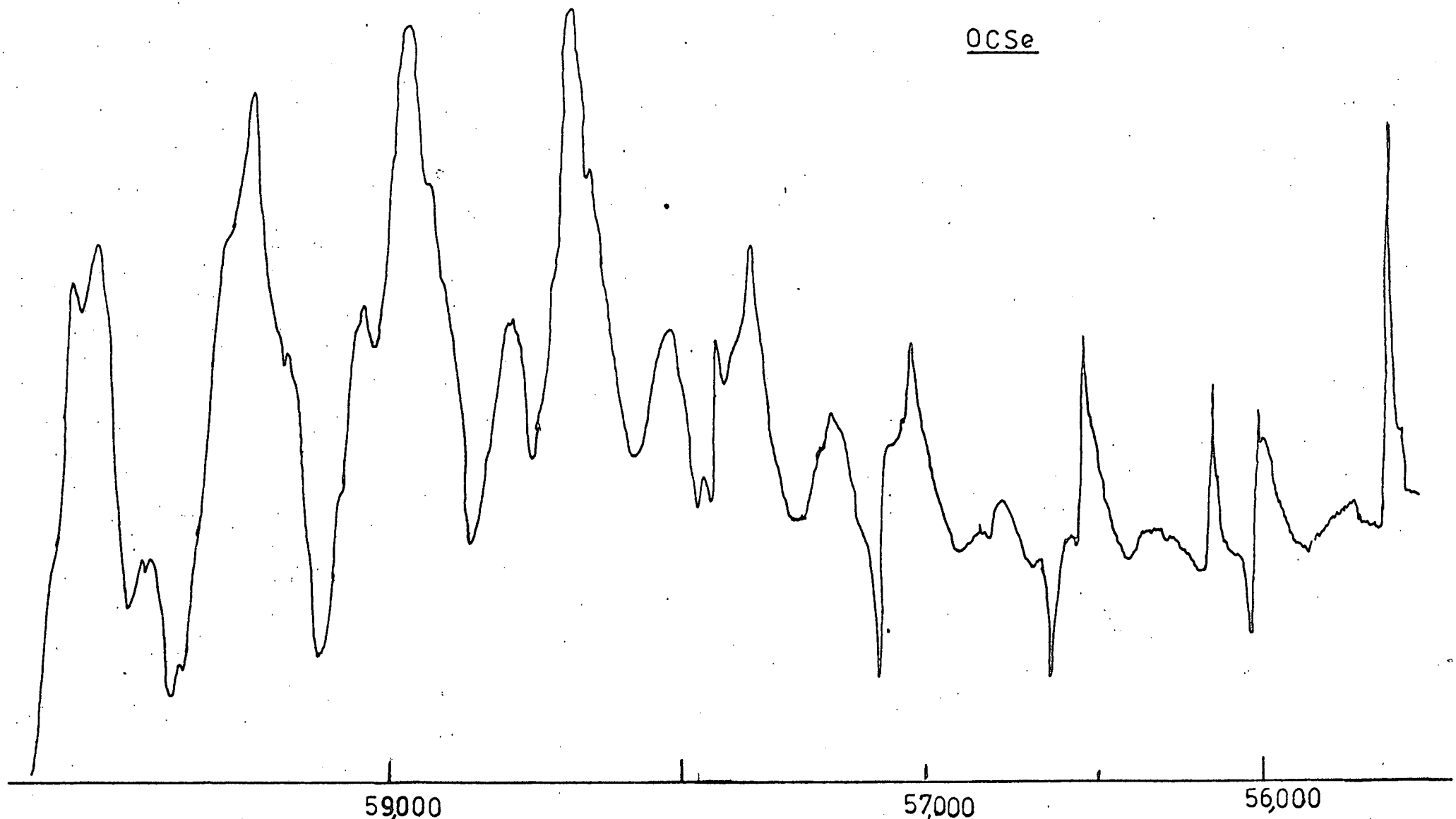

Fig. 13

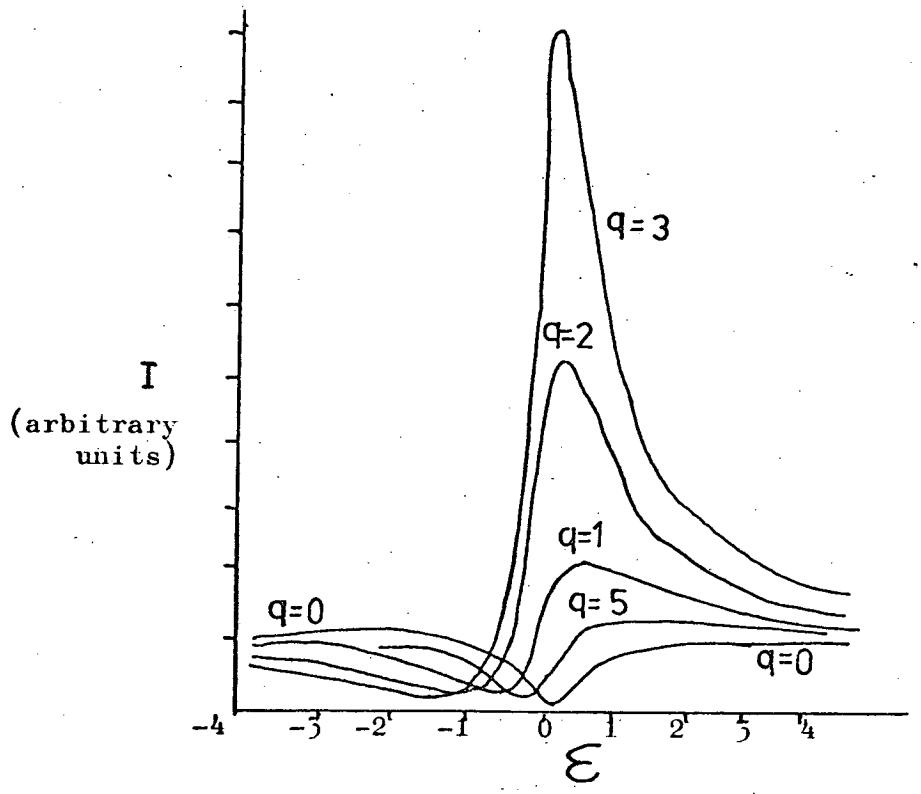

Figure 14

Line shape profiles.

In CSe_2 the states most likely to be involved are the $^3\Pi_o$ component of the Se 5s Rydberg state of $\Omega = \frac{1}{2}$ core and the Σ_u $(J = 0)$ vibronic continuum associated with the valence shell transition ($^1\Sigma_g^+ \rightarrow {}^1\Pi_g$) corresponding to the configuration ($\ldots.1\pi_g^3\ 3\sigma_g^1$). A similar analysis may apply to OCSe.[28]

REFERENCES.

1. A.D. Walsh; Chem. Soc. Revs. (1948), 2, 73.

2. H.H. Jaffe and M. Orchin; Theory and Applications of Ultraviolet Spectroscopy. Wiley and Sons, New York and London, (1962).

3. W.C. Price; Adv. At. Mol. Phys. (1974), 10, 132.

4. G. Herzberg; The Spectra and Structures of Simple Free Radicals, Cornell U.P. Ithaca, New York, (1971).

5. P.W. Atkins; Quanta, "A Handbook of Concepts," Clarendon Press, Oxford (1974).

6. S. Walker and H. Shaw; Spectroscopy Vol. II, Chapman Hall, (1962).

7. G.W. King; Spectroscopy and Molecular Structure, Holt Rinehart and Winston, New York, Chicago, San Francisco, Toronto, London, (1964).

8. V. Heine; Group Theory and Quantum Mechanics, Pergamon, New York, (1960).

9. H.G. Kuhn; Atomic Spectra, Longmans, London (1962), page 283.

10. G. Duxbury; The Electronic Spectra of Triatomic molecules and the Renner-Teller Effect; Molecular Spectroscopy, Volume 3, Chemical Society Specialist Periodical Reports, page 497.

11. R.J. Buenker, S.G. Peyerimhoff; Chem. Rev. (1974), 74, 127.

12. G.W. King and K. Srikameswaran; J. Mol. Spectros. (1969), 31, 269.

13. E.J. Finn and G.W. King; J. Mol. Spectros., (1975), 56, 39.

13a. M. Bavia, G. Dilonardo, C. Galloni and A. Trombetti; J.C.S. Faraday II, (1972), 68, 615.

14. J.W. Rabalais, J.M. McDonald, V. Scherr and S.P. McGlynn; Chem. Rev., (1971), 71, 73.

15. A.E. Douglas in, "Chemical Spectroscopy and Photochemistry in the Vacuum Ultraviolet" ed. C. Sandorfy, P.J. Ansloos and M.B. Robin; D. Reidel Publishing Co. Holland (1974), page 113.

16. S.P. McGlynn as Ref. 15 page 385.

17. M.B. Robin; Higher Excited States of Polyatomic Molecules Vol . I, Academic Press, 1974.

18. S. Cradock, R.J. Donovan, W. Duncan, H.M. Gillespie; J.C.S. Faraday II (1975) 71, 156.

19. S. Bell, S. Cradock, R.J. Donovan, W. Duncan; to be published.

20. S. Cradock, R.J. Donovan, W. Duncan, H.M. Gillespie; Chem. Phys. Letts., (1975) 31, 244.

21. J. Jortner and G.C. Morris; J. Chem. Phys. (1969), 51, 3869.

22. U. Fano; Nuovo Cimento (Series 8) (1935), 12, 154.

23. U. Fano; Phys. Revs. (1961), 124, 1866.

24. H. Beutler; Z. Physik (1935), 93, 177.

25. K. Codling; J. Chem. Physics (1966), 44, 4401.

26. U. Fano and J.W. Cooper; Phys. Revs. (1965), 137, 1364.

27. W.R.S. Garton; Adv. At. Mol. Phys. (1966), 2, 130.

28. S. Bell, S. Cradock, R.J. Donovan, W. Duncan; unpublished results.

RYDBERG TERM TABLES.

01.00	1097.37	906.92	762.06	649.33	559.88	487.72	428.66	379.71	338.70	303.98
	190.45	144.85	112.73	89.45	72.16	59.06	48.95	41.02	34.71	
00.99	1095.18	905.27	760.80	648.33	559.08	487.07	428.13	379.27	338.32	303.66
	189.91	144.48	112.46	89.25	72.01	58.95	48.86	40.95	34.66	
00.98	1093.00	903.63	759.53	647.34	558.29	486.42	427.59	378.82	337.94	303.34
	189.37	144.10	112.19	89.05	71.86	58.83	48.77	40.88	34.60	
00.97	1090.82	901.99	758.27	646.35	557.49	485.78	427.06	378.38	337.57	303.02
	188.82	143.72	111.92	88.85	71.72	58.72	48.68	40.81	34.55	
00.96	1088.65	900.36	757.01	645.36	556.70	485.13	426.53	377.93	337.20	302.71
	188.29	143.35	111.65	88.66	71.57	58.60	48.59	40.74	34.49	
00.95	1086.48	898.73	755.75	644.37	555.91	484.49	426.00	377.49	336.82	302.39
	187.75	142.98	111.39	88.46	71.42	58.49	48.50	40.67	34.43	
00.94	1084.32	897.11	754.50	643.38	555.12	483.84	425.46	377.05	336.45	302.07
	187.22	142.61	111.12	88.26	71.27	58.38	48.42	40.60	34.38	
00.93	1082.17	895.49	753.25	642.40	554.33	483.20	424.94	376.61	336.08	301.75
	186.68	142.24	110.85	88.07	71.13	58.27	48.33	40.53	34.32	
00.92	1080.02	893.87	752.00	641.41	553.54	482.56	424.41	376.17	335.70	301.44
	186.15	141.87	110.59	87.87	70.98	58.15	48.24	40.46	34.27	
00.91	1077.88	892.26	750.76	640.43	552.75	481.92	423.88	375.73	335.33	301.12
	185.62	141.50	110.33	87.68	70.83	58.04	48.15	40.39	34.21	
00.90	1075.75	890.65	749.52	639.46	551.97	481.28	423.35	375.29	334.96	300.81
	185.10	141.13	110.06	87.49	70.69	57.93	48.07	40.32	34.16	
00.89	1073.62	889.05	748.28	638.48	551.19	480.65	422.83	374.85	334.59	300.49
	184.57	140.77	109.80	87.29	70.54	57.82	47.98	40.25	34.10	
00.88	1071.50	887.45	747.05	637.51	550.41	480.01	422.30	374.41	334.22	300.18
	184.05	140.40	109.54	87.10	70.40	57.71	47.89	40.19	34.05	
00.87	1069.39	885.86	745.82	636.54	549.63	479.38	421.78	373.97	333.86	299.86
	183.53	140.04	109.28	86.91	70.25	57.60	47.81	40.12	33.99	
00.86	1067.28	884.27	744.59	635.57	548.85	478.74	421.26	373.54	333.49	299.55
	183.01	139.68	109.02	86.72	70.11	57.49	47.72	40.05	33.94	
00.85	1065.18	882.68	743.36	634.60	548.08	478.11	420.74	373.10	333.12	299.24
	182.50	139.32	108.76	86.53	69.97	57.38	47.63	39.98	33.88	
00.84	1063.08	881.10	742.14	633.64	547.30	477.48	420.22	372.67	332.75	298.93
	181.98	138.96	108.50	86.34	69.82	57.26	47.55	39.91	33.83	
00.83	1060.99	879.52	740.92	632.68	546.53	476.85	419.70	372.23	332.39	298.61
	181.47	138.60	108.25	86.15	69.68	57.16	47.46	39.84	33.77	
00.82	1058.91	877.95	739.71	631.72	545.76	476.22	419.18	371.80	332.02	298.30
	180.96	138.24	107.99	85.96	69.54	57.05	47.38	39.78	33.72	
00.81	1056.83	876.38	738.49	630.76	544.99	475.60	418.66	371.37	331.66	297.99
	180.45	137.89	107.73	85.77	69.39	56.94	47.29	39.71	33.67	
00.80	1054.76	874.82	737.28	629.80	544.22	474.97	418.14	370.93	331.29	297.68
	179.94	137.54	107.48	85.58	69.25	56.83	47.21	39.64	33.61	
00.79	1052.69	873.26	736.08	628.85	543.46	474.35	417.63	370.50	330.93	297.37
	179.44	137.18	107.22	85.39	69.11	56.72	47.12	39.58	33.56	

00.45	985.94	822.80	698.75	597.69	518.36	455.85	400.64	356.29	318.91	287.12	
	163.33	125.87	99.04	79.33	64.53	53.19	44.36	37.38	31.79		
00.44	984.07	821.18	695.62	596.81	517.64	453.25	400.16	355.88	318.57	286.82	
	162.89	125.56	98.82	79.16	64.40	53.09	44.28	37.32	31.74		
00.43	982.21	819.76	694.52	595.93	516.93	452.66	399.68	355.48	318.22	286.53	
	162.45	125.24	98.59	78.99	64.27	52.99	44.20	37.25	31.69		
00.42	980.35	818.35	693.41	595.05	516.22	452.08	399.20	355.07	317.88	286.24	
	162.01	124.93	98.36	78.83	64.14	52.89	44.12	37.19	31.64		
00.41	978.50	816.93	692.31	594.18	515.52	451.50	398.71	354.67	317.54	285.95	
	161.57	124.62	98.14	78.66	64.01	52.79	44.05	37.13	31.59		
00.40	976.66	815.53	691.21	593.30	514.81	450.93	398.23	354.27	317.20	285.66	
	161.13	124.31	97.91	78.49	63.89	52.69	43.97	37.07	31.54		
00.39	974.82	814.12	690.12	592.43	514.11	450.35	397.75	353.86	316.86	285.36	
	160.70	124.00	97.69	78.32	63.76	52.59	43.89	37.01	31.49		
00.38	972.98	812.72	689.03	591.56	513.40	449.77	397.28	353.46	316.52	285.07	
	160.26	123.70	97.46	78.16	63.63	52.50	43.81	36.95	31.44		
00.37	971.15	811.32	687.93	590.69	512.70	449.20	396.80	353.06	316.18	284.78	
	159.83	123.39	97.24	77.99	63.51	52.40	43.74	36.89	31.39		
00.36	969.33	809.93	686.85	589.83	512.00	448.62	396.32	352.66	315.84	284.49	
	159.40	123.08	97.02	77.83	63.38	52.30	43.66	36.82	31.34		
00.35	967.51	808.54	685.76	588.96	511.30	448.05	395.85	352.26	315.50	284.20	
	158.97	122.78	96.80	77.66	63.25	52.20	43.58	36.76	31.29		
00.34	965.69	807.15	684.68	588.10	510.61	447.48	395.37	351.86	315.16	283.91	
	158.54	122.48	96.58	77.50	63.13	52.11	43.51	36.70	31.25		
00.33	963.88	805.77	683.60	587.24	509.91	446.91	394.90	351.46	314.82	283.63	
	158.11	122.17	96.36	77.33	63.00	52.01	43.43	36.64	31.20		
00.32	962.08	804.39	682.52	586.38	509.22	446.34	394.42	351.07	314.49	283.34	
	157.69	121.87	96.14	77.17	62.88	51.91	43.36	36.58	31.15		
00.31	960.28	803.02	681.44	585.53	508.52	445.77	393.95	350.67	314.15	283.05	
	157.26	121.57	95.92	77.00	62.76	51.82	43.28	36.52	31.10		
00.30	958.49	801.65	680.37	584.67	507.83	445.20	393.48	350.27	313.81	282.76	
	156.84	121.27	95.70	76.84	62.63	51.72	43.20	36.46	31.05		
00.29	956.70	800.28	679.30	583.82	507.14	444.63	393.01	349.88	313.48	282.48	
	156.42	120.97	95.48	76.68	62.51	51.62	43.13	36.40	31.00		
00.28	954.91	798.91	678.23	582.97	506.45	444.07	392.54	349.48	313.14	282.19	
	156.00	120.68	95.26	76.52	62.38	51.53	43.05	36.34	30.95		
00.27	953.13	797.55	677.17	582.12	505.76	443.50	392.07	349.09	312.81	281.90	
	155.59	120.38	95.05	76.36	62.26	51.43	42.98	36.28	30.91		
00.26	951.36	796.19	676.11	581.27	505.08	442.94	391.60	348.70	312.48	281.62	
	155.17	120.09	94.83	76.19	62.14	51.34	42.90	36.22	30.86		
00.25	949.59	794.84	675.05	580.43	504.39	442.38	391.13	348.30	312.14	281.33	
	154.75	119.79	94.62	76.03	62.02	51.24	42.83	36.16	30.81		
00.24	947.83	793.49	673.99	579.58	503.71	441.82	390.67	347.91	311.81	281.05	
	154.34	119.50	94.40	75.87	61.89	51.15	42.76	36.10	30.76		
00.23	946.07	792.14	672.93	578.74	503.03	441.26	390.20	347.52	311.48	280.76	
	153.93	119.20	94.19	75.71	61.77	51.06	42.68	36.04	30.71		
00.22	944.31	790.79	671.88	577.90	502.35	440.70	389.74	347.13	311.15	280.48	
	153.52	118.91	93.98	75.56	61.65	50.96	42.61	35.98	30.67		
00.21	942.56	789.45	670.83	577.07	501.67	440.14	389.27	346.74	310.81	280.20	
	153.11	118.62	93.76	75.40	61.53	50.87	42.53	35.92	30.62		
00.20	940.82	788.12	669.78	576.23	500.99	439.58	388.81	346.35	310.48	279.91	
	152.70	118.33	93.55	75.24	61.41	50.77	42.46	35.87	30.57		
00.19	939.08	786.78	668.74	575.40	500.32	439.03	388.35	345.96	310.15	279.63	
	152.30	118.04	93.34	75.08	61.29	50.68	42.39	35.81	30.52		
00.18	937.34	785.45	667.69	574.56	499.64	438.47	387.88	345.57	309.82	279.35	
	151.89	117.76	93.13	74.92	61.17	50.59	42.31	35.75	30.48		
00.17	935.61	784.12	666.65	573.73	498.97	437.92	387.42	345.18	309.49	279.07	
	151.49	117.47	92.92	74.77	61.05	50.49	42.24	35.69	30.43		
00.16	933.89	782.80	665.62	572.90	498.29	437.36	386.96	344.80	309.17	278.79	
	151.09	117.18	92.71	74.61	60.93	50.40	42.17	35.63	30.38		
00.15	932.17	781.48	664.58	572.08	497.62	436.81	386.50	344.41	308.84	278.51	
	150.69	116.90	92.50	74.45	60.81	50.31	42.09	35.57	30.33		
00.14	930.45	780.16	663.55	571.25	496.95	436.26	386.05	344.03	308.51	278.22	
	150.29	116.61	92.30	74.30	60.69	50.22	42.02	35.51	30.29		
00.13	928.74	778.85	662.52	570.43	496.29	435.71	385.59	343.64	308.18	277.94	
	149.89	116.33	92.09	74.14	60.57	50.12	41.95	35.46	30.24		

00.78	1050.64	871.70	734.87	627.90	542.69	473.72	417.11	370.07	330.57	297.06	
	178.93	136.83	106.97	85.21	68.97	56.61	47.04	39.51	33.50		
00.77	1048.58	870.15	733.67	626.95	541.93	473.10	416.60	369.64	330.20	296.75	
	178.43	136.48	106.72	85.02	68.83	56.50	46.95	39.44	33.45		
00.76	1046.54	868.60	732.47	626.01	541.17	472.48	416.09	369.22	329.84	296.45	
	177.93	136.13	106.47	84.83	68.69	56.39	46.87	39.37	33.40		
00.75	1044.49	867.06	731.28	625.06	540.41	471.86	415.57	368.79	329.48	296.14	
	177.44	135.78	106.22	84.65	68.55	56.29	46.79	39.31	33.34		
00.74	1042.46	865.52	730.08	624.12	539.65	471.24	415.06	368.36	329.12	295.83	
	176.94	135.44	105.97	84.46	68.41	56.18	46.70	39.24	33.29		
00.73	1040.43	863.98	728.89	623.18	538.90	470.63	414.55	367.93	328.76	295.52	
	176.45	135.09	105.72	84.28	68.27	56.07	46.62	39.18	33.24		
00.72	1038.41	862.45	727.71	622.24	538.14	470.01	414.04	367.51	328.40	295.22	
	175.95	134.75	105.47	84.10	68.13	55.97	46.53	39.11	33.18		
00.71	1036.39	860.93	726.52	621.30	537.39	469.40	413.54	367.08	328.04	294.91	
	175.46	134.40	105.22	83.91	67.99	55.86	46.45	39.04	33.13		
00.70	1034.38	859.40	725.34	620.37	536.64	468.78	413.03	366.66	327.68	294.60	
	174.98	134.06	104.97	83.73	67.86	55.75	46.37	38.98	33.08		
00.69	1032.37	857.88	724.17	619.44	535.89	468.17	412.52	366.24	327.32	294.30	
	174.49	133.72	104.73	83.55	67.72	55.65	46.29	38.91	33.02		
00.68	1030.37	856.37	722.99	618.51	535.14	467.56	412.02	365.81	326.97	294.00	
	174.00	133.38	104.48	83.37	67.58	55.54	46.20	38.85	32.97		
00.67	1028.38	854.86	721.82	617.58	534.39	466.95	411.51	365.39	326.61	293.69	
	173.52	133.04	104.24	83.19	67.45	55.44	46.12	38.78	32.92		
00.66	1026.39	853.35	720.65	616.66	533.65	466.34	411.01	364.97	326.25	293.39	
	173.04	132.70	103.99	83.01	67.31	55.33	46.04	38.72	32.87		
00.65	1024.41	851.85	719.48	615.73	532.91	465.73	410.51	364.55	325.90	293.08	
	172.56	132.37	103.75	82.83	67.17	55.23	45.96	38.65	32.81		
00.64	1022.43	850.35	718.32	614.81	532.16	465.13	410.00	364.13	325.54	292.78	
	172.08	132.03	103.51	82.65	67.04	55.12	45.88	38.59	32.76		
00.63	1020.46	848.85	717.16	613.89	531.42	464.52	409.50	363.71	325.19	292.48	
	171.61	131.70	103.27	82.47	66.90	55.02	45.79	38.52	32.71		
00.62	1018.50	847.36	716.00	612.97	530.68	463.92	409.00	363.29	324.84	292.18	
	171.13	131.36	103.03	82.29	66.77	54.91	45.71	38.46	32.66		
00.61	1016.54	845.88	714.84	612.06	529.95	463.32	408.50	362.87	324.48	291.88	
	170.66	131.03	102.79	82.11	66.63	54.81	45.63	38.39	32.61		
00.60	1014.58	844.39	713.69	611.15	529.21	462.71	408.01	362.46	324.13	291.58	
	170.19	130.70	102.55	81.93	66.50	54.71	45.55	38.33	32.55		
00.59	1012.63	842.91	712.54	610.23	528.48	462.11	407.51	362.04	323.78	291.27	
	169.72	130.37	102.31	81.76	66.36	54.60	45.47	38.26	32.50		
00.58	1010.69	841.44	711.39	609.32	527.74	461.51	407.01	361.62	323.43	290.97	
	169.25	130.04	102.07	81.58	66.23	54.50	45.39	38.20	32.45		
00.57	1008.75	839.97	710.25	608.42	527.01	460.92	406.52	361.21	323.08	290.68	
	168.79	129.71	101.83	81.40	66.10	54.40	45.31	38.13	32.40		
00.56	1006.82	838.50	709.11	607.51	526.28	460.32	406.02	360.80	322.72	290.38	
	168.32	129.39	101.60	81.23	65.96	54.30	45.23	38.07	32.35		
00.55	1004.90	837.03	707.97	606.61	525.55	459.72	405.53	360.38	322.38	290.08	
	167.86	129.06	101.36	81.05	65.83	54.19	45.15	38.01	32.30		
00.54	1002.98	835.57	706.83	605.71	524.83	459.13	405.04	359.97	322.03	289.78	
	167.40	128.74	101.13	80.88	65.70	54.09	45.07	37.94	32.25		
00.53	1001.06	834.12	705.70	604.81	524.10	458.54	404.55	359.56	321.68	289.48	
	166.94	128.42	100.89	80.71	65.57	53.99	44.99	37.88	32.19		
00.52	999.15	832.66	704.57	603.91	523.38	457.94	404.05	359.15	321.33	289.19	
	166.49	128.09	100.66	80.53	65.44	53.89	44.91	37.82	32.14		
00.51	997.25	831.22	703.44	603.02	522.66	457.35	403.56	358.74	320.98	288.89	
	166.03	127.77	100.43	80.36	65.30	53.79	44.83	37.75	32.09		
00.50	995.35	829.77	702.32	602.12	521.94	456.76	403.08	358.33	320.63	288.59	
	165.58	127.45	100.19	80.19	65.17	53.69	44.75	37.69	32.04		
00.49	993.46	828.33	701.20	601.23	521.22	456.17	402.59	357.92	320.29	288.30	
	165.13	127.13	99.96	80.02	65.04	53.59	44.67	37.63	31.99		
00.48	991.57	826.89	700.08	600.34	520.50	455.59	402.10	357.51	319.94	288.00	
	164.68	126.82	99.73	79.84	64.91	53.49	44.59	37.57	31.94		
00.47	989.69	825.46	698.96	599.46	519.78	455.00	401.61	357.10	319.60	287.71	
	164.23	126.50	99.50	79.67	64.78	53.39	44.51	37.50	31.89		
00.46	987.81	824.03	697.84	598.57	519.07	454.41	401.13	356.69	319.25	287.41	
	163.78	126.18	99.27	79.50	64.65	53.29	44.43	37.44	31.84		

00.12	921.05	777.54	661.49	589.61	493.62	435.16	385.13	343.26	307.86	277.67
	149.50	116.05	91.88	73.99	60.46	50.03	41.88	35.40	30.19	
00.11	925.33	776.23	660.46	568.79	494.95	434.62	384.68	342.87	307.53	277.39
	149.10	115.77	91.68	73.83	60.34	49.94	41.80	35.34	30.15	
00.10	923.64	774.93	659.44	567.97	494.29	434.07	384.22	342.49	307.21	277.11
	148.71	115.49	91.47	73.68	60.22	49.85	41.73	35.28	30.10	
00.09	921.94	773.62	658.42	567.15	493.63	433.52	383.77	342.11	306.88	276.83
	148.32	115.21	91.27	73.53	60.10	49.76	41.66	35.23	30.05	
00.08	920.26	772.33	657.40	566.34	492.96	432.98	383.31	341.73	306.56	276.55
	147.93	114.93	91.06	73.37	59.99	49.67	41.59	35.17	30.01	
00.07	918.57	771.03	656.38	565.52	492.30	432.44	382.86	341.35	306.23	276.27
	147.54	114.65	90.86	73.22	59.87	49.58	41.52	35.11	29.96	
00.06	916.89	769.74	655.37	564.71	491.65	431.89	382.41	340.96	305.91	276.00
	147.15	114.37	90.65	73.07	59.75	49.49	41.44	35.05	29.91	
00.05	915.22	768.45	654.36	563.90	490.99	431.35	381.96	340.58	305.59	275.72
	146.77	114.10	90.45	72.92	59.64	49.40	41.37	35.00	29.87	
00.04	913.55	767.17	653.35	563.10	490.33	430.81	381.51	340.21	305.27	275.44
	146.38	113.82	90.25	72.76	59.52	49.30	41.30	34.94	29.82	
00.03	911.89	765.89	652.34	562.29	489.68	430.27	381.06	339.83	304.94	275.17
	146.00	113.55	90.05	72.61	59.40	49.22	41.23	34.88	29.78	
00.02	910.23	764.61	651.33	561.49	489.02	429.73	380.61	339.45	304.62	274.89
	145.62	113.28	89.85	72.46	59.29	49.13	41.16	34.83	29.73	
00.01	908.57	763.34	650.33	560.68	488.37	429.20	380.16	339.07	304.30	274.62
	145.23	113.00	89.65	72.31	59.17	49.04	41.09	34.77	29.68	

CHAPTER IV.

THE PHOTOELECTRON SPECTRA OF MAIN GROUP CYCLOPENTADIENYLS.

THE PHOTOELECTRON SPECTRA OF MAIN GROUP CYCLOPENTADIENYLS. Page No.

1. INTRODUCTION.

a) Main group cyclopentadienyls.

In this chapter we will be concerned with the structure and bonding in the cyclopentadiene deriatives of the heavy main group elements, Tl C_5H_5, In C_5H_5; $Sn(C_5H_5)_2$, Pb $(C_5H_5)_2$ and Hg $(C_5H_5)_2$.[1] Some of the other heavy main group elements are also known to form a cyclopentadienyl derivative e.g. Cd $(C_5H_5)_2$,[2] Sb $(C_5H_5)_3$ and Bi $(C_5H_5)_3$, but these decompose or disproportionate on heating,[3] and so were not synthesised in this study.

Accurate gas phase structures and bond lengths have been determined previously for all the compounds studied,[4,5,6] except for Hg $(C_5H_5)_2$, whose structure has been deduced from its i.r. spectrum in solution.[7]

The purpose of the study was to see how the different structures and bonding schemes which exist in these compounds would be revealed and understood using Photoelectron Spectroscopy. It will also be useful to make comparison with the p.e. spectra of other metal cyclopentadienyl compounds.[8,9,10]

b) Bonding schemes in metal cyclopentadienyls.

Given that the known range of metal cyclopentadienides compares in size and distribution throughout the periodic table with those of the metal halides and metal oxides,[3] it is not surprising that there are often marked differences in their physical and chemical properties.

Thus, largely on the basis of i.r. evidence, Fritz[11] has classified the observed spectra into 4 different groups, according to the nature of the bonding between the metal and the cyclopentadienyl ligand(s).[12] These classes are:-

1. Ionically bonded; e.g. K C_5H_5, Rb C_5H_5, $Ca(C_5H_5)_2$ and $Sr(C_5H_5)_2$. Here the metal is ionically bonded to the C_5H_5 ring and the i.r. spectrum is essentially the same as that of the $C_5H_5^-$ ion which possesses D_{5h} symmetry. These compounds can easily be understood as salts of the weak acid C_5H_6 (pK_a = 20) formed by strongly electropositive metals; the $C_5H_5^-$ ion as predicted from simple Huckel theory, has a resonance stabilised aromatic sextet of electrons.

2. Centrally σ bonded; e.g. Li C_5H_5, Tl C_5H_5, Mg $(C_5H_5)_2$. Here the metal is bonded to the centre of the C_5H_5 ring and the ring spectrum interpreted on the basis of C_{5v} symmetry. Unlike type (1), this class of complex can also show metal-ligand vibrations.

3. Centrally π bonded; e.g. Fe $(C_5H_5)_2$, Ru $(C_5H_5)_2$, $Ni(C_5H_5)_2$. The large number of transition metal cyclopentadienyl complexes are almost all of this type, in which the metal is bonded to the centre of the ring via a π bond. The C_5H_5 rings exhibit similar spectra to (2), but the CH out of plane deformation frequencies are usually higher than for type (2). In addition to the metal-ring stretching vibrations, this type of complex also exhibits other skeletal modes in the far i.r.

4. Diene σ bonded; e.g. Hg $(C_5H_5)_2$, $Me_3SiC_5H_5$. In this type of complex the metal is bonded to one of the ring carbons

through a σ bond. The i.r. spectra are similar to that of C_5H_6 and quite distinct from those exhibited by the other types of metal cyclopentadienyls.

However, it should be noted that this classification scheme relates to solids (or in some cases solutions), and may not be strictly relevant to our studies on isolated gaseous molecules.

c) Previous photoelectron studies of metal cyclopentadienyls.

A considerable amount of effort on the part of theoretical chemists has gone into devising suitable molecular orbital bonding schemes to account for the remarkable sandwich type structures of molecules like ferrocene. These schemes have largely been based on constructing m.o.'s from suitable combinations of the ligand orbitals of appropriate symmetry and energy to interact with the metal d orbitals which, under the influence of the ligand field, are no longer degenerate.[14] The results of various semi-empirical calculations have led to different estimates of the orbital energies and order;[13] likewise they have produced conflicting estimates of the charge distribution in the molecule.[15] Nevertheless, there is little dispute about the qualitative features of the bonding and it is quite clear that $Fe(C_5H_5)_2$ can only be regarded as a derivative of Fe(II) in a purely formal sense as the bonding is mostly covalent in nature. These predictions have largely been confirmed by p.e. spectroscopy

Comparison of the p.e. spectra of $Fe(C_5H_5)_2$ and $Mg(C_5H_5)_2$[8] in which the d orbitals of Mg are assumed to take no part in the bonding, reveal two additional bands of relative intensity 2:1 at approximately 7 e.V. in the spectrum of $Fe(C_5H_5)_2$.

These must be due to ionisation from the predominantly metal

3d orbital levels in $Fe(C_5H_5)_2$. The higher ionisation energy bands, which are common to both spectra, appear to be characteristic of the $C_5H_5^-$ species, and can be attributed to ionisation from the essentially ligand π and σ levels in the complex.

Such an analysis in which direct comparison is made between the molecular levels in the neutral species and the results of the photoelectron spectrum, (which relates to the molecular ion), assumes the validity of Koopmans' Theorem.[16] However, recent ab initio calculations have cast serious doubt upon its validity in $Fe(C_5H_5)_2$[17] and C_5H_5NiNO.[18] Essential to the application of Koopmans' Theorem is the assumption that no electronic reorganisation of the orbital energies takes place on ionisation, and such are the differences in charge delocalisation possible when ionisation takes place from an orbital largely localised on the metal atom, compared with that possible for ionisation from orbitals delocalised over the C_5H_5 rings, that a substantial degree of electronic rearrangements may in fact occur on ionisation from the predominantly metal m.o.'s. In the case of the essentially Ni 3d levels of C_5H_5NiNO this energy has been estimated to be about 6 e.V.

This breakdown in Koopmans' Theorem is likely to occur for most of the metal cyclopentadienyl systems under discussion, but it is to be hoped that the deviations which will occur within a group of related molecules will be sufficiently systematic to at least allow a reasonably valid indication of trends within the group to be determined.

Using this as a justification the photoelectron spectra of several of the transition metal cyclopentadienyl compounds and their ring substituted deriatives have been analysed assuming Koopmans'

Theorem.[8,9] Of particular interest are the spectra of the species $V(C_5H_5)_2$, $Cr(C_5H_5)_2$, $Co(C_5H_5)_2$, and $Ni(C_5H_5)_2$,[9] all of which exhibit complex metal 3d ionisation bands in the low energy region of the spectrum. This is due to the larger number of ion states accessible from the open shell electronic configurations of the neutral molecule compared with a closed shell species e.g. $Fe(C_5H_5)_2$.

The photelectron spectrum of $Mn(C_5H_5)_2$[9] has been interpreted in terms of a high spin, partially ionic structure, which is consistent with the analysis of its i.r. spectrum.[11]

d) Relationship between structure and bonding.

In the discussion and analysis of the results to be presented we will see much of the fundamental relationship between structure and bonding. These two largely complementary features are related by molecular symmetry. The structure imposes restrictions on all molecular wavefunctions which must conform to the symmetry properties of the molecular geometry. As a result, the symmetry properties are fundamental in determining the bonding possible for a particular structure, as only atomic and molecular orbitals of the same symmetry can combine. In addition, although the symmetry conditions may be satisfied, significant bonding will not occur when there is too great an energy difference between the orbitals involved. When drawing up qualitative m.o. bonding schemes it will therefore be necessary to consider both the energy and the symmetry species of the component molecular or atomic orbitals. Thus prior to the analysis and discussion of the p.e. spectra it will be necessary to estimate the energy

levels and determine the symmetries of the cyclopentadienyl ligand and metal orbitals. This we shall now do.

2. THALLIUM DICYCLOPENTADIENYL AND INDIUM DICYCLOPENTADIENYL.

a) Molecular orbital energy levels of C_5H_5.

Unfortunately, as p.e. spectroscopy is not yet sufficiently developed in the techniques required to obtain the spectra of species as short-lived as $C_5H_5^-$, directly determined values of the molecular orbital energies have not been recorded. However, it is possible to make estimates of these levels from a knowledge of the p.e. spectrum of C_5H_6.[19]

This has been recorded and the results analysed with the aid of both extended Huckel[19] and spectroscopically parameterised INDO (SPINDO) calculations.[20] In addition, the results of the SPINDO calculations agree well with those of a recent ab initio calculation,[21] the assignments of which are shown in Figure 1.

On changing from C_5H_6 to $C_5H_5^-$ the molecular symmetry also changes, from C_{2v} to D_{5h}, and using group correlation methods,[22] the symmetry of the corresponding molecular oribitals in $C_5H_5^-$ are readily obtained from those of C_5H_6. It is worth noting that this leads to the result, also demonstrated to be the case in C_6H_6,[23] that the uppermost σ levels of the ring are intermediate in energy between the two occupied π levels, e_1'' and a_2''.

We can check the number and symmetry of the molecular orbitals of $C_5H_5^-$ from consideration of the manner in which the atomic orbitals of C and H can combine in $C_5H_5^-$. Each C will contribute 4 electrons and each H will contribute 1 electron, making a total of 25 + 1 = 26 in $C_5H_5^-$. These 26 electrons form $5(C-C)\sigma$, $5(C-H)\sigma$ and $3(C-C)\pi$ bonds of symmetry

$$\left.\begin{array}{ll}(C-C)\sigma & : \; a_1' + e_1' + e_2' \\ (C-H)\sigma & : \; a_1' + e_1' + e_2'\end{array}\right\} \quad 20 \text{ electrons}$$

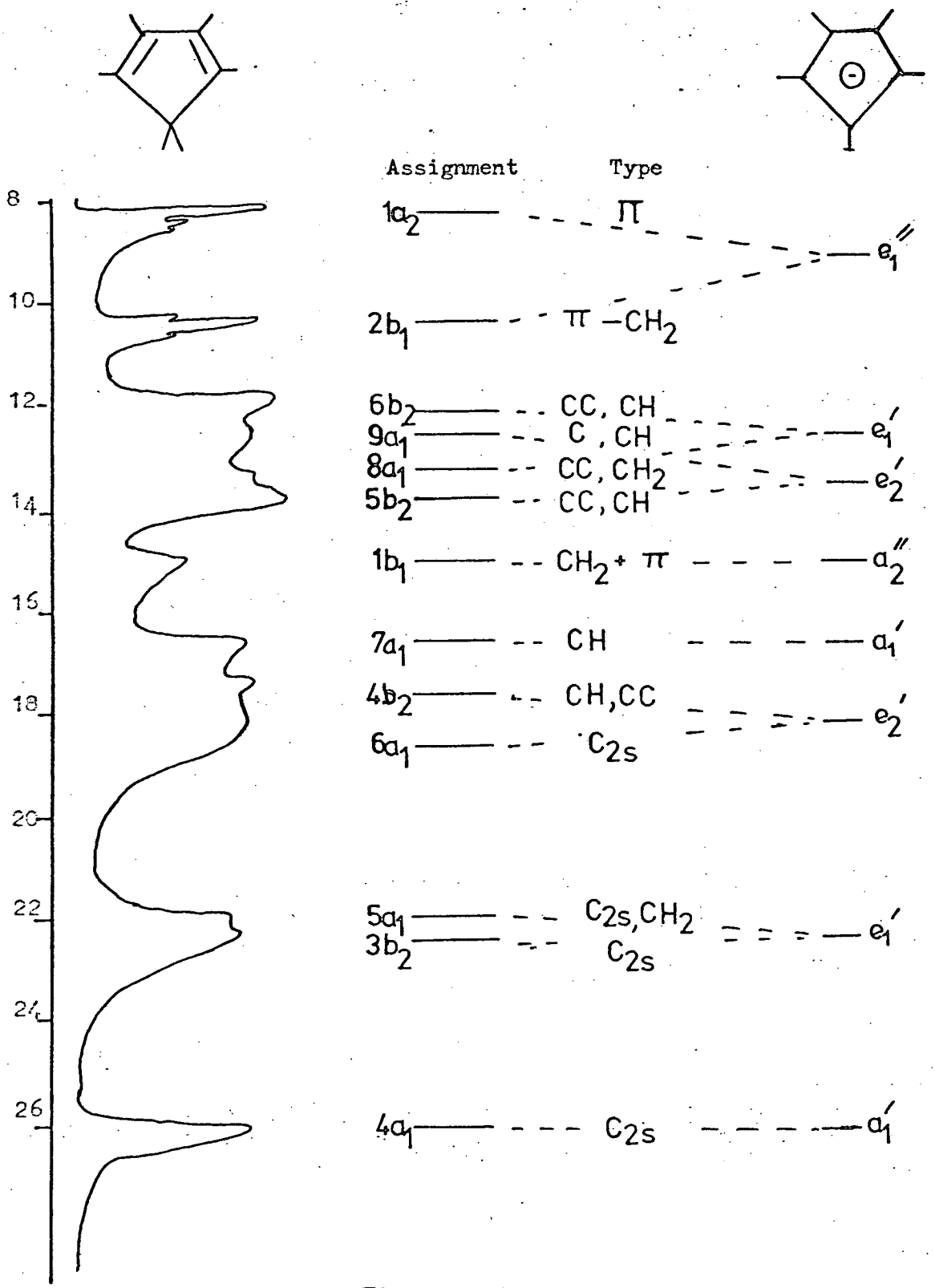
Assignment
Type
8
10
12
14
16
18
20
22
24
26
1a2 — π — e1''
2b1 — π — CH2
6b2 — CC, CH
9a1 — C, CH
8a1 — CC, CH2
5b2 — CC, CH
e1'
e2'
1b1 — CH2 + π — a2''
7a1 — CH — a1'
4b2 — CH, CC
6a1 — C2s
e2'
5a1 — C2s, CH2
3b2 — C2s
e1'
4a1 — C2s — a1'

Figure 1

$(C - C)\ \pi$: $a''_2 + e''_1$ 6 electrons

and comparison of these with the results of Figure 1 bears out the original assignments.

b) Atomic energy levels of Thallium and Indium.

Of the metals under consideration, only the gas phase u.v. p.e. spectra of Hg and Pb have been reported.[24,33] However, in the case of the other metals we can estimate the binding energies of the atomic orbitals from optical absorption spectra.[25]

In the case of Tl, the relevant transitions are:-

		cm^{-1}
Tl(I) $^2P_{\frac{1}{2}}$ $(..5d^{10}6s^26p)$	$\longrightarrow$ Tl(II) ^1S_o $(.,5d^{10}6s^2)$	49250
	$\longrightarrow$ Tl(I) $^2P_{\frac{1}{2}}$ $(..5d^{10}6s6p^2)$	67150
	$\longrightarrow$ Tl(I) $^2D_{\frac{3}{2}}$ $(..5d^{10}6s^26d)$	36200
Tl(II) ^1So $(..5d^{10}6s^2)$	$\longrightarrow$ Tl(II) 1^o $(5d^96s^26p)$	110390

and using this information we can derive the energy level diagram shown in Figure 2a, as follows.

The transition $Tl(I)\,^2P_{\frac{1}{2}} \longrightarrow Tl(II)\,^1S_o$ gives us the ionisation of the Tl 6p level as 6·1 e.V. and the other transitions give the energies of the 6s, 6d and 5d levels relative to the Tl 6p level. It must be emphasised that although care was taken to choose transitions to states which are fairly representative of the energy differences between the centres of the various configurations possible on excitation, the analysis of the spectrum just performed can only give a rough indication of the ionisation energies of the atomic levels involved. Nevertheless, these values will be sufficiently accurate for our purposes and provied we choose the same transitions in systems of related configuration then valid

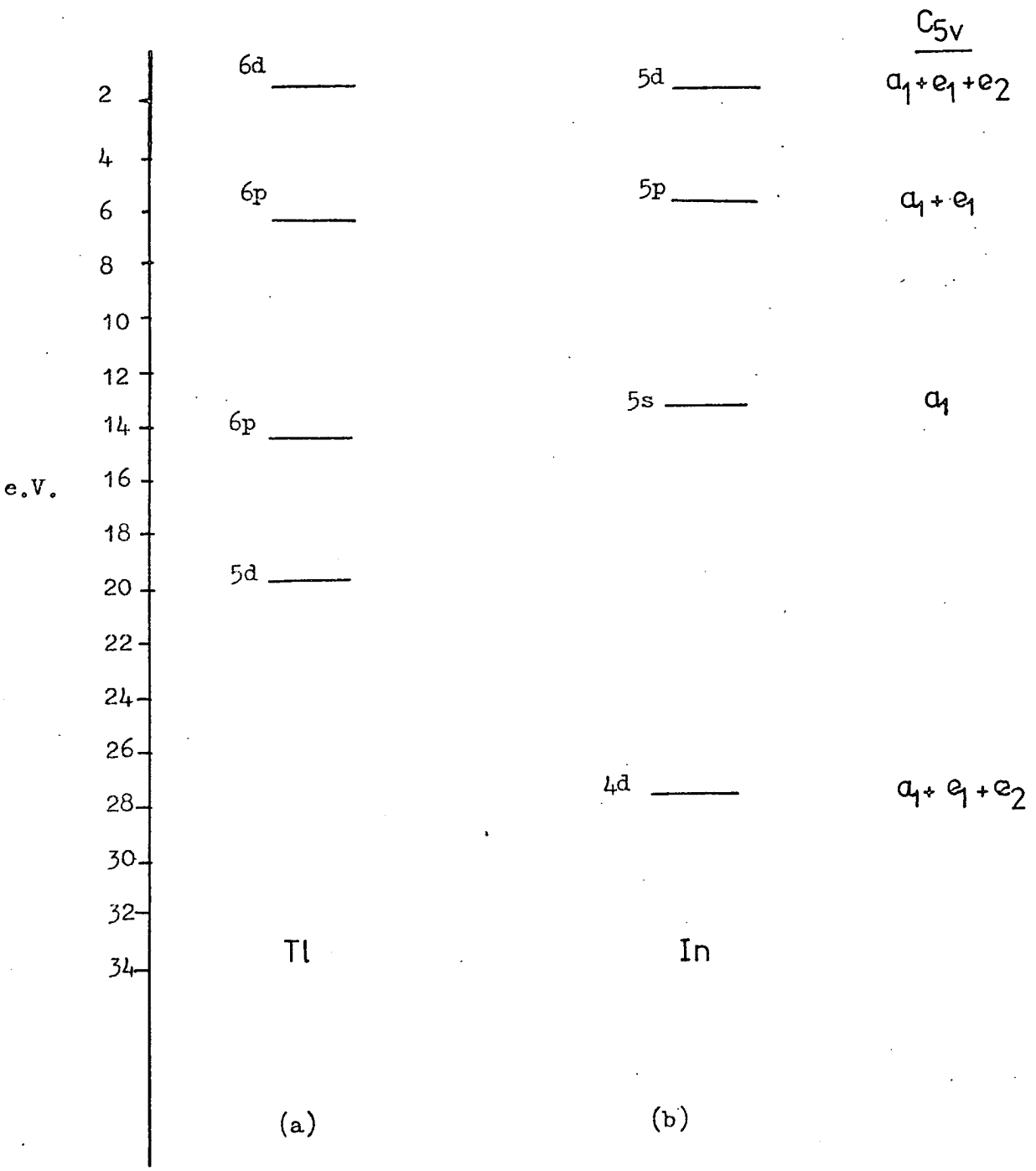
C_{5v}
6d
5d
$a_1 + e_1 + e_2$
2
4
6p
5p
$a_1 + e_1$
6
8
10
12
5s
a_1
14
6p
e.V.
16
18
5d
20
22
24
26
4d
$a_1 + e_1 + e_2$
28
30
32
Tl
In
34
(a)
(b)

Figure 2.

comparison may be made.

The corresponding transition energies in In are found to be:-

		cm^{-1}
In (I) $(4d^{10}5s^25p)\ ^2P_{\frac{1}{2}}$	$\longrightarrow$ In(II)$(4d^{10}5s^2)\ ^1So$	46,470
	$\longrightarrow$ In (I)$(4d^{10}5s5p^2)\ ^2P_{\frac{1}{2}}$	59,650
	$\longrightarrow$ In (I)$(4d^{10}5s^25d)\ ^2D_{\frac{3}{2}}$	32,890
In(III) $(4d^{10}5s)$	$\longrightarrow$ In(III)$(4d^9 5s^2)$	115,570

and using the same procedure as in Tl, the approximate atomic ionisation energies derived for In are shown in Figure 2b.

Comparing the levels in Tl and In, it should be noted that the In 5s level is higher in energy than the Tl 6s level. However the reverse is true for the d levels, in which the In 4d electrons appear more tightly bound than the Tl 5d electrons. These observations are also reflected in the trends in the successive I.P.s[25] i.e.

M	I	II	III	IV	
Tl	6.1	20·4	29.8	50.7	e.V.
In	5.7	18.8	28.0	54	e.V.
Configuration	ns^2	ns^1	$(n-1)d^{10}$	$(n-1)d^9$	

M(II) is the energy required to remove an ns level electron from $M^+(ns^2np^o)$ to give $M^{++}(ns^1np^o)$. The difference between the M(IV) and M(III) energies is due to ionisation of an (n - 1) d level electron.

c) Structure of TlC_5H_5 and InC_5H_5.

Although polymeric as solids[26], in the gas phase both Tl C_5H_5 and In C_5H_5 consist of monomeric open sandwich structure species in which the metal is symmetrically placed above the centre

Gas phase Structures of InC_5H_5 and TlC_5H_5.

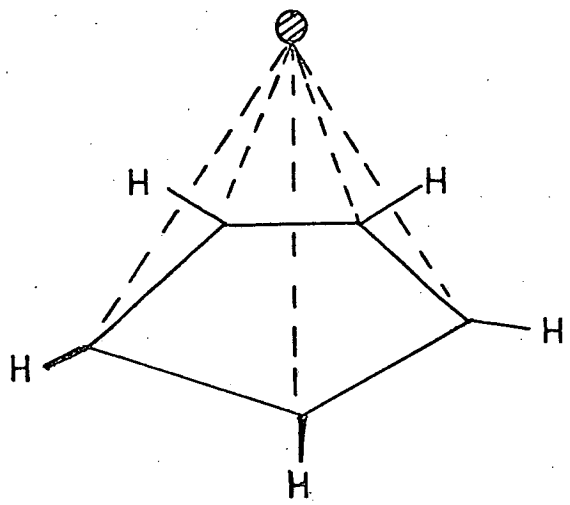

Tl - C	2.67 Å	Gas phase structure
In - C	2.41 Å	bond lengths in
C - C	1.43 Å	TlC_5H_5 and InC_5H_5.

Figure 3.

as shown in Figure 3. The bond lengths in Tl C_5H_5 and In C_5H_5 have been determined from electron diffraction studies,[4,5]. This structure has molecular symmetry C_{5v} and in this point group the metal a.o.s possess symmetry as shown in Figure 2c.

d) Molecular orbital energy diagram for TlC_5H_5 and interpretation of the p.e. spectrum.

Having carefully considered the symmetry properties and energy of the ligand molecular orbitals and the metal a.o.s we can now attempt to construct an m.o. energy level diagram for TlC_5H_5 and this is shown in Figure 4. With the aid of this diagram we can attempt to analyse the He(I) and He(II) p.e. spectra of TlC_5H_5, which are shown in Figures 5 and 6.

Also of some assistance in the assignment, is comparison with the He(I) spectra of TlCl and TlBr,[27] which both show three bands and have been analysed as follows:-

One band, approximately 13.5 e.V., σ bonding level derived from halogen p_σ and Tl 6s a.o.s.

Two overlapping bands, approximately 10 e.V.; π level, essentially halogen p_π very little mixed with Tl $6p_\pi$; σ bonding level, derived from Tl 6s, $6p_\sigma$ and halogen p_σ.

Thus the first band in the p.e. spectrum of TlC_5H_5, is largely derived from the e_1'' (π) level of C_5H_5 and contains only a small contribution from Tl $6p_\pi$ orbitals which lie to higher energy but are of the same e_1 symmetry. There is no resolvable vibrational structure to the band, although the shoulder to higher ionisation energy may arise as a result of Jahn-Teller interactions[28] in the ^2E state of the molecular ion.

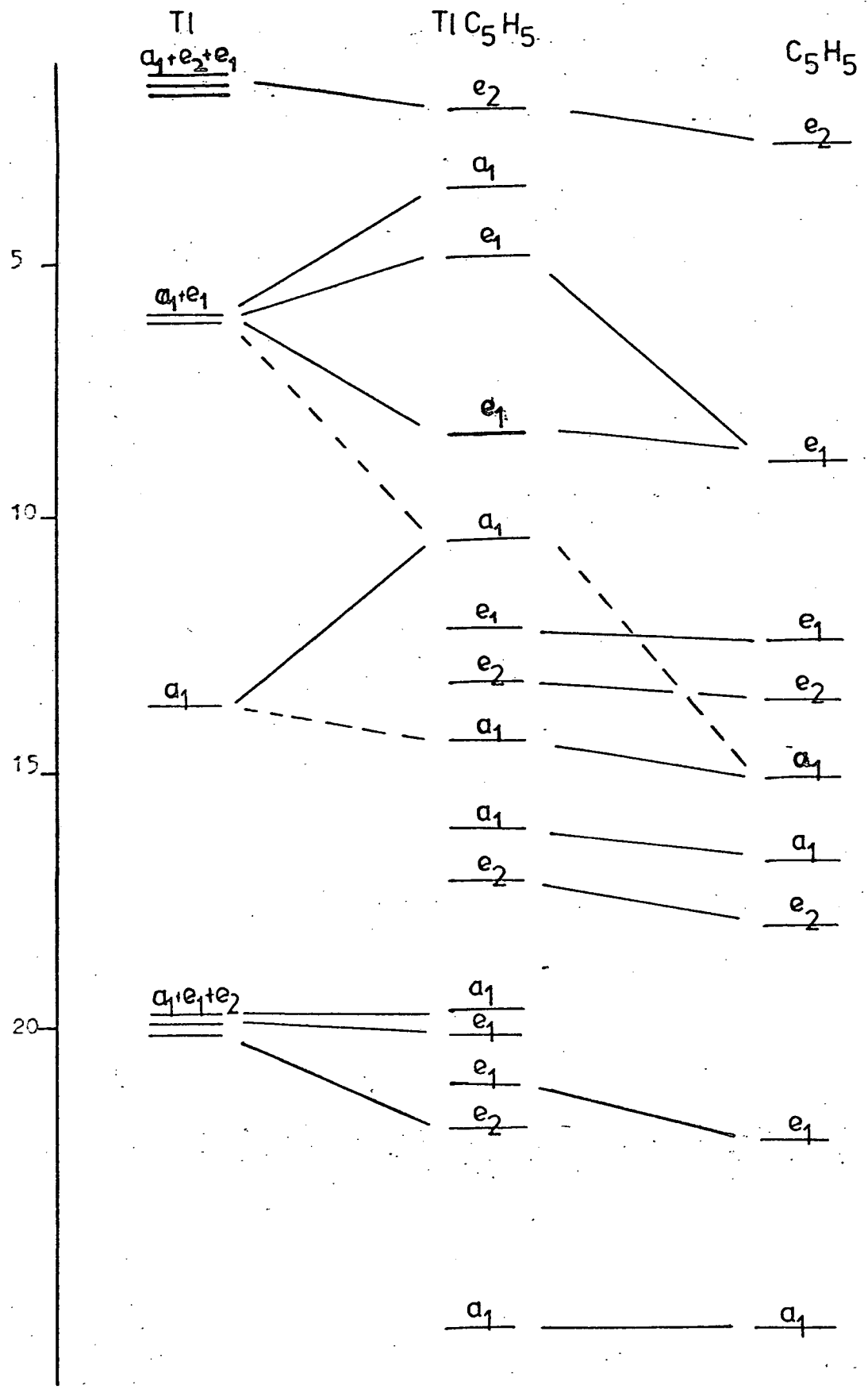
Tl
$a_1+e_2+e_1$
$Tl C_5H_5$
C_5H_5
e_2
e_2
a_1
e_1
5
a_1+e_1
e_1
e_1
10
a_1
e_1
e_1
e_2
e_2
a_1
a_1
15
a_1
a_1
e_2
e_2
$a_1+e_1+e_2$
a_1
e_1
e_1
20
e_2
e_1
a_1
a_1

Figure 4

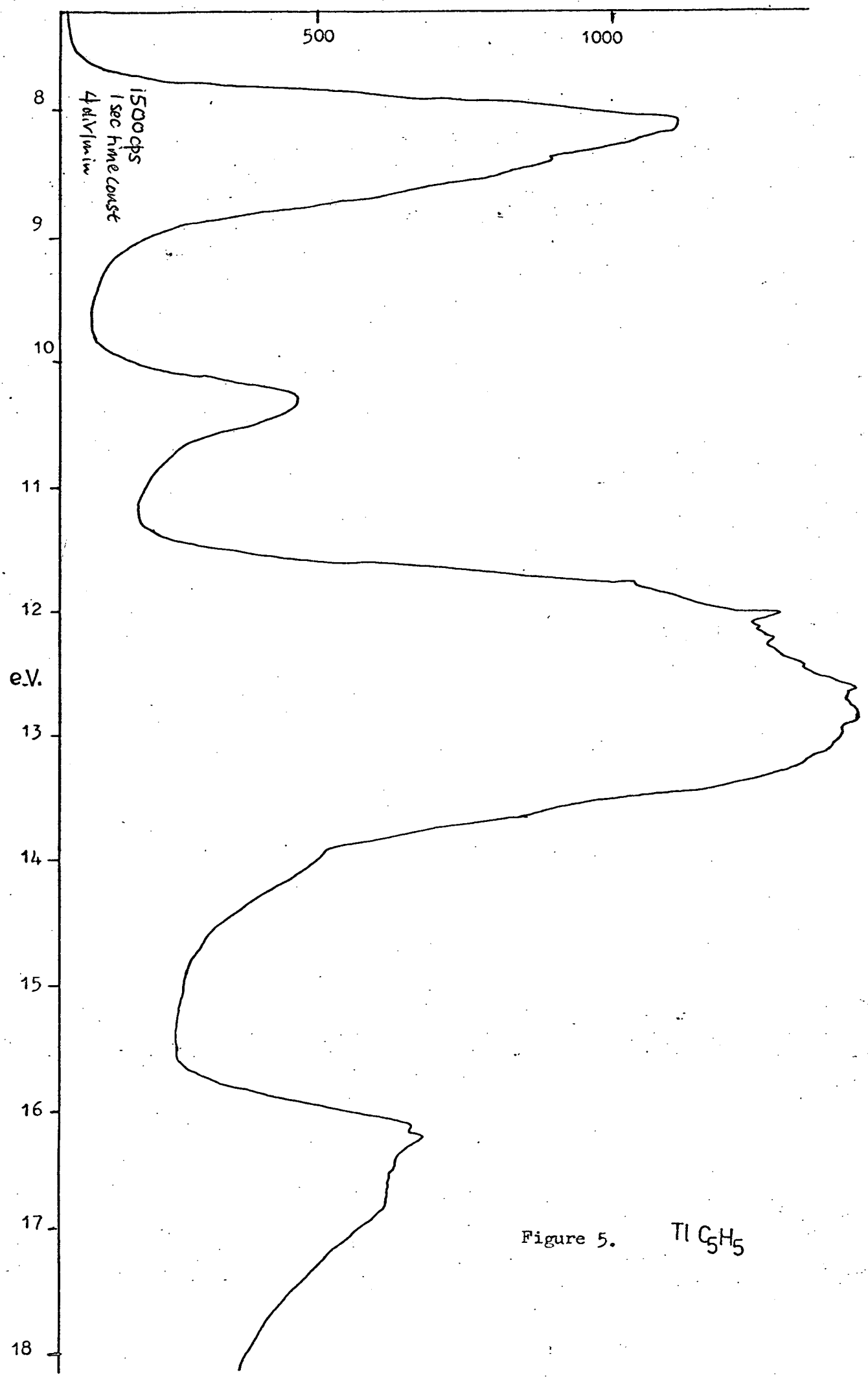

Figure 5. $Tl\,C_5H_5$

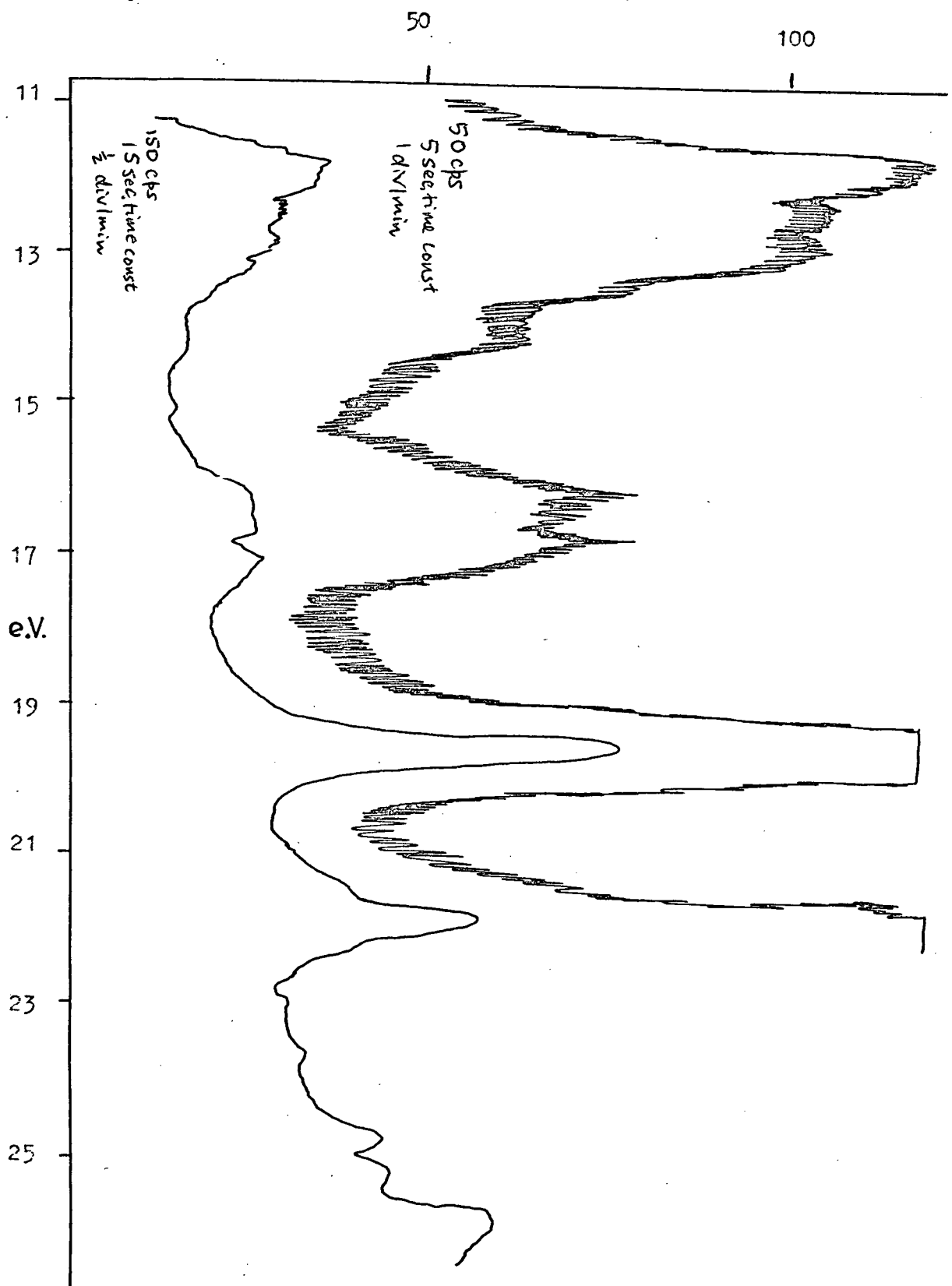

He(II) Photoelectron spectrum

of

TlC_5H_5

Figure 6.

The next band in the spectrum at 10.3 e.V. is weaker than the first and is attributed to a σ lone pair level derived mainly from Tl 6s, $6p_\sigma$ atomic orbitals, but with a small contribution from the ring a_2'' level.

The next band, the strongest in the He(I) spectrum, corresponds to the uppermost of the ligand σ orbitals, e_1' and e_2' and again shows no resolvable vibrational features. These levels are essentially unchanged in energy between ligand and complex because there are no metal a.o.s either of appropriate energy, or in the case of e_2' ring level, of appropriate symmetry with which to overlap. The fact that the p.e. spectra of other metallocenes containing both transition metal and main group metals,[8] all show an almost identical strong featureless band in this region, further points to the lack of metal orbital contribution to these essentially ligand σ levels. These levels are more clearly distinguished in the He(II) p.e. spectrum where the relative photoionisation cross-sections appear reversed in comparison to those of the He(I) spectrum. Unfortunately, such intensity effects are only imperfectly understood at present and although several of the contributing factors have been recognised[29] they do not in this case provide additional information to aid assignment. As in the first band of the spectrum, there is the possibility of Jahn-Teller broadening in the molecular ion states contributing to the overall width of the bands.

As a high energy shoulder to these bands is another, clearly seen in the He(II) spectrum which is attributed to the ligand π level, a_2'' with a small contribution from the Tl 6s orbital.

The next band in the spectrum is again broad and is due to ionisation from the largely ligand CH and CC σ bonding levels a_1' and e_2'. Although of the same symmetry as the metal $5d_{z^2}$, and

$5d_{x^2-y^2}$, and $5d_{xy}$ orbitals, there does not appear to be much mixing. Again, the second of these overlapping levels is more clearly distinguished in the He(II) spectrum.

Subsequent bands were only observed using He(II) radiation. The first of these at 19.6 e.V. and the band at 22 e.V. are attributed to ionisation from the largely metal 5d orbitals. The magnitude of the separation between these bands makes it clear that the splitting is essentially due to spin orbit coupling rather than "ligand field" effects relating to molecular symmetry. The two bands are thus designated as the $^2D_{\frac{5}{2}}$ and $^2D_{\frac{3}{2}}$ components of the Tl5d levels.

The low energy shoulder to the $^2D_{\frac{3}{2}}$ band at about 21.6 e.V. is attributed to the largely $C_{2s}\,\sigma$ bonding level of the ligand.

It is difficult to be sure whether the subsequent features observed in the He(II) spectrum correspond to higher energy ionisation levels of TlC_5H_5 or are due to "shadow" features which arise from the He(I)β, γ lines[31] also present in the spectrometer discharge and which could give rise to bands in this region. Certainly a fairly strong feature deriving from the other $C_{2s}\,\sigma$ bonding level, a_1', would be expected to occur at about 26 e.V., but it is impossible to be certain whether the bands observed at that part of the spectrum, are either wholly or in part due to this.

e) Molecular orbital energy diagram and interpretation of p.e. spectrum of InC_5H_5.

The corresponding m.o. level diagram and the He(I) p.e. spectrum of InC_5H_5 are shown in figures 7 and 8.

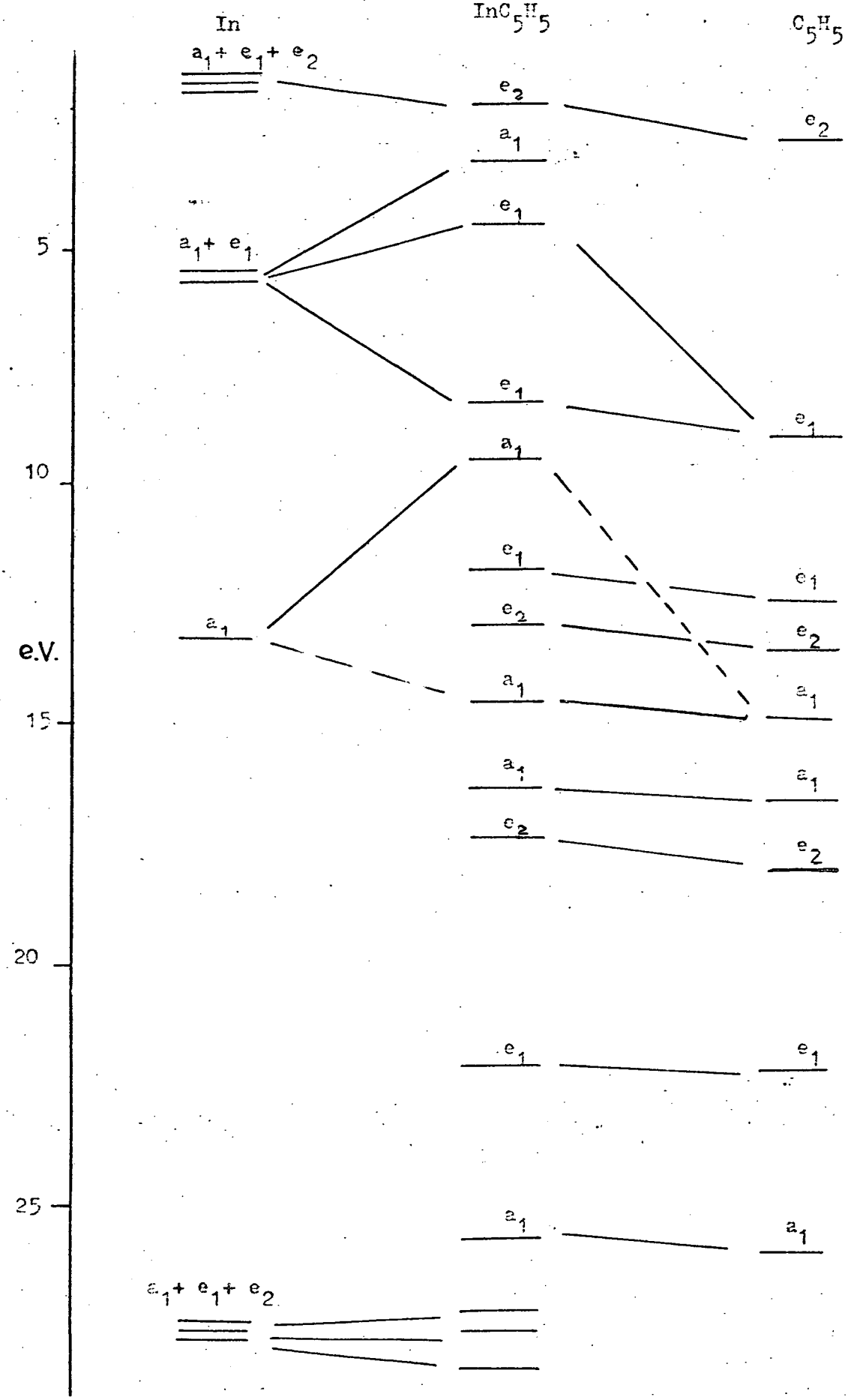
In
InC5H5
C5H5
a1+ e1+ e2
e2
a1
e1
a1+ e1
e1
e1
a1
e1
e1
e2
e2
a1
a1
a1
e2
e2
e1
e1
a1
a1+ e1+ e2
5
10
e.V.
15
20
25

Figure 7.

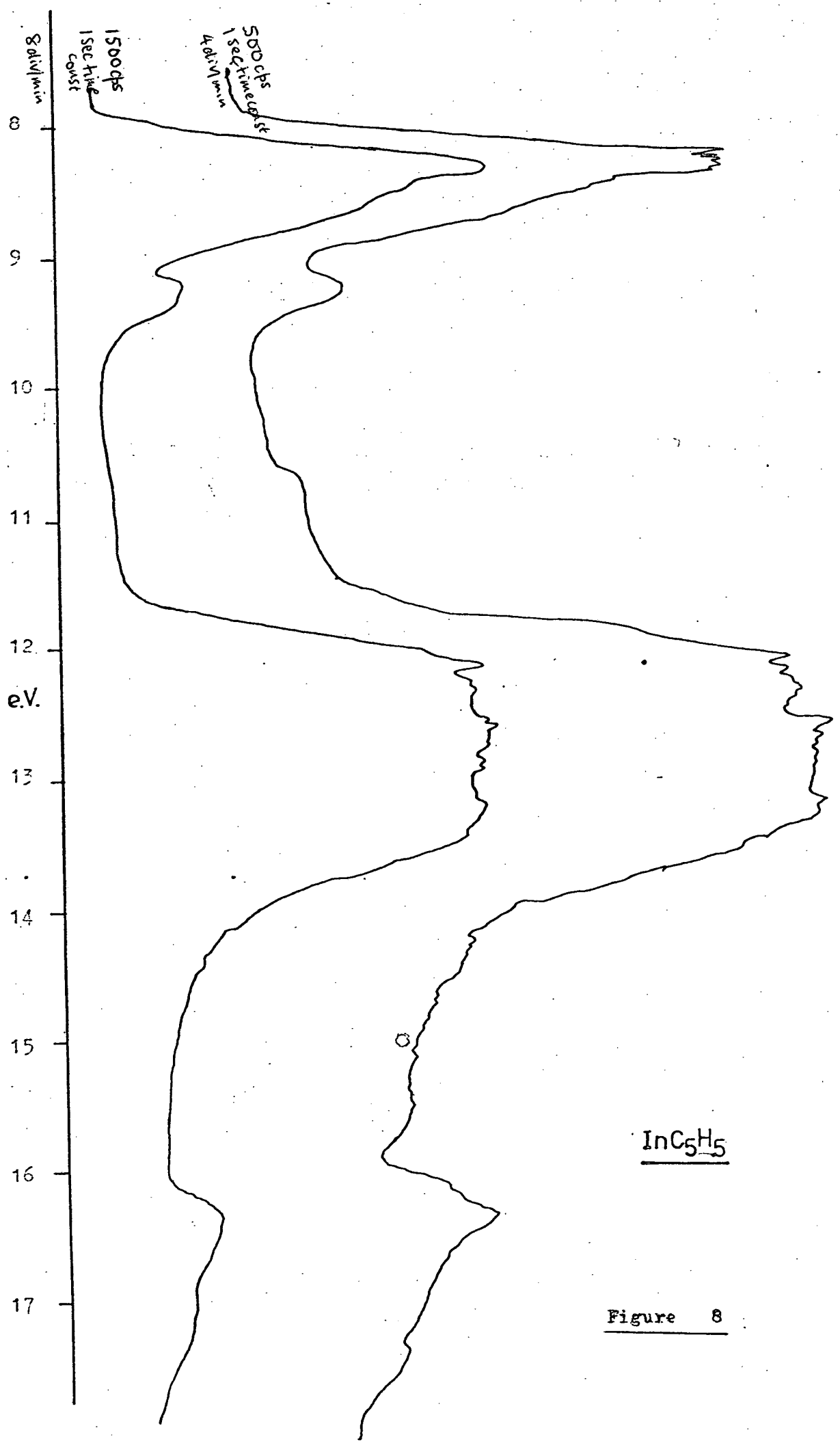
8 abi/min
1500cps
1 sec time const
500 cps
1 sec time const
4 abi/min
8
9
10
11
12
e.V.
13
14
15
16
17
InC5H5

Figure 8

TlC_5H_5		InC_5H_5	
Adiabatic	Vertical	Adiabatic	Vertical
7.67	8.12	7.81	8.3
9.87	10.28		9.3
11.37	12.77	11.61	12.7
15.77	16.28	16.0	16.3

TABLE I (IP's in e.V.)

Although essentially similar to that of TlC_5H_5; see Table 1, the spectrum of InC_5H_5 shows certain features which in fact corroborate the assignments made for TlC_5H_5. The only significant difference expected between the spectra would be associated with levels in which the metal a.o.s have a major contribution; for as we have already seen there is a difference in energy of approximately 1 e.V. between the ionisation energies of the In 5s and Tl 6s levels in the free atom.

In the analysis of the TlC_5H_5 spectrum the second band, at 10.3 e.V., was assigned to an essentially metal σ level and on such a basis would be predicted to shift to lower ionisation energy in the case of InC_5H_5. This prediction is observed to occur, the second band in InC_5H_5 being at 9.3 e.V.

Also, the small change in the I.P. of the first band in the spectrum, see table 1 and Figures 5 and 8, may indicate an even smaller degree of mixing between the uppermost ring π level, e_1', and the metal p_π orbitals of the same symmetry, in the case of InC_5H_5 , than in TlC_5H_5.

The fact that the remaining bands do not shift in the Indium compound compared with the Thallium one, supports their origin as essentially ligand ionisations.

It would be most instructive to compare the He(II) p.e. spectra of InC_5H_5 and TlC_5H_5, for on the basis of the metal orbital ionisation energies of Figure 2, the Indium compound should not exhibit any of the features in the 20 - 22 e.V. region which were ascribed to mainly Tl 5d level ionisations. Unfortunately, experimental difficulties in obtaining usable He(II) output from discharge lamp have made it impractical to record satisfactory

He(II) spectra of any of the other metallocene compounds in this study.

f) Ionic versus covalent bonding in TlC_5H_5.

As a result of calculations of the overlap integrals between the metal and ring orbitals, InC_5H_5 and TlC_5H_5[40] were originally thought to be truly ionic compounds. This calculation has subsequently been shown to be in error[5] and the recalculated values are in agreement with the other evidence which suggests covalent bonding.[11] Likewise the p.e. spectra of both compounds do not indicate any strongly ionic character to the bonding. If this had been the case, we would have expected the uppermost ligand π ionisation to occur at lower I.P.[9] Also as the I.P. of Tl(II) is 20.4 e.V. we would have expected the metal s level ionisations at a much higher energy than were in fact observed.[27]

3. LEAD DICYCLOPENTADIENYL AND TIN DICYCLOPENTADIENYL.

We shall now turn our attention to the second pair of main group metallocenes studied by p.e. spectroscopy, viz., $Pb(C_5H_5)_2$ and $Sn(C_5H_5)_2$. Following the same sequence of analysis and discussion leading to the construction of the m.o. energy level diagrams used to interpret the TlC_5H_5 and InC_5H_5 spectra, we shall begin by considering the atomic energy levels of the metal atoms.

a) Atomic levels of tin and lead.

The electronic transitions in Pb and Sn used to estimate the a.o. energy levels shown in Figures 9(a) and (b) are:-[25]

				cm^{-1}
Pb(I)(..$5d^{10}6s^26p^2$)	^3P_o	→ Pb(II) ($5d^{10}6s^26p^1$)	$^2P_{\frac{1}{2}}$	59,821
			$^2P_{\frac{3}{2}}$	73,901
		→ Pb(I) (..$6s^26p^16d^1$)	$^3D_1^o$	46,060
Pb(II)($5d^{10}6s^26p^1$)	$^2P_{\frac{1}{2}}$	→ Pb(II) ($5d^{10}6s6p^2$)	$^4P_{\frac{3}{2}}$	66,124
Pb(V) ($5d^{10}$)	$^1S_o^2$	→ Pb(V) ($5d^96s$)	$^3D_2$	114,705

and the corresponding transitions in Sn are:-

				cm^{-1}
Sn(I) ($4d^{10}5s^25p^2$)	^3P_o	→ Sn(II) ($4d^{10}5s^25p^1$)	$^2P_{\frac{1}{2}}$	59,236
			$^2P_{\frac{3}{2}}$	63,483
		→ Sn(I) ($5s^25p^15d^1$)	$^3D_1^o$	44,508
Sn(II) ($4d^{10}5s^25p^1$)	$^2P_{\frac{1}{2}}$	→ Sn(II) ($4d^{10}5s5p^2$)	$^4P_{\frac{3}{2}}$	48,368
Sn(V) ($4d^{10}$)	^1S_o	→ Sn(V) ($4d^95s$)	$^3D_2$	185,058

A recently reported gas phase p.e. spectrum of Pb gave identical values for the energies of the $^2P_{\frac{1}{2}}$, $^2P_{\frac{3}{2}}$ and $^4P_{\frac{3}{2}}$ states and so corroborates the above analysis of the electronic spectrum.[33]

The same trends as were observed in the Tl and In atomic levels are repeated in Pb and Sn. Thus, the uppermost filled s and p levels occur at slightly lower I.P. in the lighter element, whereas the d level ionisations are at lower I.P. in the heavier element. This

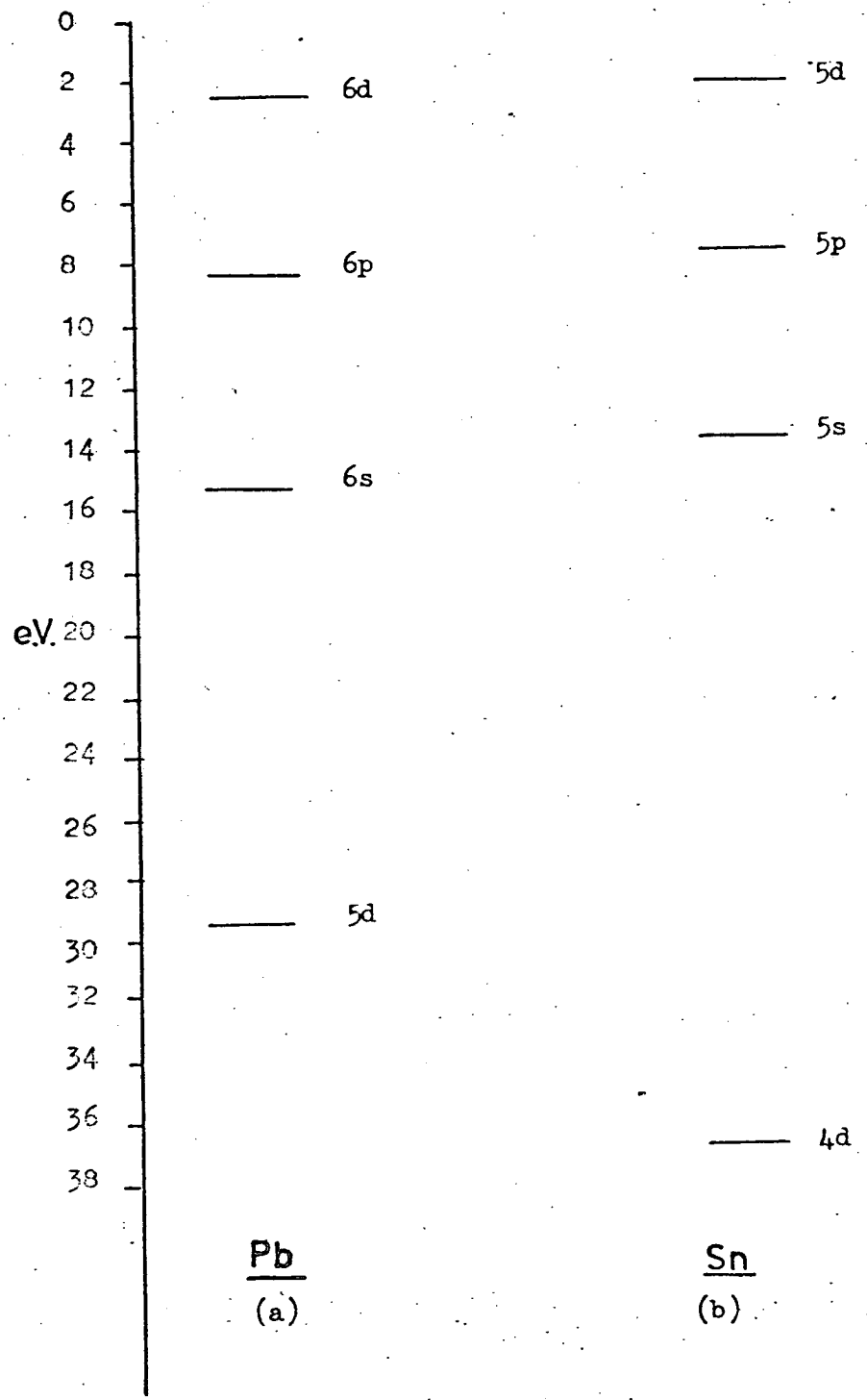
0
2
4
6
8
10
12
14
16
18
eV. 20
22
24
26
28
30
32
34
36
38
6d
6p
6s
5d
Pb
(a)
5d
5p
5s
4d
Sn
(b)

Figure 9

means that it should again be possible to distinguish between molecular levels of $Pb(C_5H_5)_2$ and $Sn(C_5H_5)_2$ which are largely derived from the metal a.o.s.

Comparison of Figures 3 and 9 also shows that the Pb a.o.s occur to higher binding energy than the corresponding Tl a.o.s and that the same relationship is true for the I.P.s of Sn and In.

b) Symmetry classification of molecular orbitals in $(C_5H_5)_2$ systems.

The molecular orbital levels of the $C_5H_5^-$ ligand shown in Figure 1 will require to be reclassified in terms of the new molecular symmetry to take account of the interactions between the ring levels. Two possible orientations of the rings which it will be useful to consider are the parallel and skew ring structures. i.e.

Strictly speaking, the parallel ring structure can exist in either of two forms with the rings staggered (D_{5d}) or eclipsed (D_{5h}), but as this is not essential to our assignments or the energy difference between these forms large, we shall regard the parallel structure as only possessing D_5 symmetry. In this point group (which is isomorphous with C_{5v}) the ligand π m.o.s combine as follows:-

$(C_5H_5)_2$ π	D_5
2 x a_2''	$a_1 + a_2$
2 x e_1''	$2e_1$
2 x e_2''	$2e_2$

In the skew structure, which has C_{2v} symmetry, the doubly

degenerate e levels split into a and b combinations although the splitting is expected to be small. Thus the ring π levels combine to give:-

$(C_5H_5)_2$ π	C_{2v}
2 x a_2''	$a_1 + b_2$
2 x e_1''	$a_1 + b_2$; $a_2 + b_1$
2 x e_2''	$a_1 + b_2$; $a_2 + b_1$

with the axes and b_1, b_2 convention shown in Figure 10.

c) Structures of $Sn(C_5H_5)_2$ and $Pb(C_5H_5)_2$.

The gas phase structures of $Sn(C_5H_5)_2$ and $Pb(C_5H_5)_2$ have been determined and both compounds possess the skew ring structure.[6] This type of structure is fairly common in transition metal cyclopentadienyl derivatives with other ligands also present e.g. $(C_5H_5)_2$ MX_2 where M = Ti, Zr, Mo; X = Halide, H, R. Details of the structure and bond lengths in $Sn(C_5H_5)_2$ are given in Figure 10(a).

d) Molecular orbital energy level diagrams and interpretation of the p.e. spectra of Sn $(C_5H_5)_2$ and $Pb(C_5H_5)_2$.

In constructing the m.o. energy level diagrams for $Sn(C_5H_5)_2$ and $Pb(C_5H_5)_2$ it is helpful to distinguish the interactions possible for each symmetry class in the manner shown in Figures 11 and 12. In this way we may avoid the confusion which could arise from the proliferation of a and b levels. It is also assumed that the π level splittings are small. This effect has been noted previously in the p.e. spectra of 1,1 substituted derivatives of $M(C_5H_5)_2$; (M = Fe, Ru, Os) in which the symmetry is also reduced to C_{2v} or C_{2h},[8]

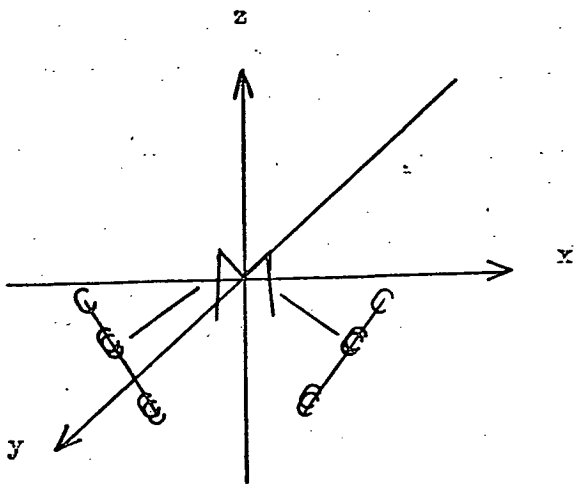

C_{2v}	E	C_2	σ_{xz}	σ_{yz}
A_1	+	+	+	+
A_2	+	+	−	−
B_1	+	−	−	+
B_2	+	−	+	−

Figure 10

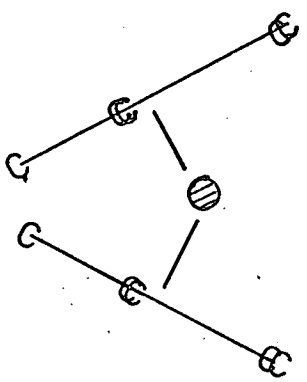

C - C 1.431

C - H 1.142

Sn - C 2.706

All C - H, C - C distances equal.

Figure 10 (a).

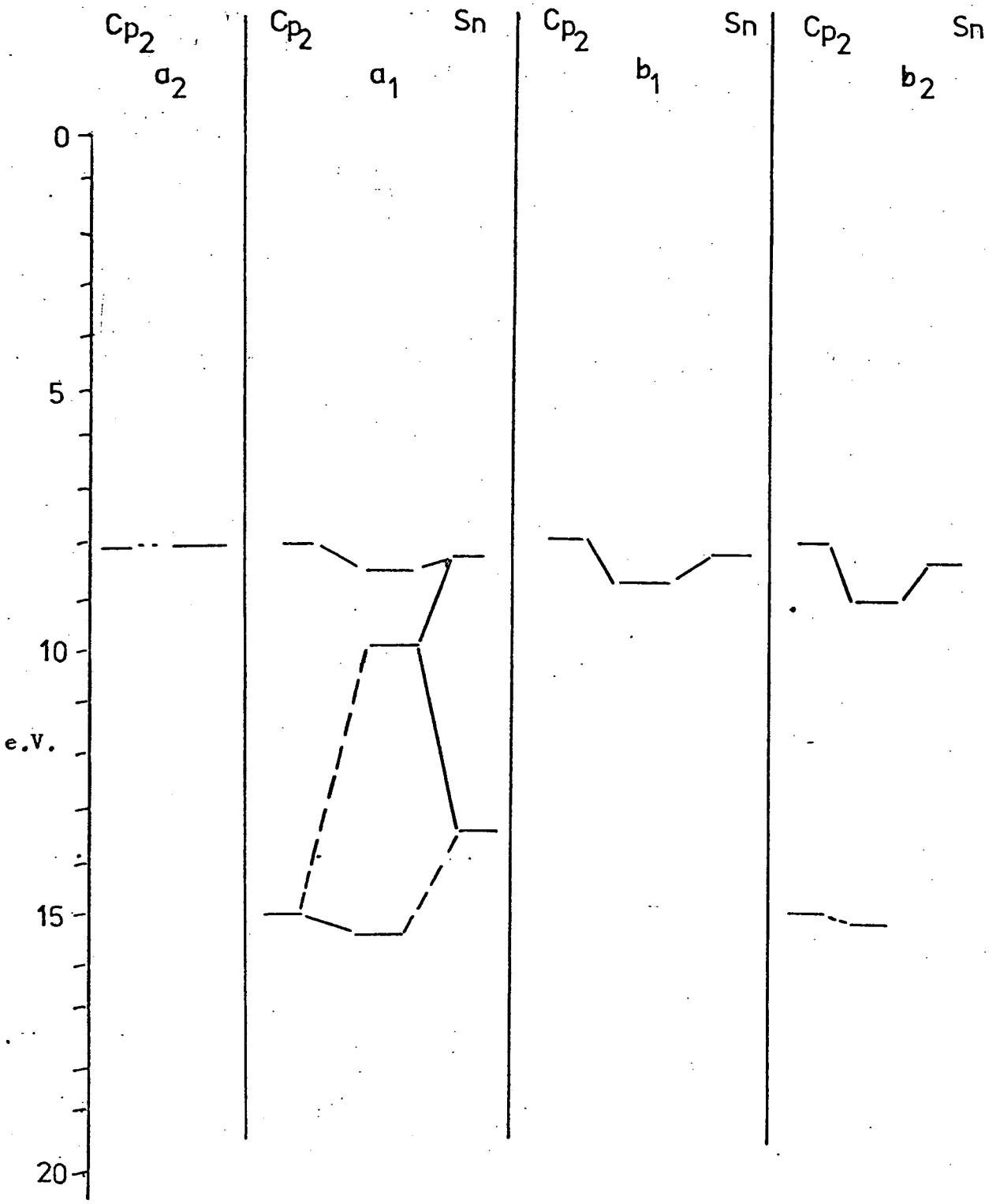

Figure 11

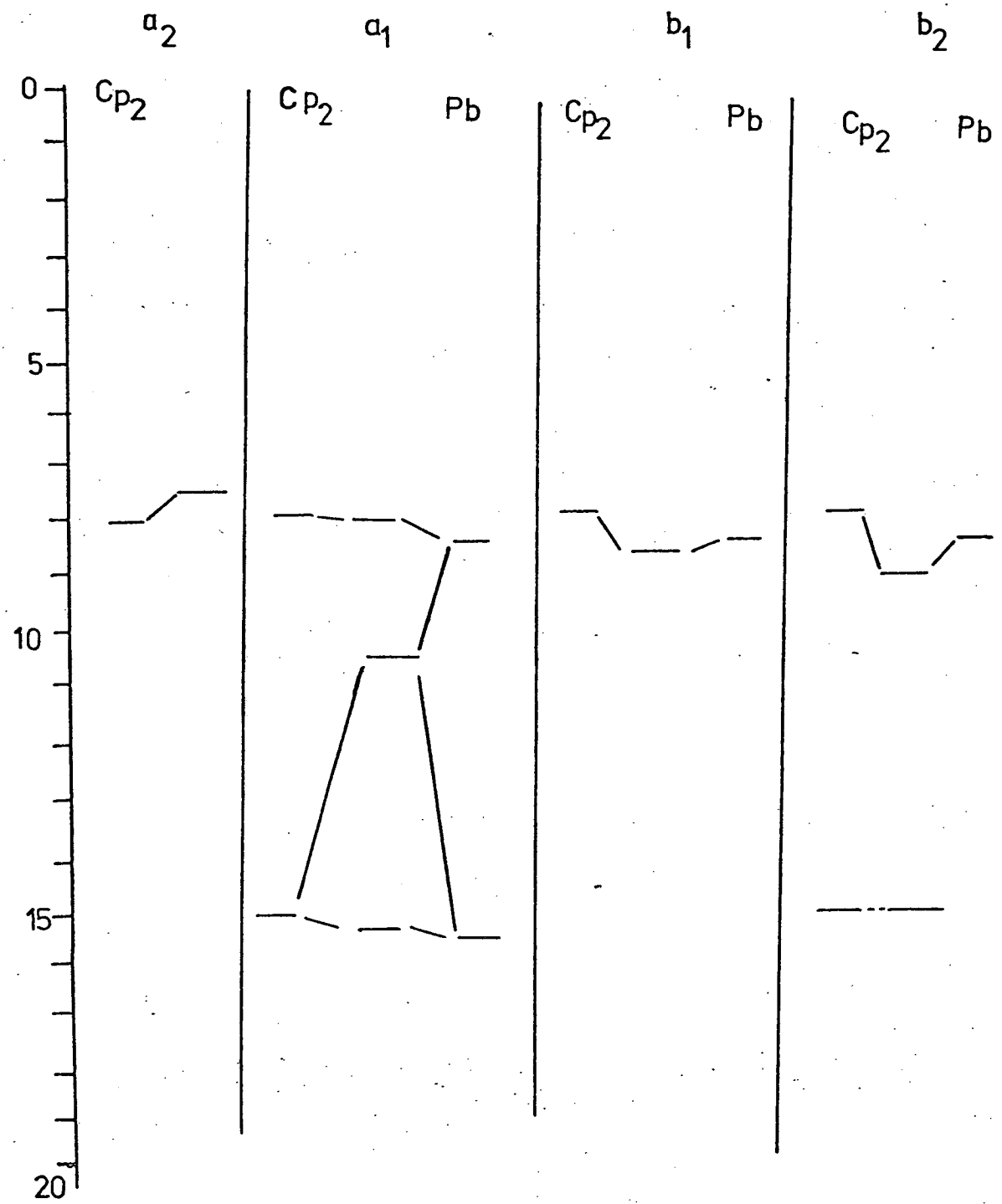

Figure 12

but with only a slight diffuseness occurring on some of the bands. Thus it would appear as if the m.o.s behaved as if they possessed higher symmetry properties than they in fact have.

We can use the m.o. diagrams to interpret the He(I) spectra of $Sn(C_5H_5)_2$ and $Pb(C_5H_5)_2$ which are shown in Figures 13 and 14. Both spectra contain 5 bands (denoted A to E in table 2) and show considerable overall similarity. However in the spectrum of $Pb(C_5H_5)_2$ (Figure 14) bands A and B are clearly split whereas this effect is not resolved in the spectrum of $Sn(C_5H_5)_2$.

The A and B bands largely derive from the ligand $e_1''\pi$ levels mixing with the metal p orbitals. However there is no metal p orbital of the same symmetry to overlap with the ligand $a_2\pi$ level and so we assign the low I.P. component of the first band (A) to this level. The next band (B) is assigned to the b_1 and b_2 levels derived from the metal px,py and ligand$\pi e_1'$ orbitals of the same symmetry. The remaining level deriving from the ring a_1 and metal p_z orbital is therefore assigned to the higher energy shoulder of band A.

However it should be pointed out that plausible alternative assignments exist for these bands and it is possible that band B derives from overlap of the a_1 and b_2 ring π levels with py,pz; the px orbital contributing to the high energy shoulder of band A.

The next band, C, is substantially shifted in position between the two spectra; in $Sn(C_5H_5)_2$ it is just apparent as a high energy shoulder to the previous band B, but in $Pb(C_5H_5)_2$ it is completely distinct. This shift would strongly suggest that it derives from a molecular level of essentially metal orbital character and is attributed to the metal s level of symmetry a_1.

The similarity both in shape, position and intensity of the

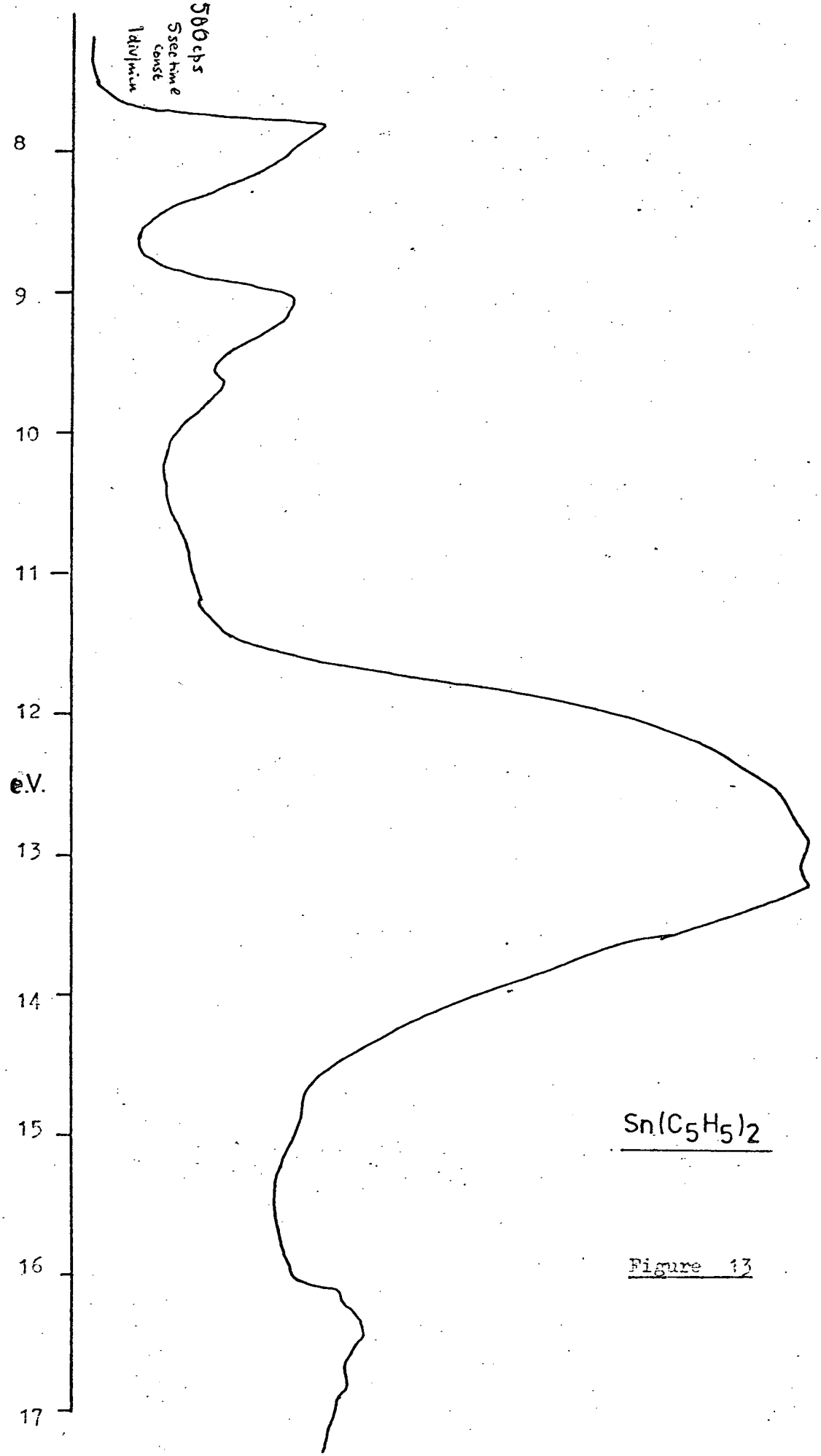

$Sn(C_5H_5)_2$

Figure 13

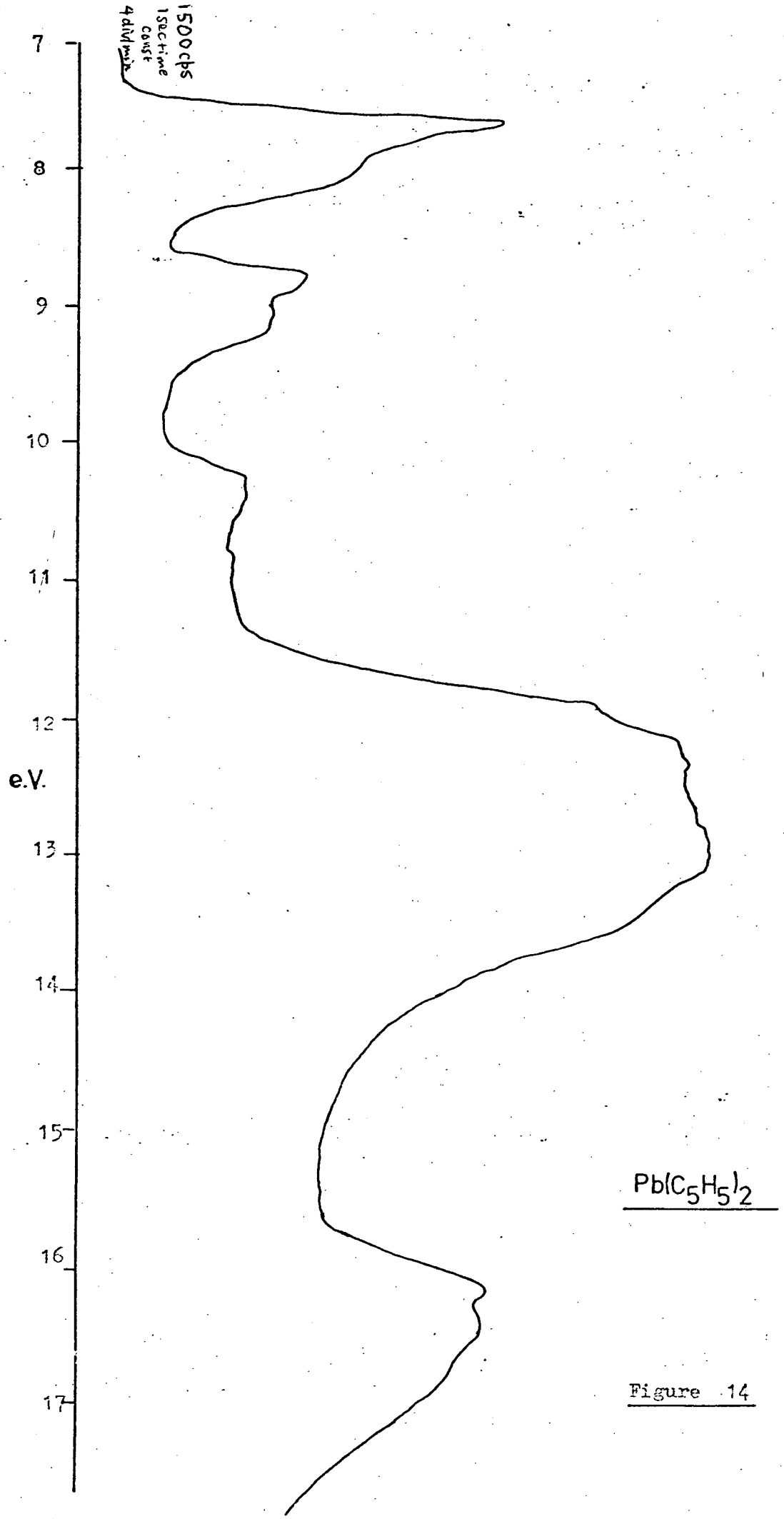

$Pb(C_5H_5)_2$

Figure 14

$Pb(C_5H_5)_2$			$Sn(C_5H_5)_2$	
Adiabatic	Vertical		Adiabatic	Vertical
7.4	7.53 8.00	A		7.75
	8.6 9.0	B		9.1
	10.3	C		9.7
11.6	12.7	D	11.6	12.8
15.8	16.4	E	16.0	16.4

TABLE 2 (IP's in e.V.)

two remaining featureless bands D and E, in both spectra is wholly consistent with their assignment to ligand σ levels and as assumed earlier, the splitting of these σ levels as a result of interactions between the two rings is too small to be apparent. The other two ligand π levels a_1 and b_2 are also not resolved, but presumably lie buried beneath the high energy tail of the bands labelled D.

e) Comparison with p.e. spectra of other $M(C_5H_5)_2$ species.

It is instructive at this point to compare the spectra of the Pb and Sn cyclopentadienyls with that of $Mg(C_5H_5)_2$.[8] This compound has a parallel ring structure of D_{5d} symmetry in the gas phase. But in the case of Mg there are no occupied p orbitals, and although the 3s level is of comparable energy to the e_{1g} and e_{1u} ligand levels, it is of a_{1g} symmetry and therefore does not mix with the ligand levels. Consequently the first two bands, of approximately equal intensity, at 8.23 and 9.26 e.V. (vertical I.P.s) are almost entirely derived from the e_{1g} and e_{1u} combination of the upper ligand π levels but perhaps slightly stabilised by interaction with empty p orbitals of Mg. These may be compared with the bands denoted A and B in $Pb(C_5H_5)_2$ which occur at slightly lower ionisation energy. This largely corroborates the earlier assignment of these bands in $Pb(C_5H_5)_2$ (and $Sn(C_5H_5)_2$), as possessing some metal p_π character as a result of mixing between the ligand π and metal p_π levels which lie to higher energy (lower I.P.).

Comparison of the p.e. spectra of Pb and Sn cyclopentadienyls with those of the skew ring transition metal derivatives[9] e.g. $(C_5H_5)_2$ MoCO is also instructive. In these compounds the first two bands are attributed to largely metal d orbital ionisations.

However, the next set of bands arise from the ligand π levels which split into the a_1, b_2, a_2 and b_1 components. In the case of $(C_5H_5)_2$-MoCO these occur at 8.8, 9.3 and 9.6 e.V. and may again be compared with the $Pb(C_5H_5)_2$ ionisations at 7.53, 8.63 and 9.00 e.V. Once more we see the $Pb(C_5H_5)_2$ I.P.s occur to lower energy and the observed splittings of the higher I.P. bands in both spectra are of comparable size.

4. MERCURY DICYCLOPENTADIENYL.

Finally, we turn our attention to $Hg(C_5H_5)_2$. This compound is sensitive to both heat and light. Unfortunately the analogous Cd derivative is so unstable[3] that it cannot be sublimed without substantial decomposition and so was not suitable for this study.

a) Atomic energy levels in mercury.

The energies of the atomic levels of Hg are readily obtainable from the p.e. spectrum[24,34]. This shows bands at 10.4, 14.84 and 16.71 e.V. corresponding to the $^2S_{\frac{1}{2}}$, $^2D_{\frac{5}{2}}$ and $^2D_{\frac{3}{2}}$ states of Hg (II).

However it is instructive to compare these values with the results arrived from the optical spectrum.[25] The transitions:-

			cm^{-1}
Hg(I)($5d^{10}6s^2$) ^1S_o	$\longrightarrow$ Hg(II) ($5d^{10}6s^1$)	$^2S_{\frac{1}{2}}$	84,184
	$\longrightarrow$ Hg(I) ($5d^{10}6s6p$)	$^3P_1^\circ$	39,412
	$\longrightarrow$ Hg(I) ($5d^96s^26p^1$)	$^3F_4$	76,945
	$\longrightarrow$ Hg(II) ($5d^96s^2$)	$^2D_{\frac{5}{2}}$	119,692
	$\longrightarrow$ Hg(II) ($5d^96s^2$)	$^2D_{\frac{3}{2}}$	134,732

lead to estimates of the 6s and 5d levels which are in good agreement with the p.e. results. In addition the optical spectrum gives an estimate for the energy of the unoccupied 6p level. These results are shown in Figure 15. This agreement between optical and p.e. data gives an additional measure of confidence to the type of analysis performed on the optical spectra of the other metals in deriving their orbital energies.

b) Structure of $Hg(C_5H_5)_2$.

After many years of dispute, the evidence of the solution i.r.[35]

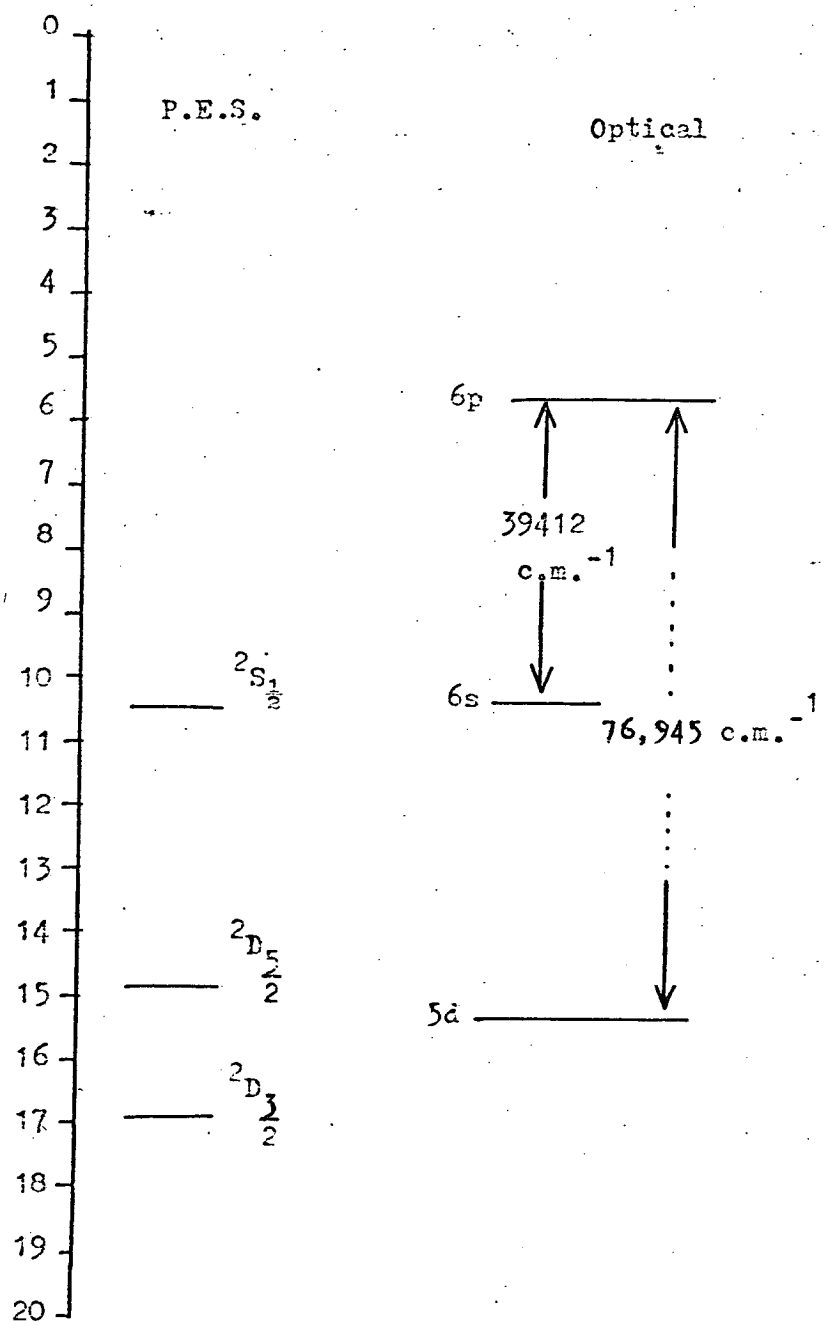
0
1
2
3
4
5
6
7
8
9
10
11
12
13
14
15
16
17
18
19
20
P.E.S.
Optical
$^2S_{\frac{1}{2}}$
$^2D_{\frac{5}{2}}$
$^2D_{\frac{3}{2}}$
6p
39412
c.m.$^{-1}$
6s
76,945 c.m.$^{-1}$
5d

Figure 15

and n.m.r.[36] has finally been resolved and points to an extremely fast "fluxional" diene structure. No structure determination of the molecule in the gas phase has been reported and an attempt to record the electron diffraction pattern of $ClHgC_5H_5$ was abandoned as a result of the substantial decomposition of the sample which occurred on heating.[37] This decomposition would lead to such a complex mixture of gas phase species, that it would be impossible to analyse the resulting diffraction pattern to give reliable data for $ClHgC_5H_5$. A similar situation would obtain for $Hg(C_5H_5)_2$ which is thermally less stable.

The possible structures for $Hg(C_5H_5)_2$ as deduced from the i.r. are shown in Figure 16. However, the transoid structure, of symmetry C_{2v}, is considered unlikely on the basis of the measured dipole moment.[7]

c) Diene energy levels in C_5H_5.

In a σ diene structure the ligand levels are best compared with the molecular levels in C_5H_6 as this allows for the considerable localisation of the ring π levels which still exists in these compounds. Furthermore we will assume that there is no significant interaction between the levels of the different rings.

d) Molecular energy level diagram and p.e. spectrum of $Hg(C_5H_5)_2$.

We can now construct the m.o. level diagram for $Hg(C_5H_5)_2$ shown in Figure 17. Also of considerable assistance in the interpretation of the p.e. spectrum, is comparison with other σ diene compounds, notably $SiH_3C_5H_5$, the p.e. spectrum of which has recently been analysed with the aid of ab initio calculations.[21]

The p.e. spectrum of $Hg(C_5H_5)_2$ is shown in Figure 18. Also

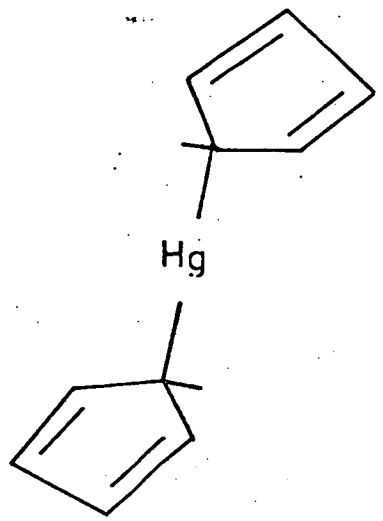

C_{2h}

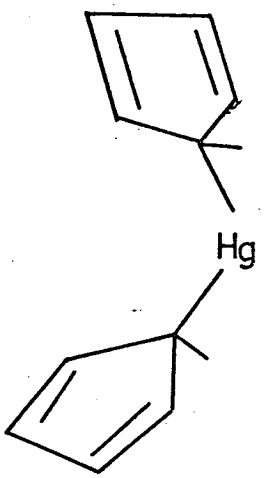

C_{2v}

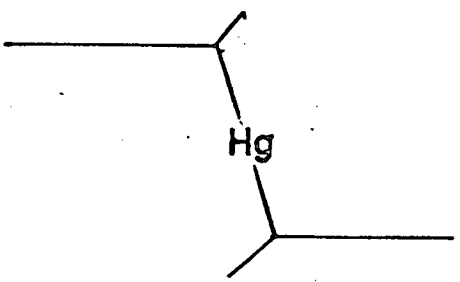

Transoid

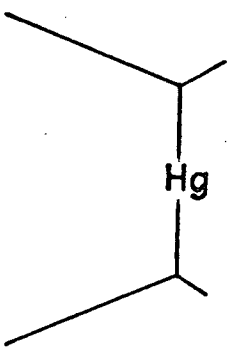

Cisoid

Figure 16

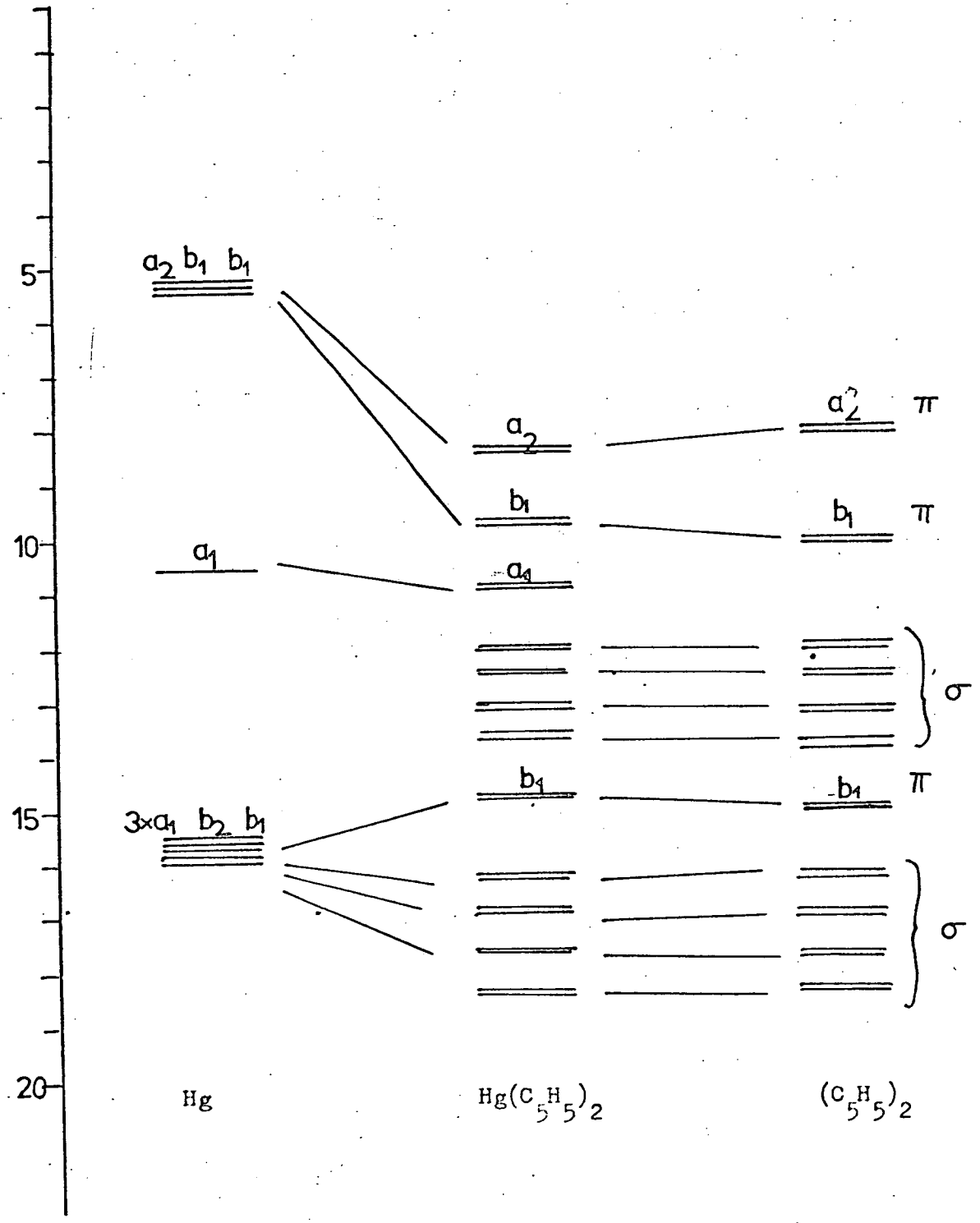
5
10
15
20
a2 b1 b1
a1
3×a1 b2 b1
a2
b1
a1
b1
a2
b1
b1
π
π
π
σ
σ
Hg
Hg(C5H5)2
(C5H5)2

Figure 17.

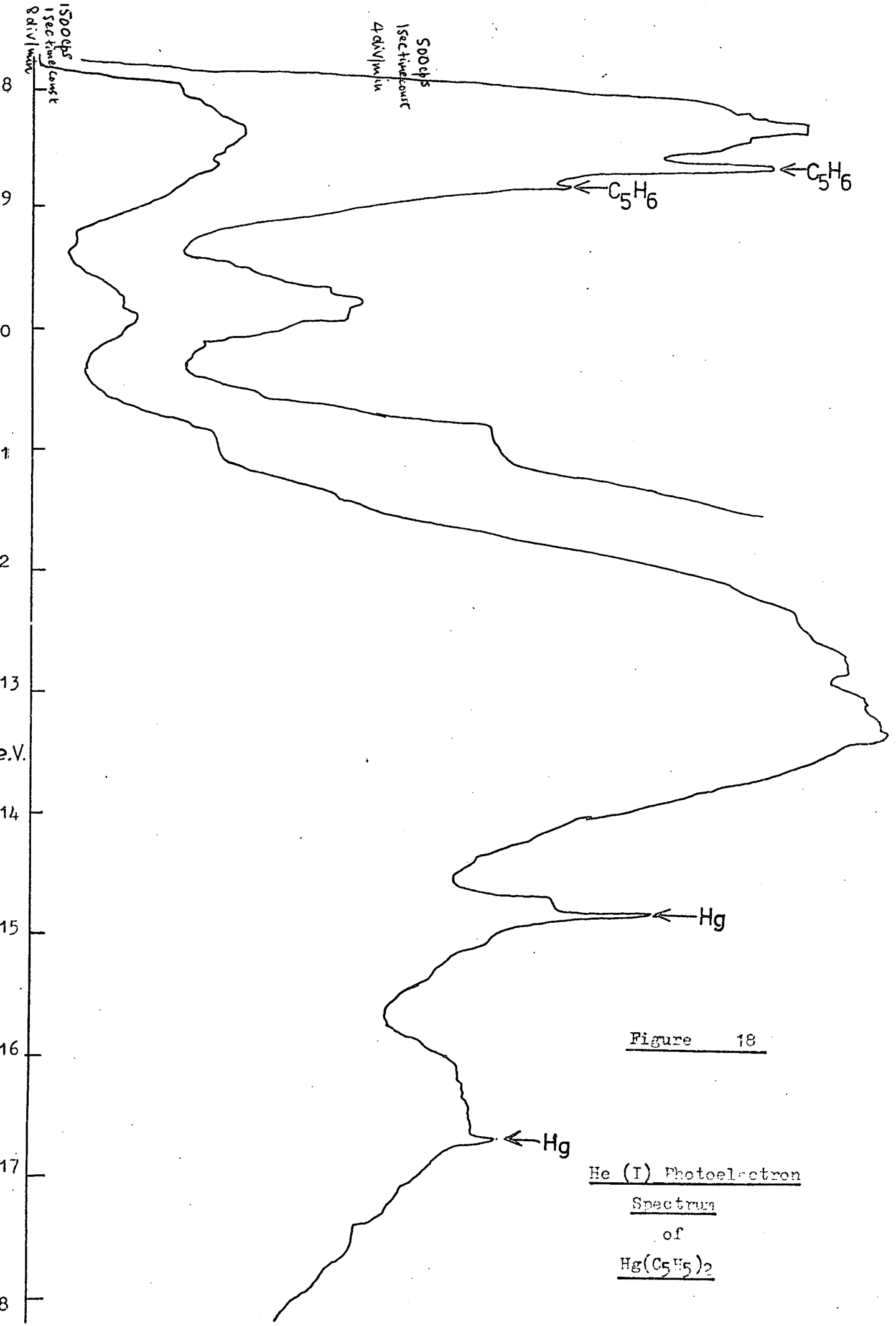

Figure 18

He (I) Photoelectron Spectrum of $Hg(C_5H_5)_2$

$Hg\ (C_5H_5)_2$

Adiabatic	Vertical
7.8	8.4
9.4	9.8
10.5	10.9
	13.4
14,65	14.8
	16.4

TABLE 3 (IP's in e.V.)

apparent are bands of Hg and C_5H_6 which result from some decomposition of the $Hg(C_5H_5)_2$ sample.

The first band of $Hg(C_5H_5)_2$ overlaps with the sharp features (denoted with arrows) which are attributed to traces of C_5H_6.[19] This similarity in position and the fact that it occurs to much higher energy than the first band of $Pb(C_5H_5)_2$, confirm the assignment of the band to levels of essentially C_5H_6 $^1a_2$ character. The possibility of some mixing with a higher energy (lower I.P.), unoccupied 6p level of Hg may account for the fact that the bands lie to slightly lower I.P. in the Hg compound than in C_5H_6.

The next band largely derives from the $2b_1$ level of C_5H_6 and again the possibility of mixing with the b_1 levels of Hg6p may account for its slightly lower I.P. By analogy to a similar band in $SiH_3C_5H_5$ assigned to the (π - SiC) level,[21] this band is attributed to the (π - HgC) bonding level.

The next band appears as a low ionisation energy shoulder to the ligand σ bands and is attributed to the HgC σ bonding levels formed by overlap of the Hg 6s level and ligand levels of the same symmetry, a_1.

The broad featureless band between 11 and 14.5 e.V. will contain the remaining ligand σ levels.

The low ionisation energy shoulder to the Hg $^2D_{\frac{3}{2}}$ line observed at 14.9 e.V. is attributed to the remaining ring π orbitals derived from the $1b_1$ level of C_5H_6, perhaps slightly mixed with the b_1 level of Hg 5d orbitals.

The final band in the spectrum, containing a very weak feature at 16.75 e.V. corresponding to the $^2D_{\frac{5}{2}}$ state of Hg^+, is due to ionisation from the C - C and C - H σ bonding levels corresponding to the $7a_1$, $4b_2$ and $6a_1$ levels of C_5H_6. Underlying this band and

and probably responsible for the long tail which extends from about 17 e.V. to about 18.5 e.V., will be ionisations from the largely Hg 5d levels which would be expected to occur in this region of the spectrum.[38,39]

REFERENCES.

1. G. E. Coates, M.L.H. Green and K. Wade; Organometallic Elements Volume 1, 3rd edition 1967, Methuen and Co. Ltd., London.

2. J. Lorberth; J. Orgmet. Chem. (1969), 19, 189.

3. E.O. Fischer and H.P. Fritz; Adv. Inorg. Nucl. Chem. (1959), 1,55.

4. M. McConnell and D.W.H. Rankin; unpublished results.

5. S. Shibata, L.S. Bartell and R.M. Gavin; J. Chem. Phys. (1964), 41, 717.

6. A. Almenningen, A. Haaland and T. Motzfeldt; J. Orgmet. Chem. (1967), 7, 97.

7. E. Maslowsky, Jnr. and K. Nakamoto; Inorg. Chem. (1969), 8, 1108.

8. S. Evans, M.L.H. Green, B. Jewitt, A.F. Orchard and C.F. Pygall; J. Chem. Soc. Faraday Trans. II, (1972), 68, 1847.

9. S. Evans, M.L.H. Green, B. Jewitt, G.H. King and A.F. Orchard; J. Chem. Soc. Faraday Trans. II, (1974), 70, 356.

10. J.C. Green, S.E. Jackson and B. Higginson; J. Chem. Soc. Dalton Trans. (1975), 403.

11. H.P. Fritz; Adv. Orgmet. Chem. (1964), 1, 262.

12. K. Nakamoto; Infra-red Spectra of Inorganic and Organometallic Compounds; 2nd edition (1970), Pages 268-271: Wiley-Interscience, John Wiley and Sons, New York, London, Sydney and Toronto.

13. F.A. Cotton and G. Wilkinson; Advanced Inorganic Chemistry; 3rd edition (1972), page 736; Interscience Publishers, John Wiley and Sons, New York, London, Sydney, Toronto.

14. L.E. Orgel; An introduction to Transition Metal Ligand Field Theory Chemistry; 2nd edition, page 166, Methuen and Co. Ltd., London.

15. C.A. Coulson; Valence, 2nd edition, page 299; Oxford University Press.

16. T. Koopmans; Physica (1933), 1, 104.

17. M-M. Coutiere, J. Demuynck and A. Veillard; Theor. Chim. Acta (1972), 27, 281.

18. S. Evans, M.F. Guest, I.H. Hillier, and A.F. Orchard; J. Chem. Soc. Faraday Trans. II, (1974), 70, 417.

19. P.J. Derrick, L. Asbrink, O. Edqvist, B.O. Jonsson and E. Lindholm; Int. J. Mass Spect. Ion Phys. (1971), 6, 203.

20. C. Fridh, L. Asbrink and E. Lindholm; Chem. Phys. Letts. (1972), 15, 408.

21. S. Cradock, R.H. Findlay, M.H. Palmer; J. Chem. Soc. Dalton Trans. (1974), 1650.

22. J.A. Salthouse and M.J. Ware; Point Group Character Tables and Related Data, (1972), Cambridge University Press.

23. L. Asbrink, O. Edqvist, E. Lindholm and L.E. Selin; Chem. Phys. Letts, (1970), 5, 192; ibid, page 609.

24. A.J. Blake; Proc. Roy. Soc. Lond. A, (1971), 325, 555.

25. C.E. Moore, Nat. Bur. Std. (U.S.) Circ. No. 467, Atomic Energy levels, Volume III, (1958).

26. E. Frasson, F. Meriegus, C. Panattoni; Nature, (1963), 199, 1087.

27. J. Berkowitz; J. Chem. Phys. (1972), 56, 2766.

28. D.W. Turner, C. Baker, A.D. Baker, and C.R. Brundle Molecular Photoelectron Spectroscopy (1970) Wiley, London.

29. W.C. Price, A.W. Potts, and D.G. Streets; Electron Spectroscopy edited D.A. Shirley, North Holland Amsterdam. (1972) page 187.

30. as reference 13, page 556.

31. A.D. Baker and D. Betteridge; Photoelectron Spectroscopy; Pergamon Press (1972).

32. L.D. Dave, D.F. Evans and G. Wilkinson; J. Chem. Soc. (1959), 3684.

33. S. Suzer, M.S. Banna and D.A. Shirley; J. Chem. Phys. (1975), 63, 3473.

34. J. Berkowitz, J.L. Dehmer, Y.K. Kim and J.P. Desclaux; J. Chem. Phys. (1974), 61, 2556.

35. F.A. Cotton and T.J. Marks; J. Amer. Chem. Soc. (1969), 91, 7281.

36. P. West, M.C. Woodville, and M.D. Rausch, J. Amer. Chem. Soc. (1969), 91, 5649.

37. D.E.J. Arnold, W. Duncan and D.W.H. Rankin; unpublished results.

38. J.H.D. Eland; Int. J. Mass Spect. Ion Phys. (1970), 4, 37.

39. P. Burroughs, S. Evans, A. Hamnett, A.F. Orchard and N.V. Richardson, Chem. Comm. (1974), 22, 921.

40. F.A. Cotton and L.T. Reynolds; J. Amer. Chem. Soc. (1958), 80, 269.

APPENDIX

on

EXPERIMENTAL

PROCEDURES

and

TECHNIQUES.

APPENDIX.

THE PHOTOELECTRON SPECTROMETER

The spectrometer used was a commercially available Perkin Elmer P.S. 16 instrument. This model, which was first produced about six years ago, has since undergone several minor modifications and is currently available as the PS18 model.

Likewise several alterations and additions, including the use of a heated sample inlet probe and an He(I)/He(II) discharge lamp were made to the PS16 instrument to obtain some of the results presented in the preceding chapters.

The basic design features and components are largely similar to those of the 'typical' spectrometer described in the introduction and are as shown in Figure I and Figure 2.

The water cooled helium discharge lamp is connected to the ionisation chamber by a fine capillary tube allowing the radiation to pass through the sample but preventing excessive diffusion of the helium, which is continuously pumped out from the lamp. The photoejected electrons leave the target region through a narrow slit and enter the electrostatic analyser. This consists of two concentric plates of 127^{o} $(\frac{\Pi}{\sqrt{2}})$ section, the voltage between which may be varied continuously to deflect electrons of different energy. The exit from the analyser to the electron multiplier, is controlled by a narrow slit of width variable up to a maximum of 1 mm. In recording high resolution He(I) spectra, this slit is kept at the minimum width compatible with reasonable intensity, with a resolution of $\geqslant$ 30 meV being readily obtainable. However, when recording He(II) spectra it is usually necessary to open the slit considerably wider in order to obtain useful intensity, even although this is at the expense of inferior resolution.

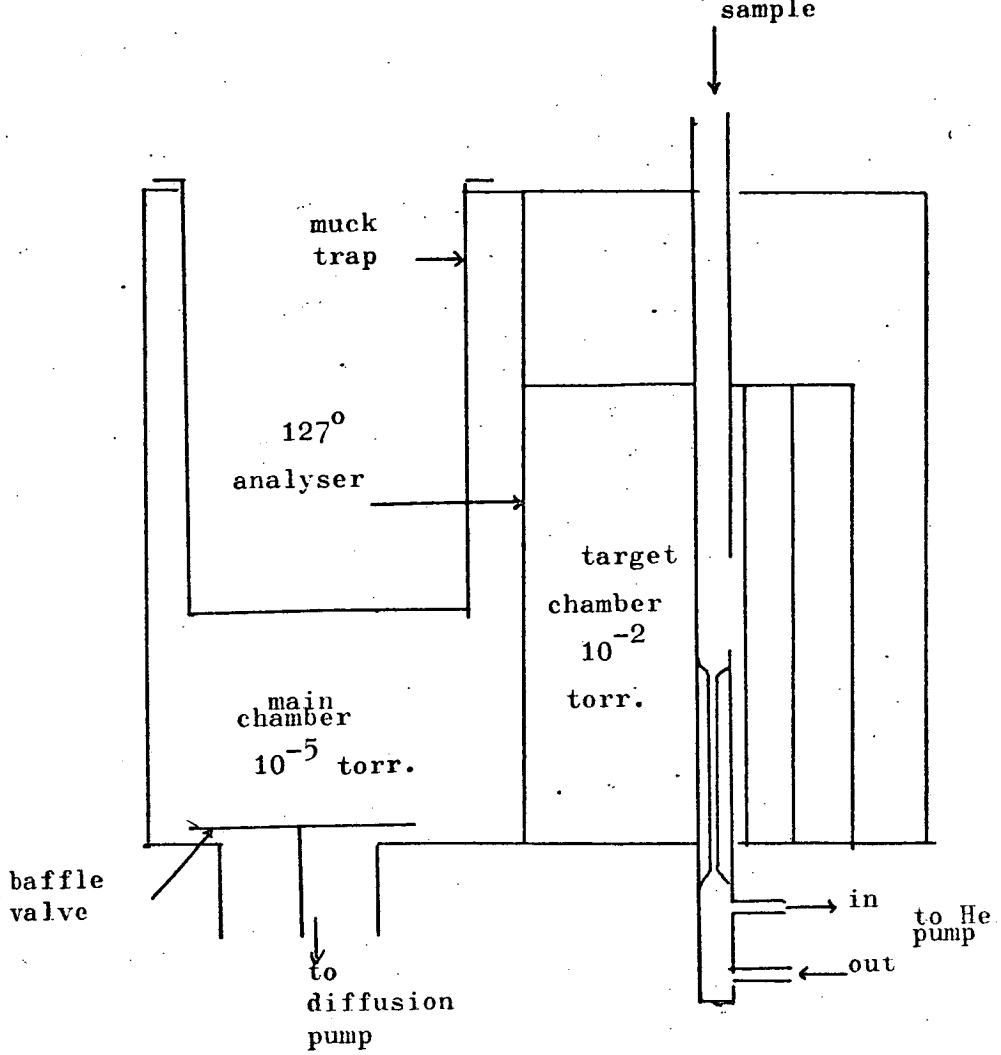

Figure 1

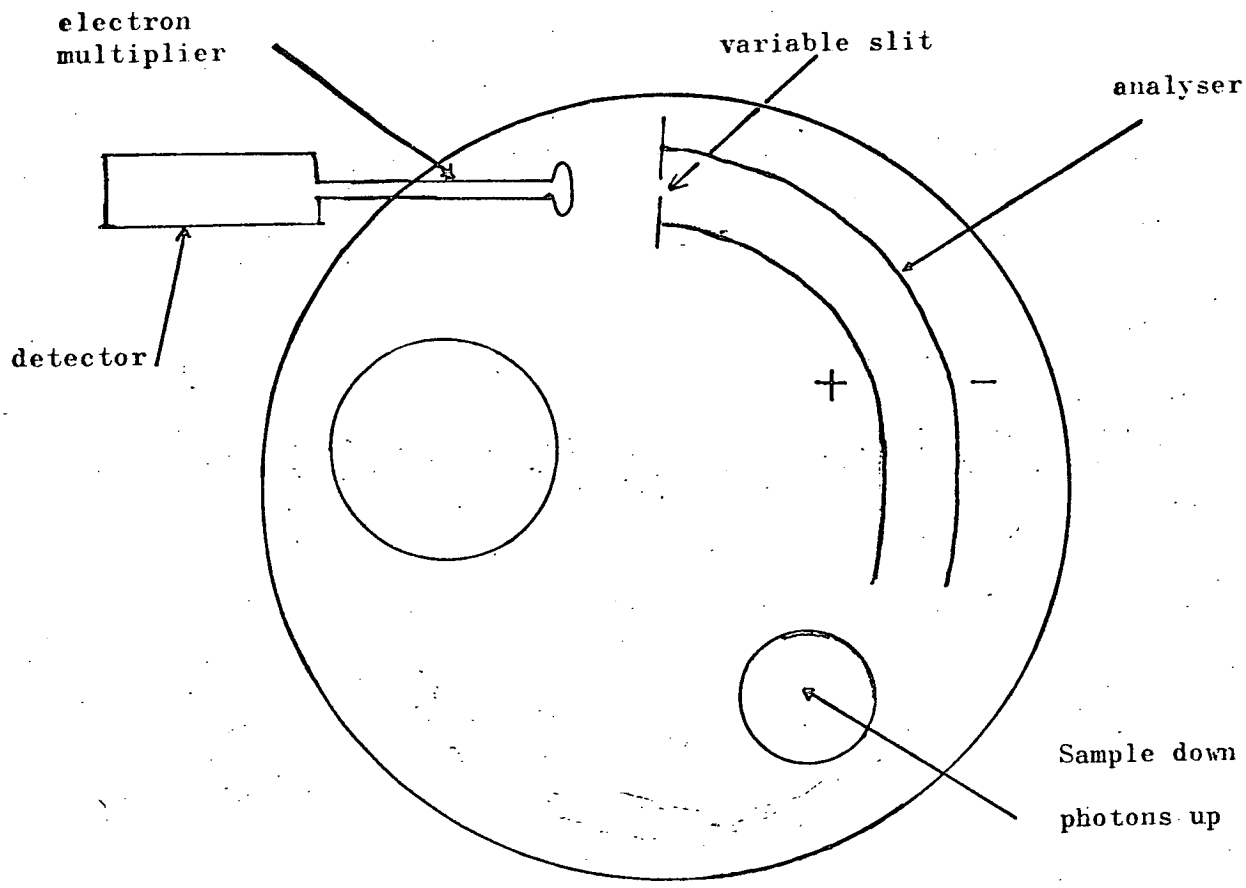

Figure 2.

The amplified pulses generated by the electrons then pass from the electron multiplier into a solid state counting system consisting of a linear amplifier and a ratemeter capable of handling count rates of up to 5000 counts per second (cps). The principal features of the He(I) spectra were recorded at count rates in the range 500 - 5000 cps, but as a consequence of the low He(II) intensity from the discharge lamp even at optimum conditions, most He(II) spectra were recorded at count rates in the range 150 - 500 cps. To improve the signal to noise ratio in this latter range it is necessary to use an integrating time constant which averages the signal over 5, 15 or 60 second periods as necessary.

The counting equipment is connected to a variable speed X - Y plotter which records the intensity of each band as a function of its apparent ionisation potential (measured in eV). It is possible (and indeed more convenient) to record the I.P.'s directly, rather than the experimentally determined kinetic energy (KE) of the electrons, by using the relationship,

$$K.E. = I.P. - 21.2 \text{ eV}.$$

In recording the spectrum on the X - Y plotter the chart speed has to be appropriate to the count rate and integrating time constant employed, otherwise there will be considerable loss in apparent resolution and accuracy of intensity and energy values.

The band positions of the spectra thus obtained are calibrated by comparison with known standards such as Ar, Kr or N_2 introduced into the target chamber during the course of the experiment from samples kept in the instrument reservoir.

The vacuum system employed in the spectrometer (as shown in Figure 1), indicates the conflicting pressure requirements of the

different spectrometer regions. The main chamber, which contains the analyser, and electron multiplier must be maintained at pressures better than 5×10^{-5} Torr by an oil diffusion pump backed by a rotary pump. This allows the photoelectrons a collison free path to the electron multiplier. If the pressure exceeds this limit then anomalous effects such as those presented in Chapter 2 are likely to occur.

However, the pressure of He in the discharge lamp necessary to maintain a continuous self sustaining discharge is in the range 0.I to 10 Torr; the limiting value depending critically on the voltage, distance between, and surface conditions of the electrodes. Likewise, the sample pressure in the target region required to generate sufficient photoelectrons is again in the $\geqslant 10^{-1}$ Torr range. In order to maintain these different pressures in the absence of suitable window materials it is necessary to employ differential pumping on the sample and He supply as well as connect-:ing the ionisation chamber to the main chamber by a narrow slit.

Gaseous and volatile samples are introduced into the instrument through a 'Hoke' needle valve connected via a stainless steel manifold to a simple conventional all glass vacuum line fitted with greaseless 'Rotaflo' taps. The appropriate needle valve position is determined by opening the valve until the optimum signal strength of the strongest peak in the spectrum is obtained. Typical sample consumption is between 1 to 10 mg $hour^{-1}$ and samples introduced into the spectrometers are condensed on to a liquid N_2 cooled 'muck' trap. By closing the baffle valve between the main chamber and the diffusion pumps it is possible to let the

chamber up to atmospheric pressure whilst maintaining the pumping system intact. By filling the chamber with dry N_2 samples could be recovered from the muck trap by use of a specially constructed glass pot, the ground glass top of which formed a seal with the rubber O ring of the trap. This was then attached to a vacuum line and the sample pumped off as the trap warmed up. This was useful not only as it allowed precious samples to be recovered, but also because it was necessary to prevent unpleasant smelling or toxic samples from escaping to the atmosphere.

For samples which do not possess the necessary vapour pressure of at least 10^{-2} torr. at room temperature, but which do have such vapour pressures when heated to temperatures up to 250°C it is possible to use an alternative inlet system.

In this case the sample is placed in a small glass capillary tube inserted directly into the probe ionisation chamber. By controlling the flow rate of the air or water coolant to the dis-:charge lamp, it is possible to use the ionisation chamber as a small oven with which to heat the sample to the required temperature. It is important that this temperature is stable and is not allowed to vary by more than $\pm$ 2°C during the recording of each spectrum, otherwise misleading relative intensity patterns will be obtained. The temperature is thus monitored continously by a thermocouple located in the all-metal sample probe.

When handling air or water sensitive samples by this method, it is necessary to perform such manipulations as filling the capil-:lary tube and fitting it into the heated probe in an inert (usually dry N_2) filled glove bag. The probe and sample is then removed from the bag and inserted into the spectrometer as quickly as possible.

The provision of a vacuum lock on the spectrometer allows this to be performed rapidly and the total time for which the sample is exposed less than 5 seconds. Thus except in the case of extremely sensitive or spontaneously inflammable samples, it is normally not necessary to employ further precautions.

Another useful alteration made to the spectrometer was the modification of the He discharge lamp to give, in addition to the usual He(I) lines, the higher energy He(II) resonance lines.

By working with very high voltages and low He pressures it is possible to make the discharge emit radiation from He ions, the major output from which is the He(II) line at 40.8 eV. The successful operation of the discharge under such conditions required the construction of a much more powerful supply system. The work was carried out by Mr. Alan King (Departmental Electronic Workshop) in collaboration with Mr. Hans Lempka of Perkin Elmer. The design of the power unit is shown in Figure 3, and is capable of delivering 25kV at 250 m.A. current.

The mains input voltage is controlled by a variable transformer with a secondary winding capable of producing up to 18,000 V. AC. This is then rectified into an unsatibilised halfwave DC supply by a series of 40 diodes contained in two stacks. The power then passes through the resistor R2, which is air cooled whilst the unit is in operation. For safety, the entire unit is contained in an earthed metal cage and the power is led to the discharge lamp using car ignition cable contained in an earthed conduit.

To operate the lamp under He(II) conditions, the following procedure is adopted. The He pressure in the lamp is increased

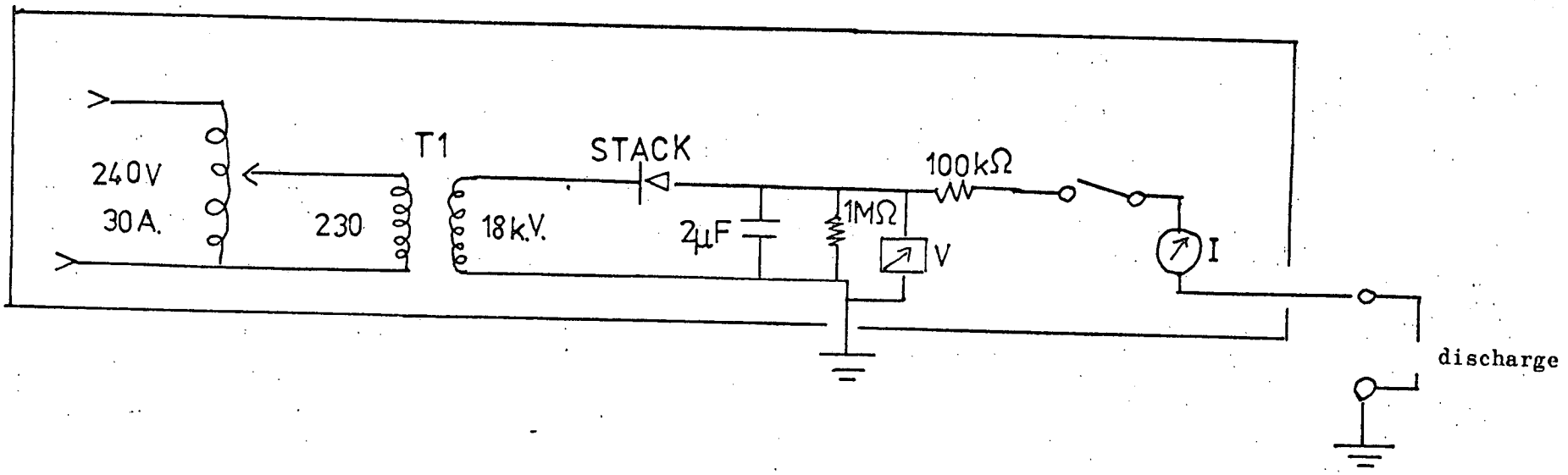

Bird's eye view
of power unit.

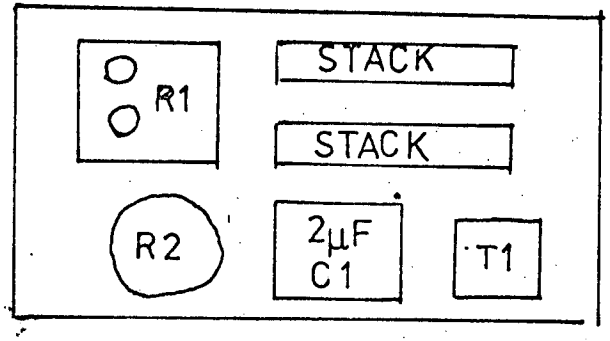

Figure 3.

to approximately 5 Torr and the power unit switched on. The voltage is slowly increased to 15 to 18 kV by which time the discharge should ignite. Immediately this occurs a reading of approximately 150 m.A should show on the ammeter and the voltage reading drops by 2 - 3 kV. If ignition of the discharge has not occurred when the voltage reading has reached 20kV then it is necessary to increase the pressure of He. When ignition has occurred the voltage is reduced to approximately 13k.V. and the He pressure lowered slowly and carefully to the minimum pressure at which the discharge will operate. Usually this is at a pressure between ·1 to ·2 Torr and the lower the pressure, the greater the He(II) output.

When recording He(II) spectra the range of electron kinetic energies which are required to be analysed is almost twice that of He(I) spectra. As a result, the voltage range across the analyser plates must also be doubled and this is achieved by means of a two way switch located behind the spectrometer fascia.

However as the X - Y plotter records apparent ionisation potentials (assuming $h\nu$ = 21.2 1 eV) and not electron kinetic energies, the calibration of the spectra involves a little care. For a normal routine He(I) scan, the apparent IP scale begins at 6 eV. This corresponds to an electron kinetic energy of 15.2 eV. On changing to He(II) operation, the highest kinetic energy electron measured on this scan will therefore be 15.2 x 2 = 30.4 eV and will correspond to an apparent IP of (40.8 - 30.4) = 10.4 eV. In fact, it is possible to record lower energy IP's on other expansion scanning modes. However very slow scan speeds were necessary (because of the very low count rates associated with He(II) spectra) and so it was

not usual to record routine spectra using expansion modes.

Another consequence of the low scan speeds was the significantly larger quantity of sample required.

Normally at least 1 m. mole was needed to obtain all the necessary spectra. But in the case of involatile samples which required the use of the heated probe inlet system the restricted sample size proved troublesome. It was difficult to obtain a high enough rate of sublimation compatible with maintaining sufficient sample to complete a full scan, which could easily take up to $1\frac{1}{2}$ hours.

Another drawback having to use such a large quantity of sample was the increased amount of material which decomposed in the spectro-:meter. The successful operation of the discharge lamp in the He(II) mode requires particular care not only over the purity of the He supply but also over the cleanliness of the electrode surfaces. As a result it was frequently necessary to dismantle and clean the dis-:charge and target chamber surfaces.

VACUUM ULTRAVIOLET SPECTROMETERS.

Two different vacuum u.v. spectrometers were used to obtain the results presented in Chapter 3. The preliminary work was performed on a Hilger Watts 1 metre vacuum grating monochromator and the subsequent higher resolution studies were obtained at the University of Dundee using a Macpherson Model 241.

The basic design and operation of both instruments is very similar. As shown in Figure 4, both consist of a large cylindrical chamber evacuated to about 10^{-6} Torr to eliminate atmospheric absorption. Light from the source passing through the sample, which is contained in a glass cell fitted with Li F windows, falls on to the concave grating. The light is dispersed by it, refocussed into the focal curve and passes through the exit slit to be recorded on a photographic film.

The major differences between the spectrometers lie in the light sources employed, the grating characteristics, and the size of the photographic film used to record the spectrum.

In the Hilger Watts instrument the source was a pulsed Lyman discharge lamp filled with either Ar or Kr and it was usually necessary to fire the lamp 10 to 15 times per exposure. The Macpherson instrument was operated using a continuous microwave sustained discharge in either H_2, Kr or Ar. In this case it was possible to vary either the sample pressure or exposure time to obtain suitable intensity.

The exposure times depend critically on the microwave power, the cleanliness of the cell windows and the absorption of the

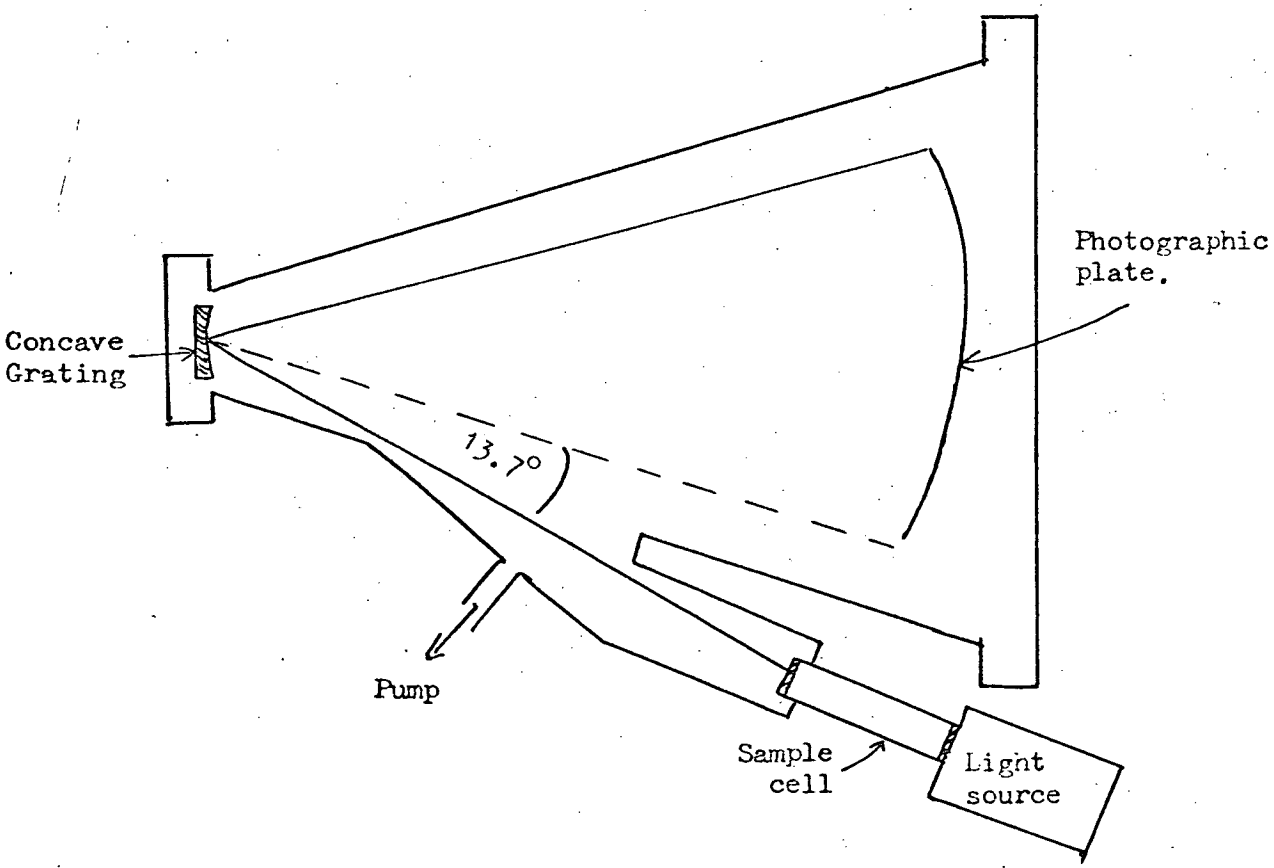

Vacuum u.v. spectrometer design

Figure 4 .

sample and usually ranged from between 5 to 10 minutes. Once a suitable exposure time had been determined, it was customary to use the same time for each exposure and increase the pressure of sample to reveal the weaker spectral features. After each exposure the plateholder containing the photographic film was raised, enabling several exposures (usually up to 5) to be recorded on each film. In this way the spectra obtained with the Macpherson instrument presented in Chapter 3 shows clearly the effect of increasing sample pressure.

The grating in the Hilger Watts instrument was ruled with 2000 lines/mm and had a radius of curvature of 99.98 cm. In the Macpherson instrument the 3 metre radius grating had 1200 lines/mm with a linear dispersion of 2.8 Å/mm which is almost twice that of the smaller instrument.

In order to photograph the spectrum, specially prepared film was used. For the Hilger Watts instrument Ilford HB4 film sensitised by a .5M Sodium Salicylate solution in methanol was developed using microphen. In the Macpherson instrument the film was available either in the form of cellulose strips or, for more accurate work, on glass plates.

The spectrum thus obtained can then be enlarged photographi-:cally or by a microdensitometer attached to an X - Y chart recorder. By this latter technique it is possible to produce a more convention-:al representation of the spectrum in which the intensity of each band is plotted against wavelength. The distance of each band in the spectrum is then measured relative to accurately known standard lines (usually atomic emission lines occurring naturally in the

lamp) either from the densitometer trace or preferably directly from the photographic plate. It is for this reason that glass plates are used in preference to cellulose strips since these latter are much more liable to distort or change size and so produce erroneous band position measurements.

The distances may be measured directly from the photograph or plate either with a ruler and magnifying glass or preferably using a travelling microscope linked to an accurate micrometer screw. The wavelength dispersion of the plate is then calculated from the distances between the emission lines and in this way the wavelength of each unknown line obtained by linear interpolation. If greater accuracy of wavelength measurement is required it is customary to use higher order terms to define the wavelength dispersion of the plate.

PREPARATION AND CHARACTERISATION OF METAL CYCLOPENTADIENYL COMPOUNDS.

PREPARATIONS.

The heavy metal cyclopentadienyl compounds were all prepared according to standard literature methods. As a result it will only be necessary to give a brief indication of the methods used as further details are included in the references given.

a) Thallium Cyclopentadienyl $Tl\,C_5H_5$ [1]

This was prepared by adding 3 ml of freshly distilled cyclopentadiene monomer to 5.04g Thallous Sulphate dissolved in 15ml of 4N aqueous Sodium Hydroxide . The mixture was shaken vigourously for twenty minutes and the reaction proceeded smoothly according to the equation:

$$TlOH + C_5H_6 \longrightarrow TlC_5H_5 + H_2O .$$

The curdy white precipitate was filtered off rapidly, washed and left to dry in a vacuum desicator filled with fresh potassium hydroxide KOH. A pure sample of Thallium cyclopentadienyl was obtained by vacuum sublimation of the dried product at 100°C. This produced 3.5g of fine yellow needle shaped crystals, representing an overall yield of 65% (based on the quantity of Thallous Sulphate used).

b) Indium Cyclopentadienyl.[2]

Owing to the sensitivity to moisture and atmospheric oxygen it is not possible to prepare this, or the other cyclopentadienyls by routes analogous to the preparation of Thallium Cyclopentadienyl. Instead the compounds are prepared by the reaction of sodium cyclopentadiene with the metal halide in

ether.

In such cases particular care has to be taken to ensure that the ether and metal halide are dry and that all manipulations are performed in an inert atmosphere (usually dry nitrogen).

Sodium Cyclopentadiene is prepared by refluxing 4.8g finely divided metallic sodium for 4 - 6 hours under nitrogen with 15 ml of freshly distilled cyclopentadiene monomer in 500 mls dry peroxide free diethyl ether. The Sodium Cyclopentadiene is formed with the evolution of hydrogen according to the equation:

$$2Na + 2C_5H_6 \longrightarrow 2Na\,C_5H_5 + H_2 \ .$$

When reaction is complete the resulting solution is pale pink in colour. To this is added, with stirring, 13 g. Indium trichloride dissolved in excess dry diethyl ether.

The Indium trichloride used was dried prior to use, by refluxing with thionyl chloride ($SOCl_2$) and filtering off the anhydrous Indium trichloride.

The mixture of $Na\,C_5H_5$ and $InCl_3$ is refluxed with continuous stirring under N_2 for 12 - 14 hours. The solvent is then reduced to small bulk by distillation at atmospheric pressure, and is removed completely by further distillation at reduced pressure. The resulting solid residue is transferred in an inert atmosphere to a vacuum sublimation tube and a pure sample obtained by gradually raising the temperature to 150°C.

c) Tin Dicyclopentadienyl and Lead Dicyclopentadienyl.[3]

These were prepared by the addition of slight excess of the

appropriate anhydrous metal halide to sodium cyclopentadiene in dry diethyl ether, or tetra hydrofuran, according to the equations:

$$Sn\ Cl_2 + 2Na\ C_5H_5 \xrightarrow{solvent} Sn\ (C_5H_5)_2 + 2NaCl$$

$$PbCl_2 + 2Na\ C_5H_5 \xrightarrow{solvent} Pb\ (C_5H_5)_2 + 2NaCl \quad .$$

The mixtures were stirred continuously under reflux in an atmosphere of dry N_2 for 10 - 12 hours. The anhydrous metal halide was prepared by treating the hydrated metal salt with acetic anhydride for $1\frac{1}{2}$ hours and filtering off the solid. After reaction was complete, the solvent was removed by distillation and pure samples obtained by sublimation of the solid residue at $100^{o}C$ in vacuum.

Like Indium cyclopentadienyl both Tin dicyclopentadienyl and Lead dicyclopentadienyl are air and moisture sensitive com-:pounds which require to be manipulated in dry inert condi-:tions.

d) Mercury dicyclopentadienyl $Hg\ (C_5\ H_5)_2$ [5]

Like the Indium, Tin and Lead derivatives, mercury dicyclo-:pentadienyl may also be prepared by the action of the metal halide on sodium cyclopentadiene in ether, i.e.

$$Hg\ Cl_2 + 2Na\ C_5\ H_5 \longrightarrow Hg(C_5H_5)_2 + 2NaCl$$

However an alternative, and better, synthesis uses the low temperature exchange reaction between mercuric chloride and thallium cyclopentadiene in dry tetra hydrofuran described by the equation: [6]

$$Hg\ Cl_2 + 2Tl\ C_5H_5 \xrightarrow[N_2]{THF} 2\ Tl\ Cl + Hg\ (C_5H_5)_2 \quad .$$

By stirring vigourously for 30 minutes a suspension of 6g Thallium cyclopentadiene in circa 30 ml Tetrahydrofuran was prepared. This was cooled to about $-40^{\circ}C$. using a chlorobenzene/liq. nitrogen slush bath and 3g. of Mercuric chloride dissolved in 10 ml. Tetrahydrofuran was added slowly. After stirring for one hour at $-40^{\circ}C$ the solution was filtered rapidly under nitrogen. The filtrate was immediately reduced to dryness using a rotatory evaporator. The remaining yellow solid was dissolved in 2 - 3 ml dry diethyl ether, the solution filtered, and the filtrate cooled to $-40^{\circ}C$ to precipi-:tate fine yellow crystals of mercury dicyclopentadienyl. These were then filtered off and stored in the dark. The yield is quanta-:tive.

(e) Attempted preparation of Cadmiumdicyclopentadienyl.

An attempted preparation of the known[7], but highly sensitve compound cadmium dicyclopentadienyl, by an analogous preparation to that outlined above, but using cadmium chloride, $CdCl_2$ in place of mercuric chloride, was not successful and did not lead to isolable products.

(f) Characterisation of Metal Cyclopentadienyls.

The purity of the samples thus prepared was confirmed by record-:ing their mass spectra using an AEI MS 902.

The samples were manipulated in an inert atmosphere and intro-:duced into the spectrometer via an all glass heated inlet system. The spectra, which were recorded at various temperatures up to $120^{\circ}C$. with 70 eV. ionising voltage, all showed parent ion peaks with the correct metal isotope pattern. All other peaks could reasonably

be attributed to likely fragmentation product ions, and no impurities were found to be present in the vapour above the heated solid. Thus, as a result of the basic similarity in experimental techniques used to record both the mass spectra and photoelectron spectra, we can be certain that the photoelectron spectra do, in fact, correspond to the compounds chosen for study and not to other, or decomposition, pro-:ducts.

PREPARATION AND PURIFICATION OF THE Se CONTAINING DERIVATIVES CSe_2, SCSe, OCSe.

INTRODUCTION.

In recording the photoelectron and vacuum ultra-violet spectra of CSe_2, SCSe and OCSe several attempts were necessary to obtain all the material required. As a result, slightly different methods and/or modifications to the apparatus employed on each occasion, occurred. The methods described below detail the systems employed on the final occasion on which each method was used.

In the design and execution of these experiments considerable attention needed to be given to safety. Not only were the compounds involved often particularly unpleasant but some were also highly inflammable and toxic. As a result all the experiments were carried out under the supervision (and with the prior consent) of a safety officer.

CARBON DISELENIDE.[8]

This was produced in low yield by the direct reaction of methylene chloride vapour and Se at 500 - 600°C.

i.e. $CH_2Cl_2 + Se \longrightarrow CSe_2 + 2HCl$.

The apparatus used is shown in Figure 5.

PREPARATION of SELENIUM.

The Selenium required (80g.), was prepared by passing sulphur dioxide through an acidified solution of selenium dioxide.

i.e. $H_2O + SeO_2 + SO_2 + 2H^+ \longrightarrow H_2SO_4 + H_2O + Se$

The selenium was filtered off and dried in a oven at 150°C for 2 days. Final traces of water were removed by heating to 300° for 4 hours in a stream of dry nitrogen. After allowing to cool, the selenium was pulverised and stored in a desiccator until required.

PREPARATION OF CARBON DISELENIDE.

The finely divided Se was loosely packed into one end of a silica tube and heated to approximately 520°C. A slow stream of dry N_2 was passed through the apparatus to carry the methylene chloride vapour and selenium to the reaction zone of the furnace tube at 560°C. Under optimum conditions a white mist was produced in the receiver flask. If the flow rate of nitrogen or the temperature of the bulk Selenium was too high, then excess Selenium was swept through the apparatus so blocking the outlet from the furnace tube to the receiver flask. However when the furnace temperatures and flow rates had stabilised the experiment could be left to continue undisturbed for several hours. At the end of this time, the receiver flasks would contain a dark, foul smelling liquid.

PURIFICATION.

The first stage in the isolation of pure CSe_2 was to distil the

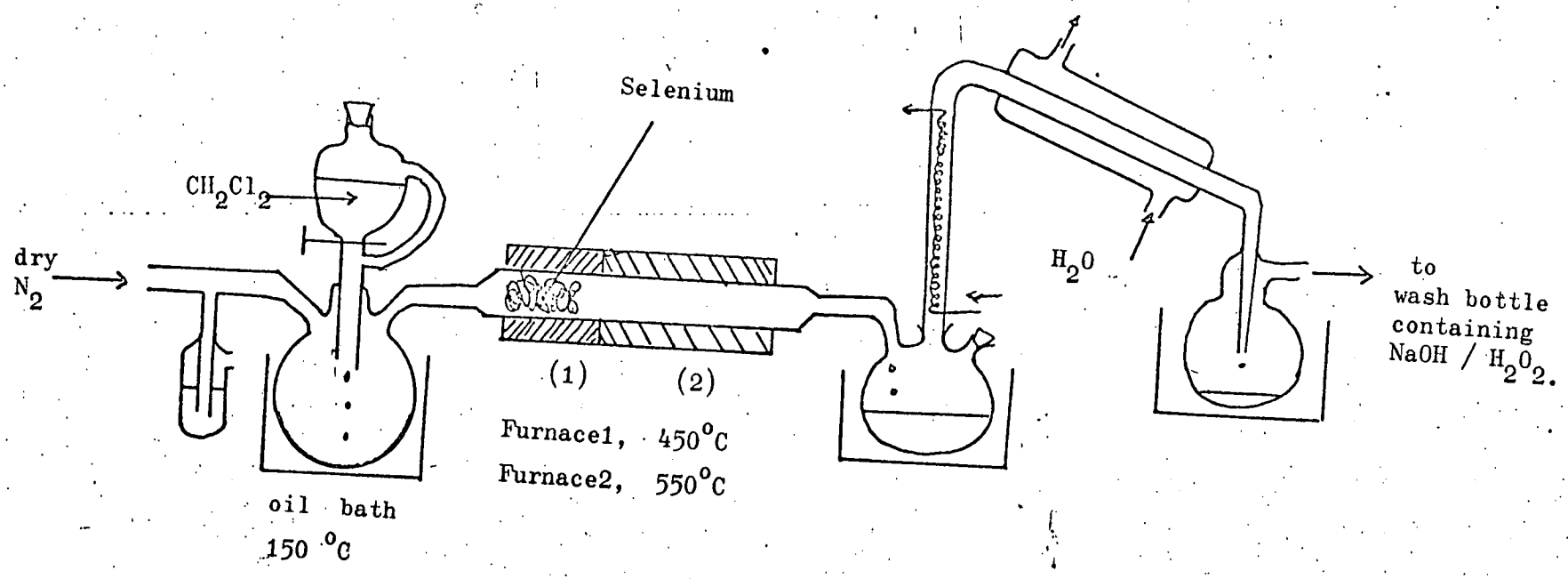
Selenium
CH_2Cl_2
dry
N_2
(1)
(2)
Furnace1, 450°C
Furnace2, 550°C
oil bath
150 °C
H_2O
to
wash bottle
containing
NaOH / H_2O_2.

Figure 5.

liquid fractionally at atmospheric pressure, using a 30 cm. glass bead filled column, to remove excess methylene chloride. The remaining dark red liquid was then transferred to a vacuum line fitted with Rotaflo greaseless taps and the mixture freed from dissolved selenium by pumping.

The Carbon Diselenide was further purified by repeated trap to trap distillation using an acetone-solid carbon dioxide ($-78^{o}C$) and Toluene-liquid nitrogen ($-96^{o}C$) slush baths. Despite assertions to the contrary in the literature[9], it was possible by this method to obtain a sample of carbon diselenide whose infra-red spectrum showed it to be free of methylene chloride or other impurities. The bulk of the golden yellow liquid thus obtained was stored in a refrigerator and in the absence of light to prevent polymerisation. Small samples kept at $-196^{o}C$ on the vacuum line, showed no sign of decomposition.

10

CARBON SULPHOSELENIDE.

This was prepared by the reaction between carbon disulphide vapour and selenium at 750°C.

$$\text{i.e. } CS_2 + Se \longrightarrow SCSe + S.$$

The method and apparatus employed was essentially similar to that described above in the preparation of carbon diselenide, as shown in Figure 6.

PREPARATION.

The Se, prepared as above, was placed at one end of the silica furnace tube and heated to 450 - 500°C. A current of carbon disulphide vapour was carried in a stream of dry nitrogen through the heated Selenium and the resulting vapours passed along the tube where it was heated to 750°C to form carbon sulphoselenide in about 1% yield. The vapours were then collected in ice cooled receivers.

PURIFICATION.

The resulting orange red liquid was freed from the bulk of the carbon disulphide by distillation at atmospheric pressure using a 30 cm. long glass bead filled column. The distillate was maintained at 40 - 50°C until no more carbon disulphide could be removed. The remaining dark red liquid was then transferred to a vacuum line and the mixture freed from carbon disulphide by repeated trap to trap distillation and by using a low temperature fractionating column at -50°C. The purity of the remaining pale yellow liquid was confirmed by its infra-red spectrum which showed no carbon disulphide or other impurites to be present. Samples of purified carbon sulphoselenide were stored in the dark at -196°C to prevent decomposition.

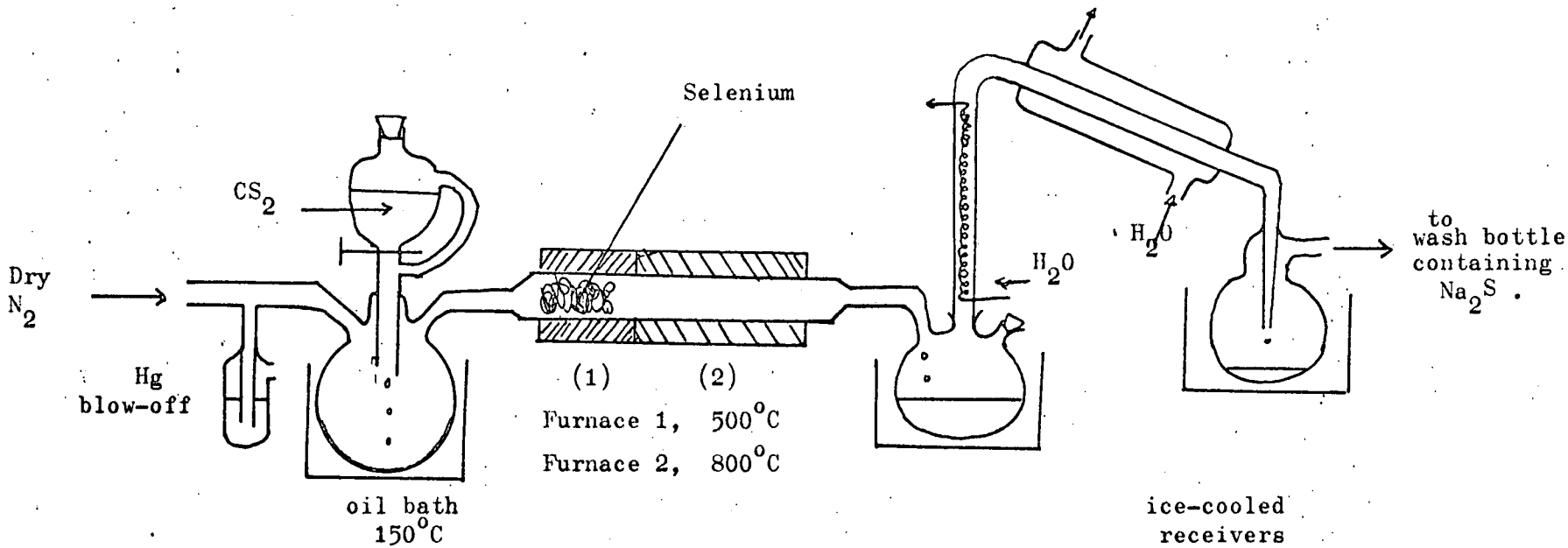
Selenium
CS_2
Dry
N_2
Hg
blow-off
(1)
(2)
Furnace 1, 500°C
Furnace 2, 800°C
oil bath
150°C
H_2O
H_2O
to
wash bottle
containing
Na_2S .
ice-cooled
receivers

Figure 6

11

CARBON OXYSELENIDE.

The synthesis of this compound was performed using two different methods and the samples obtained gave identical spectra.

The basis for the first method was the reaction between aluminium selenide and phosgene at 220°C

$$\text{i.e. } Al_2Se_3 + 3COCl_2 \longrightarrow 2AlCl_3 + 3COSe.$$

which was performed using the apparatus shown in Figure 7.

PURIFICATION OF PHOSGENE.

The phosgene required was obtained by repeated freezing and thawing of a 12% solution of phosgene in benzene and condensing the vapours above the solid. These were fractionated by trap to trap distillation using a pentane-liquid nitrogen (-130°C) and an actone-solid carbon dioxide (-78°C) slush bath to remove impurities such as carbon dioxide, hydrogen chloride and benzene. The purity of the remaining phosgene was confirmed by its infra-red spectrum.

PREPARATION OF ALUMINIUM SELENIDE.

The Aluminium Selenide was prepared by igniting a 3:5 mixture by weight of finely powdered Aluminium and Selenium in a clay pot with a lighted magnesium ribbon. The resulting mass was finely powdered and stored in a desiccator.

PREPARATION OF CARBONYL SELENIDE.

With the Aluminium Selenide heated to 220°C the phosgene was slowly passed over it by carefully opening the needle valve. The bulk of the unreacted phosgene was trapped in the -78°C bath, with the remainder, and any carbonyl selenide produced, condensing in the -196°C liquid nitrogen trap.

PURIFICATION OF CARBONYL SELENIDE.

Small amounts of carbon dioxide, hydrogen chloride and hydrogen

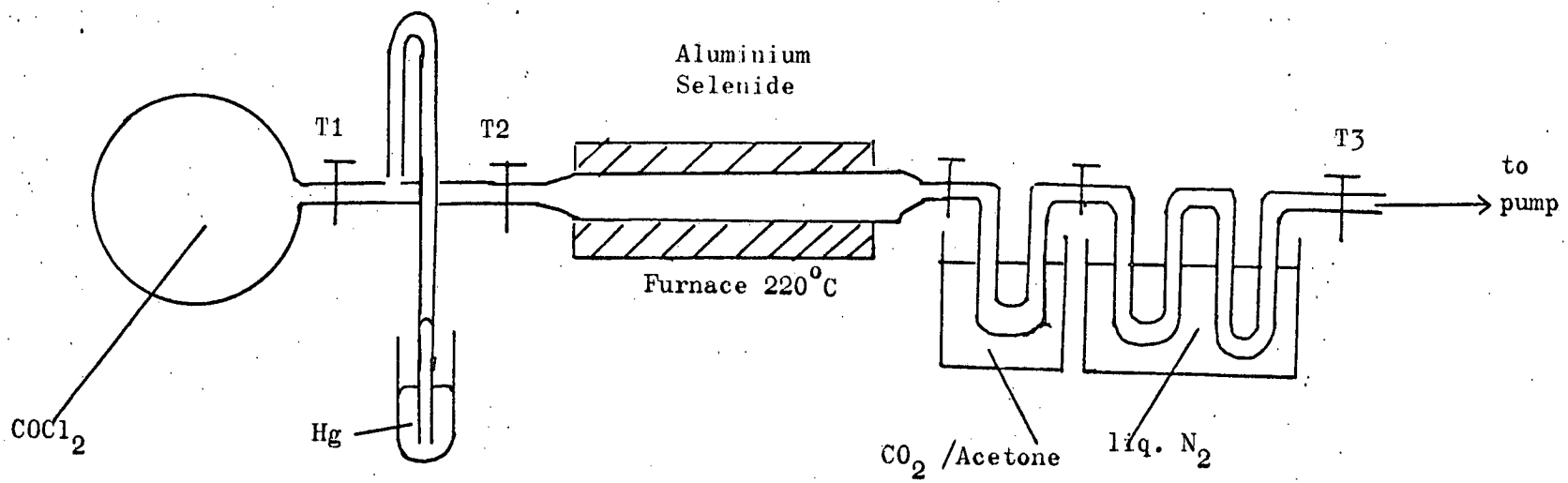
Aluminium
Selenide
T1
T2
T3
to
pump
Furnace 220°C
COCl2
Hg
CO2 /Acetone
liq. N2

Figure 7.

selenide produced by hydrolysis, and unreacted phosgene were removed by repeated trap to trap distillation using -145°C, -130°C and -120°C slush baths.

As a result of impurities in the aluminium selenide, the overall yield was much lower than anticipated and it was necessary to repeat the experiment and subsequent fractionation several times to obtain a reasonable quantity of carbonyl selenide. In the original report of this method it was noted that the Aluminium trichloride produced by the reaction had a marked catalytic effect on the yield. However the aluminium selenide had been prepared by heating a stoichiometric mixture of powdered Aluminium and Selenium in a sealed glass tube, but an attempt to prepare a sample by this method resulted in a violent explosion and so was not repeated.

The alternative preparative route based on the direct reaction

$$CO + Se \xrightarrow{750^{\circ}C} COSe$$

was also employed.[12]

The apparatus required, was basically similar to that described previously for the preparation of carbon diselenide and carbon sulphoselenide but with several important modifications as shown in Figure 8.

These were necessary because carbon monoxide does not condense at liquid nitrogen temperatures, but has a vapour pressure of almost 40 cm. Hg. Thus the manometers, blow offs and long bubbler placed between the apparatus and the pump enabled a steady pressure of approximately 30 cm. Hg to be maintained in the apparatus. At this pressure the carbonyl selenide readily condensed in the -196°C trap, without too much vapourised Selenium being swept out of the furnace.

PURIFICATION OF CARBONYL SELENIDE.

The only impurity present in the carbonyl selenide prepared by

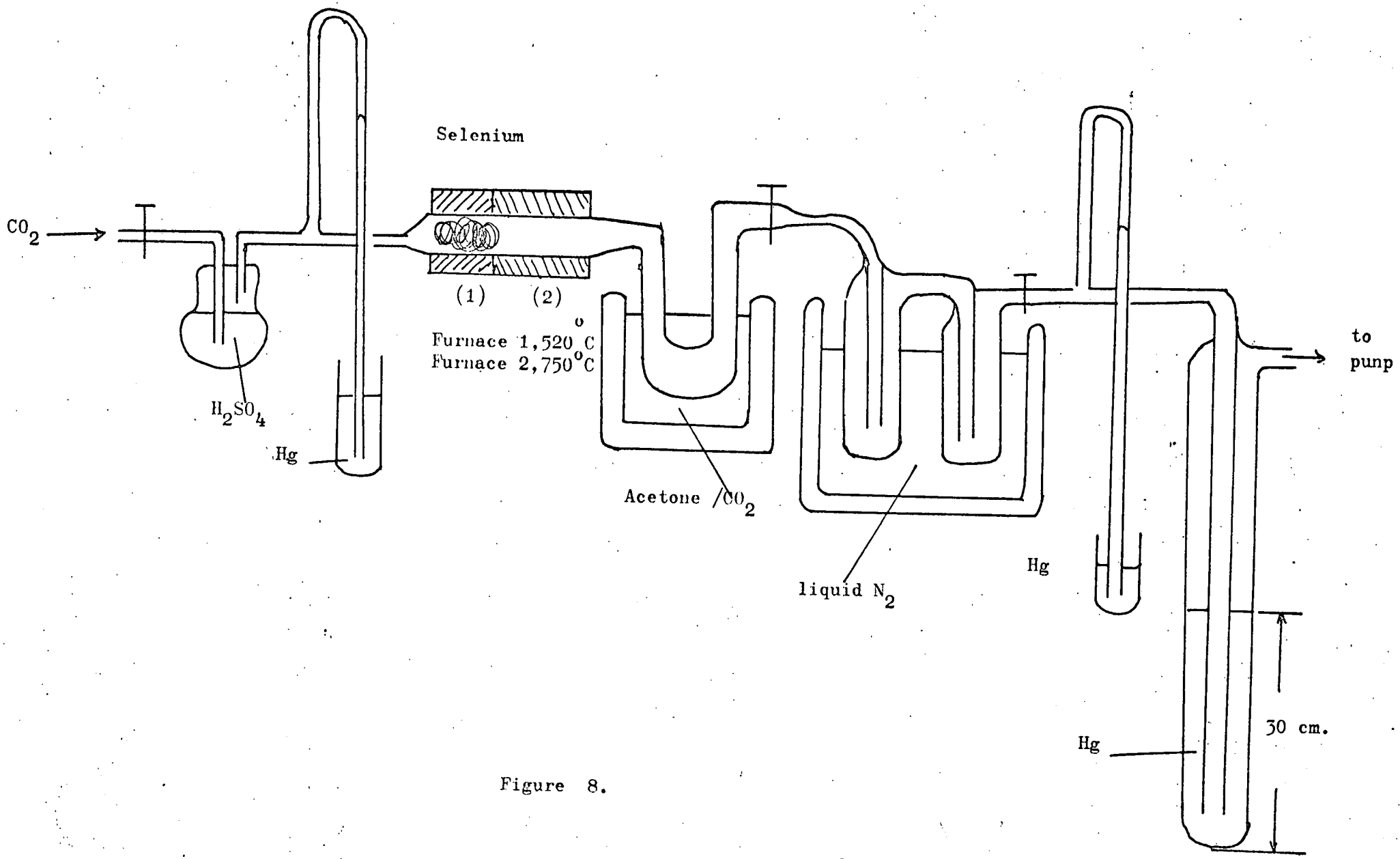
CO_2
Selenium
(1)
(2)
Furnace 1,520 °C
Furnace 2,750 °C
H_2SO_4
Hg
Acetone /CO_2
liquid N_2
Hg
to pump
30 cm.
Hg

Figure 8.

this method was carbon dioxide, which was removed by trap to trap distillation using -120° and $-130^{\circ}C$ slush baths. After fractionation, the infra-red spectrum of the carbonyl selenide showed it to be free from impurities.

Carbon oxyselenide is sensitive to water and light and readily decomposes in contact with metal surfaces or stopcock grease. As a result it was manipulated in the absence of light in a greaseless tap vacuum line and stored in the dark at $-196^{\circ}C$ in all glass ampoules.

REFERENCES.

1. L.D. Dave, D.F. Evans and G. Wilkinson; J. Chem. Soc. (1959), 3684.

2. J.M. Lalancette, A. Lachance; Can. J. Chem. (1971), 49, 2997.

3. A. Almennigen, A. Haaland and T. Motzfeldt; J. Orgmet. Chem. (1967), 7, 97.

4. G.Brauer ; 'Handbook of Preparative Inorganic Chemistry' Vols. 1 and 2. Academic Press New York, London.

5. G. Wilkinson and T.S. Piper; J. Inorg. and Nuclear Chemistry (1956), 2, 35.

6. A.N. Nesmeyanov, R.B. Materikova, and N.S. Kotcheva; Bull. Acad. Sci U.S.S.R. (1963), 1211.

7. J. Lorbeth; J. Orgmet Chem. (1969), 19, 189.

8. Henriksen and Kristiansen; Int. J. Sulphur Chemistry, (1972), 2, 133.

9. T. Wentink; J. Chem. Phys. (1958), 29, 188.

10. L. Ya Markovskii, N.V. Veshina and T.K. Voivodskaya, Zhur. Priklad. Khim., (1970), 43, 1149.

11. O. Glemser and T. Risley, Z. Naturforsch, 1948, 3b, 1.

12. T.G. Pearson, P.L. Robinson, J. Chem. Soc. (1932), 652.

MOLECULAR PHYSICS, 1974, VOL. 27, NO. 4, 837–841

The photoelectron spectrum of CSe_2

by S. CRADOCK and W. DUNCAN
Department of Chemistry, University of Edinburgh, West Mains Road, Edinburgh, EH9 3JJ

(*Received* 8 *May* 1973 ; *revision received* 24 *September* 1973)

The He I photoelectron spectrum of CSe_2 has been recorded and four of the bands observed assigned to ionization from valence shell levels that correlate well with those found for CO_2 and CS_2. Weak bands in the spectra of CS_2 and CSe_2 are assigned to shake-up processes in which electronic excitation of the ion accompanies ionization.

1. INTRODUCTION

The photoelectron (PE) spectra of CO_2 [1] and CS_2 [2] are well known, having been investigated in detail by many workers. We have recorded the PE spectrum of CSe_2 with He I (21·22 eV) excitation to enable a comparison of the upper valence shell levels with those of the lighter molecules to be made. The electronic spectrum in the near ultra-violet and visible regions, which has been reported by Tyerman [3], is discussed here in relation to the PE spectrum. The PE spectrum of CSe_2 is particularly interesting as it contains fairly prominent bands that we assign to shake-up processes, formally forbidden transitions involving electronic excitation as well as ionization. While such bands are common in X-ray excited PE spectra [4] and a few examples have been reported using He II (40·8 eV) excitation [5, 6], it appears that none have been reported previously in He I spectra.

2. EXPERIMENTAL

Carbon diselenide was prepared [7] by streaming methylene chloride over molten selenium at about 600°C in a stream of nitrogen. The resultant yellow liquid was condensed at room temperature and purified by fractional distillation on a vacuum line. The infra-red spectrum of the product then showed no methylene chloride or other impurities to be present.

Photoelectron spectra were recorded using a Perkin Elmer PS16 spectrometer with He I (21·22 eV) excitation†. Near-ultra-violet spectra were recorded using samples in the vapour phase in 100 mm cells on a Unicam SP800 spectrometer.

3. RESULTS AND DISCUSSION

The PE spectrum of CSe_2 (figure 1) shows six bands, whose vertical ionization potentials are listed in table 1. The first band consists of a pair of sharp

† eV≈0·160 192 aJ.

peaks of equal intensity separated by 0·26 eV (2100 cm^{-1}). This splitting we assign to spin–orbit coupling separating the two states of the CSe_2^+ ion $X^2\Pi_{g3/2}$ and $^2\Pi_{g1/2}$. The corresponding splittings for CO_2^+ and CS_2^+ are 180 cm^{-1} and 436 cm^{-1} respectively [1, 2]. No peaks corresponding to the formation of ions in vibrationally excited states can be detected. Thus as for CS_2 the highest occupied level of $CSe_2(1\pi_g)$ is essentially non-bonding.

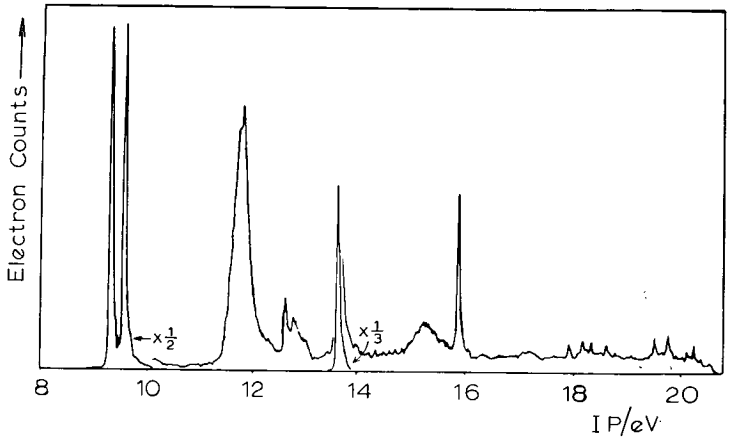

Figure 1. The He I photoelectron spectrum of CSe_2.

CO_2[1]	CS_2[2]	CSe_2	Assignment
13·79	10·07	9·26	$1\pi_g$
	10·12	9·52	
17·60	12·84	11·74	$1\pi_u$
	14·1	12·75	Shake-up band
18·08	14·47	13·61	$2\sigma_u$
		15·3	Shake-up band
19·40	16·20	15·87	$2\sigma_g$
	17·1		Shake-up band

Table 1. Vertical ionization potentials/eV.

The second band in the spectrum is comparatively broad, extending from an adiabatic IP of about 11·45 eV to about 12 eV. A vibrational progression is resolvable ; the mean spacing measured over nine peaks is 0·041 eV (330 cm^{-1}), which may be compared with the symmetric stretching frequency of the ground state molecule (368 cm^{-1}) [7]. We accordingly assign this band to a strongly bonding level, $1\pi_u$.

The third *strong* band consists of a sharp (0, 0) peak at 13·61 eV with a weak (0, 1) peak about 35 meV ($\sim$300 cm^{-1}) to higher energy. The band at 15·87 eV is also sharp, but shows no (0, 1) peak. We assign these two bands to two of the four σ levels of the valence shell.

The above assignment is closely similar to those proposed for CO_2 and CS_2, as is shown in table 1. The two remaining bands in the PE spectrum of CSe_2,

at 12·75 eV and 15·3 eV, cannot reasonably be assigned to ionization from valence shell levels ; their nature will be discussed below.

We first note that these weak peaks are separated from the first strong band by about 3·4 eV and 5·9 eV respectively. These energies are comparable with those associated with near-ultra-violet transitions, suggesting that an analysis of the electronic spectrum of CSe_2 reported by Tyerman [3] may help in assigning the weak peaks in the PE spectrum. The bands observed by Tyerman are listed in table 2, which gives our estimates of band maxima and relative intensities, together with comparable data for the first bands of CS_2 [8].

It is apparent that a very close similarity exists between the electronic spectra of these two molecules, the main difference being that each band of CSe_2 occurs some 6000 cm^{-1} to the red of the corresponding band of CS_2. This energy difference is almost identical to the difference in the first ionization potentials of the two molecules, suggesting that identical assignments of the electronic spectra are appropriate.

CS_2 [8]	CSe_2 [3]	Intensity
29 000	23 000	Very weak
31 500	26 500	Weak
50 000	43 400	Strong
55 000	49 100	Weak

Table 2. Visible and ultra-violet spectra of CS_2 and CSe_2 (band maxima/cm^{-1}).

While the assignment of the CS_2 spectrum is perhaps not yet certain, the weight of evidence at present seems to favour the suggestion that all the first three bands involve transitions to states derived from the configuration . . . $(1\pi_g)^3(2\pi_u)^1(A)$, the strongest band, at 50 000 cm^{-1} involving the fully allowed transition to the $^1\Sigma_u$ state, that near 31 500 cm^{-1} the $^1\Delta_u$ component and the very weak bands near 29 000 cm^{-1} the $^3\Delta_u$ component†. The great complexity of the bands is ascribed to the fact that the upper states are all bent, because of the occupation of the $2\pi_u$ level, so that extensive progressions in the bending vibration occur, and the bands due to the two components of the bent ion overlap, while several sets of hot bands arise because of the low bending frequency in the ground state.

Taking the analogous assignment for CSe_2, we see that the two singlet states ($^1\Delta_u$ and $^1\Sigma_u$) of the . . . $(1\pi_g)^3(2\pi_u)^1$ configuration of CSe_2 lie 3·3 eV and 5·4 eV respectively above the ground state $^1\Sigma_g$ of the configuration . . . $(1\pi_g)^4$. The similarity of these energies to those separating the weak peaks in the photoelectron spectrum from the first strong band leads us to consider what states may arise from a similar excitation $1\pi_g \rightarrow 2\pi_u$ in the ion CSe_2^+ (ground-state configuration . . . $(1\pi_g)^3$).

The resulting configuration . . . $(1\pi_g)^2(2\pi_u)^1$ gives rise to five states for a linear ion ; these may be classified in terms of the states of the . . . $(1\pi_g)^2$ . . . part of the configuration that they arise from. This part gives $^1\Delta_g$, $^1\Sigma_g$ and $^3\Sigma_g$

† We are greatly indebted to a referee for a clear exposition of this assignment, which is in no sense our own.

states, each of which combines with an additional $2\pi_u$ electron to give a $^2\Pi_u$ state ; in addition $^1\Delta_g$ gives rise to a $^2\Phi_u$ state whereas $^3\Sigma_g$ gives rise to a $^4\Pi_u$ state :

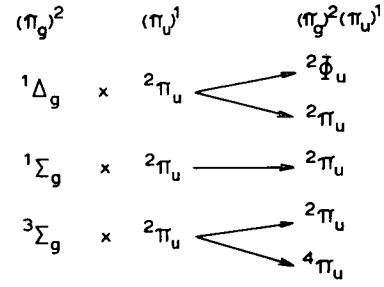

States derived from the configuration . . . $(1\pi_g)^2(2\pi_u)^1$.

Shake-up bands correspond to transitions formally forbidden under photon-excitation ; they are held [5] to derive their intensity by mixing of the upper state with nearby states of the same symmetry to which transitions are allowed. There are no nearby state of $^2\Phi_u$ or $^4\Pi_u$ symmetry to which transitions are allowed in this case, but the photoelectron band at 11·7 eV corresponds to the allowed transition to the $^2\Pi_u$ state derived from the configuration . . . $(1\pi_u)^3(1\pi_g)^4$. Thus all the $^2\Pi_u$ states arising from the configuration . . . $(1\pi_g)^2(2\pi_u)^1$ may give rise to weak bands ; we assign the two weak bands we observe at 12·7 eV and 15·3 eV to two of them. Other weak peaks appear in our spectra of CSe_2 in the 18–21 eV region ; while most of these may plausibly be accounted for in terms of ionization by ' impurity lines ' in the output of the lamp [such as those due to traces of H atoms (10·2 eV, 12·1 eV) and N atoms (10·95 eV)] we cannot be certain that there are no further genuine ionizations in this region.

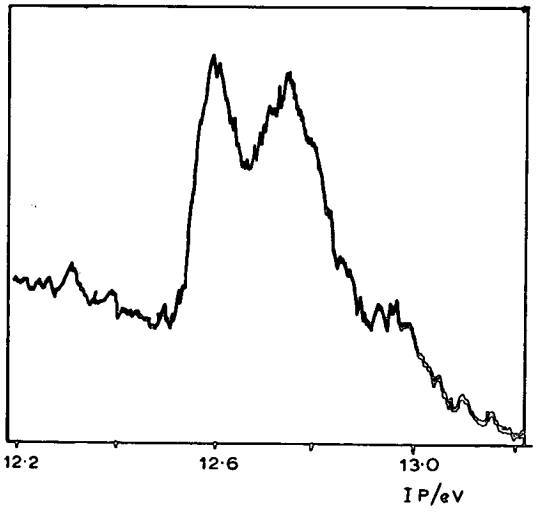

Figure 2. A portion of the photoelectron spectrum of CSe_2 showing the shake-up band near 12·75 eV.

It should be noted that the $^2\Pi_u$ states involved in the shake-up transitions, with electrons in the antibonding $2\pi_u$ level, are expected to be bent, as are the state of the molecule arising from the . . . $(1\pi_g)^3(2\pi_u)^1$ configuration. Under the resulting C_{2v} symmetry each $^2\Pi_u$ state should split into $^2A_1$ and $^2B_1$ states, but it does not seem likely that this splitting will be large. It may well contribute to the breadth of the 15·3 eV band. The weak peak at 12·6 eV (figures 1, 2) varies in intensity relative to the 12·75 eV band, so we assign it to traces of H_2O. It is possible that some of its intensity may in fact be due to a second component of the 12·75 eV band of CSe_2, as we have been unable to remove it completely and it appears broader than expected for H_2O in figure 2.

A similar pair of weak bands to those we observe in CSe_2 has been reported in the spectrum of CS_2 (see table 1). It seems possible that they may be due to shake-up processes similar to those we have invoked for CSe_2.

4. Conclusions

We have observed and analysed the photoelectron spectrum of CSe_2; the valence shell levels $2\sigma_g$, $2\sigma_u$, $1\pi_u$ and $1\pi_g$ give rise to bands similar in position and structure to those found for CO_2 and CS_2. Weak peaks in the spectra of CSe_2 are assigned to shake-up processes leading to $^2\Pi_u$ states derived from the . . . $(1\pi_g)^2(2\pi_u)^1$ configuration of the ion.

References

[1] Turner, D. W., *et al.*, 1970, *Molecular Photoelectron Spectroscopy* (Wiley), p. 66.
[2] As reference [1], p. 65.
[3] Callear, A. B., and Tyerman, W. J. R., 1965, *Trans. Faraday Soc.*, **61**, 2395.
[4] Gelius, U., Allan, C. J., Allison, D., Siegbahn, H., and Siegbahn, K., 1971, *Chem. Phys. Lett.*, **11**, 224.
[5] Lorquet, J. C., and Cadet, C., 1970, *Chem. Phys. Lett.*, **6**, 198.
[6] Price, W. C., 1972, *Discuss. Faraday Soc.*, **54**, 115.
[7] Wentink, T., 1958, *J. chem. Phys.*, **29**, 188.
[8] Herzberg, G., 1966, *Electronic Spectra of Polyatomic Molecules* (Van Nostrand Reinhold) p. 600.

Offprinted from the *Journal of The Chemical Society, Faraday Transactions II*, 1975, vol. 71.

VACUUM ULTRAVIOLET SPECTRUM OF CARBON DISELENIDE

Vacuum Ultraviolet Spectrum of Carbon Diselenide

By Stephen Cradock,* R. J. Donovan, W. Duncan and H. M. Gillespie

Department of Chemistry, University of Edinburgh,
West Mains Road, Edinburgh EH9 3JJ

Received 8th July, 1974

The vacuum ultraviolet spectrum of CSe_2 is reported in the region 210-130 nm. Rydberg series leading to the first ionisation potential are identified and vibrational structure associated with the long wavelength members assigned. The effects of spin-orbit coupling and configuration mixing on the observed spectrum, in the 200 nm region, are discussed.

The vacuum ultraviolet spectra of CO_2 and CS_2 have been investigated by many workers; the results have recently been reviewed.[1] These spectra contain extensive Rydberg series leading to several distinct ionisation potentials. By contrast the spectrum of CSe_2 has been reported only in the quartz ultraviolet region; Callear and Tyerman [2] published plates showing bands down to 190 nm, but did not analyse this region. We have suggested an assignment for these bands in connection with our analysis [3] of the He I photoelectron spectrum of CSe_2. This study has provided values for the ionisation potentials of the molecule due to removal of electrons from the $1\pi_g$, $1\pi_u$, $2\sigma_u$ and $2\sigma_g$ valence-shell molecular orbitals.

Photoelectron data make it possible to analyse Rydberg series with a greater degree of confidence than has been the case hitherto, as the number of unknown parameters in the series formula

$$E_n = I - R/(n-\delta)^2$$

is reduced from three (I, n and δ) to two if I is known. Accordingly we have investigated the spectrum of CSe_2 in the range 130-210 nm and analysed the observed bands into Rydberg series leading to the first ionisation potential, found from the photoelectron study.

This first ionisation potential corresponds to removal of an electron from the $1\pi_g$ level and is associated with two states of the ion, $^2\Pi_{g,\frac{3}{2}}$ and $^2\Pi_{g,\frac{1}{2}}$. The energy difference between these states, 0.26 eV (2100 cm^{-1}) is a measure of the spin-orbit coupling in the ion. This may be expected to manifest itself in Rydberg states leading to the first ionisation potential, as these contain the ionic " core " together with an electron in a diffuse Rydberg orbital. The interaction of the Rydberg electron with the core electrons is expected to be weak.

The most prominent feature in the 160-210 nm region of the absorption spectrum is a pair of very strong bands, separated by ~2100 cm^{-1}, at 180.2 and 173.6 nm. The term value ($I-E$) calculated using the photoelectron ionisation potential is 2.42 eV for the long-wavelength member. Comparison of this with the Rydberg levels of atomic Se suggests the assignment of these bands to Se $5p$ (atomic term about 2.3 eV). The selection rules for a symmetric linear triatomic molecule are such that transitions from the $^1\Sigma_g^+$ ground state are fully allowed only to $^1\Sigma_u^+$ and $^1\Pi_u$ upper states; as the core has symmetry $^2\Pi_g$ allowed transitions may occur to states with π_u or σ_u Rydberg levels occupied. It seems likely that these very strong bands correspond to Rydberg

states with the Se $5p\ \sigma_u$ level occupied, as transitions to Se $5p\ \pi_u$ level would be expected to be weak ($\Delta l = 0$).

Close to these two strong bands are a number of other fairly intense features attributable to vibrational excitation (see table 1). The symmetric stretching frequency of the molecule in the ground state [4] is 368 cm^{-1}, and appreciable populations of vibrationally excited states are expected at 300 K. In addition to the strong (0, 0) band there are weaker bands assigned to the (1, 0) and (0, 1) vibrational transitions. The vibration frequencies v_1'' and v_1' are found to be $\sim$380 and $\sim$320 cm^{-1} respectively from these bands. The appreciable difference between these frequencies leads to the appearance of sequences; the transitions (1, 1), (2, 2), (2, 1) and (1, 2) give rise to the most prominent features of this type.

TABLE 1.—ABSORPTION SPECTRUM OF CSe_2 BETWEEN 210 AND 170 nm

				assignment	
λ(vacuum)/*nm	intensity	$\bar{\nu}/cm^{-1}$	description	vibration	electronic (upper state)
~205		~48 780	continuum		$^1\Pi_g(\ldots 1\pi_g^3 3\sigma_g^1)$
203.0 min	m	49 260	resonance		$^3\Pi_{u,0}(\ldots 1\pi_g^3(\Omega_c = \frac{1}{2})5s\sigma_u^1)$ see text
201.9_8 max		49 510			
200.0_0	m	50 000	broad, diffuse†	(0, 0)	$^1\Pi_{u,1}(\ldots 1\pi^3(\Omega_c = \frac{3}{2})5s\sigma_u^1)$
198.2_0	w	50 454	broad, diffuse†	ν_2?	
197.4_4	w	50 648	diffuse†	$2\nu_1$?	
196.4_8	w	50 896	broad, diffuse†	$2\nu_2$?	
196.0_3	w	51 013	diffuse	$3\nu_1$?	
195.4_3	vw	51 169		$\nu_1+\nu_3-\nu_1$	
195.3_0	w	51 203		ν_3	
193.9_9	vw	51 549	diffuse	$2\nu_1+\nu_3-\nu_1$	
193.8_6	m	51 584	diffuse	$\nu_1+\nu_3$	
191.3_4	vw	52 263	sharp	$\nu_1(1, 1)$	$^1\Pi_{u,1}(\ldots 1\pi_g^3(\Omega_c = \frac{1}{2})5s\sigma_u^1)$
191.1_6	m	52 312	sharp	(0, 0)	
181.6_0	vw	55 066		$\nu_1(1, 2)$	
181.4_3	w	55 118	sharp	(0, 1)	
181.1_1	vw	55 215		?	
180.5_8	m	55 377	sharp	(2, 2)‡	
180.3_8	s	55 438	sharp	(1, 1)	
180.1_9	vs	55 497	sharp	(0, 0)	$^1\Pi_u(\ldots 1\pi_g^3(\Omega_c = \frac{3}{2})5p\sigma_u^1)$
179.3_6	vw	55 754	diffuse	(2, 1)	
179.1_6	m	55 816	diffuse	(1, 0)	
178.6_9	vw	55 963		?	
178.6_0	vw	55 991		?	
174.7_3	w	57 231		$\nu_1(0, 1)$	
173.7_5	s	57 554	diffuse	(1, 1)	$^1\Pi_u(\ldots 1\pi_g^3(\Omega_c = \frac{1}{2})5p\sigma_u^1)$
173.5_8	vs	57 610	diffuse	(0, 0)	
172.6_3§	vw	57 927	diffuse	(1, 0)	

* wavelengths accurate to ±0.05 nm; † other weaker diffuse bands in this region; ‡ Si emission line at 180.8 nm may obscure the (3, 3) band; § other very weak bands in the region 173.6-172.6 nm.

Although the bending frequency v_2'' is lower than v_1'' it is of π_u symmetry and should only appear in double quanta. It is not impossible that such transitions are involved in the sequences observed, but the indicated change in ν_1 seems adequate explanation for them. A very weak band possibly assignable to excitation of $2v_2'$ is observed at 178.7 nm.

The bands associated with the shorter-wavelength transition ($^2\Pi_{g,\frac{1}{2}}$ core) are more diffuse than those belonging to the longer-wavelength transition, and fewer of them

are measurable. This diffuseness must be due to a predissociation affecting the higher-energy Rydberg state.

The Rydberg states with Se 5*s* levels occupied would be expected to give transitions of lower energy than those with Se 5*p* levels occupied. The atomic term value for Se 5*s* is about 3.6 eV. Again the strongest transitions are to states with the σ_u combination of Se 5*s* levels occupied, together with either the $\Omega_c = \frac{3}{2}$ or the $\Omega_c = \frac{1}{2}$ ionic core. The sharp band, showing a sequence of peaks, near 191.2 is best assigned to the Se 5*s* σ_u Rydberg state correlating with the $\Omega_c = \frac{1}{2}$ state of the ion. The other component apparently gives rise to a complex progression of bands around 200 nm. We place the origin at 200.0_0 corresponding to a term value of about 3.2 eV.

A broad continuum that extends from 200 to 210 nm is probably due to the valence-shell transition $3\sigma_g \leftarrow 1\pi_g$. This transition is formally forbidden, and the observed band will derive its intensity from transitions involving excitation of σ_u or π_u vibrations. No discrete vibrational peaks are apparent, so the transition must lead to dissociation. As the upper electronic state associated with this band has Π_g symmetry, excitation of σ_u and π_u vibrations will give allowed vibronic transitions of Π_u and Σ_u symmetry respectively. The Se 5*s* σ_u Rydberg state has Π_u symmetry, and the vibrational progression associated with the $\Omega_c = \frac{3}{2}$ core state will arise from coupling with the Π_u vibronic continuum.

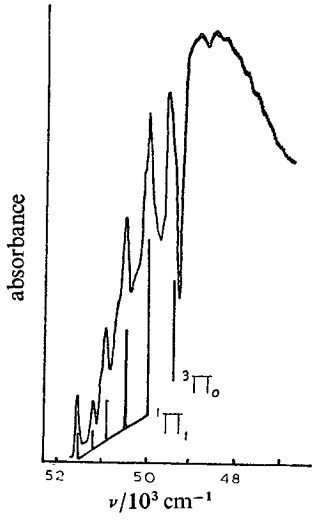

FIG. 1.—Tracing of 200 nm region of CSe_2 absorption spectrum recorded on Unicam SP800 spectrophotometer.

A further phenomenon associated with the interaction of the Se 5*s* Rydberg states and the excited valence-shell level with electronic configuration . . . $1\pi_g^3 3\sigma_g^1$ is the abrupt variation of intensity in the continuum at 203 nm. We interpret this as being a "resonance",[5-7] here involving configuration mixing of a Rydberg state and a *dissociation* continuum of the same energy, like parity and with the same total angular momentum (J). Fig. 1 shows a tracing of this region.

The dissociation continua have J values of $0(\Sigma_u)$ and $1(\Pi_u)$. As the Rydberg states correlating with the Ω_c, $= \frac{3}{2}$ and $\Omega_c = \frac{1}{2}$ ionic states are so clearly separated we must use (Ω_c, ω) coupling between the core and Rydberg levels. The $\Omega_c = \frac{3}{2}$ core then gives rise to states with $J = 1$ and $J = 2$, while the $\Omega_c = \frac{1}{2}$ core gives rise to states with $J = 1$ and $J = 0$. We have already assigned peaks to the two singlet

states, so the only remaining possibility is interaction of the $^3\Pi_0$ Rydberg state correlating with the $\Omega_g = \frac{1}{2}$ core with the $\Sigma_u(J = 0)$ vibronic continuum. This enables us to define the energy of the triplet Rydberg state; the singlet–triplet separation is $\sim 3050\ cm^{-1}$.

Other Rydberg transitions appear between 170 nm and the ionisation limit near 130 nm; some show vibrational satellites, while all show the large spin-orbit coupling and can be divided into two distinct sets of series. Table 2 shows the energies of all band origins and our suggested assignments. In addition to Rydberg series a number of other weaker features have been observed, and are assigned as follows: a diffuse band at 169.8 nm, as arising from the allowed valence shell transition $3\sigma_u \leftarrow 1\pi_g$ [a weaker band at 169.1 nm could then be the (1, 0) transition]. Several diffuse bands between 154.4 and 151.6 nm are assigned to the $2\pi_u \leftarrow 1\pi_u$ transition. A continuum and a number of bands between 147.0 and 144.8 nm are assigned to the $3\sigma_g \leftarrow 1\pi_u$ transition.

The Rydberg series have been assigned as pairs of s levels ($\delta \approx 3.1$), p levels ($\delta \approx 2.4_5$), and d levels ($\delta \approx 1.2$). In each case the first members of the series are perturbed and displaced from the predicted positions. As the ionisation limits are approached the d series become more prominent; the s series merge with the d series because the quantum defects differ by almost exactly 2, but the p series appear to become weak. This is to be expected as the Rydberg states become more atom-like in nature. The series leading to the second limit ($\Omega_c = \frac{1}{2}$ core) are considerably more

TABLE 2.—RYDBERG SERIES FOR CSe_2

n	λ/nm	intensity	$\bar{\nu}$/cm^{-1}	core state	quantum defect δ	spin-orbit splitting/cm^{-1}	comments
				(*a*) *nd* series			
4	~ 161.4	w	61 960	$^2\Pi_{\frac{3}{2}}$	1.06	~ 2300	weak, and
	~ 155.6	w	64 270	$^2\Pi_{\frac{1}{2}}$	1.04		diffuse
5	148.3_9	s	67 390	$^2\Pi_{\frac{3}{2}}$	1.12	2141	two bands
	143.8_2	s	69 531	$^2\Pi_{\frac{1}{2}}$	1.12		(sequence structure?)
6	142.8_5	s	70 004	$^2\Pi_{\frac{3}{2}}$	1.16	2078	strong diffuse band,
	138.7_3	s	72 082	$^2\Pi_{\frac{1}{2}}$	1.19		overlaps, $7s(^2\Pi_{\frac{1}{2}})$
7	140.0_0	s	71 429	$^2\Pi_{\frac{3}{2}}$	1.19	2133	overlaps $7p(^2\Pi_{\frac{1}{2}})$
	135.9_4	s	73 562	$^2\Pi_{\frac{1}{2}}$	1.19		
8	138.2_9	s	72 312	$^2\Pi_{\frac{3}{2}}$	1.19	2132	coincidence with
	134.3_3	s	74 444	$^2\Pi_{\frac{1}{2}}$	1.20		$8s(^2\Pi_{\frac{1}{2}})$
9	137.2_2	m	72 876	$^2\Pi_{\frac{3}{2}}$	1.19	2137	coincidence with
	133.3_1	s	75 013	$^2\Pi_{\frac{1}{2}}$	1.19		$11s(^2\Pi_{\frac{3}{2}})$
10	136.5_0	s	73 260	$^2\Pi_{\frac{3}{2}}$	1.21	2148	overlaps $8p(^2\Pi_{\frac{1}{2}})$
	132.6_2	s	75 403	$^2\Pi_{\frac{1}{2}}$	1.19		
11	135.9_8	m	73 540	$^2\Pi_{\frac{3}{2}}$	1.19	2137	overlaps $7d(^2\Pi_{\frac{1}{2}})$
	132.1_4	s	75 677	$^2\Pi_{\frac{1}{2}}$	1.19		
12	135.6_1	m	73 741	$^2\Pi_{\frac{3}{2}}$	1.18	2137	coincidence with
	131.7_9	m	75 878	$^2\Pi_{\frac{1}{2}}$	1.20		$9s(^2\Pi_{\frac{1}{2}})$
13	~ 135.4	w	$\sim 73\ 860$	$^2\Pi_{\frac{3}{2}}$		2130	
	~ 131.6	m	$\sim 75\ 990$	$^2\Pi_{\frac{1}{2}}$			
14	~ 135.3	vw	$\sim 73\ 910$	$^2\Pi_{\frac{3}{2}}$		2190	
	~ 131.4	w	$\sim 76\ 100$	$^2\Pi_{\frac{1}{2}}$			
15	~ 135.0	vw	$\sim 74\ 070$	$^2\Pi_{\frac{3}{2}}$		2110	
	$\sim 131.2_7$	vw	$\sim 76\ 180$	$^2\Pi_{\frac{1}{2}}$			
16	~ 134.9	vw	$\sim 74\ 130$	$^2\Pi_{\frac{3}{2}}$		2150	
	~ 131.1	vw	$\sim 76\ 280$	$^2\Pi_{\frac{1}{2}}$			
17	~ 130.9	vw	$\sim 76\ 400$	$^2\Pi_{\frac{1}{2}}$			

TABLE 2.—*continued*

n	λ/nm	intensity	$\bar{\nu}$/cm^{-1}	core state	quantum defect δ	spin-orbit splitting/cm/$^{-1}$	comments
				(*b*) *np* series			
5	180.1_9	vs	55 497	$^2\Pi_{\frac{3}{2}}$	2.61	2113	well developed sequence structure
	173.5_8	vs	57 610	$^2\Pi_{\frac{1}{2}}$	2.61		
6	151.0_0	s	66 225	$^2\Pi_{\frac{3}{2}}$	2.40	2044	two bands (sequence structure?)
	146.4_8	s	68 269	$^2\Pi_{\frac{1}{2}}$	2.42		
7	144.0_1	vs	69 440	$^2\Pi_{\frac{3}{2}}$	2.42	2004	two bands (sequence structure?)
	139.9_7	vs	71 444	$^2\Pi_{\frac{1}{2}}$	2.48		
8	140.6_0	s	71 124	$^2\Pi_{\frac{3}{2}}$	2.44	2115	sequence structure overlaps $10d(^2\Pi_{\frac{3}{2}})$
	136.5_4	s	73 239	$^2\Pi_{\frac{1}{2}}$	2.46		
9	138.6_3	s	72 134	$^2\Pi_{\frac{3}{2}}$	2.43	2133	sequence structure?
	134.6_5	m	74 267	$^2\Pi_{\frac{1}{2}}$	2.44		
10	137.4_0	m	72 780	$^2\Pi_{\frac{3}{2}}$	2.40	2115	sequence structure?
	133.5_2	m	74 895	$^2\Pi_{\frac{1}{2}}$	2.45		
11	136.6_7	w	73 169	$^2\Pi_{\frac{3}{2}}$	2.48	2144	
	132.7_8	m	75 313	$^2\Pi_{\frac{1}{2}}$	2.46		
				(*c*) *ns* series			
5	200.0_0	s	50 000	$^2\Pi_{\frac{3}{2}}$	2.89	2312	irregular progressions
	191.1_6	m	52 312	$^2\Pi_{\frac{1}{2}}$	2.89		sequence only
6	~160.9	w	62 150	$^2\Pi_{\frac{3}{2}}$	3.04	~2400	diffuse
	154.8_4	m	64 583	$^2\Pi_{\frac{1}{2}}$	3.01		diffuse
7	147.1_8	s	67 944	$^2\Pi_{\frac{3}{2}}$	2.96	2109	diffuse
	142.7_5	s	70 053	$^2\Pi_{\frac{1}{2}}$	2.97		diffuse, overlaps $6d(^2\Pi_{\frac{3}{2}})$
8	142.1_8	vw	70 333	$^2\Pi_{\frac{3}{2}}$	2.98	1979	
	138.2_9	s	72 312	$^2\Pi_{\frac{1}{2}}$	3.06		coincidence with $8d(^2\Pi_{\frac{3}{2}})$
9	139.8_5	m	71 505	$^2\Pi_{\frac{3}{2}}$	3.12	2236	
	135.6_1	m	73 741	$^2\Pi_{\frac{1}{2}}$	3.03		coincidence with $12d(^2\Pi_{\frac{3}{2}})$
10	138.3_5	w	72 280	$^2\Pi_{\frac{3}{2}}$	3.24	2236	
	134.2_0	m	74 516	$^2\Pi_{\frac{1}{2}}$	3.10		
11	137.2_4	w	72 865	$^2\Pi_{\frac{3}{2}}$	3.22	2176	coincidence with $9d(^2\Pi_{\frac{3}{2}})$
	133.2_6	m	75 041	$^2\Pi_{\frac{1}{2}}$	3.14		

intense than those leading to the first limit, and because of chance coincidences between members of the different series it is less easy to pick out the latter. The ($\Omega_c = \frac{1}{2}$) *nd* series can be followed up to $n \approx 17$, only about 400 cm^{-1} from the ionisation limit.

What appears to be the first member of another Rydberg series leading to the $A^2\Pi_u$ state of the ion, gives rise to a number of broad bands between 140.9 and 142.6 nm. We assign it to the $5s\sigma_u \leftarrow 1\pi_u$ transition, as the energy difference between the strongest band and the band at 200 nm attributed to the $5s\sigma_u \leftarrow 1\pi_g$ transition is equal to that observed in the u.v. photoelectron spectrum between the $1\pi_g$ and $1\pi_u$ levels (2.48 eV). The next Rydberg transition of this type, the $5p\sigma_u \leftarrow 1\pi_u$ transition, would be expected to give a band at about 132.5 nm, where the spectrum is dominated by the closely spaced *nd* series leading to the second ionisation limit at 130.3 nm. As the $(1\pi_u)^{-1}$ band in the photoelectron spectrum is broad, consisting of a progression of vibrational peaks in v_1', we may expect Rydberg transitions associated with this level to give broad bands too, going to a limit at 11.74 eV (≡ 105.6 nm).

Finally, a diffuse band around 120 nm is observed that could correspond to the allowed $3\sigma_g \leftarrow 2\sigma_u$ valence shell transition. Further Rydberg series are to be expected

below 120 nm associated with the $B^2\Sigma_u$ state of the ion (vertical ionisation potential = 13.61 eV; ionisation limit 91 nm). These series should give rise to single peaks like that found for the $(2\sigma_u)^{-1}$ transition in the photoelectron spectrum.

We are indebted to the Royal Society and the S.R.C. for equipment grants and to the S.R.C. for the award of a Research Fellowship to H. M. G. We are also indebted to Dr. S. Bell for his advice and helpful discussions.

[1] J. W. Rabalais, J. M. McDonald, V. Scherr and S. P. McGlynn, *Chem. Rev.*, 1971, **71**, 73.
[2] A. B. Callear and W. J. R. Tyerman, *Trans. Faraday Soc.*, 1965, **61**, 2395.
[3] S. Cradock and W. Duncan, *Mol. Phys.*, 1974, **27**, 837.
[4] T. Wentink, *J. Chem. Phys.*, 1958, **29**, 188.
[5] G. Herzberg, *The Spectra and Structures of Simple Free Radicals* (Cornell U.P., Ithaca, New York, 1971), p. 195.
[6] U. Fano and J. W. Cooper, *Phys. Rev. A*, 1965, **137**, 1364.
[7] W. R. S. Garton, *Adv. Atom. Mol. Phys.*, 1966, **2**, 130.

PRINTED IN GREAT BRITAIN AT
THE UNIVERSITY PRESS
ABERDEEN

Offprinted from the *Journal of The Chemical Society, Faraday Transactions II,* 1975, vol. 71.

PHOTOELECTRON SPECTRA OF OCSe AND SCSe

Photoelectron Spectra of OCSe and SCSe

By Stephen Cradock* and William Duncan
Department of Chemistry, University of Edinburgh, West Mains Road, Edinburgh EH9 3JJ

Received 22nd October, 1974

The He I photoelectron spectra of OCSe and SCSe have been studied and the strong bands observed assigned to ionisation from four valence-shell levels in each case. Weaker bands in the spectrum of SCSe are attributed to the formation of doubly-excited species in which an electron has been excited in addition to the ionisation. The positions of these bands are shown to be related to the transition energies found in the electronic spectrum of the molecule. The same relationship holds for other molecules in which similar " shake-up " bands have been reported.

We have recently reported [1] the He I photoelectron spectrum of CSe_2, which contains bands arising from electronic excitation during ionisation (shake-up bands) as well as bands due to direct ionisation. A similar feature in the spectrum [2] of CS_2 was attributed to the same effect. We have now prepared the unsymmetrical compounds OCSe and SCSe, and recorded their spectra to see if similar bands were present. The spectrum of SCSe does contain such bands; the corresponding bands for OCSe probably underlie the much stronger bands due to direct ionisation.

Meanwhile, the He I photoelectron spectra of all these compounds have been published [3] and discussed in detail by other workers. They report no bands due to shake-up effects, despite efforts to find bands analogous to the " fifth band " of CS_2. It was suggested that the photoionisation cross-sections for transitions of this type were too small for them to be detected in this set of molecules. Our earlier results for CSe_2 and our present results for SCSe show that this conclusion is incorrect.

EXPERIMENTAL

Photoelectron spectra were recorded using a Perkin Elmer PS16 spectrometer with He I (21.22 eV) excitation.† U.v./visible spectra were recorded using 100 mm gas cells on a Pye Unicam SP800 spectrophotometer.

Carbon oxide selenide (OCSe) was prepared in low yield both by direct reaction [4] of carbon monoxide and selenium vapour at 750°C and by reaction [5] of phosgene ($COCl_2$) with heated Al_2Se_3. The latter method gave lower yields than expected from the literature reports. Subsequent purification was carried out by trap-to-trap and low-temperature column distillation in a vacuum line until no impurities could be detected by infra-red spectroscopy.

SCSe was prepared [6] in very low yield (1 %) by passing CS_2 and selenium vapours together through a tube furnace at 750°C. The resulting golden liquid, containing CS_2, SCSe and dissolved selenium, was distilled fractionally at atmospheric pressure using a 300 mm column packed with glass beads to remove most of the CS_2. The dark liquid remaining was transferred to a vacuum line and distilled to remove selenium and the remaining CS_2. Particular attention was given to the purification of this sample, which was distilled repeatedly until no traces of impurity could be detected by infra-red spectroscopy.

† Working resolution was in the range 25-40 meV; no structure resolvable at this level was observed on the *weak* bands reported here. The stronger bands showed vibrational structure as reported by other workers.[3]

RESULTS AND DISCUSSION

The photoelectron spectra of OCSe and SCSe are shown in fig. 1 and 2, and the ionisation potentials collected in table 1, which also shows our assignments. Details of the weak bands of SCSe are shown in fig. 3 and 4.

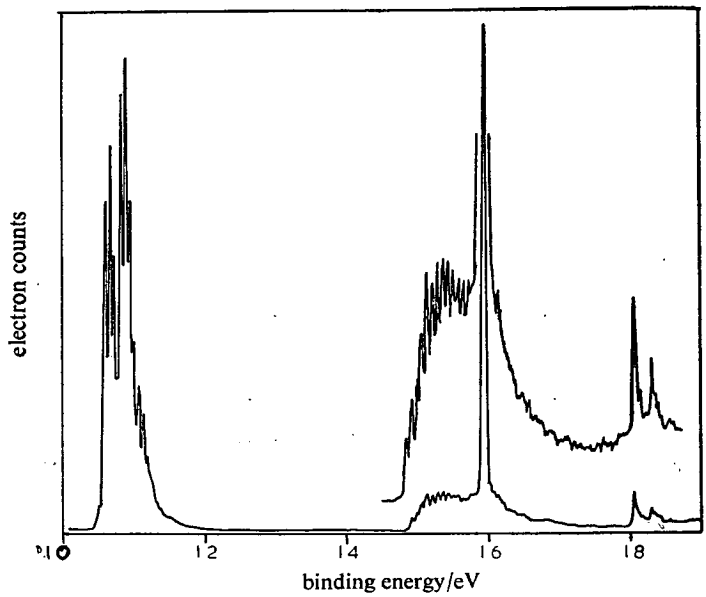

FIG. 1.—The He I photoelectron spectrum of OCSe.

The four intense bands in each spectrum are assigned to direct ionisation of valence electrons from the levels 2π, 1π, 4σ and 3σ, in order of increasing binding energy, by analogy with the spectra of OCS and the symmetrical triatomic molecules CO_2, CS_2 and CSe_2. This assignment is identical to that proposed in ref. (3), and we do not propose to discuss it or the detailed structures of the main bands further.

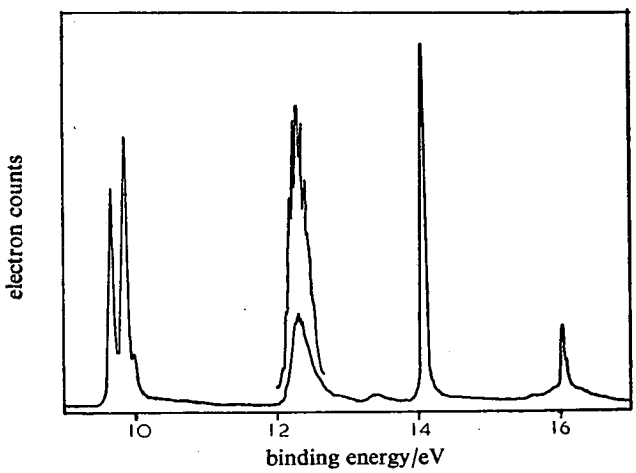

FIG. 2.—The He I photoelectron Spectrum of SCSe.

In addition to these strong bands, the spectrum of SCSe contains weaker bands which cannot be assigned to direct ionisation from valence levels. As for CSe_2, a clue to their assignment comes from the fact that they are displaced from the first strong band of the spectrum by about 3.6 eV and 6.3 eV respectively. These are

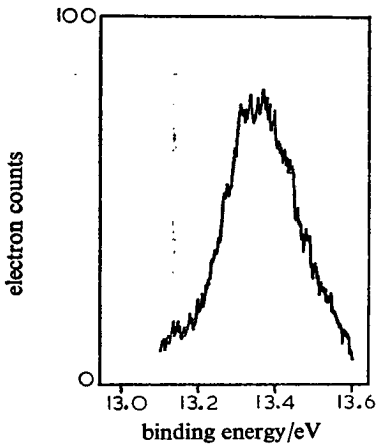

FIG. 3.—The first shake-up band in the photoelectron spectrum of SCSe.

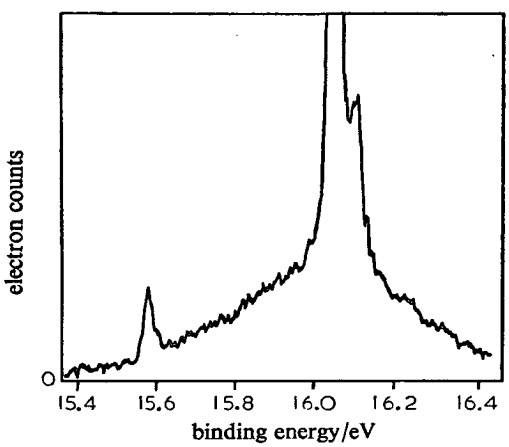

FIG. 4.—Portion of the photoelectron spectrum of SCSe showing the fourth main band and the second shake-up band.

close to the energies associated with the optical transitions observed for the molecule, at about 28 000 cm^{-1} (3.5 eV) and 46 000 cm^{-1} (5.7 eV), as shown in fig. 5. We suggest that the two sets of bands can be ascribed to the same excitation $2\pi \rightarrow 3\pi$, occurring respectively in the ion and in the molecule.

TABLE 1.—PHOTOELECTRON SPECTRA OF OCSe AND SCSe

state of ion	IP/eV for OCSe adiabatic	IP/eV for OCSe vertical	IP/eV for SCSe adiabatic	IP/eV for SCSe vertical	electron configuration
$X^2\Pi_{\frac{3}{2},\frac{1}{2}}$	10.37		9.58		$3\sigma^2\,4\sigma^2\,1\pi^4\,2\pi^3$
	10.57		9.76		
$A^2\Pi$	14.62	15.14	12.05	12.25	$3\sigma^2\,4\sigma^2\,1\pi^3\,2\pi^4$
$^2\Pi$			13.13	13.14	$3\sigma^2\,4\sigma^2\,1\pi^4\,2\pi^2\,3\pi^1$
$B^2\Sigma$	15.72		14.05		$3\sigma^2\,4\sigma^1\,1\pi^4\,2\pi^4$
$^2\Pi$			15.62	15.98	$3\sigma^2\,4\sigma^2\,1\pi^4\,2\pi^2\,3\pi^1$
$C^2\Sigma$	17.92		16.02		$3\sigma^1\,4\sigma^2\,1\pi^4\,2\pi^4$

In the neutral molecule, this excitation leads to a configuration (. . . $1\pi^4\,2\pi^3\,3\pi^1$) which gives rise to states $^{1,3}\Sigma^+$, $^{1,3}\Delta$ and $^{1,3}\Sigma^-$. By analogy with the proposed [1] assignment of the optical spectra of CS_2 and CSe_2, the two absorption bands shown in fig. 5 will correspond to the $^1\Sigma^+$ and $^1\Delta$ upper states respectively. In the ion the same excitation leads to the configuration (. . . $1\pi^4\,2\pi^2\,3\pi^1$), which gives rise to states $^2\Phi$, $^4\Pi$ and *three* $^2\Pi$ states.

The $^2\Pi$ states of this configuration cannot be reached by one-electron excitation from the ground state molecule, and would not be expected to give rise to bands in the photoelectron spectrum by interaction with a photon. However, configuration mixing with the $^2\Pi$ states of the ion resulting from simple removal of an electron from the 1π or 2π levels can provide a mechanism by which transitions to the " doubly

excited " states can be observed. As for CSe_2, only two of the three states give bands in our spectrum.

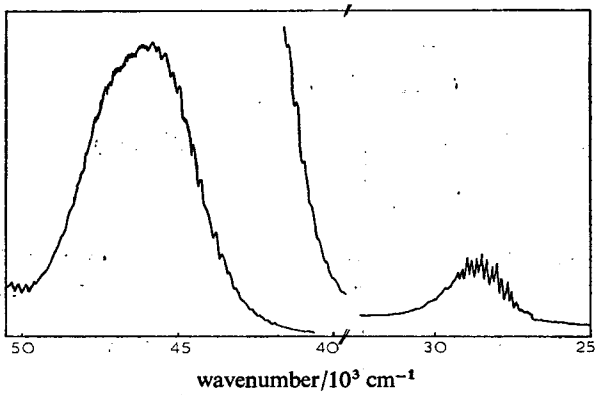

FIG. 5.—Ultraviolet spectrum of SCSe between 25 000 and 50 000 cm^{-1}.

In the photoionisation process the intensity I of any transition may be represented by the expression : $I \propto |\langle \Psi'' | P | \Psi' \rangle|^2$ where P is the electric dipole moment, Ψ'' is the wavefunction of the initial state (ground state neutral molecule) and Ψ' is the wavefunction of the final state (ion *plus* the ionised electron). The selection rule that only one-electron transitions are allowed (give finite intensity) follows if it is assumed that the core orbitals remain unperturbed in the process and are orthogonal to the orbital containing the electron to be ionised.

If the wavefunctions Ψ'' and Ψ' are regarded as derived purely from one electron configuration each this selection rule forbids the appearance of shake-up bands in the photoelectron spectrum, for such bands correspond to states of the ion differing by two electron changes from the ground state molecule. This prohibition is relaxed, however, if configuration mixing between states of the same symmetry is taken into account, for each overall wavefunction now is a linear combination of the wavefunctions of the ideal configurations.

$$\Psi_i = a_i\phi_1 + b_i\phi_2 + c_i\phi_3 + \ldots$$

Now provided at least one of the ideal wavefunctions ϕ of the excited state corresponds to a configuration differing from the ground state (which will normally be well described by a single configuration) by only a one-electron change, a mechanism exists for intensity to be " borrowed " from a formally allowed band by a formally forbidden band. The intensity is proportional to the square of the appropriate configuration mixing coefficient (m_i). The intensity of the formally allowed band should be correspondingly reduced by such borrowing, as the sum of the squares of the coefficients relating to the configuration that supplies the intensity must equal unity.

Recently there have been several attempts [7, 8] to calculate the position and intensities of shake-up bands in the spectra of diatomic and triatomic molecules using, for the most part, semi-empirical methods to derive the configuration mixing coefficients and hence the intensities and energies involved. The results have not been unsatisfactory in some instances, though the parameterisation needed in any semi-empirical calculation makes it difficult to be sure of the exact significance of the agreement with experiment.

We would point out that it is possible to infer the positions (energies) of some shake-up bands from information experimentally available from the electronic spectrum of the neutral molecule. The scheme shows that energy cycles can be

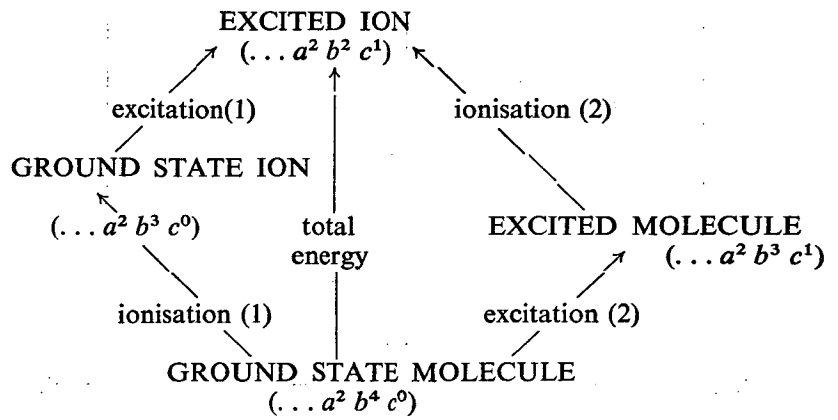

SCHEME 1.—The right-hand path is the one adopted in the text.

written giving the energy required to form an excited state ion from the ground state molecule in two ways :— by way of the ground state ion followed by excitation of an electron in the ion, *or* by way of an excited state molecule followed by ionisation of a non-excited electron from this molecule.

From experiment we know the energies associated with ionisation of the ground state molecule (Ionisation 1) and with excitation of the ground state molecule (Excitation 2). The other energies are not directly determinable, but it seems a reasonable approximation to take the ionisation energy of the excited molecule (Ionisation 2) as being equal to that of the ground state molecule; the same electron is ionised from the same orbital in each case, though the different disposition of the remaining electrons will certainly cause some difference in the net energies for the two processes.

The cycle then provides a convenient method of calculating the energies of excited state ions, such as those involved in shake-up bands, from experimentally determined data. We would emphasise that its use carries no implication whatsoever about the mechanism by which shake-up bands arise; as we have already stated, this involves configuration mixing between ionic states of the same symmetry.

Applying the cycle to SCSe, we note that the optical transition of energy 3.5 eV leads to the $^1\Delta$ state of the excited molecule; removal of an electron from the 2π level can now lead to one of the $^2\Pi$ states of the ion with the configuration (. . . $1\pi^4\ 2\pi^2\ 3\pi^1$). As the energy required to remove an electron from the 2π level of the ground state molecule is 9.6 eV we may expect the total energy for the process to be roughly $3.5+9.6 = 13.1$ eV. The shake-up band at 13.3 eV is thus very close to the predicted position.

Similarly, removal of an electron from the 2π level in the $^1\Sigma^+$ excited state of the molecule, for which the excitation energy from the electronic spectrum is 5.7 eV, should give rise to another excited state $^2\Pi$ ion whose production in a one-step process requires $5.7+9.6 = 15.3$ eV. The corresponding shake-up band appears to coincide more-or-less exactly with the intense fourth main band at 16.0 eV, causing the marked broadening of the foot of the peak (see fig. 4). The third $^2\Pi$ state of the ion with this

configuration arises from the $^1\Sigma^-$ state of the excited molecule by removal of a 2π electron; this molecular state has not been definitely located in this or any similar molecule because the transition between it and the ground state molecule is strongly forbidden.

TABLE 2.—ENERGIES OF IONISATION AND EXCITATION FOR MOLECULES/eV

molecule	1st IP	optical transition $^1\Delta \leftrightarrow {}^1\Sigma^+$	shake-up band position calc.	shake-up band position obs.	optical transition $^1\Sigma^+ \leftrightarrow {}^1\Sigma^+$	shake-up band position calc.	shake-up band position obs.
CSe_2	9.3[a]	3.3[a]	12.6	12.7[a]	5.4[a]	14.7	15.3[a]
CS_2	10.1[b]	3.9[e]	14.0	14.1[b]	6.3[e]	16.4	17.1[b]
CO_2	13.8[b]	8.4[e]	22.2	22.6[h]	11.1[e]	24.9	—
SCSe	9.6[c]	3.5[g]	13.1	13.3[g]	5.7[g]	15.3	16.0[g]
OCSe	10.4[c]	4.9[d]	15.3	o	5.8[d]	16.2	o
OCS	11.2[b]	5.2[e]	16.4	o	8.1[e]	19.3	20.1[h]
N_2O	12.9[b]	6.8[e]	19.7	19.5[f]	9.7[e]	22.6	22.5[f]

[a] ref. (1), [b] ref. (2), [c] ref. (3), [d] ref. (9), [e] ref. (10), [f] ref. (7), [g] this work, [h] ref. (11).
—, not reported; o, obscured by strong bands arising from direct ionisation.

We have made a similar analysis of possible shake-up bands in the spectra of CSe_2, CS_2, CO_2, OCSe, OCS and N_2O.† The predicted positions for the bands formally related to the $^1\Delta$ and $^1\Sigma^+$ excited state molecules are shown in table 2. Our observed bands for CSe_2 and SCSe, the bands noted for CS_2 by earlier workers [2] and the bands found [7] for N_2O with He II (40.8 eV) excitation are also shown. The agreement in all cases is excellent for the lower energy band and reasonable for the second band. Most of the other bands predicted will require He II excitation, as the total energy required is 21 eV or more. It is apparent that the predicted positions for the shake-up bands in the spectrum of OCSe (15.3 and 16.2 eV) lie in regions of the spectrum dominated by the strong bands due to direct ionisation from the 1π and 4σ levels. It is thus quite reasonable that they are not observed.

CONCLUSIONS

The He I photoelectron spectra of OCSe and SCSe have been recorded. In contrast to an earlier report, we find weak bands attributable to shake-up processes in the spectrum of SCSe. An analysis of their positions in terms of a cycle involving the electronic transition energies of the molecule and its normal first ionisation potential suggests that any such bands in the spectrum of OCSe are obscured by direct ionisation bands of much greater intensity. An extension of the analysis to the known and unknown shake-up bands of CO_2, CS_2, CSe_2, OCS and N_2O is proposed; the good agreement between calculated and observed band positions suggests that the cycle employed here will be a useful aid to the understanding of shake-up bands in other molecules.

[1] S. Cradock and W. Duncan, *Mol. Phys.*, 1974, **27**, 837.
[2] C. R. Brundle and D. W. Turner, *Int. J. Mass Spectr. Ion Phys.*, 1969, **2**, 195.
[3] D. C. Frost, S. T. Lee and C. A. McDowell, *J. Chem. Phys.*, 1973, **59**, 5484.

† A referee has drawn our attention to a paper [11] proposing a similar analysis for " configuration interaction " bands of, among other molecules, CO_2, COS, CS_2 and N_2O. Except for N_2O, however, no specific assignments were profferred for the bands we deal with here, though their positions are reported. A band fitting closely our predicted position for CO_2 (predicted 22.2 eV; observed 22.6 eV) is also reported in this paper. The band reported for COS at 20.1 eV may well correlate with our predicted band at 19.3 eV (table 2).

[4] T. G. Pearson and P. L. Robinson, *J. Chem. Soc.*, 1932, 652.
[5] O. Glemser and T. Risler, *Z. Naturforsch.*, 1948, **3b**, 1.
[6] L. Ya. Markovskii, N. V. Veshina and T. K. Voivodskaya, *Zhur. priklad. Khim.*, 1970, **43**, 1149.
[7] J. C. Lorquet and C. Cadet, *Int. J. Mass Spectr. Ion Phys.*, 1971, **7**, 463.
[8] H. Lefebvre-Brion, *Chem. Phys. Letters*, 1971, **9**, 463.
[9] M. Bavia, G. Di Lonardo, C. Galloni and A. Trombett, *J.C.S. Faraday II*, 1972, **68**, 615.
[10] J. W. Rabalais, J. M. McDonald, V. Scherr and S. P. McGlynn, *Chem. Rev.*, 1971, **71**, 73.
[11] A. W. Potts and T. A. Williams, *J. Electron Spectr.*, 1974, **3**, 3.

PRINTED IN GREAT BRITAIN AT
THE UNIVERSITY PRESS
ABERDEEN